Harmonic propagation studies in offshore wind power clusters

Marco Vinicio Chávez Báez

A thesis presented in fulfilment of the requirements for the degree of

Doctor of Philosophy

Institute of Energy and Environment
Department of Electronic and Electrical Engineering
University of Strathclyde
Glasgow G1 1XW
Scotland, UK

December, 2018

Declaration

This thesis is the result of the author's original research. It has been composed by the author and has not been previously submitted for examination which has lead to the award of a degree.

The copyright of this thesis belongs to the author under the terms of the United Kingdom Copyright Acts as qualified by University of Strathclyde Regulation 3.50. Due acknowledgement must always be made of the use of any material contained in, or derived from, this thesis.

Marco Vinicio Chávez Báez   December, 2018

Dedication

Dedicated with all my gratitude and love to

My sons

Vini and Alexis

my daughter

Ximena

and

Sandra

Acknowledgements

I would like to thank God, because I always found strength in Him to go ahead and He never abandoned me, even in the most challenging times. Also, I would like to thank all the people who made this thesis possible. I would like to express my sincerest thanks to my supervisor Prof. Olimpo Anaya-Lara and Prof. K. L. Lo for accepting me as a PhD student. I would like to give my special thanks to Prof. Olimpo Anaya-Lara for his useful guidance, patience, keen interest and efforts at every time, his assistance and instructions during my time at the University of Strathclyde has been invaluable, for my family and me.

Also, I would like to thank especially to PhD José Antonio Domínguez Navarro for his friendship and very, very helpful guidance and because it would not have been able to complete this work without his significant contributions. I would like to thank PhD Manuel Madrigal Martínez for his friendship, help, and guidance during the process of writing up the thesis. Also, I would like to thank PhD Nathanial Gardner, PhD Adriana del Carmen Téllez Anguiano, and PhD David Campos Gaona for their friendship and help during the review of the thesis.

As well, I would like to express my sincerest thanks to my colleagues from the Instituto Tecnológico de Morelia for all their support and great help. Also, I would like to thank DGEST and COECYT of Michoacán for their economical support.

My deepest and sincere thanks to my Mom, because she has been my support since I was young, to my sisters, my uncles, and aunts, my cousins, because all of them believed in me, to my whole family, my family-in-law and all my friends, here, in Glasgow, and all my friends in Mexico, especially in Morelia, for their constant support and prayers. I would like to thank Kamila Nieradzinska, Antonio Luque, and Juan Carlos Nambo for all the exchange of ideas to continue with the project. I am so lucky and so proud to have such a beautiful family and wonderful friends.

And lastly, and most important, I owe my warm thanks to my sons, Vini and Alexis, my daughter Ximena, and Sandra, who encouraged me to keep going and because without their understanding, endless patience and encouragement it would have been impossible for me to finish this work.

Abstract

The recent growth of new renewable energy sources has necessitated fresh avenues for research that searches for new methods to optimise the electrical network and reduce power losses. As this issue represents a combinational problem, the larger electrical systems present more complexity – the reason why this problem remains unsolved.

This research aims to develop an algorithm that suggests a set of configurations in large offshore wind power clusters to maintain harmonics at levels that let the clusters operate without operational problems caused by harmonics.

The major case studies of harmonics in offshore wind farms are focused on the importance of harmonic analysis for obtaining better performance from the design of the components. The interactions between the components of the system affect harmonic performance, which, in turn, may yield adverse effects such as resonances that can cause instability and operational problems that could shut off one or more wind turbines, causing a significant fault if not controlled promptly. Consequently, it is essential to reduce these adverse effects, and it is in this context that this study locates the proposed algorithm.

This research pays attention to harmonic minimisation in combination with power losses minimisation, thus implementing an evolutionary algorithm to be applied to offshore wind power clusters. The project is divided into two primary goals:

First, developing the objective functions to calculate power flow and harmonic propagation. Second, implementing the objective functions to develop a multi-objective evolutionary algorithm that can minimise harmonic propagation and power losses between the different components of a grid. Once it is obtained a set of better configurations of the offshore wind farm, data is used and helps to the designer to make recommendations for possible control strategies in large offshore wind farm projects that will deliver the offshore capacity generated into the onshore AC grid.

Contents

List of Figures

List of Tables

Acronyms

AC	Alternate Current
CSC	Current Source Converter
DC	Direct Current
DFIG	Doubly Fed Induction Generator
DFS	Deep First Search
DPI	Driving Point Impedance
FACTS	Flexible Alternating Current Transmission Systems
FPC	Full Power Converter
FSIG	Fixed-Speed Induction Generator
HVAC	High Voltage Alternating Current
HVDC	High Voltage Direct Current
IGBT	Insulated Gate Bipolar Transistor
LCC	Line Commutated Converter
MOEA	Multi-Objective Evolutionary Algorithm
MOO	Multi-Objective Optimisation
NSGA	Non-Dominated Sorting Genetic Algorithm
PCC	Point of Common Coupling
PWM	Pulse Width Modulation
RFI	Radio Frequency Interference
THD	Total Harmonic Distortion
VI	Virtual Instrument
VSC	Voltage Source Converter

1   Introduction

1.1   Background

As interactions between elements of the network can generate harmonic distortions and resonances that can affect the elements of the network, it is necessary to optimise the network to reduce the effects of the harmonic propagation. It is imperative to reduce the adverse effects caused by harmonics to avoid the overheating or destruction of the elements. The complexity of this issue requires efficient algorithms to be implemented in large wind power parks. In the field of wind farm optimisation research, it is considered the study of harmonic propagation, but it is not included as the main issue. To solve this problem, there are different algorithms, several focused on decreasing power losses and harmonic distortion, among the implemented algorithms there are some heuristics that allow solving network design and optimization problems [1]. On this basis, the question can be posed: Is it possible to reduce the problem of harmonics propagation by changing the configuration of the offshore wind power clusters and how does it affect the onshore AC grid?

1.1.1   Algorithms to design and optimise offshore wind farms

Increasing the number and size of the offshore wind turbines has complicated the network design problem, and the design of offshore power plants can become more complicated if harmonic propagation is included in the optimisation problem constraints. The design and optimisation of wind farms is a very complex problem, because it has different objectives, modelling assumptions, constraints and numerical solution methods. As the issue is a combinational problem, the complexity is high in large electrical systems [2]. This complexity is the reason for this issue still being an unsolved problem [3], [4]. The use of several different components in the offshore wind power plants generates problems such as the following: stability, voltage distortion, resonances and so on. These problems complicate the designs in which offshore wind farms are integrated with the mainland. The design and optimisation of offshore wind farms begin with the guidelines and international standards. To solve the problem of design and to optimise offshore wind

farms several numerical solution methods are used, and these methods cover the various multidisciplinary ways of solving this problem [5].

In [6], an exhaustive review of the design and optimisation problem is presented. This review covers the following: site selection, wind turbine wakes, wind turbine infrastructure, environmental impacts (wildlife and biodiversity, visual impact, noise, electromagnetic interference), uncertainty and risk management, wind turbine technology (type, size, capacity and control), number of wind turbines, electrical interconnection layout, type and length of power lines, power collection systems (transformer number, type, size, capacity), and other electric devices. The available technology constrains variables in electrical devices. The size and number of wind turbines are constrained electrically by the actual power system capacity and the expected demand from the energy consumers. Furthermore, the review focuses on electrical power losses while considering the amount of reactive power generation, transmission line length, and transmission voltage. However, there are no references of harmonic propagation in the network.

Several optimisation algorithms are focused on the best placement of the turbines for offshore wind farms. Those algorithms use wake effect, wind direction, wind power energy production, power losses, component failures, initial investment, maintenance and installation cost as main functions. Heuristic optimisation algorithms are based on certain techniques such as the following [7], [8]: multi-objective evolutionary algorithms (MOEA) [9]–[14], genetic algorithms [15]–[25], particle swarm [26], [27], greedy algorithm [28], [29], coral reefs algorithm [30], ant colony algorithm [31], virus-based optimisation algorithm [32], Monte Carlo simulation, [33], Benders' method [34], [35], local search algorithm [36], and minimum spanning tree (MST) [37], [38].

In [39], factors to optimise the design of offshore wind farms are analysed, using the cable of minimum size that is capable of carrying the wind farm output safely. In [40], a control structure to transfer the power of offshore wind farms to the DC side and into the grid is analysed, emphasising on the optimised position of the DC-DC converter and using reactive power as an objective function.

An algorithm based on geometric programming is used in [41], and the purpose is to design the layout of wind farms. The objective function is the total cost, considering power loss and system reliability. Cable connections are considered to plan connections of large offshore wind farms in Denmark. Simulation studies were of the Horns Rev B wind farm connection. Reactive compensation is required in order to reduce adverse effects in

long high voltage alternating current (HVAC) lines. This study considers harmonic impedance.

In [42], a wind farm cluster has been modelled to study the operability of groups of 1 to 5 paralleled wind turbines. The results of modelling the system with a single machine, two machines and five machines highlight the presence of the 6th harmonic because of interactions between the harmonics produced by adjacent machines, introducing lower harmonic components. In [43], an entire transmission network model was used to calculate harmonic impedance, and a reduced model is proposed, in order to reduce the amount of data.

In [44], a decision support model is presented. This model covers the three factors that characterise the design of AC electric power systems of offshore wind farms: investment cost of the components, system efficiency and system reliability, in addition to the stochasticity of wind speed and reliability of the primary system components. The model is useful for basic engineering design.

When the network is designed, it is essential to consider all possible distortions and resonances caused by harmonics in order to optimise the connections of the future wind farms to the grid. An option to optimise networks is the use of evolutionary algorithms because those algorithms are easy to implement and the evolutionary algorithms explore different possibilities, avoiding fall into a local solution [1], [45].

1.1.2   Algorithms focused on minimising power losses in large wind farms

In the power flow problem, both load powers and generator powers are given or fixed and can be represented in mathematical terms as a set of non-linear equations. The number of equations is equal to double the number of nodes. With the new large power systems, this problem increases in its complexity, because the number of combinations increases the number of equations to solve. Furthermore, to solve the complexity of the harmonic propagation and power flow for large power systems, many algorithms have been developed [1], [46].

The network configuration with minimum line losses is a problem that has been studied since 1975 when Merlin and Back proposed a non-linear optimisation algorithm to solve a network configuration with minimum line losses. The problem was solved with a heuristic approach aimed at obtaining a global minimum of losses using a branch-and-bound method. That algorithm was improved using another heuristic algorithm that worked

by opening the switches of the lines with the lowest current determined by the optimal flow pattern [47], [48]. After these solutions, several algorithms have been proposed.

In [2], there is a review, in chronological order, of some of the papers relative to the network configuration with minimum power losses. In [49] and [50], with a two-stage solution methodology and a modified simulated annealing technique, an algorithm was developed. The algorithm allows for the identification of the most effective operations for a network reconfiguration problem which is a constrained, multi-objective, non-differentiable optimisation problem.

In [51], an approach was presented to obtain the minimum loss configuration of the distribution system using a refined genetic algorithm with a radiation distribution network to calculate the load flow. In [52], another approach is implemented to obtain minimum loss configuration using a refined genetic algorithm, and the manner in which the application of minimal loss reconfiguration can help evaluate online reconfiguration benefits is analysed.

In [53], two different algorithms are presented, one resorting to a genetic algorithm and the other solving a typical mixed-integer linear problem to examine the method. The genetic algorithm is based on a heuristic strategy, and the solution starts with a meshed system obtained by closing all the tie switches, and then, lines are opened successively based on minimum power loss increase, determined by a power flow. In [54], a branch exchange procedure was applied in the neighbourhoods of the open line switches to improve the solution.

In [55], a review of techniques for the optimisation of power distribution systems is presented, which are used to solve problems with different and limited objectives and constraints.

From the preceding section, it can be seen that the optimisation of large electrical networks in order to obtain the best configuration to minimise power losses, cost, increase power capacity, get the best location of the wind turbines and other constraints is a very complex problem [1], [46]. With the large offshore wind farms planned around the world in the near future, the problem will increase in its complexity.

From another perspective, imitating nature has led to the development of evolutionary algorithms to solve complex problems. In order to minimise the adverse effects of the interactions between the components of the network, it is essential the

configuration of the network to reduce distortions caused by harmonics. These distortions can be reduced in the planning stage of the network configuration.

1.1.3   Harmonic distortion in wind power parks

With the growth of the grid and the integration of renewable resources into the power system, several problems are emerging in the grid. One of these problems is that of the harmonic currents. Harmonic currents are generated in the electrical network by all devices that contain power converters. By their nature of the operation, these types of devices generate harmonic currents in the electrical network. Under these circumstances, the presence of resonance conditions is possible and operational condition depends on the network topology, connected generation devices and connected reactive power devices. When a power system is designed, planners seek to ensure that the connected equipment does not inject harmonics into the power system. The designs must comply with the standards of the grid codes, such as not exceeding the total harmonic distortion (THD) of the voltage waveform and limits on the distortion due to specific harmonics [56], [57].

One of the challenges for the designers is to improve the capability, controllability and reliability of electric systems [58], [59]. From the viewpoint of the system, there are still several questions regarding the operation, modelling and analysis of these controllers who need to be addressed, as harmonic instabilities and resonance problems within the system may arise as a result of unexpected interactions [60].

The extensive cable network associated with offshore wind farms will bring new technical challenges, as the harmonics associated with wind turbine converters and possible resonance effects may be a potential cause of concern [61].

Issues mainly associated with offshore wind farms include the possibility of the magnification of low order harmonic voltages from the main grid due to the large capacitance of long AC cables [62], [63].

Harmonic propagation and power flow study are essential tools to analyse the power system in normal steady-state operation in the development of wind farms. Power flow studies are fundamental to determine the best operation of existing and future systems that contain multiple load centres. Also, the study of harmonic propagation is critical to avoid operation problems caused by resonances and to assess the level of harmonic emission from the wind farms into the point of common coupling (PCC) [64].

Having a lot of different devices working in the wind farms, the interconnection between the wind farms with a long subsea cable could generate great harmonic resonance problems affecting the function of the electrical network. The resonance is the reason that the study of the harmonic propagation is essential in the actual wind farms in order of improving the design of the future offshore wind power clusters that are projected for the North Sea [65], [66].

Until 2018, only a few papers have been published on harmonic analysis for wind power plants, and in the technical literature, harmonic analysis for wind power plants have not been widely discussed [67].

The severity of the harmonics injected by wind turbines depends on the turbine technology, and, a significant challenge is to eliminate harmonics at the source or to design filters to ensure that the distortion of the waveform by harmonics remains within acceptable limits. Nonetheless, a minimal voltage distortion can cause large harmonic currents at a resonance condition [68], [69]. Resonance conditions can be generated by the long distances that connect offshore wind farms to the onshore grid, power station transformers, conventional reactive power compensation, and so on [70]. Devices for harmonic correction can be costly, but a capacitor bank as part of the electrical network can provide reactive compensation and harmonic detuning as a single unit [71]–[73].

Different aspects of the power system harmonic analysis in wind power plants are discussed in [74], and practical simulation cases are discussed in [75]. In [76], a modelling approach for a doubly fed induction generator (DFIG) and a full power converter (FPC) fed generator for harmonic penetration studies is presented. In this paper, the maximum distance proposed is 50 km and the wind farm is divided into two groups of 20 wind turbines.

In [77], Kocewiak developed a study of measurement data processing focused on harmonic analysis. Although variable-speed wind turbines are grid-friendly machines in most power quality aspects, it has been observed that the different origin of harmonics can affect the results of the network. In [78], a methodology is developed to conduct harmonic studies for wind farms that are in the process of being designed, and results are simulated for the London Array offshore wind farm. London Array is located around 20 km from the shore.

In [79], an algorithm applying voltage-source converters-high-voltage direct current (VSC-HVDC) is proposed to solve problems of harmonics, voltage fluctuation, flickering

and long-distance transmission caused by large offshore wind farms. Also, in [80], an efficiency study is used to evaluate the power loss distribution after a reduced capacitor bank makes redistribution of harmonic and reactive currents in a line-commutated converter-high-voltage direct current (LCC-HVDC) connection of offshore wind farms.

In [81], harmonic distortion emission limits for the connection of an offshore wind farm are considered when the wind farm is connected to the same node with other connections. Also, this includes a harmonic filter to comply with emission limits.

In [82], an analysis of harmonic compensation using hybrid filters is presented. The purpose of the analysis is to avoid the harmful effects of harmonics in offshore wind power plants. In [83], harmonic emission from a large offshore wind farm is addressed to avoid the fact that harmonic emissions from individual turbines at higher frequencies do not reach the harmonic limits.

In [84], total harmonic distortion and the harmonic ratio of the current of a wind farm are calculated by the summation of multi-harmonic sources and the simulation of the suppression of harmonics by filters. In [85], a technique to analyse harmonic resonance issues in megawatt wind farms that use DFIGs is used. Wind farms are connected to the grid.

A Monte Carlo simulation is implemented in [86], and the purpose is to study the aggregation of the harmonic emission from individual turbines to the public grid. In [87], an approach for the harmonic penetration of the DFIG and the resonance mitigation study for an offshore wind farm that uses DFIGs is developed.

In [88], the first experiences of some phenomena with harmonic interactions in BorWin1, which is the first HVDC system connected between an offshore wind farm and a small isolated offshore AC grid, are presented. In [89], harmonic propagation and the interaction between a small scale wind farm and non-linear load in the distribution grid is studied.

Despite many research related to the study of harmonics, the study of harmonics in offshore wind farms remains of vital importance because with the offshore wind farms planned in the next years it is imperative to consider the harmonic propagation to avoid resonances that could create instability in the system. Different algorithms can be implemented in the design and optimisation of offshore wind farms using different objective functions and parameters.

1.2   Motivation of research

In reviewing the literature about the design and optimisation of the offshore wind farms, it is seen that there is a high percentage that refers to the engineering construction, and the electrical, mechanical, design, and ecological aspects. Also, with the review of the literature, it is possible to verify that the problem is multidisciplinary and involves different points of view (physical, ecological, health, and so on), to understand the general problem and to propose a particular solution.

About the electrical design, there is technical bibliography to design wind turbines, to improve the performance of power generation, to eliminate harmonics and to reduce the cost of maintenance and construction. Furthermore, there is technical information available to optimise a wind farm. There are many methods and algorithms available to place the wind turbines in the best location to achieve the best power performance.

From the harmonic propagation, there are precedents for the optimisation and design of the wind farms to integrate the generated power to the grid. Most of the research about harmonic propagation was conducted after the electrical network was designed and the harmonic analysis is focused on the use of filters to eliminate the harmonics in the power grid.

The optimisation of offshore projects is one of the most challenging tasks in developing sizeable offshore wind power clusters with hundreds of variations to be managed, documented, and benchmarked. The harmonic propagation is an ongoing problem despite a large amount of research related to this topic.

Harmonic generation and resonance conditions could create instabilities in the network. These network instabilities can cause the turbines to remain out of service, or even worse; it can cause a cascading effect in other turbines that may overheat and damage the equipment.

In the case of power systems that will increase with the new wind farms planned, the use of a method to study the harmonic propagation is essential. Implementing a conventional method for power flow and then using the current injection method facilitates the study in calculating the harmonic propagation.

By implementing the harmonic propagation in an evolutionary algorithm, it is possible to optimise the large electrical networks planned in the next years.

1.3   Description and problem statement

As described in the previous section, some of the areas of power research directly involved with wind power parks are power flow, transient stability, power quality, and harmonic analysis. The configuration of a power network involves optimisation techniques, and typical applications are cost reduction, power losses reduction, and power capacity. The optimisation of power flow has received considerable attention in research [58], [90].

Also, as far as renewable energy issues and power quality are concerned, custom power and VSC-HVDC stations have been studied from the viewpoint of technological application. Even though these new technologies inevitably generate harmonic frequencies, very little research has been conducted on harmonic analysis. One possible reason is that low order harmonic frequencies are not generated by pulse width modulation (PWM) converters, and it may be argued that the high harmonic frequencies generated by them should not cause significant problems in the distribution and transmission system if a fixed high-frequency harmonic filter is used [91].

However, a more careful analysis of the operation of fixed harmonic filters and these electronics-based controllers indicates that they might interact with elements of the transmission and distribution system such as power generators, transformers, capacitor banks, and other switching stations. Such interactions are undesirable since they may cause stability problems, over-voltages, frequency oscillations, harmonic instabilities, and, in general, abnormal device operation [92].

Despite a large number of existing studies regarding harmonics in electrical networks, the harmonic propagation remains an ongoing problem due to large offshore wind farms planned in the near future, and also, another kind of renewable energies that will be integrated to the grid.

Therefore, the first goal of this project is to implement an algorithm to calculate harmonic propagation and power flow in order to determine the objective functions and minimise harmonic distortion and power losses. The data obtained from the functions implemented will help propose actions to optimise the network. Specifically, this research proposes an evolutionary algorithm combined with a genetic algorithm to obtain the best configurations in order to minimise harmonic propagation and power losses. The proposed algorithm is applied to projected offshore wind parks in the North Sea.

1.4   Novelty and research contributions

The primary case studies of harmonics in the offshore wind farms are focused on the importance of harmonic analysis in order to obtain a better performance of the design of the wind turbine and other components of the wind farm. The interactions between these system components can increase the harmonic distortion in the system. Therefore, minimising harmonic distortion is key to reducing adverse effects such as resonance problems that could cause instability and operating problems, and this is the context where the method for network configuration proposed in this research stands to minimise the harmonic propagation using the network configuration and reduce the problem by changing the configuration of the offshore wind power clusters and, as a consequence, minimise adverse effects in the onshore AC grid [2], [4], [61], [93], [94].

This research seeks not only the techniques available for network configuration but also the research pays attention to the minimisation of harmonic propagation, and even a combination with power losses reduction to be applied to offshore wind power networks in order to use data obtained to make recommendations for possible control strategies in the large projects and incorporate generated power to the main grid. For the above, this research is focused on the following:

- The minimisation of harmonic propagation in the design of the connection of the wind farms power clusters using an evolutionary algorithm combined with a genetic algorithm.
- Implementing an evolutionary algorithm combined with a genetic algorithm will improve the performance of the algorithm to obtain the best configuration using the THD and the power losses as the main functions and the distance of the cable and number of lines as ancillary functions.
- The evolutionary algorithm approximates the solution to the best configuration eliminating lines to minimise subsea cable and with the best chromosomes starts the genetic algorithm to obtain the best configuration.

The advantage of using evolutionary and genetic algorithms is that there are the possibilities of finding the best solutions by evaluating more options. Combining the method of power flow and harmonic propagation with evolutionary and genetic algorithms will help to obtain a better configuration to optimise the electrical networks minimising the THD and power losses.

1.5   Thesis organisation

This work is divided into seven chapters. Chapter 1 presents reviews of different papers regarding the harmonic propagation and power flow, minimisation of power losses and harmonic distortion in wind power parks. Other topics presented in this chapter are the evolutionary programming focusing on research regarding the design and optimisation of offshore wind farms and different optimisation algorithms to solve network configurations. Also, the research problem is described, and a solution is proposed. Finally, the motivation and novelty of the research are described.

Chapter 2 describes general considerations regarding wind farm technologies. It presents an introduction of the different technologies of wind turbines and a brief introduction to the offshore wind farms and substations. Furthermore, it presents a brief explanation of the cables and the calculation of parameters.

In Chapter 3 an introduction to networks design and optimisation is presented. Also, an introduction to different multi-objective optimisation (MOO) algorithms to design and optimise networks is presented. There is a brief description of the differences between evolutionary and genetic algorithms. The chapter contains the basic description of a genetic algorithm. Also, the encoding, parameters, selection, crossover and mutation of the chromosomes are described. Finally, there are some recommendations concerning implementing genetic algorithms.

Chapter 4 presents a brief introduction of the harmonics generated in electrical systems. There is a compilation of different studies regarding solution techniques of harmonic power flow analysis. Also, it presents a basic introduction to harmonic propagation and power flow in large offshore wind farms and models for harmonic studies of different wind farm components. The power flow problem is formulated, and an algorithm is implemented for harmonic power propagation analysis based on the current injection method. Also, the DPI is described. With the algorithm implemented, the objective functions of the MOEA to minimise harmonic propagation and power losses are obtained.

Chapter 5 describes the algorithm proposed. From Chapter 3, an evolutionary algorithm and the objective functions to calculate THD and power losses are implemented. These are developed upon in Chapter 4 and are implemented in an MOEA to minimise harmonic propagation and power losses. The theory to eliminate isolated nodes based on the depth-first search (DFS) is described, and an algorithm is implemented. Also, an

algorithm based on the haversine formula to calculate the distance between two points and obtain the parameters of the lines is implemented. Finally, there are comparisons of the number of chromosomes generated and the elapsed generation time.

Chapter 6 presents the results of the application for case studies. Finally, in Chapter 7, the general conclusions, the contribution of this work, and outlines for future research are stated.

Furthermore, Appendices A to G contain the description of the programs developed, and Appendix H demonstrates results generated by the developed algorithm for Scenarios 1, 2 and 3. Network data and reports are not attached because if the generation data, network voltages and loads data, lines and transformers data, harmonic current injection data, power flow report, line power flow report, and harmonic propagation report for each configuration is included, it will amount to too much information.

1.6   Publications

[C1]   M.V. Chávez-Báez, O. Anaya-Lara, K. L. Lo and J. McDonald, "Harmonics and power losses reduction in multi-technology offshore wind farms using simplex method" in *48th International Universities' Power Engineering Conference (UPEC 2013). Dublin, 2013. pp. 2-5.*

[C2]   M.V. Chávez-Báez, O. Anaya-Lara, K. L. Lo and J. McDonald, "Review of harmonics in offshore wind farms" in *48th International Universities' Power Engineering Conference (UPEC 2013). Dublin, 2013. pp. 2-5.*

2 A general review of wind farms

2.1   Introduction

Over the last decade, wind energy generation has evolved into offshore installations, mainly due to restrictions to building onshore (e.g. the UK). Up to 2017, thirteen new offshore wind farms were completed, increasing the total capacity of offshore wind power farms installed in Europe to 15.8 GW [95].

Large numbers of offshore wind farms are to be built in the next years. According to the European Commission communication '*Offshore Wind Energy: Action needed to deliver on the Energy Policy Objectives for 2020 and beyond*' the offshore wind potential exploitable by 2020 is likely to be some 30-40 times the installed capacity of 2012, and in the 2030 time horizon, the figure could reach up to 150 GW, yielding some 575 TWh. These are in line with WindEurope's scenarios of 40 GW installed capacity by 2020 and 150 GW by 2030, with clusters of wind farms appearing at favourable locations, such as the German Bight and Dogger Bank, both in the North Sea [96]–[102].

Additionally, existing concepts and proposed designs for Europe's offshore grids anticipate the use of hybrid networks (LCC-HVDC and VSC-HVDC) and combinations of AC and DC offshore transmission schemes. It is envisaged that the control requirements and dynamic performance of these future offshore wind power systems, with such a variety of technology and complex network arrangements, may be significantly different from conventional and comparatively more straightforward than existing power networks. In the case of actual offshore network planning, control and operation practices may no longer be required [61], [62], [64], [103]–[105].

Hence intensive research is required in different areas to gain knowledge and an understanding on how future offshore wind power systems should be designed, controlled, and operated to ensure, technically and economically, the security of the power supply. An aspect of the power system which becomes quite relevant in these multi-technology offshore wind power networks is the aspect of harmonics, bearing in mind the dominant

presence of power electronic components in most elements involved, namely the wind turbine, compensation equipment, and transmission link [61], [62], [64], [103]–[105].

Studies of harmonic propagation in offshore wind farms imply all the components as are wind turbines, transformers, power electronics converters, smoothing capacitors, subsea cables, and so on. The subsea cables have complicated structures consisting of many different layers (conductor, insulation, sheath, and armour), and the distance between the nodes is very important for the study. The interactions between these system components can increase the harmonic distortion in the system [2], [4], [61], [93], [94].

The configuration of the network is key to reducing adverse effects, and it is the context in which this work is placed. However, obtaining the best configuration is necessary to have a brief idea regarding the necessary components of the network.

2.2   Wind turbines

The first element in wind generation is the wind turbine. At first, wind turbines tended to use Fixed Speed Induction Generators (FSIG), which consume reactive power and have limited real power control. Because network connection codes impose technical requirements, wind turbine manufacturers have developed new systems such as DFIGs and Full Range Converters (FRCs), which meet the grid code requirements, for example, the ability to control the failure of network outages, or the ability to control active and reactive power [103], [106].

Wind turbine technology has evolved quickly over the past three decades. Wind turbines have seen an increase in the diameter of the rotor and have implemented the use of sophisticated power electronics components to allow the operation of variable speed generators [103], [106].

With the different kind of technologies of wind turbines, each wind turbine injects different levels of harmonics. Hence, the importance of developing efficient mathematical models to study the harmonic performance of wind farms and their connection with the grid becomes apparent [103], [107].

As technology has evolved, also the size of the turbines has increased dramatically over the past three decades, growing from 10 meter-diameter turbines to 164 meter-diameter turbines. In Figure 2.1, there is a comparison of the evolution of the wind turbines [4], [108], [109].

To provide an idea of the size of the turbines, the turbines can be compared to a Boeing 747-8I, which has a total length of 76 m, 68 m wingspan, and a wind turbine of 3.6 MW.

The turbine has a rotor diameter of 107 m and a height of 143 m. Furthermore, the comparison with a football field used for international matches can be employed here, as the turbine similarly has a length of 100 to 120 m and a width of 64 to 90 m, with a wind turbine of 8.0 MW capacity, a rotor diameter of 174 m, and a turbine height of 220 m.

Also, the comparison of a transmission tower with the first offshore wind turbine of 450 MW and the Statue of Liberty and The Big Ben with a wind turbine of 6 GW is shown [103], [110]–[112].

Year	70's	1985	1991	1995	2001	2004	2006	2007	2015	2016
Capacity (MW)	0.15	0.225	0.45	0.66	2	2.3	3.6	5.0	6.0	8.0
Rotor diameter (m)	10	30	35	46	66	92	107	126	154	164
Turbine height (m)	18	45	52.5	63	95	126	143	176	182.5	220
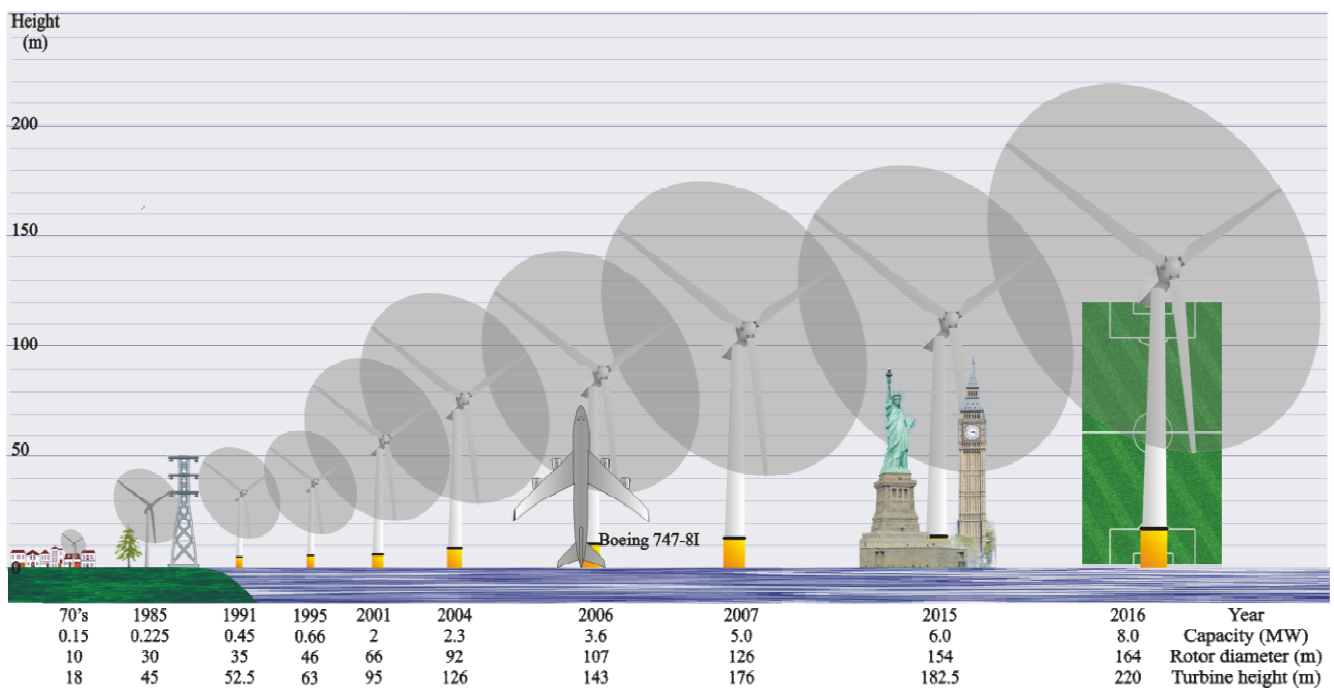
Figure 2.1. Evolution of the size of wind turbines.

2.2.1 Wind turbine operation

Wind turbines produce electricity using wind power to move a generator. The wind passes over the blades, generating a pressure that exerts a force of rotation.

The blades rotate on their axis and move the gears in a gearbox. The gearbox increases the rotational speed at an appropriate pace for the generator, which uses magnetic fields to convert rotational energy into electrical energy.

The output voltage generated is sent to a transformer, which increases the generator voltage to the appropriate voltage for the power collection system [106].

Figure 2.2 shows the wind turbine components [103].
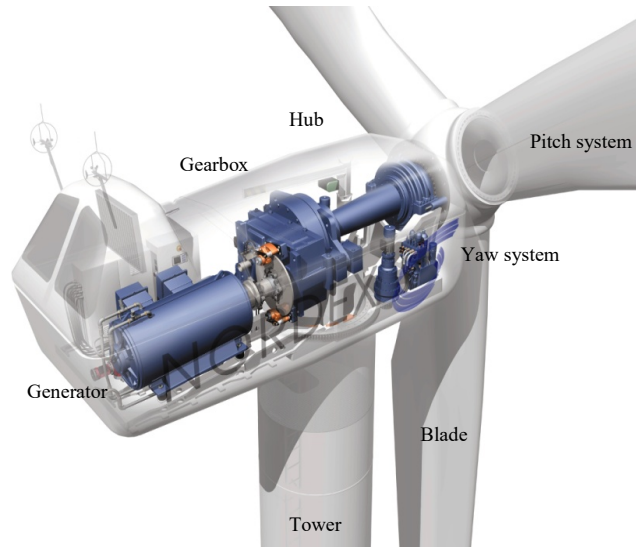
Figure 2.2. Inside the wind turbine.
Source: Coriolis Energy Ltd. 2012

2.2.2 Wind turbine generators

Wind turbine generators (WTGs) are classified into four basic types, known as Type 1 or Type A through Type 4 or Type D [113]. Generators used for wind turbines include the FSIG (Type A). If the rotor resistance of the FSIG is controlled with a slip control, then, the generator is transferred to a variable speed induction generator (Type B), or if it is used a power electronic frequency converter between the generator and the grid to get variable speed operation, synchronous or asynchronous generators are used. They can be a DFIG (Type C) or full power converter (FPC, Type D), with these being the most used DFIG wind turbines [103], [107]. Modern wind turbines, especially those with variable-speed concepts, are grid-friendly and minimise electrical emissions. However, the harmonic emissions are still a problem, so it is essential to study the different configurations of the wind turbines [114]–[116].

2.2.3 Fixed speed induction wind turbine generator

Type A, (FSIG) requires reactive power from the grid, and it is compensated with capacitor banks at the wind turbine and the PCC. However, with inadequate reactive power compensation, the voltage can collapse, or the power system can become unstable, especially in a weak grid [117], [118].

The rotor speed stability of a wind farm based on FSIG is the capability to maintain a fixed mechanical speed that is close to the speed corresponding to the actual power system frequency, even if the power system has a disturbance [117], [118].

The configuration for an FSIG wind turbine is shown in Figure 2.3 [4], [106].
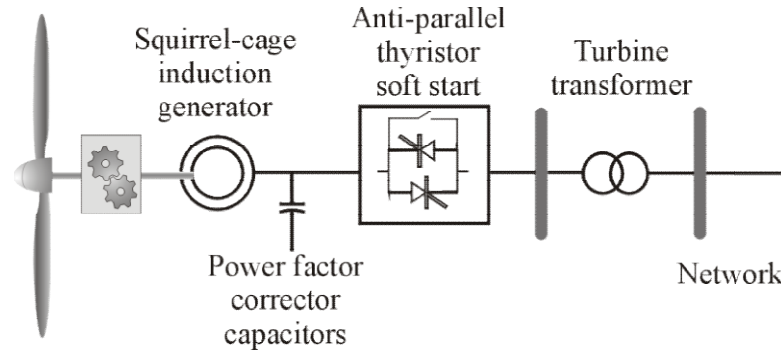
Figure 2.3. A basic configuration of a fixed speed wind turbine generator, Type A.

2.2.4 Variable speed induction wind turbine generator

Variable speed operation increases efficiency and can be achieved by controlling the rotor resistance of the fixed speed WTG, Type B, as it is shown in Figure 2.4.
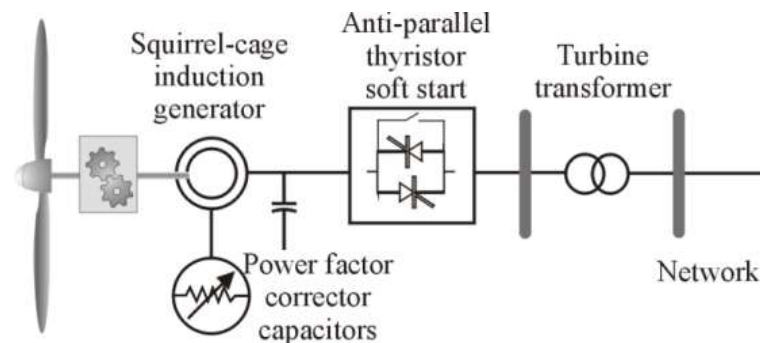
Figure 2.4. A basic configuration of a variable slip wind turbine generator, Type B.

In Type A and Type B WTGs, harmonic current generation primarily comes from the soft starter installed in the turbine to reduce the in-rush current during start-up. This harmonic current is low in magnitude and brief.

Additionally, a transformer's energisation can cause a considerable amount of low order harmonics, and the DC component can be part of the harmonic content. Another source of harmonics in a power transformer is magnetic saturation, which is an undesired operating condition. Odd harmonics are associated with overexcited transformers [4], [106], [115].

2.2.5   Doubly fed induction wind turbine generator

Type C, a typical configuration of a DFIG wind turbine system is shown schematically in Figure 2.5.
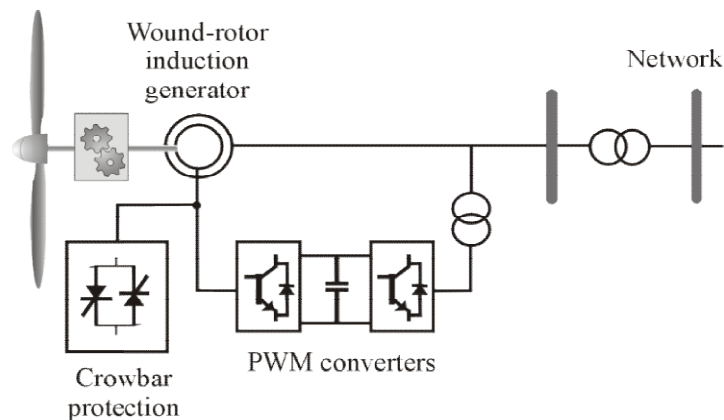
Figure 2.5. A basic configuration of a DFIG wind turbine generator, Type C.

The DFIG is constructed from a wound rotor asynchronous machine. Variable speed operation is obtained by injecting a variable voltage into the rotor at slip frequency. The injected rotor voltage is obtained using two AC-DC insulated-gate bipolar transistor-based VSCs, linked by a DC bus. The converter ratings determine the variable speed range. For harmonic analysis DFIG converters can be considered as two harmonic voltage sources: one connected to the rotor and the other connected to the stator [4], [106].

Therefore the harmonic frequencies depend on the switching technique used to switch the converter and the harmonic frequencies always are an integer (an odd value other than a triple) multiple of the fundamental frequency, 50 Hz or 60 Hz [76], [103], [107], [119]. However, the interaction between the rotor-side converter and the rotor can generate additional harmonics and interharmonics [120].

As the fundamental frequency of the rotor converter is the slip frequency, the harmonics produced by the rotor converter are a multiple of slip frequency. In the general form, k^{th} harmonic component on the rotor produces a stator current at a frequency given in Table 2.1, where f is the grid frequency [76], [103], [107], [119].

Table 2.1. Harmonic frequencies on the stator due to the rotor harmonics.

	Super-synchronous speeds	Sub-synchronous speeds
Positive sequence harmonic components	$[-(k+1)s+1]f$	$[(k-1)s+1]f$
Negative sequence harmonic components	$[-(k-1)s-1]f$	$[(k+1)s-1]f$

For the harmonic penetration studies of a power system with a wind farm connection, superposition is used to discover the harmonic currents in a particular part of the network [76].

In [76], the magnitude and frequency of the stator current sources at different torques for harmonic components produced by the rotor side PWM converter are presented. These values can be obtained by running a detailed DFIG model under different mechanical torques which represents the wind speed and then finding the fundamental frequency injected, and the voltage required. For example, according to [76], for sine-triangle PWM switching strategy with a modulation index of 15, the harmonic components present at the output are 13th, 17th, 29th, 31st, and so on.

In Type C WTGs, harmonics can be generated by power converters [121], [122]. In the study presented in [123], relatively high harmonic levels are shown for Type C WTGs. Predominantly low order harmonics are present (5th, 7th, 11th, and 13th). According to [75], these low order harmonics are introduced because of the interaction of a wind power plant with the source power system, and the most significant components reported by [75] include the 39th and 41st.

2.2.6 Full power converter wind turbines

In the FPC wind turbine known as Type D, the harmonics are produced by the full power PWM converter which directly feeds into the grid. The configuration of an FPC wind turbine is shown in Figure 2.6 [106], [124].
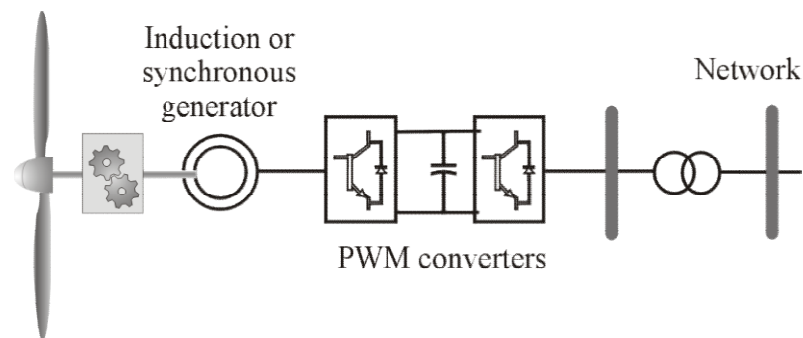
Figure 2.6. A basic configuration of an FPC wind turbine generator, Type D.

Type C and Type D WTGs are equipped with controlled back-to-back power electronic converters, and they may produce harmonics to the grid [74]. Harmonic distortion from wind power farms could interact with pre-existing harmonic network distortion and cause several issues if some of the harmonic frequencies involve exciting a resonance point [74].

2.3   Offshore substation

The purpose of an offshore substation is to minimise transmission losses by transforming the voltage of the electricity generated at the wind turbine to a higher voltage suitable for transmission to shore. The substation is sized with the appropriate power rating for the project capacity and steps up the line voltage from the collection system voltage to a higher voltage level, usually the voltage of the point of interconnection. Higher voltage lines will minimise line losses and increase the overall efficiency of the system [125], [126].

All offshore wind farms require substations, but not all substations are located offshore. The need for offshore substations depends upon the electrical power generated and the distance to the mainland, which determines the tradeoffs between capital expenditures and transmission losses. Among other things, the compensation equipment and other power electronic-based components are located in the offshore substation [125], [126].

2.4   Cables

HVAC subsea transmission schemes are commonly used by offshore wind farms (e.g. Horns Rev, Denmark). However, the distances over which AC transmission systems can be used are limited, mainly because of their charging current requirements. HVDC schemes offer an alternative method for subsea transmission. Different methods for interconnecting offshore wind generation farms and onshore utility transmission systems are addresses in [127].

An initial approach might be to examine cable models provided in commercially available packages, such as PSCAD/EMTDC [128], which is a commercially available computer-based simulation tool, providing a powerful analysis of multilayer cable models. However, there are limitations with the cable models used by such commercial software packages.

For example, it is a common feature which models only nonmagnetic material layers are considered. Only the outermost conducting layers are bonded to ground, and limited cable arrangements with often only single-core cable models are available for simulation purposes [127].

The aim of [129] was to study the steady-state harmonic behaviour of a long-distance VSC-HVDC system when accurate harmonic models for the cables are used. This

reference also examines the effects of different subsea cables upon the performance of a VSC-HVDC system. The results presented show harmonic resonances in the waveforms for different operating conditions (e.g. different switching functions, capacitor bank size, cable materials, and transmission methods-monopolar and bipolar arrangements).

Cables can be modelled as π equivalents, and usually, this representation is enough for short cable lengths, but the length of the main high voltage submarine cable to shore is longer, so it could be solved by subdividing the cable and representing it as a series of π sections, which provides reasonable accuracy for frequencies up to a few kHz. To represent frequencies that differ from the fundamental frequency can be used distributed models of the cable that are suitable for load flow analysis [76], [130], [131].

In cable transmission line, the capacitive effect is considerable, and the capacitive reactive power increases with the voltage and length of the cable. Cable overheating can be avoided limiting the current capability limited by the capacitive charging current. The reactive power of the cable depends not only on the capacitive component of the cable, as the inductive component has influence over the voltage, for compensating the reactive power are used shunt reactor as inductive components [61], [132].

A subsea power cable has a multilayered structure, and it is generally heavily armoured as is shown in Figure 2.7 [133].

Figure 2.7. DC subsea cable cross-section.
Source: NSW. 2014

Figure 2.8 demonstrates components of a subsea cable line. For DC subsea cables, the insulation is usually designed to withstand higher voltage strengths compared to an equivalent AC subsea cable, just because of the voltage stress requirements [129].
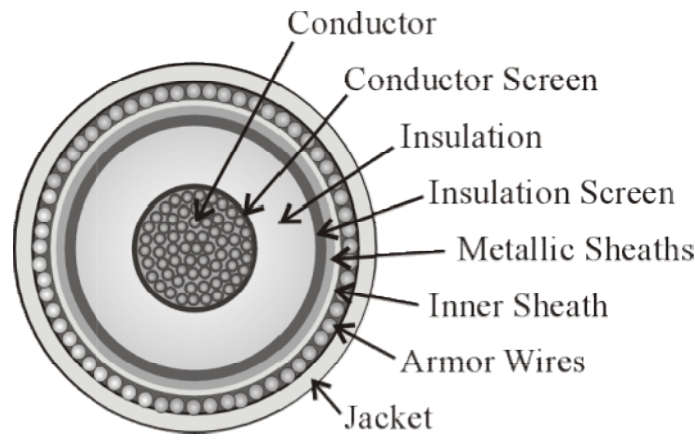
Figure 2.8. Components of DC subsea cable line.

Figure 2.9 shows the armouring hang-off of the five inter-array 33kV cables and the 150kV export cable on the substation at Horns Rev.

Figure 2.9. Armouring hang-off of the five inter-array 33kV cables and the 150kV export cable on the substation at Horns Rev.
Source: Offshore Energy, Denmark, 2012

2.4.1   Calculation of the electrical parameters of the subsea cable

As the offshore wind farms projected are located several kilometres from the shore, it is necessary to know the electrical parameters to mitigate the possible problems in the network connections. In the power system analysis, a simplified calculation of a per-unit system is used, because quantities do not change on the two sides of a transformer. The per-unit system is especially helpful in a power system where the number of transformers is large. The per-unit system absorbs large differences in absolute values, making unit values more uniform. Units provided are for power, voltage, current, impedance, and admittance [134].

To calculate the parameters for subsea cables, the usual base values are power and voltage, and they are labelled as per-unit (pu) [135]. Electrical data depends on each subsea cable, and it is essential to obtain it in order to calculate the performance of the cable in the grid [136]–[138].

2.5   Offshore wind power clusters

In the past, wind turbines were grouped into wind farms, but with the evolution of wind energy management, wind farms are being grouped into wind power clusters to allow the transmission system operators to manage wind energy more like a conventional power plant [115].

The International Offshore Wind Market to 2020 Report predicts that by the end of 2020, the global offshore wind farm capacity will be around 55 GW, but there are projects in Europe and the entire world to generate more power using offshore wind farms.

Offshore wind power farms are required to provide energy with constant voltage, frequency, and low harmonic emission to ensure the reliability and stability of the power system network. As more offshore wind farms have been integrated into the main grid, harmonic distortion issues have increased [65], [66], [103].

Since October 2008 the UK has been the world leader in offshore wind power, with as much capacity already installed as the rest of the world combined, with 24 projects and 1,184 turbines installed with an offshore capacity of 4,049 MW [96].

The sector has been developed with a series of licensing 'Rounds' co-ordinated by the Crown Estate, the landlord and owner of the seabed [96], [97], [104].

Round 3, released in 2010, is the largest so far and features nine zones across the UK.

The largest, Dogger Bank, has the potential to generate up to 13 GW of power, and it is one of the most significant energy projects anywhere in the world [5], [98], [139]–[141].

Figure 2.10 shows an example of the connection of offshore wind power clusters in the North Sea for Round 3 [65], [66], [103], [142].

Figure 2.10. Connection of offshore wind power clusters in Europe for Round 3.

Hence, it is essential to consider the main elements when modelling wind farms. These elements include the wind turbine technology, subsea cables, transformers, and transmission network components. Figure 2.11 shows the diagram of an example offshore wind farm with the main components [76]. These elements are interconnected in the most suitable location to satisfy the operational requirements of the AC grid.

It is important to remark that because of a large number of cables to connect wind turbines, and the interaction of different components of the offshore wind power farms, and even more, interaction between different offshore wind power farms, could be generated harmonic problems.

Even more, with the long distances between offshore wind power farms, the subsea cables could generate additional resonance effects that may cause instabilities within the main AC grid [106], [115].
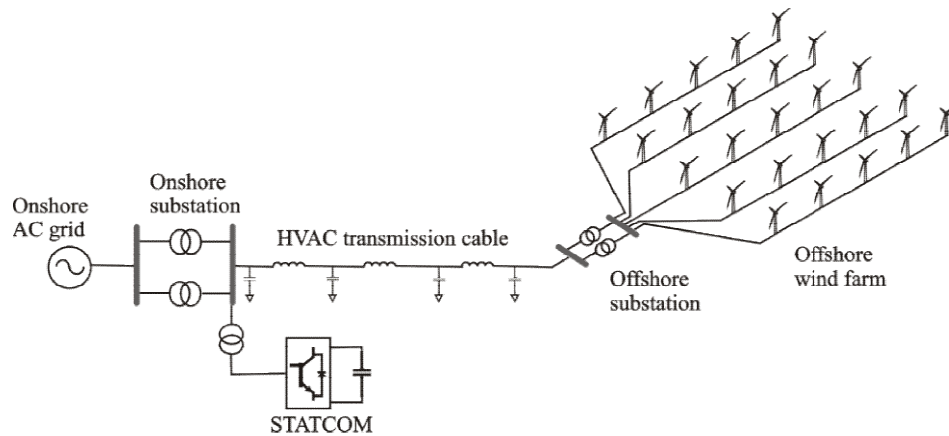
Figure 2.11. Diagram of an example offshore wind farm.

2.6   Modelling and simulations

Before installing high-voltage electrical equipment, it is necessary to model their electrical systems using computer software with the purpose of analysing different scenarios from the steady-state to transient behaviour of the electrical system [103], [104]. Time and costs of development can be reduced considerably, and components can be tested without exposing physical prototypes to the influence of destructive full-scale tests, for instance. Thus, computer simulations are a very cost-effective way to perform thorough research before a prototype is exposed to real and full-scale tests [56], [107].

However, the quality of computer simulation can only be as good as the quality of the built-in models and that of the applied data. Therefore, it is strongly recommended that the purpose of the computer simulations be clearly defined in order to ensure that the model and data quality are sufficiently accurate for the problem in question and that the simulations will provide adequate results. Otherwise, the results may be insufficient and unreliable [56], [107].

2.7   Summary

This chapter provides a general description of the electrical components of an offshore wind farm, including the components of the offshore substation and the problems related to cable layout.

A brief review of the evolution of the size of wind turbines in three decades allows for the observation of the quick development of the offshore wind power clusters regarding their capacity in the future. Also, projects provide an idea of the significant problems that could emerge due to harmonic propagation and the need to avoid harmonics.

It is essential to know the necessary components in order to implement data and obtain a better execution of the algorithm proposed to optimise the network previously mentioned.

Assuming that an offshore wind power cluster is integrated by offshore wind turbines that could be of different technologies, an offshore substation or substations, depending on the capacity of the offshore wind farm, medium voltage cables that connect the offshore wind turbines to the offshore substation, it is possible that the generation of harmonics could be present in the network.

Harmonics generated could be treated as one unit to be connected to other offshore wind farms to create a large offshore wind power cluster that will interact with other offshore wind power clusters as well.

The interaction of different offshore wind power clusters will generate harmonics, and with the long distances between offshore wind power clusters, the subsea cables could generate resonances that may cause instabilities when generated power is connected to the grid. Instability could shut off one or more wind turbines, causing a significant fault if not controlled quickly.

As was demonstrated in this chapter, large offshore wind farms are a reality. At present, power electronics and long cable lines are the core of the wind farms. In this sense, the problem of harmonics can easily present itself in the wind farms in the AC interconnection grid. These are good reasons to optimise the connection between offshore wind power clusters in order to minimise harmonic propagation and avoid resonance problems, using only the configuration of the wind power clusters.

3 Evolutionary programming to design and optimise networks

3.1 Introduction

There are several areas of research examining new optimisation methods to reconfigure the network system in order to reduce the power losses. In this chapter, the evolutionary programming and the advantage of using it to design, reconfigure, and optimise electrical power systems is introduced [1], [46], [143].

The power network reconfiguration problem consists of identifying a new network topology, and this is an important tool in the design of electric power systems. One of the main goals in the electrical power system reconfiguration problem is to minimise power losses. All the electrical system constraints must be satisfied [1], [45], [46], [51], [144], [145].

The problem can be generalised by attaching different objectives to the original power flow problem. As long as the power flow model remains without changes, more variables depending on the objective can be considered. Experience shows that the performance of solution methods in the power system analysis area is dominated on the nature of the system model, on the type of non-linearities, on the type of constraints, and the number of constraints [1], [46], [94], [143].

From the foregoing, it can be seen that the optimisation of large electrical networks in order to obtain the best configuration to minimize power losses, cost, increase power capacity, get the best location of the wind turbines and other constraints, is a very complex problem [1], [46]. With the large offshore wind farms planned around the world the problem will increase its complexity. It is very important consider all possible distortions and resonances caused by harmonics to optimise the connections of the future wind farms to the grid. To minimize negative effects of the interactions between the components of the network, configuration is important to reduce distortions caused by harmonics. These distortions can be reduced using an evolutionary algorithm to propose the network configuration [1], [46].

3.2   Evolutionary algorithms to optimise power flow in large wind farms

Since 1975, several algorithms based on heuristic methods to optimise power flow have been proposed. In [146], it is proposed a method based on artificial neural networks to evaluate the distribution system reliability. In [147], it is presented a heuristic-based two-stage solution approach in which weights were assigned to multi-objective functions.

In [148], it was developed a heuristic method suitable for real-time applications based on optimality condition using a fast load flow solution technique with new and efficient algorithms for the inspections of the network elements. In [149], another method combined with heuristic rules was proposed to determine the configuration with minimum energy loss for a given period. In [150], it was proposed a heuristic approach for reconfiguration, which reduced operating cost over a specified time period. In [151], a constructive heuristic method that started with all switches open, and at each step, the switch that resulted in the least increase in the objective function is closed.

In [152], a multi-objective evolutionary programming method for feeder reconfiguration in a practical system is proposed, in this algorithm an interactive fuzzy algorithm has been used for obtaining a solution. In [153], it is proposed another method based on genetic algorithms that is formulated as a fuzzy multi-objective problem, the algorithm takes normal conditions and contingencies and a vertex encoding is used for encoding the strings. In [154], a method based on heuristic rules and fuzzy multi-objective approach is presented. Heuristic rules are incorporated to the algorithm for minimizing the number of tie-switch operations.

In [155], it is used a genetic algorithm, the searching space is reduced when a new codification strategy is gotten, also there are accentuated crossover and directed mutation operators, this strategy reduce drastically the computational time. In [156], an improved search algorithm is presented as an efficient meta-heuristic searching algorithm where a mutation operation is introduced in the algorithm to weaken the dependence of global search ability. Also, the candidate neighbourhood is designed to improve local search efficiency saving a large amount of computational time.

In [157], a heuristic technique based on the direction of the branch power flows, despite of its simplicity, has good effectiveness. In [158], a new fuzzy multi-criteria decision making algorithm is proposed for the proper processing of the information sources available at the utilities in the context of distribution network reconfiguration.

In [159], a genetic algorithm is used for reconfiguration of radial distribution systems; a forward and backward algorithm is used to calculate load flows in unbalanced distribution systems, this process simulate the survival of the fittest elements among the strings, and performing crossover and mutation helps to obtain the optimum string.

In [160], a meta-heuristic algorithm to minimize active power loss based on modified honey-bee-mating optimisation is presented, heuristic functions with a higher contribution in solution improvement will be used in the next process, limiting unnecessary objective function evaluation. In [161], it is presented an algorithm based on simple heuristic rules where an effective switch status configuration for maximizing the line maximum load ability of the system is identified. Then a profile calculation of the best switching combination is found by load flow solution. In [162], a heuristic algorithm based on the branch-and-bound strategy, the search tree is obtained by subdividing the feasible set using the branch exchange technique.

In [163], it is introduced a genetic algorithm that uses the edge-window-decoder-encoding technique for network representation and building up spanning trees, using efficient operators in order to explore the search space. In [164], it was developed a method that combines reliability and efficiency to minimize active energy losses using a non-sequential Monte Carlo simulation based on the branch reliability and a genetic algorithm makes the optimisation that has been discussed.

As can be noted, the complexity of the power systems implies more than one objective, and this is the reason for the necessity of using the multi-objective algorithms to optimise a network considering power losses and harmonic propagation [1], [46], [94], [143].

3.3   Multi-objective optimisation

The MOO problem has two or more objectives that involve many decisions concerning variables and constraints. Usually, optimisation problems involve n objective functions [1], [45], [46],

$$f(x) = (f_1(x), f_2(x), ..., f_n(x)), \tag{3.1}$$

subject to l inequality constraints and m equality constraints:

$$g_i(x) \leq 0 \quad i = 1, 2, ..., l \tag{3.2}$$

$$h_i(x) = 0 \quad i = 1, 2, ..., m \tag{3.3}$$

Multi-objective problems can be solved using mathematical programming techniques or using metaheuristic methods. However, in both cases, normally, the concept of Pareto optimality is used to obtain the best possible solution among all the objectives. Given an initial allocation of resources among a set of individuals, a shift from the initial allocation to a different allocation that makes at least one individual better off without making any other individual worse off is called Pareto optimality or Pareto improvement. The option *x* is Pareto optimal if there exists no feasible vector of the decision variables of the universe which would decrease some criterion without causing a simultaneous increase in at least one other criterion. This concept provides a set of solutions called the Pareto optimal set or Pareto front [1], [46], [143].

Figure 3.1 presents a Pareto front. All options are compared individually. Two options are compared. To minimise, if $f_1(a) \leq f_1(c)$ and $f_2(a) \leq f_2(c)$, then the option $f(a)$ is *No Dominant* and is part of the Pareto front. If both conditions are not met, then it is a *Dominant* option and is eliminated [46], [143], [165], [166].
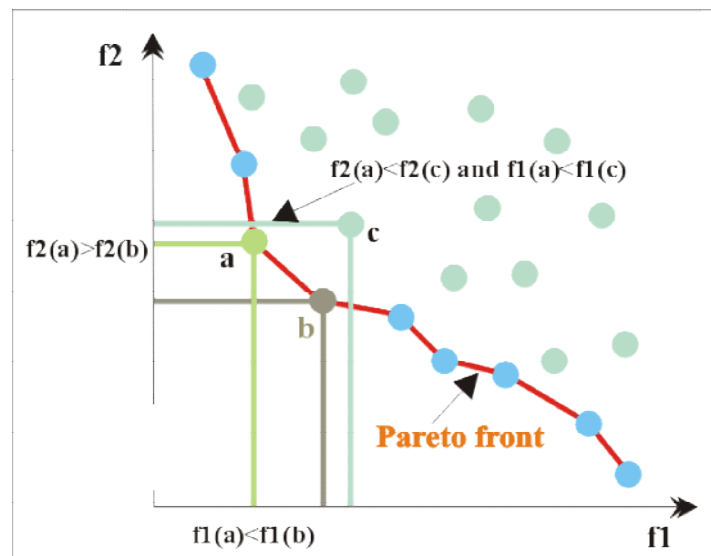
Figure 3.1. Pareto front.

3.4 Evolutionary algorithms

Of the many metaheuristic algorithms available, evolutionary algorithms have become popular because of their ease of implementation and high effectiveness. Evolutionary algorithms are inspired by Darwin's theory regarding evolution, based on an emulation of the natural selection mechanism. The beginning of the use of evolutionary strategies in solving these problems dates back to 1960 when John Holland proposed the possibility of incorporating natural selection mechanisms to solve problems of Artificial Intelligence (AI). The simulation of the processes of the natural evolution of species results

in a stochastic optimisation technique that was later referred to as evolutionary algorithms, which were framed as non-conventional optimisation techniques to address real-world problems [46], [143], [165].

From the creation of these evolutionary strategies emerged other types of research such as the following: genetic algorithms (Goldberg), genetic programming (Koza), evolutionary programming (Fogel) and evolution strategies (Rechenberg / Schwefel), where the strategies of evolution best known are genetic algorithms [46], [143], [165].

3.4.1   Multi-objective evolutionary algorithm

In 1989, Goldberg proposed a ranking scheme based on Pareto optimality. Such a mechanism, which was called *Pareto ranking*, would soon become standard within modern MOEAs.

The basic idea of Pareto ranking is to find the set of individuals in the population that are Pareto no dominant concerning the rest of the population. These individuals are then assigned the highest rank and eliminated from further contention. Another set of individuals that are no dominant concerning the remainder of the population is then determined, and these individuals are assigned the next highest rank. This process continues until the population is suitably ranked.

The first generation of MOEAs was based on non-dominated solutions. Modern MOEAs consider the method of elitism multi-objective evolutionary search. Elitism in a single-objective evolutionary algorithm consists of retaining the best individual from the current generation and passing it intact to the following generation.

In MOO, elitism is not straightforward, since all the Pareto optimal solutions are equally viable and, in theory, all of them should be retained. There are different types of MOEAs, and the non-dominated sorting algorithm is described below [46], [143], [165].

3.4.1.1   *Non-dominated sorting genetic algorithm*

NSGA is based on several layers of classifications of the individuals. Before the selection is performed, the population is ranked by the non-dominated individuals. All non-dominated individuals are classified into one category (with a dummy fitness value, which is proportional to the population size, to provide equal reproductive potential for these individuals). To maintain the diversity of the population, fitness sharing is applied to these classified individuals using their dummy fitness values. Then, this group of classified individuals is ignored, and another layer of non-dominated individuals is considered.

The process continues until all individuals in the population are classified. Stochastic remainder proportional selection is adopted for this technique. Since individuals in the first front have the maximum fitness value, they always get more copies than the rest of the population [46], [143], [165].

3.5   Genetic algorithms

Genetic algorithms are a powerful search and optimisation technique with a highly parallel behaviour, inspired by the Darwinian principle of natural selection and genetic reproduction. With this principle of selection, fittest individuals have a higher probability of reproduction, and the offspring of these individuals have a higher chance of transmitting their genetic codes to future generations. Solutions to a problem solved by genetic algorithms have evolved because many optimisation problems are complicated to solve using traditional techniques [46], [143], [165].

3.5.1   Basic description of a genetic algorithm

Genetic algorithms are an adaptive heuristic search algorithm based on the evolutionary ideas of natural selection and genetics.

Genetic algorithms operate regarding a population of individuals. Each is a potential solution to a given problem, and each is typically encoded as a fixed-length binary string, which is analogous to an actual chromosome.

An algorithm starts with a set of solutions that are called population (represented by chromosomes). Solutions from one population are taken and used to form a new population. The solution is motivated by hope, that the new population will be better than the old one.

At each step, the genetic algorithm selects individuals from the current population to be parents and uses them to produce the children for the next generation.

After an initial population is randomly or heuristically generated, the algorithm evolves the population through a sequential and iterative application of three operators: selection, crossover, and mutation.

Selection is applied to create an intermediate population, and then, crossover and mutation are applied to the intermediate population to create the next generation of potential solutions.

Solutions that are selected to form new solutions (offspring) are selected according to their fitness - the more suitable they are, the more chances they have to reproduce. This is repeated until some condition (for example, the number of populations or improvement of the best solution) is satisfied [1], [46], [145], [167], [168].

The diagram of a genetic algorithm is shown in Figure 3.2 [1], [46], [145], [167], [168].
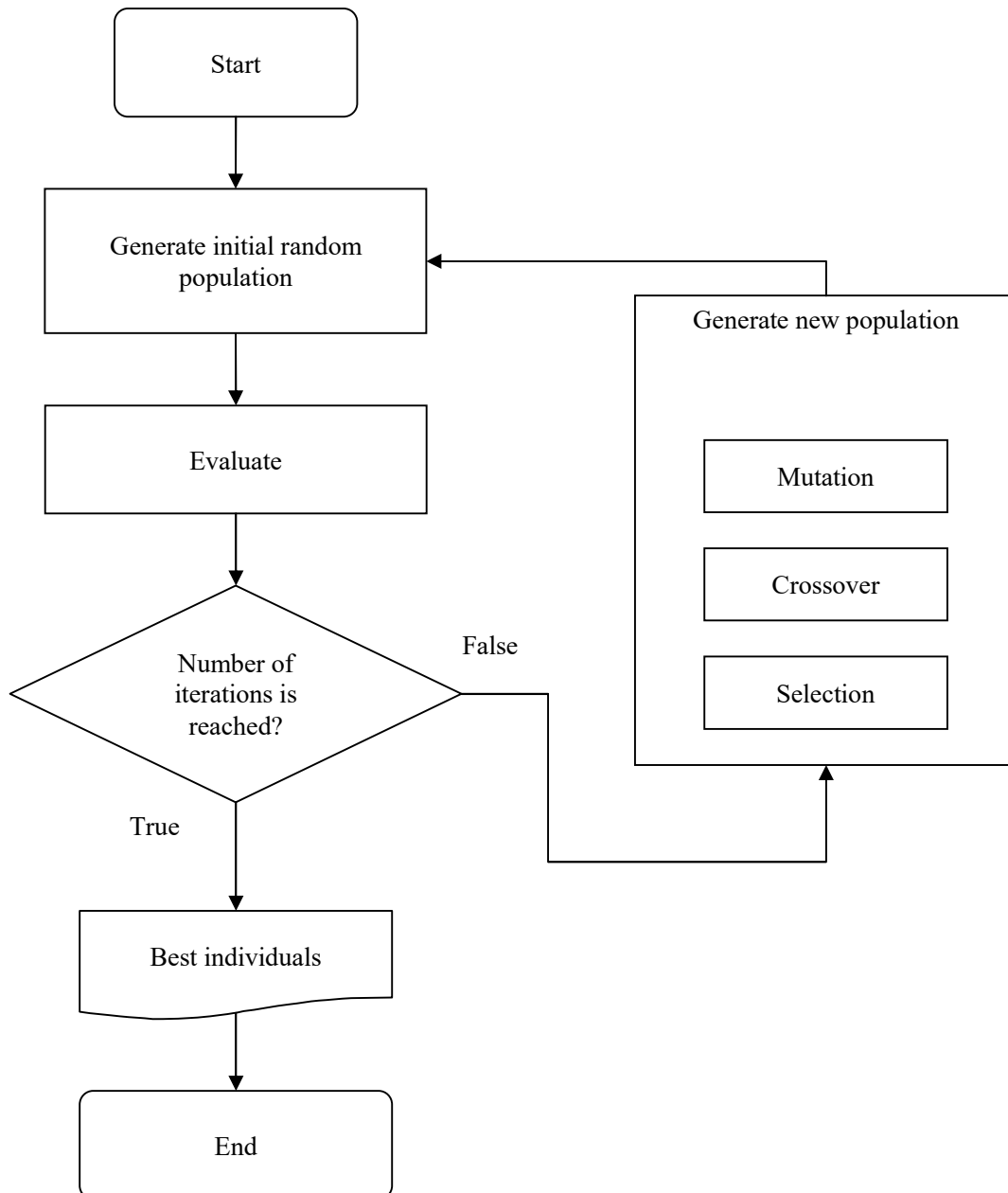
Figure 3.2. Diagram of a genetic algorithm.

3.5.2   Encoding of a chromosome

The encoding of chromosomes is one of the issues that emerge while starting solve problems with genetic algorithms, and encoding depends on the solution expected. The chromosome should, in some way, contain information about the solution that it represents.

Each chromosome has one string, and each part in this string can represent some characteristic of the solution, or the whole string can represent a number.

Of course, there are many ways of encoding, and this depends mainly on the solved problem. Each chromosome can directly encode integers or real numbers, and sometimes, it is useful to encode some permutations and so on. There are different kinds of encoding that have already been used with some success [1], [165].

3.5.2.1   Binary encoding

Binary encoding is the most common, mainly because several works regarding genetic algorithm used this type of encoding. In binary encoding, every chromosome is a string of bits, 0 or 1. Each bit of the string can represent a characteristic of the solution, or the whole string can represent the solution.

Examples of chromosomes with binary encoding are shown in Figure 3.3.

Chromosome A   101100101100101011100101

Chromosome B   111111100000110000011111

Figure 3.3. Pair of chromosomes encoded as a binary string.

Binary encoding provides many possible chromosomes, even with a small number of alleles.

On the other hand, this encoding is often not natural for many problems, and sometimes, corrections must be made after crossover and mutation [1], [165].

3.5.2.2   Tree encoding

Tree encoding is used mainly for evolving programs or expressions for genetic programming. In tree encoding, every chromosome is a tree of some objects, such as functions or commands in a programming language.

In Figure 3.4 an example of chromosomes with tree encoding is shown.

Chromosome A   Chromosome B

(+ x (/ 5 y))   (do_until step wall)
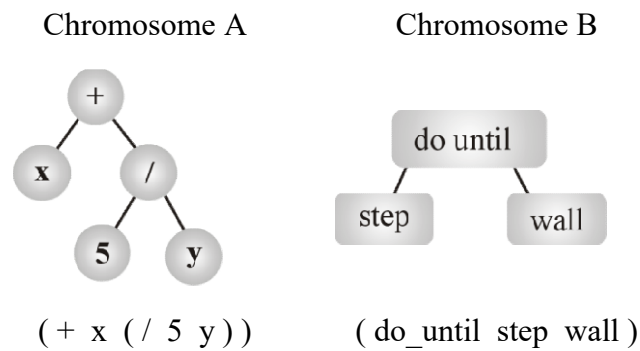
Figure 3.4. Chromosomes with tree encoding.

Tree encoding is apt for evolving programs. The programming language LISP is often used for this because programs in LISP can be easily parsed as a tree, so the crossover and mutation can be done in a relatively easy manner [1], [165].

3.5.3 Selection of a chromosome

Chromosomes are selected from the population to crossover and be parents. The problem is about the selection of these chromosomes. According to Darwin's theory of evolution, the best ones should survive and create new offspring. There are many methods to select the best chromosomes, for example, roulette wheel selection, entropy-Boltzmann selection, tournament selection, rank selection, steady-state selection and so on [1], [165].

3.5.3.1 Rank selection

Roulette wheel selection could have problems when the fitness differs too much. Rank selection first ranks the population, and then, every chromosome receives fitness from this ranking. The worst will have fitness 1, second worst 2, and so on. And the best will have fitness N that is the number of chromosomes in the population. Figure 3.5 and Figure 3.6 demonstrate how the situation changes after changing fitness to order by number.
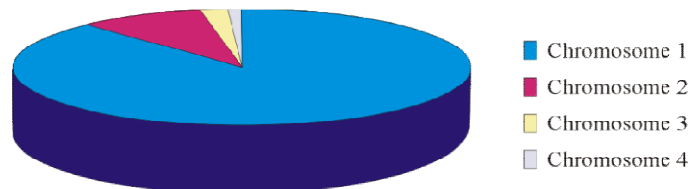
Figure 3.5. Situation before ranking (graph of fitness).
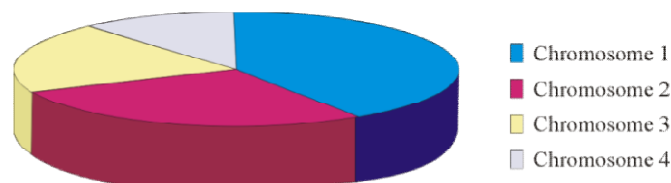
Figure 3.6. Situation after ranking (graph of ordered numbers).

After this, all the chromosomes have a chance to be selected. However, this method can lead to slower convergence because the best chromosomes do not differ so much from other ones [1], [165].

3.5.3.2 Elitism

When a new population is created by crossover and mutation, there is a high possibility of losing the best chromosome. The elitism method first copies the best chromosome (or a few best chromosomes) to the new population. The rest is done using any other method. Elitism can very quickly increase the performance of the genetic algorithm because it prevents the loss of the best solution found [1], [165].

3.5.4 Parameters of genetic algorithms

There are two basic parameters of genetic algorithms: crossover probability and mutation probability. The performance of genetic algorithms depends on them. After the decision is made regarding the type of encoding that will be used, the step to crossover can be made.

Crossover probability states how often the crossover will be performed. If there is no crossover, the offspring is an exact copy of the parents. If there is a crossover, the offspring is made from parts of the chromosome of the parents. If the crossover probability is 100%, then all of the offspring are made by crossover. If it is 0%, a whole new generation is made from exact copies of the chromosomes from the old population, but this does not mean that the new generation is the same. The crossover is made in the hope that the new chromosomes will contain the beneficial parts of the old chromosomes, and maybe, the new chromosomes will be better. However, it is appropriate to leave some parts of the population to survive for the next generation.

Mutation probability denotes how often the parts of the chromosome will be mutated. If there is no mutation, the offspring is taken after crossover without any change. If a mutation is induced, part of the chromosome is changed. If the mutation probability is 100%, the whole chromosome is changed, and if it is 0%, nothing is changed. Mutation is conducted to prevent genetic algorithms from falling into a local extreme, but it should not occur very often, because then, the genetic algorithms will change to random search.

There also exist some other parameters of genetic algorithms. An important parameter is population size.

Population size states how many chromosomes are in a population in one generation. If there are too few chromosomes, genetic algorithms have fewer possibilities to perform a crossover, and only a small part of the search space is explored. On the other hand, if there are too many chromosomes, the genetic algorithms will slow down. Research shows that after some limit, which depends mainly on encoding and the problem, it is not useful to increase the population size because it does not speed up the problem-solving process [1], [165].

3.5.5 Crossover

The method of crossover selects genes from parent chromosomes and creates a new offspring. The type and implementation of operators depend on encoding and also depends on the type of the problem. There are many ways to conduct crossover, for example, single point crossover, two-point crossover, uniform crossover, and arithmetic crossover.

3.5.5.1 Tree crossover

When trees are used, in both parents, one crossover point is selected. Parents are divided at this point, and they exchange parts below the crossover point to produce a new offspring. This is shown in Figure 3.7 [1], [165].
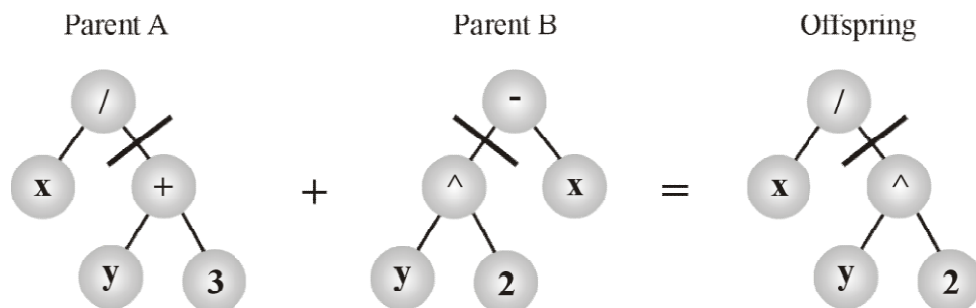
Figure 3.7. Tree crossover example.

3.5.6 Mutation

After a crossover is performed, mutation takes place to prevent the solutions in population from falling into a local optimum of solved problems. Mutation randomly changes the new offspring. For binary encoding, it can switch a few randomly chosen bits from 1 to 0 or from 0 to 1.

The mutation depends on the encoding as well as the crossover. For example, when permutations are being encoded, the mutation could be exchanging two genes [1], [165].

3.5.6.1   Tree mutation

When trees are used, an operator or number can be changed, and the selected nodes are changed [1], [165].

3.5.7   Recommendations

Recommendations are often the results of some empiric studies of genetic algorithms, which were often performed only regarding binary encoding.

- The crossover rate should generally be high, about 80% - 95%. However, some results show that for some problems, the crossover rate of about 60% is the best.

- Mutation rate, on the other hand, should be meager. The best rates reported are about 0.5% - 1%.

- Population size. It may be surprising, that a considerable population size usually does not improve the performance of genetic algorithms, regarding the speed of finding a solution. Good population size is about 10 - 30 times the number of variables. However, sometimes, sizes of 50 - 100 are reported as being the best. Some research also demonstrates the fact that the best population size depends on the size of the encoded string. If a chromosome has 16 bits, the population should be two times more.

- Selection. A basic roulette wheel selection can be used, but sometimes rank selection can be used as well. Some other sophisticated methods change the parameters of selection in genetic algorithms. Elitism could be used if there is no use of another method in saving the best solution found. Also a steady-state selection can be used.

- Encoding depends on the problem and of the size of the problem.

- The types of crossover and mutation operators depend on encoding and the problem.

- The number of generations recommended is about ten times the number of generated chromosomes, but this can be programmed to stop after a certain number of generations without change [1], [46], [145], [167], [168].

3.6   Summary

Evolutionary algorithms are different from the conventional optimisation methods and converge to the global optimum solutions because of their parallelism. Genetic algorithms travel in a search space with more individuals, so they are less likely to be stuck

in a local extreme as in other methods. Genetic algorithms are also easy to implement but, on the other hand, choosing an encoding and fitness function can be quite tricky. However, if the functions and encoding are identified and defined, genetic algorithms generate highly efficient results.

It is complicated to consider all the possible variables in the optimisation of electrical networks, and because evolutionary algorithms are generally used to solve specific problems, the implementation of a genetic algorithm was proposed. Pareto optimal solutions can be handy to the design of electrical networks. In the case of the optimisation of an electric network, when harmonic distortion and power losses are used as functions, the problem is not linear, and it could be solved with evolutionary algorithms.

After the review of the literature, the conclusion is that the best genetic algorithm that could be implemented to solve the task is the Non-Dominated Sorting Genetic Algorithm (NSGA). The NSGA is selected because for the nature of the problem is the best option to implement the chromosomes in the algorithm proposed. To represent chromosomes, it is better to use a binary tree encoding and to create offspring; it is better to choose the methods of tree crossover and tree mutation. To select chromosomes, it is better to use the elitism selection combined with rank selection. The reason to use NSGA is because it was easier to implement and provided the classification rank it is needed, it is possible to classify Pareto fronts, and although this algorithm adopts a stochastic remainder of proportional selection, it is possible to get more copies of the first front because its chromosomes are the strongest and most capable of overcoming the first front. Some other evolutionary algorithms do extra work that it is considered not necessary to obtain the results of this problem decreasing computational time and getting the same results. Furthermore, it is possible to explore other possibilities with weaker chromosomes to avoid falling into a local optimum solution.

4 Harmonic propagation in wind power parks

4.1 Introduction

Power flow and harmonic propagation studies are essential for planning future offshore wind power clusters as well as in determining the best operation of existing systems and the integration of offshore power generation into the existing grid [169]. Power flow analysis is the basis on which harmonic propagation in large electrical networks is carried out on [170].

The impedance of the long transmission cable generates the harmonic impedance that causes the parallel resonances to have a frequency shift depending on the number of array cables connected. When the number of array cables is reduced, there is a shift to lower frequencies. Additionally, a longer submarine cable would produce parallel resonances at lower frequencies, and it can cause a situation when a parallel resonance occurs at the same frequency as one of the harmonics produced by the wind turbines, in which harmonics have a frequency shift according to the wind speed and the number of turbines, and cables in operation [76]. It is essential to know the harmonic content at the PCC of the offshore wind farm in order to ensure acceptable harmonic voltages at this point and also to assess possible resonance conditions and improve solutions to these issues [171].

4.1.1 International standards associated with harmonics levels

There are numerous international standards available to guide the system operators, transmission owners, and wind farm developers. These standards are associated with the control, mitigation and monitoring of harmonic distortion, about shifts in resonances within the host network, the modification of existing harmonic distortion, and the propagation of injected harmonics into the network and through cables and substations. Some of the international standards are UK ER G5/4-1, IEEE 519, EN 50160 and IEC 61000-3-6 [74], [75], [103], [172]–[184].

4.2   Harmonic propagation methods review

Harmonics in power systems could cause an increase in the heating in the conductors and equipment, misfiring in variable speed drives, and torque pulsations in motors. The increase in the proportion of the non-linear loads has prompted more stringent recommendations in international standards and stricter limits imposed by public utilities. Incidences of harmonic-related problems are low, but an awareness of harmonic issues can help improve the reliability of plant power systems. On the rare occasions that harmonic distortions are a problem, these are either due to the magnitude of the harmonics produced or due to the power system resonance [185].

The work on harmonic power flow analysis solution techniques was pioneered by D. Xia and G. T. Heydt [186], [187] where the conventional Newton-Raphson power flow method was reformulated to include the harmonic current flows and to solve fundamental frequency parameters and harmonics simultaneously using Newton's method. In [188], the method was extended to include unbalanced systems, and in [189] a converter model was included in the algorithm.

In the methods presented in [190]–[192] the concentrated linear loads, for which their active and reactive powers are assumed to be known, are represented by an equivalent admittance at harmonic frequencies. The disadvantage of this representation is that many types of equivalent circuits exist, with their very different responses at high harmonic frequencies. In the case of an unknown non-linear load, an injected current or harmonic voltage source usually is used. According to [192], a further characteristic of most of these methods is that the addition of a new electronic-based controller requires its analytical representation and an ensuing non-straightforward reformulation of the Jacobian matrix.

In [170], a harmonic power flow methodology is implemented based on the instantaneous power flow balance concept, the harmonic domain, and the Newton-Raphson method. The method is based on the instantaneous power balance as opposed to the active and reactive power balance, followed by traditional harmonic power flow methods. The power system is modelled entirely in the harmonic domain.

With different methods to calculate harmonic propagation and power flow, it is essential to select one that can quickly obtain a solution. Choose a quickly method is important, because with the large electrical networks, there are many components to be analysed, and in consequence, there are several possible combinations of connections.

Another method is the harmonic power flow. A difficult task associated with this method is that its analytical expressions must represent each non-linear load type and included in the Jacobian matrix. Also, it is reported that this method takes a few iterations to reach convergence in the presence of non-linear loads [193].

In electrical networks, there are different methods to study harmonic propagation. One such method is the injection method, which is the simplest and most used in large electrical networks. This method allows a linear approach to representing, by a current or voltage source at different frequencies, the non-linear elements, and this simplification reduces the harmonic propagation problem to the solution of a set of linear equations solved at each harmonic frequency of interest [192], [193].

In this chapter, the harmonic current injection method is explained, and it is also used in this thesis. The harmonic current injection method is chosen because the information for each node can be proposed to represent the non-linear elements reducing the solution to a set of linear equations.

The harmonic current injection method, for harmonic propagation studies, requires an operation point based on the power flow study. The power flow formulation is explained in the following section.

4.3   Power flow analysis

The power flow analysis is carry on at fundamental frequency and steady state. The formulation of the problem is as follows.

In a transmission line, as shown in Figure 4.1, power S_{12} is given by the following:

$$S_{12} = V_1 I_{12}^* = V_1 \left(\frac{V_1 - V_2}{jx} \right)^* = \frac{|V_1|^2 - V_1 V_2^*}{-jx} = j \left(\frac{|V_1|^2}{x} - \frac{V_1 V_2^*}{x} \right)$$

$$= j \left(\frac{|V_1|^2}{x} - \frac{|V_1||V_2|}{x} e^{j(\delta_1 - \delta_2)} \right) = j \left(\frac{|V_1|^2}{x} - \frac{|V_1||V_2|}{x} \left[\cos(\delta_1 - \delta_2) + j \sin(\delta_1 - \delta_2) \right] \right)$$

$$= \frac{|V_1||V_2|}{x} \sin(\delta_1 - \delta_2) + j \left(\frac{|V_1|^2}{x} - \frac{|V_1||V_2|}{x} \cos(\delta_1 - \delta_2) \right) \qquad (4.1)$$

$$V_1 = |V_1| \angle \delta_1 \qquad\qquad V_2 = V_2 | \angle \delta_2$$

$$jx$$
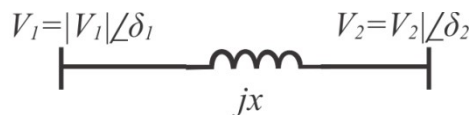
Figure 4.1. Transferred power between two buses.

Separating S_{12} from Equation (4.1) in real and imaginary parts, active and reactive power is obtained:

$$P_{12} = \text{Re}(S_{12}) = \frac{|V_1||V_2|}{x}\sin(\delta_1 - \delta_2) \qquad (4.2)$$

$$Q_{12} = \text{Im}(S_{12}) = \frac{|V_1|^2}{x} - \frac{|V_1||V_2|}{x}\cos(\delta_1 - \delta_2) \qquad (4.3)$$

And as $(\delta_1 - \delta_2)$ is very small, then $cos(\delta_1 - \delta_2) \approx 1$, reactive power is given by the following:

$$Q_{12} \approx \frac{|V_1|}{x}\left(|V_1| - |V_2|\right) \qquad (4.4)$$

Equations (4.2) and (4.4) show the basic powers flowing in a transmission line. There is a strong dependence between P and δ, and because δ is related to frequency, then an excess of generated MW tends to increment the frequency. Also, there is a strong dependence between Q and $|V|$ and an excess of reactive power (MVAR) tends to increment $|V|$. It must be observed that while f is a global variable and any change affects the whole system, $|V|$ is a variable of local effect, and as a consequence, its changes are not uniform, and these changes are more significant on buses with more excess of Q.

A more realistic system is shown in Figure 4.2, where a transmission line is included instead of the reactance. The electric system has two buses, and each bus has a generator that injects power, respectively, an S_{G1} and S_{G2} power and a load that demands an S_{D1} and S_{D2} power, and both buses are connected by a π circuit [1], [57], [170].
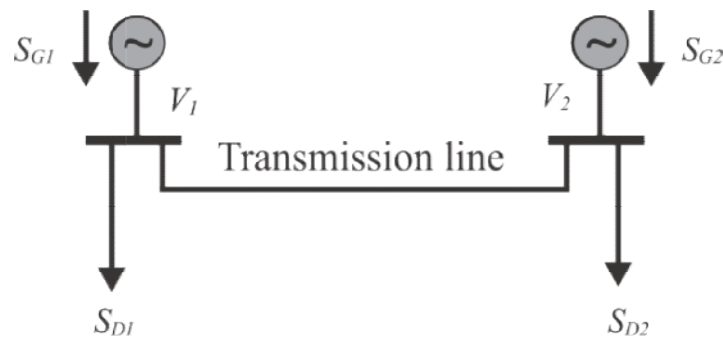
Figure 4.2. Two buses transmission line.

The transmission line model represented by the π equivalent is shown in Figure 4.3.
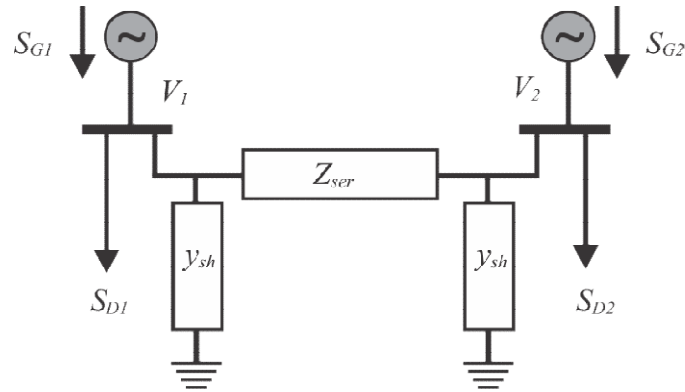
Figure 4.3. Two buses transmission line including Z_{ser} and Y_{sh}.

In Figure 4.4 total injection power at each bus is shown and it is given for each bus by the following:

$$S_1 = S_{G_1} - S_{D_1} = (P_{G_1} - P_{D_1}) + j(Q_{G_1} - Q_{D_1}) \qquad (4.5)$$

$$S_2 = S_{G_2} - S_{D_2} = (P_{G_2} - P_{D_2}) + j(Q_{G_2} - Q_{D_2}) \qquad (4.6)$$
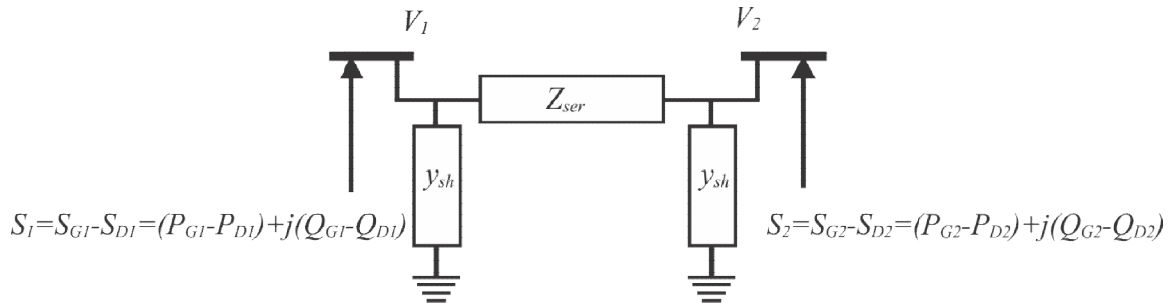
Figure 4.4. Two buses transmission line with total power injection.

The real part is the generator active power, and it complies with power balance. This means that generated power is equal to demand plus losses and the balance is maintained because the frequency is constant.

The imaginary part is reactive power, and it is maintained by the generator current to keep the voltage constant in each bus at a predetermined level [1], [57], [170].

In the general form [1], [57], [170], the active and reactive power injected in node i of an electrical network is obtained by the following,

$$S_{Gi} - S_{Di} = S_i = \sum_{k=1}^{n} S_{ik} \qquad (4.7)$$

From Equation (4.7) it must be noted that the generated power S_{Gi} and the demanded power S_{Di} in node i, must be equal to the sum of the powers that flow from node i towards the nodes of the rest of the network through the n transmission lines. Equation (4.8) is used to obtain these power flows in the electrical network.

$$S_i = P_i - jQ_i = V_i^* \sum_{k=1}^{n} Y_{ik} V_k \qquad\qquad (4.8)$$

Equation (4.7) represents the equation of power balance in all the nodes of the network, and it is the primary equation of the power flow study, and furthermore, it must be met for all nodes. The solution is explained in the following section.

4.3.1 Formulation of the power flow problem

Electrical power systems are modelled as a network of electrical nodes (buses) and are interconnected by admittances (branches) that represent transmission lines, cables, transformers, and similar power system equipment. Buses are referenced by the nodes with index $i \in N$, while branches are referenced as arcs between nodes $(i, k) \in L$, where $i, k \in N$ [1], [194].

The network in Figure 4.5 has $N = 5$ buses and $L = 6$ branches, with corresponding sets as follows:

$N = \{1, 2, 3, 4, 5\}$

$L = \{(1, 2), (1, 3), (2, 4), (3, 4), (3, 5), (4, 5)\}$.
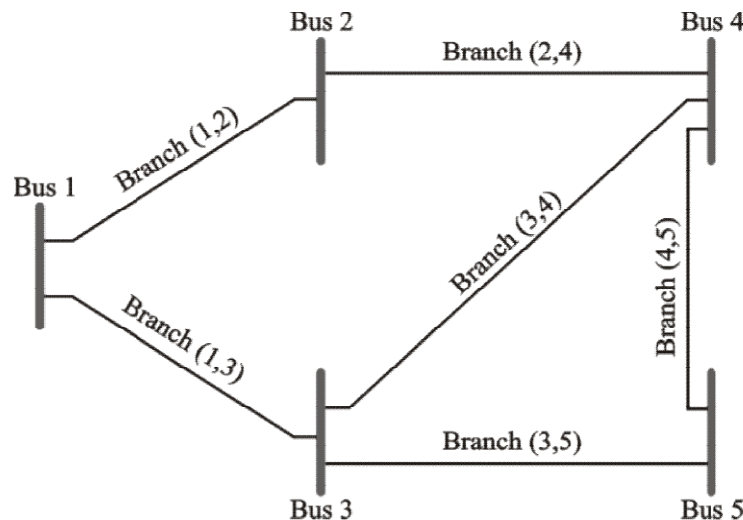
Figure 4.5. Buses and branches in a 5-bus electrical network.

In conventional power flow, all system buses are assigned to one of three bus types:

Slack bus: At the slack bus, the voltage magnitude and angle are fixed, and the power injections are free. There is only one slack bus in a power system.

Load bus: At a load bus, or P_Q bus, the power injections are fixed while the voltage magnitude and angle are free. There are M P_Q buses in the system.

Voltage controlled bus: At a voltage controlled bus, or P_G bus, the real power injection and voltage magnitude are fixed, while the reactive power injection and the voltage angle are free. This corresponds to allowing a local source of reactive power to regulate the voltage to the desired set point. There are $N-M-1$ P_G buses in the system.

Assigning buses in this manner establishes an equal number of equations and unknown quantities. Table 4.1 summarizes the three bus types [1], [194].

TABLE 4.1. BUS TYPES AND CHARACTERISTICS FOR CONVENTIONAL POWER FLOW

Bus type	*Slack*	P_Q	P_G
Number of buses in the system	1	*M*	*N-M-1*
Known quantities	δ, V	P, Q	P, V
Unknown quantities	P, Q	δ, V	δ, Q
Number of equations	0	2	2

The goal of a power flow study is to obtain the nodal voltages of the network, active and reactive power generated by the generator, power flowing in the power lines, power losses, and more conditions obtained to fulfil a steady-state operating condition of the network. Due to the non-linear nature of this problem, numerical methods are employed to obtain a solution that is within an acceptable tolerance [1], [194]–[196].

The basic equations to be used are power balance equations, which can be written for the real and reactive power for each bus. The real power balance equation is the following [1], [194]:

$$0 = -P_i(V, \delta) + |V_i| \sum_{k=1}^{N} |V_k| \left(G_{ik} \cos \delta_{ik} + B_{ik} \sin \delta_{ik} \right) \tag{4.9}$$

where:

P_i is the net power injected at bus i, G_{ik} is the real part, and B_{ik} is the imaginary part of the element in the admittance matrix corresponding to the ith row and k^{th} column.

δ_{ik} is the difference in voltage angle between the ith and k^{th} buses ($\delta_{ik} = \delta_i - \delta_k$).

In the same way, the reactive power balance equation is the following:

$$0 = -Q_i(V, \delta) + |V_i| \sum_{k=1}^{N} |V_k| \left(G_{ik} \sin \delta_{ik} + B_{ik} \cos \delta_{ik} \right) \tag{4.10}$$

where:

Q_i is the net reactive power injected at bus i.

Equations (4.9) and (4.10) include real and reactive power balance equations for each load bus and real power balance equations for each generator bus. Only a real power balance equation is written for a generator bus, because the net reactive power injected is not assumed to be known, and therefore, to include a reactive power balance equation would result in an additional unknown variable. For similar reasons, there are no equations written for the slack bus [1], [194].

There are different methods to solve the power flow problem. The majority of current methods are based on the Newton-Raphson method. The convergence rate is typically fast, but it may sometimes fail because of the inherent problems of fractality in the basins of attraction of the underlying iterative map [1].

4.3.2 Newton-Raphson method

This method begins with initial guesses of all unknown variables (voltage magnitude and angles at load buses, and voltage angles at generator buses).

Next, a first-order Taylor series approximation regarding the current estimate V and δ and the values are written, with the higher order terms ignored, for each of the power balance equations included in the system of equations. The result is a linear system of equations that can be expressed as the following [170], [192], [197]:

$$\begin{bmatrix} \Delta\delta \\ \Delta|V| \end{bmatrix} = -J^{-1} \begin{bmatrix} \Delta P \\ \Delta Q \end{bmatrix} \tag{4.11}$$

or

$$\begin{pmatrix} \Delta P \\ \Delta Q \end{pmatrix} = J \begin{pmatrix} \Delta\delta \\ \Delta|V| \end{pmatrix} \tag{4.12}$$

Where J is a matrix of partial derivatives known as a Jacobian:

$$J = \begin{bmatrix} \dfrac{\partial \Delta P}{\partial \delta} & \dfrac{\partial \Delta P}{\partial |V|} \\ \dfrac{\partial \Delta Q}{\partial \delta} & \dfrac{\partial \Delta Q}{\partial |V|} \end{bmatrix} \tag{4.13}$$

From (4.12) and (4.13)

$$\begin{pmatrix} \Delta P \\ \Delta Q \end{pmatrix} = \begin{bmatrix} \dfrac{\partial P}{\partial \delta} & \dfrac{\partial P}{\partial |V|} \\ \dfrac{\partial Q}{\partial \delta} & \dfrac{\partial Q}{\partial |V|} \end{bmatrix} \begin{pmatrix} \Delta\delta \\ \Delta V \end{pmatrix} \tag{4.14}$$

Where ΔP and ΔQ are called mismatch equations. At each iteration, mismatches in the power flow equations are as follows:

$$\Delta P_i = -P_i + \sum_{k=1}^{N} |V_i| |V_k| \left(G_{ik} \cos \delta_{ik} + B_{ik} \sin \delta_{ik} \right) \tag{4.15}$$

$$\Delta Q_i = -Q_i + \sum_{k=1}^{N} |V_i| |V_k| \left(G_{ik} \sin \delta_{ik} + B_{ik} \cos \delta_{ik} \right) \tag{4.16}$$

The method consists of iteratively solving (4.14) for the $\Delta\delta$ and ΔV required to correct the mismatch in the power flow equations computed from (4.15) and (4.16). This method is locally quadratically convergent. Therefore, given a sufficiently appropriate starting point, the method reliably finds the correct solution to the power flow equations [170], [192], [197].

The linearised system of equations is solved to determine the next guess *(m + 1)* of voltage magnitude and angles based on the following:

$$\delta^{m+1} = \delta^m + \Delta\delta \tag{4.17}$$

$$|V|^{m+1} = |V|^m + \Delta|V| \tag{4.18}$$

The process continues until a stopping condition is met. A common stopping condition is to terminate if the norm of the mismatch equations is below a specified tolerance [1], [57], [170].

4.3.3 Calculation of power losses

When the system converges to a solution, then it is possible to calculate power flow and power losses in each transmission line. As a consequence, it is possible to calculate power losses in the whole network. The power flow of each branch is obtained by subtracting active and reactive power values of each node of the line in both ways. That means from node A to B and from node B to A. And with data obtained for each branch, it is possible to calculate total power losses by subtracting demanded power from generated power as is given by the following:

$$P_{Losses} = P_{Generated} - P_{Demanded} \tag{4.19}$$

4.4 Harmonic propagation using current injection method

The harmonic propagation problem in electrical networks is a problem in steady state. Under normal operation conditions, voltages and currents are periodical balanced non-sinusoidal signals. In this sense, the Fourier series of a periodic signal is the basis of

the harmonic analysis in electrical networks. Harmonics should not be confused with spikes, dips, impulses, oscillations or other forms of transients [72], [185]. An index that describes the harmonic distortion of a signal is the THD.

Voltage THD (THD_v) is defined as the following:

$$THD_V = \frac{\sqrt{\sum_{n=2}^{\infty} V_n^2}}{V_1} \times 100\%$$ (4.20)

where:

V_1 is the rms or peak value of the fundamental component of voltage.

V_n is the rms or peak value of the nth harmonic component of voltage.

4.4.1 Nodal harmonic voltage calculation

The harmonic studies aim is to quantify harmonic voltage distortion at points of interest in the system, determine the existence of dangerous resonance conditions and verify violations within the limits of harmonics allowed. A harmonic study consists of the following steps [170], [192], [197]:

• Definition of a harmonic generator device.

• Determination of the models to represent system components including external networks.

• Simulation of the system for different scenarios.

In practice, a large number of problems related to harmonics involve small systems with relatively low distortion and, often, a single dominant harmonic source. In these cases, the simplified calculations of the resonance frequency can be manually performed, and distortion calculations can be made using a spreadsheet [170], [192], [197].

For large systems and multiple harmonic generating loads, analysis methods of harmonic propagation are necessary.

Mathematically, the method of harmonic injection current or the linear harmonic propagation method involves solving simultaneous equations. The nodal harmonic voltage in an electrical network can be obtained from the solution of Equation (4.21) for each specific harmonic h [170], [192], [197]:

$$
\begin{bmatrix} I_h^1 \\ I_h^2 \\ \vdots \\ I_h^N \end{bmatrix} = \begin{bmatrix} Y_h^{1,1} & Y_h^{1,2} & \cdots & Y_h^{1,N} \\ Y_h^{2,1} & Y_h^{2,2} & \cdots & Y_h^{2,N} \\ \vdots & \vdots & \ddots & \vdots \\ Y_h^{N,1} & Y_h^{N,2} & \cdots & Y_h^{N,N} \end{bmatrix} \begin{bmatrix} V_h^1 \\ V_h^2 \\ \vdots \\ V_h^N \end{bmatrix}
\tag{4.21}
$$

and in a compact form

$$
[I_h] = [Y_h]\,[V_h]
\tag{4.22}
$$

where

N is the number of nodes of the network.

$[I_h]$ is the vector of the nodal harmonic current injections of each bus of the network by harmonic h.

$[V_h]$ is the vector of the resulting harmonic voltages for each harmonic h.

$[Y_h]$ is the network admittance matrix at harmonic h and it is easily obtained from network data and network configuration.

The harmonic injection current vector is obtained from all the harmonic sources which are represented by their typical harmonic content. In the case of harmonics emerging from wind turbines in an offshore wind farm, they could be represented by the harmonic content.

The formulation of the admittance matrix of the network is a standard power system analysis practice, using characteristic equations for all network elements (transmission lines, transformers, rotating machines, capacitor banks, magnetic non-linearity, and FACTS devices). All these elements change with the frequency of operation, and in this sense, the admittance matrix changes for every harmonic h [170], [192], [197].

4.4.2 Power system element models for harmonic analysis

In order to solve Equation (4.21), the admittance matrix of the network $[Y_h]$ needs to be obtained. This admittance matrix is obtained with all the models, for harmonic analysis, of the electric components, mainly.

• Generator.

• Transmission line.

• Transformer.

• Capacitor banks.

• Wind generators.

• Loads.

These models are described below. When linear elements are modelled in electrical networks, it is assumed that a frequency-dependent equivalent circuit represents those elements. Linear elements have a resistive and a reactive part, and this feature is known as impedance. Both, inductive and capacitive reactance, depend on frequency.

In this way, the impedance of an element at h harmonic is given by the following:

$$Z(h) = R + jX(h) \tag{4.23}$$

With this concept, the modelling of other elements starts from an equivalent model represented by linear elements that depend on the frequency [106], [191], [192], [198], [199].

4.4.2.1 Collector cable and lines

Cables and lines can be represented by their equivalent π circuit at different frequencies, considering the effects caused by length, transposition, and by imbalance in the lines. The π circuit must be used only in lines that are less than several hundreds of kilometres in length and those with a low harmonic order.

In Figure 4.6 the π model for the power cable is shown. This model is adequate for resonance studies because distances between nodes are relatively short, and furthermore, this model considers the capacitive effect [106], [191], [199].
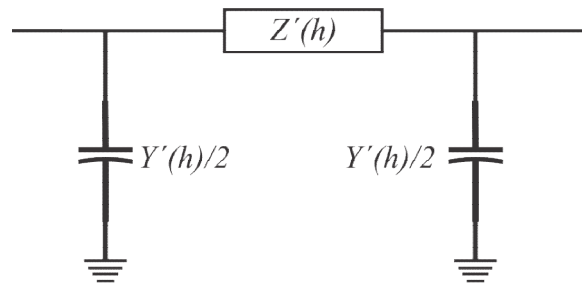
Figure 4.6. π model for a power cable.

This model is described mathematically by the following:

$$Z'(h) = Z(h)\frac{\sinh \gamma(h)l}{\gamma(h)l} \tag{4.24}$$

and

$$\frac{Y'(h)}{2} = \frac{Y(h)}{2} \frac{\tanh\frac{\gamma(h)}{2}l}{\frac{\gamma(h)}{2}l} \qquad (4.25)$$

where *Z'(h)* and *Y'(h)* are the series impedance and shunt admittance for the π model. *Z(h)* and *Y(h)* are given by the following:

$$Z(h) = (r(h) + jX_L(h))l \qquad (4.26)$$

$$Y(h) = jB_C(h)l \qquad (4.27)$$

where

$$X_L(h) = h2\pi fL \qquad (4.28)$$

$$B_C(h) = h2\pi fC \qquad (4.29)$$

and if *h<2.35f* then,

$$r(h) = r \qquad (4.30)$$

or else if *h≥2.35f*, then

$$r(h) = r(0.187 + 0.532\sqrt{h}) \qquad (4.31)$$

Resistance *r(h)* includes a correction factor to approximate the value of skin effect [191], and this factor is given by the following:

$$\gamma(h) = \sqrt{(r(h) + jX_L(h))jB_C(h)} \qquad (4.32)$$

where

r is cable resistance in ohms per unit length.

L is cable inductance in henries per unit length.

C is cable capacitance in farads per unit length.

f is the system frequency.

l is the cable length in unit length.

4.4.2.2 Transformers

Transformers are considered as linear elements, and their harmonic impedances are obtained as passive elements. The basic transformer model is represented by the equivalent circuit and it is shown in Figure 4.7. This model includes transformer leakage reactance, X_t, and total equivalent resistance, R_t.

Figure 4.7. Transformer equivalent circuit.

Transformer harmonic impedance is given by the following:

$$Z_t(h) = R_t(h) + jX_t(h) = R_t\sqrt{h} + jX_t h \tag{4.33}$$

where

R_t determines transformer power losses and

X_t is the transformer short circuit reactance.

The connection of the transformer must be used if there are harmonics of sequence zero. The transformer saturation effect can be represented by a harmonic current injection source [106], [191], [199].

4.4.2.3   Synchronous generator

Generators are considered linear elements in cases where harmonic impedance can be represented as passive elements. An equivalent circuit of a synchronous generator is shown in Figure 4.8. The harmonic impedance model is given by the following:

$$Z_g(h) = R_g(h) + jX_g(h) = R_g\sqrt{h} + jX_d"h \tag{4.34}$$

where

R_g is the generator resistance and

$X_d"$ is the inductive reactance that includes generator power losses and sub-transient reactance [106], [116], [191], [199].
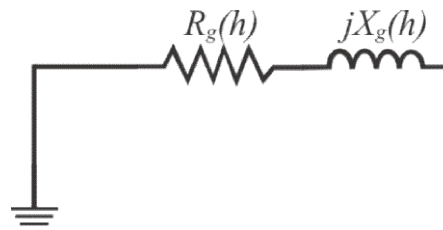
Figure 4.8. Synchronous generator equivalent circuit.

4.4.2.4   Load models

Each load can be represented by a passive load model and CIGRE models can be used [190], [199]. Figure 4.9 shows the conventional CIGRE model: *parallel R-X_L load model.* For CIGRE load model type 1, harmonic impedance is given by Equations (4.35) and (4.36) and for CIGRE load model type 2, by Equation (4.37) and (4.38):

$$R = \frac{V_{LL}^2}{P} \tag{4.35}$$

$$X_L(h) = j\frac{hV_{LL}^2}{Q} \tag{4.36}$$

$$R(h) = \frac{V_{LL}^2}{(0.1h+0.9)P} \tag{4.37}$$

$$X_L(h) = j\frac{hV_{LL}^2}{(0.1h+0.9)Q} \tag{4.38}$$

where

X_L is the load inductive reactance

R is the load resistance

V_{LL} is the load voltage (line to line)

Q is the demanded reactive power by the load

P is the demanded active power by the load
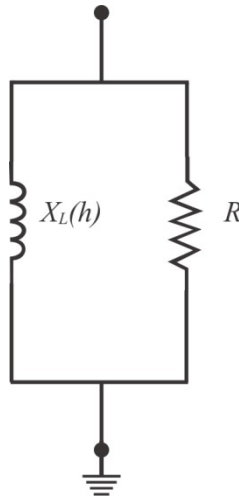
Figure 4.9. Conventional CIGRE load model.

Figure 4.10 shows the CIGRE load model type 3: *R-Xs series X_L parallel*. This model was obtained by experimentation [199], and harmonic impedance is given by the following:

$$R = \frac{V_{LL}^2}{P} \tag{4.39}$$

$$X_S(h) = j0.073hR \tag{4.40}$$

$$X_L(h) = j\frac{hR}{6.7\left(\frac{Q}{P}-0.74\right)} \tag{4.41}$$
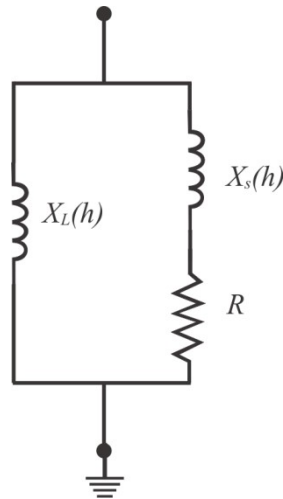
Figure 4.10. CIGRE load model type 3.

4.4.2.5 DFIG wind turbine model

In Figure 4.11 an equivalent electrical circuit of a DFIG wind turbine model for harmonic analysis is shown. This model is represented by its equivalent circuit at harmonic frequencies and an injection current source.
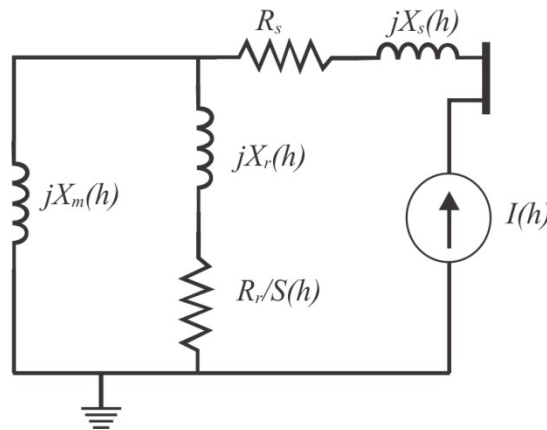
Figure 4.11. DFIG wind turbine equivalent circuit.

Where $X_r(h)$, $X_s(h)$, and $X_m(h)$ are rotor, stator, and magnetizing reactances at harmonic h, and these parameters are calculated by the following:

$$X_r(h)=hX_r \tag{4.42}$$

$$X_s(h)=hX_s \tag{4.43}$$

$$X_m(h)=hX_m \tag{4.44}$$

R_r and R_s are rotor and stator resistance, and s_h is the apparent slip at harmonic frequencies, and it is calculated by the following:

$$s_h = \frac{\pm h\omega_s - \omega_r}{\pm h\omega_s} \tag{4.45}$$

where ω_r and ω_s are the rotor and stator angular velocities, and symbol $\pm$ is for positive and negative harmonic sequences, and *I(h)* are the harmonics injected to the network due to the power electronic converter of the DFIG. These harmonics are in percentage of the fundamental voltage of the DFIG [106], [191].

4.4.2.6   Harmonic injection current source

In the implemented algorithm only two non-linear elements are considered that generate harmonics. Non-linear loads and wind power clusters.

The non-linear loads are represented by its injection current as a percentage of the fundamental frequency.

And the wind power clusters are represented by the model described in Figure 4.11.

4.4.2.7   Driving point impedance

With all these element models for harmonic analysis, the admittance matrix of the network $[Y_h]$ can be obtained in order to solve Equation (4.22) which is the harmonic propagation problem.

The inverse of the admittance matrix, $[Y_h]$, is equal to the impedance matrix, $[Z_h]$ and is given by the following:

$$[Z_h] = [Y_h^{-1}] \tag{4.46}$$

Inverting $[Y_h]$ yields the network harmonic impedance matrix $[Z_h]$. Its diagonal elements $Z_h^{j,j}$ are the harmonic self-impedances of the respective buses, in this case bus *j*.

The non-diagonal elements $Z_h^{i,j}$ are transferred impedances, related to the effect on the voltage of bus *i* when a harmonic current is injected at bus *j* [170], [192], [197].

$$[Z_h] = \begin{bmatrix} Z_h^{1,1} & \cdots & Z_h^{1,j} & \cdots & Z_h^{1,N} \\ \vdots & \ddots & \vdots & \ddots & \vdots \\ Z_h^{j,1} & \cdots & Z_h^{j,j} & \cdots & Z_h^{j,N} \\ \vdots & \ddots & \vdots & \ddots & \vdots \\ Z_h^{N,1} & \cdots & Z_h^{N,j} & \cdots & Z_h^{N,N} \end{bmatrix} \tag{4.47}$$

where impedance $Z_h^{j,j}$ is known as the Thévenin impedance seen by the node *j* at the harmonic *h*, and Thévenin impedance seen by the node *j* at a range of harmonic frequencies, as *h = 1, 2, ..., 50* is known as the driving point impedance (DPI) of the node *j* at the harmonic frequencies [170], [192], [197]. The DPI is obtained from the passive network through the impedance matrix $[Z_h]$.

Calculating $[Z_h]$ for varying frequencies $f_h=hf_1$ is obtained the DPI.

A frequency scan or impedance scan is presented as a graph of a DPI or Thévenin impedance on a system bus versus frequency [192]. DPI reveals possible harmonic resonance conditions of self or transfer impedances.

The DPI shows the impedance vs. frequency graph, where impedance peaks indicate parallel resonance and impedance valleys indicate series resonances that can help to design the network [200].

In much commercial software, the DPI is obtained by injecting a current of one per unit at an appropriate frequency in the bus of interest, where other currents are set to zero, and the equation of current injection is solved to find the nodal voltages that are equal to the nodal impedance. The calculation is repeated in the range of the harmonic frequency of interest. Typically, a scan is performed for networks of positive and zero sequences in the case of three-phase networks [170], [192], [197].

4.5   Harmonic propagation and power flow algorithm

The power flow and harmonic algorithm implemented to obtain the results in this research are a traditional Newton-Raphson and harmonic current injection method. The methods to calculate power flow and harmonic propagation, described in section 4.3 and 4.4, were implemented.
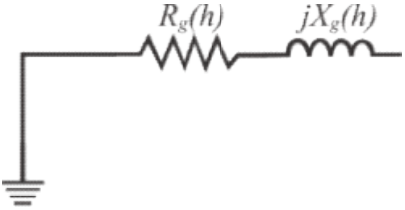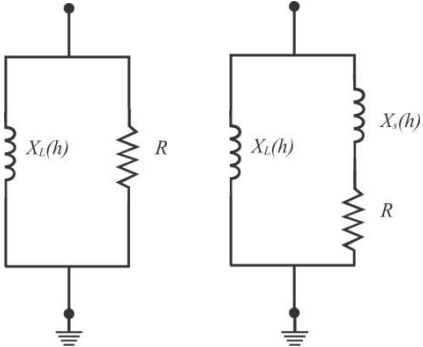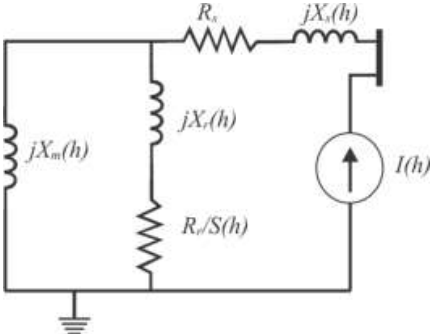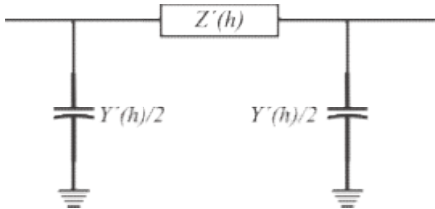
It is important to remark that in the developed algorithm, both, conventional generation and wind power clusters are P_G nodes as described in Table 4.1, but the wind power clusters include an injection harmonic current in order to conform $[I_h]$ in Equation (4.22).

All data is introduced to let the program know the conditions of the system. With all the data, the algorithm uses the Newton-Raphson method to calculate the power flow and to obtain the harmonic propagation.

The study of harmonic propagation is calculated using the current injection method. Table 4.2 shows the different elements, described before, used in the networks and the models used to calculate power flow and harmonic propagation.

TABLE 4.2. MODELS USED FOR POWER FLOW AND HARMONIC PROPAGATION

Element	Power flow model	Harmonic propagation model
Generator	P, V	$R_g(h)$ $jX_g(h)$
Load	P, Q	$X_L(h)$, R / $X_L(h)$, $X_s(h)$, R
Wind power cluster	P, V	$jX_m(h)$, $jX_r(h)$, $R_r/S(h)$, R_s, $jX_s(h)$, $I(h)$
Collector cable and lines	$Z'(h)$, $Y'(h)/2$, $Y'(h)/2$	idem
Transformer	$R_t(h)$ $jX_t(h)$	idem
Formulation	$[\Delta P] = [J]\,[\Delta V]$	$[V_h] = [Z_h]\,[I_h]$

The algorithm calculates the number of lines and transformers, nodes of generation (conventional and wind power clusters), nodes of load, the total number of nodes, number of elements in derivation, load nodes with harmonic injected, number of harmonics to be considered, and the processing time of the study.

For each node, the final voltage, as well as active and reactive power for demand and for generation, is shown.

The report generated by the algorithm includes the following: number of iterations to find the solution, calculated error, generated and demanded power, total power losses including harmonics, and power losses only by harmonics.

The report shows that for each line, the complex current flows in both directions, and with the sum of both, the power losses are calculated.

The harmonic propagation report shows the voltage and angle in each node, the voltage rms and the THD. Also, the harmonic voltages and angle for each harmonic calculated are shown.

With the THD of each node, a logarithm average of the THD is calculated. The purpose of using a logarithm average instead of an arithmetic average is to consider a greater weighing for the higher harmonic distortion.

The algorithm automatically generates the report. Additionally, the report shows the DPI of the system and the harmonic voltage for each node.

Finally, the report shows the front panel of the virtual instrument developed. The front panel includes all input and output data.

The data of power flow, harmonic propagation, power generation and power losses that the algorithm returns will be used in a genetic algorithm as objective functions.

Figure 4.12 shows the diagram of the algorithm implemented. The harmonic propagation and power flow algorithm is detailed in Appendix A.
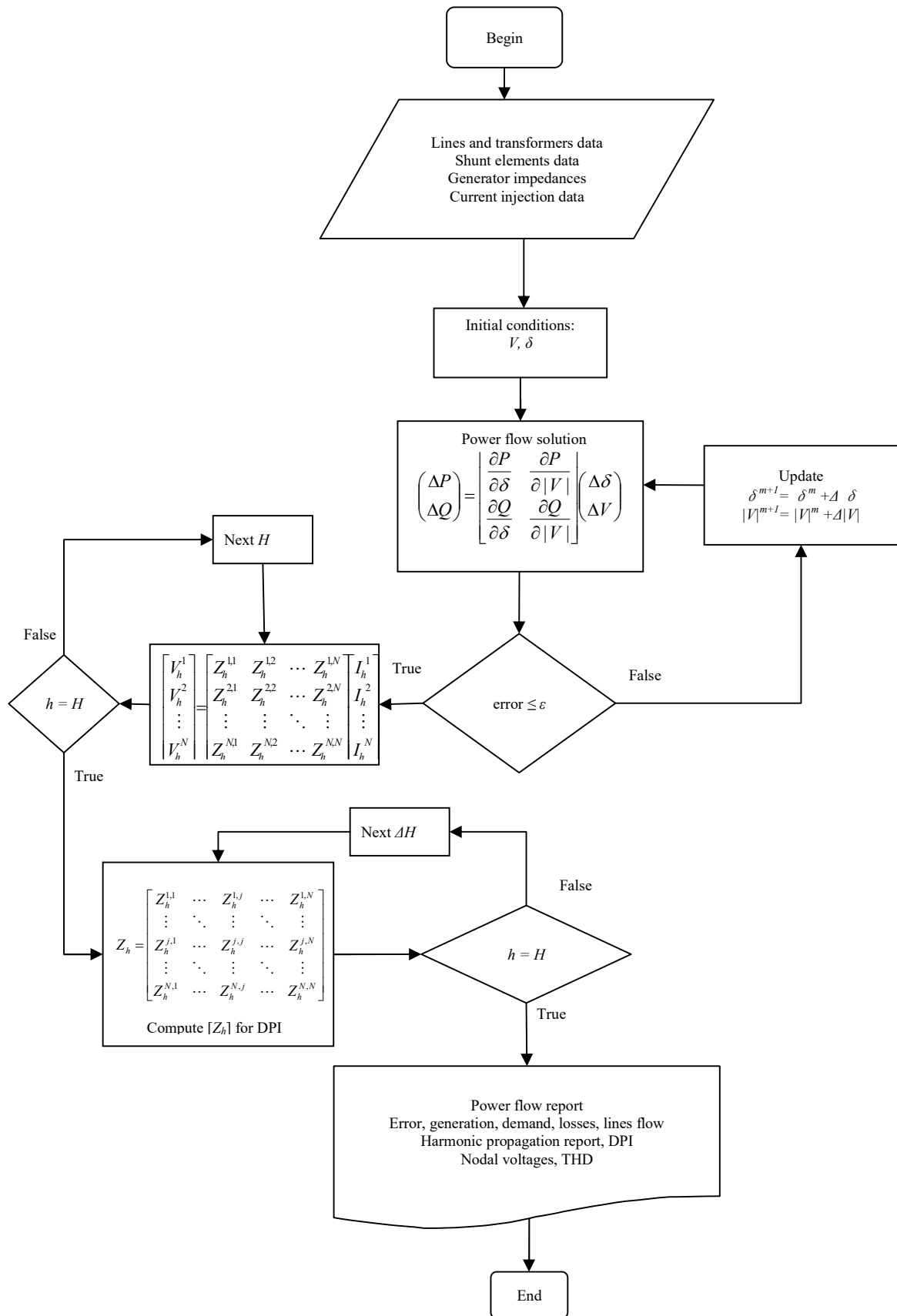
Figure 4.12. Diagram of power flow and harmonic propagation algorithm.

4.5.1 5 -bus network

A test system of the 5-bus network will be used to probe the algorithm. Figure 4.13 shows the 5-bus network used.
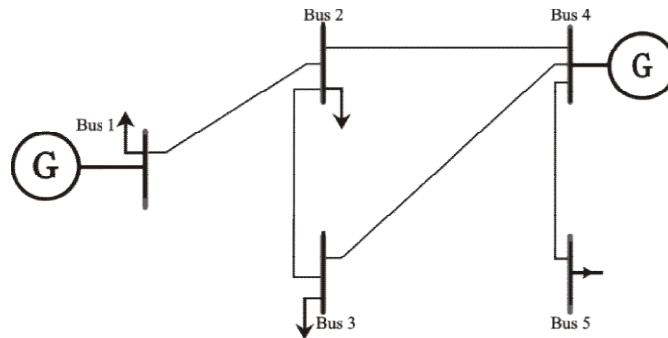
Figure 4.13. 5-Bus example.

Table 4.3 shows the number of lines, transformers, generation and load nodes, elements in derivation, load nodes with harmonics injected, and harmonics to be considered. Table 4.4 shows nodes with shunt elements and the impedance of the generators. Table 4.5 shows the current injection data, nodes with injected harmonics, and the percentage of injected harmonics in each node.

TABLE 4.3. INPUT DATA TO CALCULATE POWER FLOW AND HARMONIC PROPAGATION, REQUESTED NUMBER OF NODES AND ALL THE NETWORK CONNECTIONS.

Type of nodes and load					
nl: number of lines and transformers	5				
ng: generation nodes	2				
nc: load nodes	3				
ned: number of elements in derivation	0				
ni: load nodes with harmonics injected	2				
na: number of harmonics to be considered	6				
H: highest harmonic	50				
dH: increase of *h* for DPI frequency response	0.1				
Lines and transformers data					
tn: node type, S: slack, V: voltage, C: load	S	C	C	V	C
Pm: load model CIGRE, U-1 D-2 T-3	U	U	U	U	U
Pg: generation active power	0	0	0	0.8	0
Qg: generation reactive power	0	0	0	0	0
Pd: demand active power	0	0.45	0.51	0	.3
Qd: demand reactive power	0	.35	.4	0	.25
V: initial nodal voltages	1	1	1	1.01	1
D: angles of initial nodal voltages	0	0	0	0	0
Type of element L-line, T-transformer	L	L	L	L	L
n1: output node	1	2	3	2	4
n2: input node	2	3	4	4	5
rl: resistance between n1 and n2	.02	.04	.02	.04	.04
xl: inductance between n1 and n2	.04	.2	.04	.2	.2
b2l: susceptance between n1 and n2	.02	.02	.02	.02	.02
tap: taps of transformer	1	1	1	1	1

TABLE 4.4. REQUESTED NODES WITH SHUNT ELEMENTS AND GENERATOR IMPEDANCES.

Shunt elements data, RLC-series branch					
n10: connection nodes	-	-	-	-	-
shr: shunt resistance	-	-	-	-	-
shl: shunt inductive reactance, XL=wL	-	-	-	-	-
shc: shunt inductive reactance, Xc=1/wC	-	-	-	-	-
Generator impedances					
nng: generator node connection	1	4			
rg: generator resistance	.0001	.0001			
xg: generator sub-transient reactance	.001	.001			

TABLE 4.5. REQUESTED NODES WITH INJECTION OF HARMONICS.

Current injection data						
Nfi:	2	3				
Ari: injected harmonics	3	5	7	11	13	15
Mari: percentage of injected harmonics	1/3	-1/5	1/7	-1/11	1/13	-1/15
	1/15	1/5	1/7	1/9	1/11	1/13
Aari: angle of injected harmonic in degrees	0	0	0	0	0	0
	15	0	0	0	25	0

With data introduced, power flow results are shown in Figure 4.14. For each node, the following is calculated: voltage, active and reactive power generated, and active and reactive power demanded. Also, the number of iterations, errors, total power generated, total power demanded, and power losses including harmonics and only by harmonics is calculated.

Figure 4.14. Power flow for 5-Bus example.

Figure 4.15 shows the report of the power flow in each line.

Figure 4.15. Lines power flow report for 5-Bus example.

Figure 4.16 shows the harmonic propagation report, with voltage rms and THD for each node. There is a logarithm average of THD to determine the effect of the harmonics in the network.

Figure 4.16. Nodal voltages for 5-Bus example.

Figure 4.17 shows the harmonic voltages and angles for harmonics 3rd, 5th, 7th, 11th, 13th, and 25th.

3 Harmonic		5 Harmonic		7 Harmonic		11 Harmonic		13 Harmonic		25 Harmonic	
Vh	Ah	Vh	Ah	Vh	Ah	Vh	Ah	Vh	Ah	Vh	Ah
0.0004	-163.3371	0.0003	91.0765	0.0005	-21.514	0.0004	-49.958	0.0007	-166.199	0.0017	36.29
0.0182	-169.3463	0.0143	88.0044	0.0223	-23.3862	0.0158	-50.8081	0.0301	-166.7926	0.0693	36.3041
0.0075	-165.0049	0.0201	-97.2405	0.0273	-26.5068	0.0279	116.7299	0.0373	-154.3187	0.0811	-130.5628
0.0003	-162.3214	0.0004	-94.5622	0.0008	-24.6748	0.0006	115.9599	0.0011	-155.9035	0.0017	-127.8942
0.0003	-173.2475	0.0004	-113.7028	0.0008	-53.0917	0.0006	64.1484	0.0011	138.1819	0.0008	101.8952

Figure 4.17. Harmonic voltages for 5-Bus example.

Figure 4.18 shows the graphic of the DPI of the system. The DPI compares the magnitude of the impedance for each node.
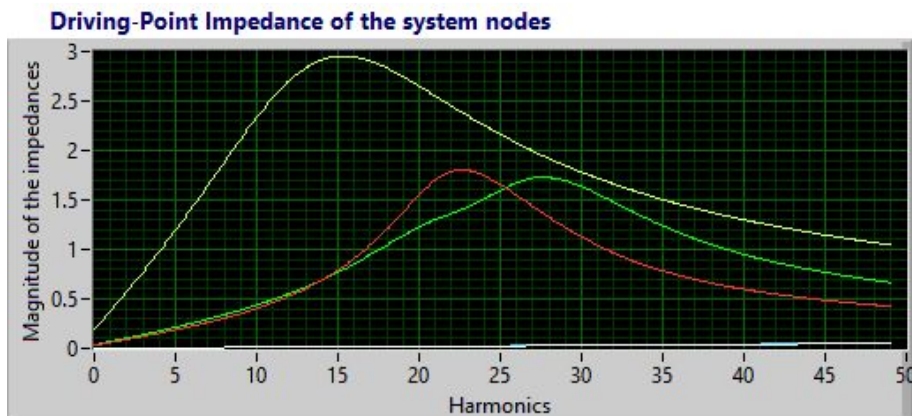
Figure 4.18. 5-Bus driving point impedance.

Figure 4.19 shows the harmonic voltage for each node. The graph is scaled to show the harmonics in detail, and this is the reason that the fundamental is not fully shown.
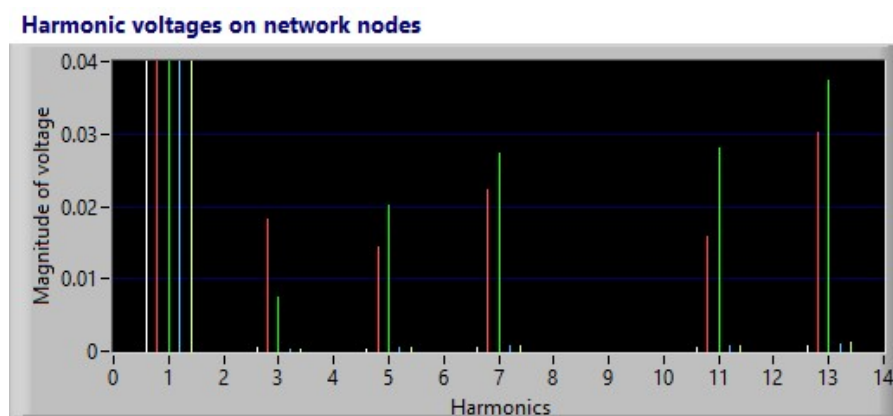
Figure 4.19. 5-Bus harmonic response.

4.5.2   30 -bus IEEE network

Figure 4.20 shows a network of the American Power Service Corporation, and this network, is known as the 30-Bus IEEE. This network data is used as the fundamental data of the algorithm.
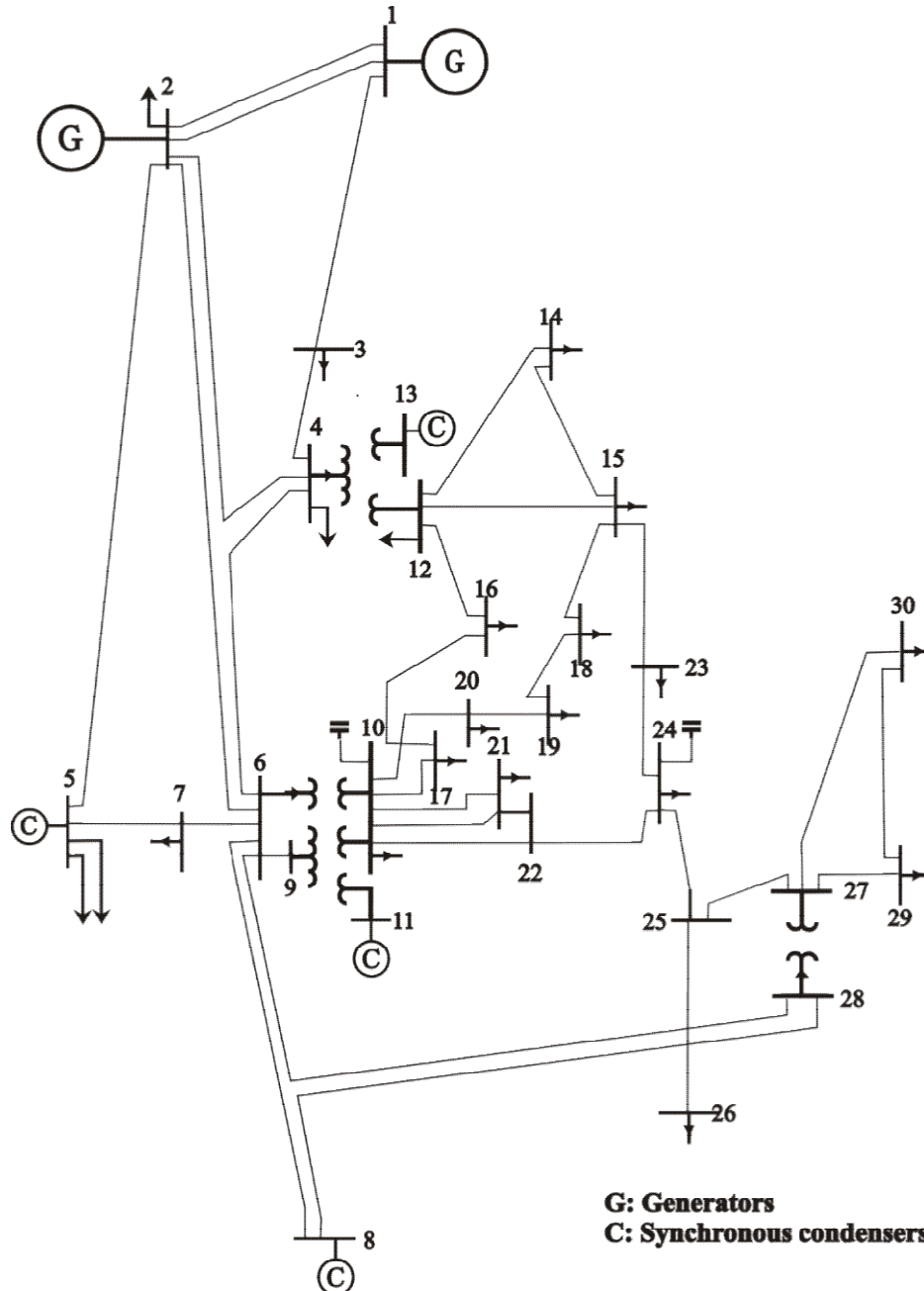
Figure 4.20. 30-Bus IEEE network.

Given below is the data network for the 30-bus IEEE. The base is 100 MW. The generation data is shown in Table 4.6. Table 4.7 shows the data of the reactive power of the capacitance bank. Voltages and loads of the network are shown in Table 4.8. Table 4.9 shows the data of the lines and transformers. Table 4.10 shows the data of the taps of transformers and Table 4.11 shows data of the harmonic current injection.

TABLE 4.6. GENERATION DATA

Node	P_g (MW)	V (pu)	X_g (pu)	R_g (pu)
1	0	1.06	0.001	0.0001
2	40	1.043	0.001	0.0001
5	0	1.010	0.001	0.0001
8	0	1.010	0.001	0.0001
11	0	1.082	0.001	0.0001
13	0	1.071	0.001	0.0001

TABLE 4.7. REACTIVE POWER OF CAPACITANCE BANK

N	MVAr	V (pu)
10	19	1.0
24	4.3	1.0

TABLE 4.8. NETWORK VOLTAGES AND LOADS

Node	Type	Magnitude	Angle	MW	MVAr
1	Slack	1.06	0	0	0
2	Voltage	1.043	0	21.7	12.7
3	Load	1	0	2.4	1.2
4	Load	1	0	7.6	1.6
5	Voltage	1.01	0	94.2	19
6	Load	1	0	0	0
7	Load	1	0	22.8	10.9
8	Voltage	1.01	0	30	30
9	Load	1	0	0	0
10	Load	1	0	5.8	2
11	Voltage	1.082	0	0	0
12	Load	1	0	11.2	7.5
13	Voltage	1.071	0	0	0
14	Load	1	0	6.2	1.6
15	Load	1	0	8.2	2.5
16	Load	1	0	3.5	1.8
17	Load	1	0	9	5.8
18	Load	1	0	3.2	0.9
19	Load	1	0	9.5	3.4
20	Load	1	0	2.2	0.7
21	Load	1	0	17.5	11.2
22	Load	1	0	0	0
23	Load	1	0	3.2	1.6
24	Load	1	0	8.7	6.7
25	Load	1	0	0	0
26	Load	1	0	3.5	2.3
27	Load	1	0	0	0
28	Load	1	0	0	0
29	Load	1	0	2.4	0.9
30	Load	1	0	10.6	1.9

TABLE 4.9. LINES AND TRANSFORMERS DATA

N1	N2	R	X	B/2
1	2	0.0192	0.0575	0.02640
1	3	0.0452	0.1852	0.02040
2	4	0.0570	0.1737	0.01840
3	4	0.0132	0.0379	0.00420
2	5	0.0472	0.1983	0.02090
2	6	0.0581	0.1763	0.01870
4	6	0.0119	0.0414	0.00450
5	7	0.0460	0.1160	0.01020
6	7	0.0267	0.0820	0.00850
6	8	0.0120	0.0420	0.00450
6	9	0	0.2080	0
6	10	0	0.5560	0
9	11	0	0.2080	0
9	10	0	0.1100	0
4	12	0	0.2560	0
12	13	0	0.1400	0
12	14	0.1231	0.2559	0
12	15	0.0662	0.1304	0
12	16	0.0945	0.1987	0
14	15	0.2210	0.1997	0
16	17	0.0824	0.1923	0
15	18	0.1073	0.2185	0
18	19	0.0639	0.1292	0
19	20	0.0340	0.0680	0
10	20	0.0936	0.2090	0
10	17	0.0324	0.0845	0
10	21	0.0348	0.0749	0
10	22	0.0727	0.1499	0
21	22	0.0116	0.0236	0
15	23	0.1000	0.2020	0
22	24	0.1150	0.1790	0
23	24	0.1320	0.2700	0
24	25	0.1885	0.3292	0
25	26	0.2544	0.3800	0
25	27	0.1093	0.2087	0
27	28	0	0.3960	0
27	29	0.2198	0.4153	0
27	30	0.3202	0.6027	0
29	30	0.2399	0.4533	0
8	28	0.0636	0.2000	0.0214
6	28	0.0169	0.0599	0.065

TABLE 4.10. TAPS OF TRANSFORMERS

Connection Nodes	Tap (pu)
6-9	0.978
6-10	0.969
9-11	1
9-10	1
4-12	0.932
12-13	1
28-27	0.968

TABLE 4.11. HARMONIC CURRENT INJECTION DATA

	Node 14		Node 15		Node 30	
Harmonic	Magnitude %	Angle (grades)	Magnitude %	Angle (grades)	Magnitude %	Angle (grades)
3	20%	15	0%	-15	0%	30
5	15%	25	25%	45	17%	45
7	10%	-40	18%	10	12%	18
11	4%	20	10%	65	9%	-32
13	0%	0	7%	-12	6%	18
17	0%	0	0%	0	5%	14
19	0%	0	0%	0	2%	10

The algorithm calculates harmonic propagation and power flow and generates the report of results.

*** Results ***
Number of lines and Transformers: 41
Generation Nodes: 6
Load Nodes: 24
Total Nodes: 30
Number of elements in derivation: 2
Load nodes with harmonics injected: 3
Number of harmonics to be considered: 7
Processing time of Power Flow and Harmonic Propagation Study: 0.083000 seconds

Table 4.12 shows the power flow report. For each node, the final voltage and angle, active and reactive power for demand, and active and reactive power for generation are shown.

TABLE 4.12. POWER FLOW REPORT

	Final Voltage, Vf	Final Angle, Af	Demand Active Power Pd	Demand Reactive Power Qd	Generation Active Power Pg	Generation Reactive Power Qg
1	1.0600	0.0000	0.0000	0.0000	0.0134	0.3744
2	1.0430	0.2704	0.2170	0.1270	0.2170	0.0342
3	1.0394	0.2685	0.0240	0.0120	0.0240	0.0120
4	1.0343	0.3678	0.0760	0.0160	0.0760	0.0160
5	1.0100	0.7616	0.9420	0.1900	0.9420	-0.1152
6	1.0293	0.4298	0.0000	0.0000	0.0000	0.0000
7	1.0222	0.5292	0.2280	0.1090	0.2280	0.1090
8	1.0100	0.7412	0.3000	0.3000	0.3000	-0.3010
9	1.0813	0.3902	0.0000	0.0000	0.0000	0.0000
10	1.0959	0.3700	0.0580	0.0200	0.0580	0.0200

11	1.0820	0.3902	0.0000	0.0000	0.0000	0.0038
12	1.0926	0.3838	0.1120	0.0750	0.1120	0.0750
13	1.0710	0.3838	0.0000	0.0000	0.0000	-0.1649
14	1.0958	0.3278	0.0620	0.0160	0.0620	0.0160
15	1.0985	0.2073	0.0820	0.0250	0.0820	0.0250
16	1.0939	0.3758	0.0350	0.0180	0.0350	0.0180
17	1.0953	0.3709	0.0900	0.0580	0.0900	0.0580
18	1.0976	0.2649	0.0320	0.0090	0.0320	0.0090
19	1.0970	0.2991	0.0950	0.0340	0.0950	0.0340
20	1.0967	0.3173	0.0220	0.0070	0.0220	0.0070
21	1.1019	0.2198	0.1750	0.1120	0.1750	0.1120
22	1.1038	0.1701	0.0000	0.0000	0.0000	0.0000
23	1.1110	-0.1531	0.0320	0.0160	0.0320	0.0160
24	1.1278	-0.6169	0.0870	0.0670	0.0870	0.0670
25	1.1065	0.0006	0.0000	0.0000	0.0000	0.0000
26	1.1065	0.0006	0.0350	0.0230	0.0350	0.0230
27	1.0930	0.3699	0.0000	0.0000	0.0000	0.0000
28	1.0320	0.3761	0.0000	0.0000	0.0000	0.0000
29	1.0930	0.3699	0.0240	0.0090	0.0240	0.0090
30	1.0930	0.3699	0.1060	0.0190	0.1060	0.0190

Table 4.13 shows the nodal report that demonstrates for each line, the complex current flow from node 1 to node 2 and the complex current flow from node 2 to node 1.

Number of iterations: 4
Error: 1.993842E-7
Generation: 2.847384 p.u.
Demand: 2.834000 p.u.
Power Losses without harmonics: 0.013384 p.u.
Power Losses with harmonics: 0.0227 p.u.
Power Losses by harmonics: 0.0093 p.u.

<div align="center">

TABLE 4.13. LINES POWER FLOW REPORT

</div>

N1 - N2	Flow 1 -2 (P, Q)		Flow 2 – 1 (P, Q)	
1 - 2	0.013	0.280	-0.011	-0.333
1 - 3	0.001	0.095	-0.000	-0.137
2 - 4	0.006	0.031	-0.006	-0.070
3 - 4	0.000	0.137	0.000	-0.146
2 - 5	-0.004	0.152	0.005	-0.190
2 - 6	0.009	0.058	-0.009	-0.097
4 - 6	0.007	0.117	-0.007	-0.126
5 - 7	-0.005	-0.115	0.006	0.095
6 - 7	0.006	0.078	-0.006	-0.095
6 - 8	0.001	0.468	0.002	-0.469
6 - 9	0.004	-0.257	-0.004	0.270
6 - 10	0.002	-0.123	-0.002	0.131
9 - 11	0.000	-0.004	0.000	0.004
9 - 10	0.004	-0.143	-0.004	0.145
4 - 12	-0.001	-0.236	0.001	0.249
12 - 13	0.000	0.168	0.000	-0.165

12 - 14	-0.002	-0.013	0.002	0.013
12 - 15	0.003	-0.051	-0.002	0.051
12 - 16	-0.002	-0.007	0.002	0.007
14 - 15	-0.002	-0.013	0.002	0.013
16 - 17	-0.002	-0.007	0.002	0.007
15 - 18	-0.003	0.006	0.003	-0.006
18 - 19	-0.003	0.006	0.003	-0.006
19 - 20	-0.003	0.006	0.003	-0.006
10 - 20	0.003	-0.006	-0.003	0.006
10 - 17	0.002	0.007	-0.002	-0.007
10 - 21	0.001	-0.089	-0.001	0.089
10 - 22	0.000	-0.058	0.000	0.058
21 - 22	0.001	-0.089	-0.001	0.089
15 - 23	0.003	-0.070	-0.003	0.071
22 - 24	0.000	-0.148	0.002	0.151
23 - 24	0.003	-0.071	-0.003	0.072
24 - 25	0.001	0.073	-0.000	-0.072
25 - 26	0.000	0.000	0.000	0.000
25 - 27	0.000	0.072	0.000	-0.071
28 - 27	0.000	-0.159	-0.000	0.168
27 - 29	0.000	0.000	0.000	0.000
27 - 30	0.000	0.000	0.000	0.000
29 - 30	0.000	0.000	0.000	0.000
8 - 28	-0.002	-0.132	0.003	0.090
6 - 28	0.003	-0.117	-0.003	-0.021

The harmonic propagation report is shown in Table 4.14. It shows the voltage and current in each node, the voltage rms and the THD. Furthermore, the harmonic voltage and angle for each harmonic calculated, and 3rd, 5th, 7th, 11th, 13th, 17th, and 19th are shown.

TABLE 4.14. HARMONIC PROPAGATION REPORT

Nodal Voltages ----- Harmonic Voltages Magnitude --- Harmonic Voltage Angle

	V	A	Vrms	THD	1	3	5	7	11	13	17	19	1	3	5	7	11	13	17	19
1	1.060	0.000	1.060	0.003	1.060	0.000	0.000	0.000	0.000	0.000	0.000	0.000	0.000	125.820	89.246	166.897	173.954	-157.421	72.226	90.627
2	1.043	0.270	1.043	0.008	1.043	0.000	0.000	0.000	0.000	0.000	0.000	0.000	0.270	125.233	86.569	159.626	157.710	-157.647	76.136	93.308
3	1.039	0.268	1.039	0.588	1.039	0.000	0.002	0.001	0.000	0.005	0.002	0.001	0.268	124.447	89.103	167.327	175.688	-156.885	72.678	91.147
4	1.034	0.368	1.034	0.626	1.034	0.001	0.002	0.001	0.000	0.006	0.002	0.001	0.368	124.306	89.199	167.565	176.109	-156.396	73.305	91.857
5	1.010	0.762	1.010	0.004	1.010	0.000	0.000	0.000	0.000	0.000	0.000	0.000	0.762	120.580	79.987	144.667	146.564	-163.860	73.735	89.577
6	1.029	0.430	1.029	0.767	1.029	0.000	0.003	0.001	0.001	0.007	0.002	0.000	0.430	119.537	82.184	148.389	151.860	-158.206	79.891	95.976
7	1.022	0.529	1.022	0.491	1.022	0.000	0.002	0.000	0.001	0.005	0.001	0.000	0.529	116.598	78.358	143.880	146.638	-163.601	74.199	90.072
8	1.010	0.741	1.010	0.027	1.010	0.000	0.000	0.000	0.000	0.000	0.000	0.000	0.741	120.601	86.214	146.560	149.370	-158.445	87.843	99.571
9	1.081	0.390	1.081	0.920	1.081	0.001	0.009	0.001	0.001	0.004	0.002	0.000	0.390	122.304	68.328	19.549	-69.924	-156.073	21.856	-39.872
10	1.096	0.370	1.096	1.635	1.096	0.002	0.017	0.001	0.002	0.004	0.004	0.001	0.370	122.579	67.174	6.588	-56.901	-154.211	12.357	-52.117
11	1.082	0.390	1.082	0.004	1.082	0.000	0.000	0.000	0.000	0.000	0.000	0.000	0.390	119.016	65.780	17.395	-71.643	-157.654	20.473	-41.180
12	1.093	0.384	1.093	0.860	1.093	0.003	0.006	0.004	0.004	0.003	0.001	0.000	0.384	133.571	114.065	-169.690	-45.000	-106.000	26.699	16.820
13	1.071	0.384	1.071	0.006	1.071	0.000	0.000	0.000	0.000	0.000	0.000	0.000	0.384	130.290	111.522	-171.839	-46.715	-107.577	25.320	15.515
14	1.096	0.328	1.096	1.808	1.096	0.008	0.011	0.010	0.009	0.005	0.001	0.000	0.328	131.741	140.601	175.352	-56.095	-89.714	18.885	-10.813
15	1.098	0.207	1.099	1.631	1.098	0.004	0.009	0.009	0.009	0.007	0.001	0.000	0.207	130.938	121.071	-160.654	-37.358	-80.383	17.206	-25.428
16	1.094	0.376	1.094	1.007	1.094	0.002	0.009	0.002	0.003	0.003	0.002	0.000	0.376	128.770	79.476	-169.374	-49.869	-131.834	12.784	-48.879

17 1.095	0.371	1.095	1.408	1.095	0.002	0.014	0.000	0.002	0.004	0.003	0.001	0.371	123.976	68.361	-2.321	-55.598	-150.512	10.775	-53.229
18 1.098	0.265	1.098	1.322	1.098	0.004	0.010	0.005	0.006	0.004	0.002	0.000	0.265	126.084	89.399	-163.283	-43.657	-101.635	7.830	-53.915
19 1.097	0.299	1.097	1.307	1.097	0.003	0.012	0.003	0.005	0.004	0.002	0.000	0.299	123.263	76.815	-165.076	-48.830	-121.089	6.791	-56.112
20 1.097	0.317	1.097	1.356	1.097	0.003	0.013	0.002	0.004	0.004	0.003	0.001	0.317	122.950	73.433	-163.967	-50.182	-130.404	8.391	-54.967
21 1.102	0.220	1.102	2.063	1.102	0.002	0.022	0.003	0.002	0.003	0.003	0.001	0.220	120.375	65.062	6.360	-56.939	-158.808	10.896	-53.696
22 1.104	0.170	1.104	2.220	1.104	0.002	0.024	0.004	0.001	0.003	0.003	0.001	0.170	120.350	65.423	7.262	-55.515	-159.575	11.661	-53.048
23 1.111	-0.153	1.111	2.182	1.111	0.004	0.023	0.001	0.005	0.003	0.000	0.000	-0.153	125.439	74.998	-119.944	-37.267	-70.236	32.144	63.334
24 1.128	-0.617	1.129	4.213	1.128	0.003	0.046	0.010	0.000	0.002	0.000	0.000	-0.617	117.739	65.130	8.553	14.990	44.137	138.319	111.094
25 1.106	0.001	1.107	3.250	1.106	0.002	0.031	0.006	0.010	0.011	0.006	0.003	0.001	114.405	82.602	114.669	145.635	-152.303	-101.249	-79.103
26 1.106	0.001	1.107	3.149	1.106	0.002	0.031	0.006	0.010	0.010	0.006	0.002	0.001	112.512	79.810	111.256	141.713	-156.239	-104.988	-82.694
27 1.093	0.370	1.094	3.688	1.093	0.002	0.026	0.013	0.018	0.019	0.010	0.005	0.370	111.403	104.516	144.150	147.543	-150.041	-98.978	-77.782
28 1.032	0.376	1.032	1.829	1.032	0.000	0.005	0.002	0.005	0.017	0.002	0.001	0.376	114.159	93.777	143.316	146.944	-157.800	115.140	115.006
29 1.093	0.370	1.095	5.466	1.093	0.002	0.033	0.025	0.028	0.026	0.019	0.008	0.370	104.159	119.606	147.794	146.447	-148.220	-98.215	-78.468
30 1.093	0.370	1.096	7.781	1.093	0.002	0.043	0.038	0.042	0.035	0.030	0.013	0.370	99.055	131.948	151.725	148.817	-144.071	-95.461	-76.389

With the THD of each node, a logarithm average that is 7.6328% is calculated.

In Figure 4.21, the DPI of the system is shown. Figure 4.22 shows the harmonic voltage for each node including the fundamental and Figure 4.23 shows only scaled harmonic voltages.
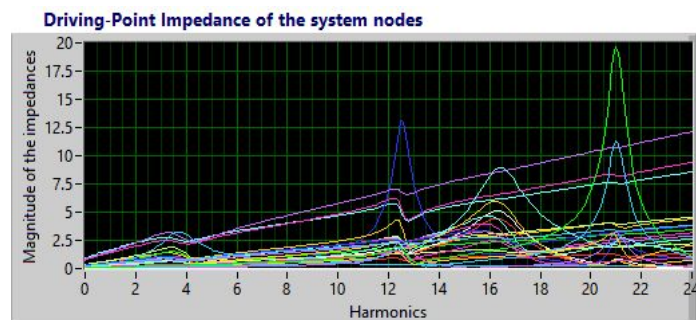
Figure 4.21. 30-Bus IEEE DPI.
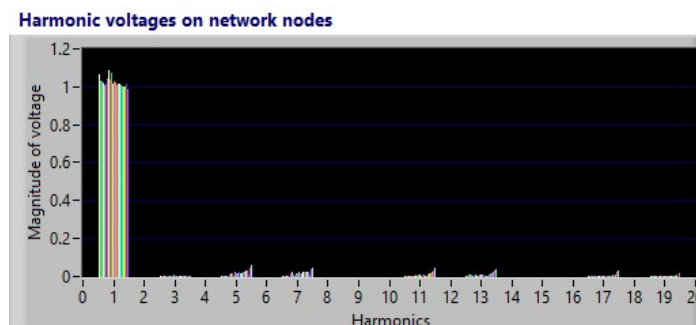
Figure 4.22. 30-Bus IEEE harmonic voltages on network nodes including fundamental.
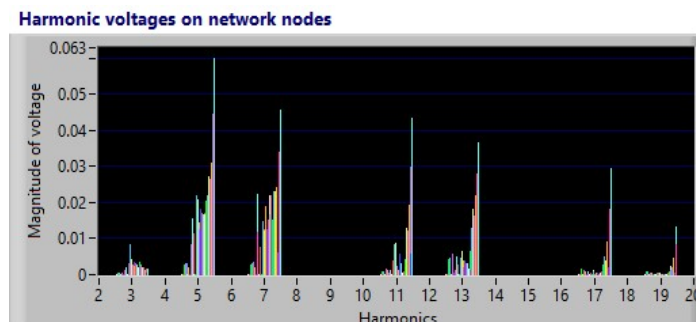
Figure 4.23. 30-Bus IEEE harmonic voltages on network nodes.

4.5.3   33 -bus network with three Wind Turbines

Figure 4.24 shows a network modified from the 30-bus of IEEE to include three non-linear loads to represent wind turbines, each of 10 MW, and this network is used to connect all the nodes generated by the algorithm. With the three wind turbines, the entire network is affected, mainly around nodes 14, 15, and 30. The power generation and demand is increased, but power losses are increased too, mainly due to resonances caused by the 15th harmonic generated by the three new nodes.
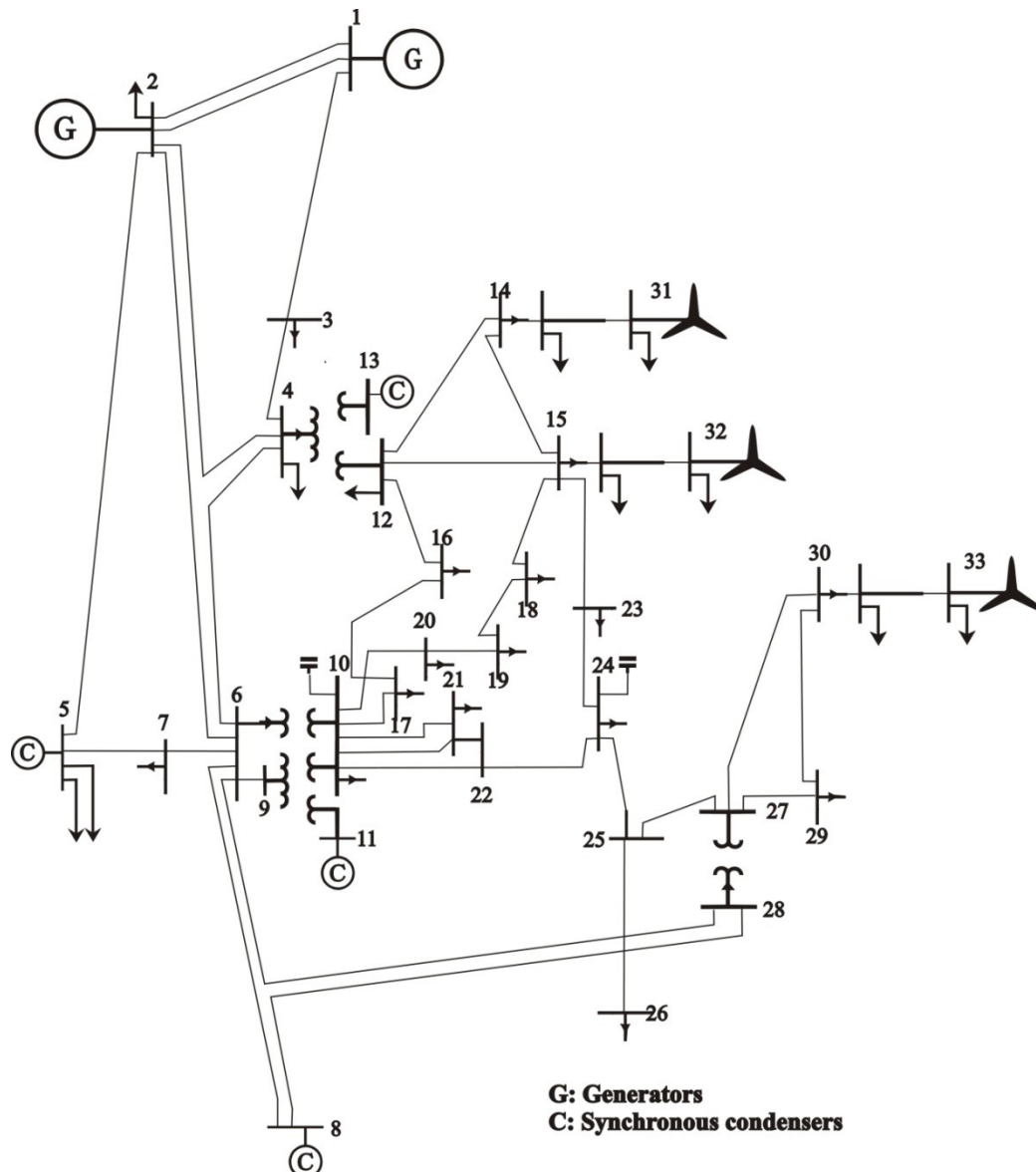
Figure 4.24. IEEE 30-Bus network with three wind turbines.

All data network and the complete report are shown in Appendix H, Section H.1. Given below are the power flow report, nodal report, and harmonic propagation report generated by the algorithm.

Table 4.15 shows the power flow report. For each node, the final voltage and angle, active and reactive power for demand, and active and reactive power for generation are shown.

TABLE 4.15. POWER FLOW REPORT FOR IEEE 30-BUS NETWORK WITH THREE WIND TURBINES

	Final Voltage, Vf	Final Angle, Af	Demand Active Power Pd	Demand Reactive Power Qd	Generation Active Power Pg	Generation Reactive Power Qg
1	1.0600	0.0000	0.0000	0.0000	2.7178	-0.1640
2	1.0430	-5.7406	0.2170	0.1270	0.4000	0.5697
3	1.0167	-8.3051	0.0240	0.0120	0.0000	0.0000
4	1.0072	-10.0330	0.0760	0.0160	0.0000	0.0000
5	1.0100	-14.8209	0.9420	0.1900	0.0000	0.3871
6	1.0068	-11.9180	0.0000	0.0000	0.0000	0.0000
7	1.0003	-13.6390	0.2280	0.1090	0.0000	0.0000
8	1.0100	-12.7126	0.3000	0.3000	0.0000	0.4551
9	1.0308	-15.9065	0.0000	0.0000	0.0000	0.0000
10	1.0062	-18.0632	0.0580	0.0200	0.0000	0.0000
11	1.0820	-15.9065	0.0000	0.0000	0.0000	0.2662
12	1.0427	-15.7777	0.1120	0.0750	0.0000	0.0000
13	1.0710	-15.7777	0.0000	0.0000	0.0000	0.2165
14	1.0184	-15.5009	0.0620	0.0160	0.0000	0.0000
15	1.0140	-16.4226	0.0820	0.0250	0.0000	0.0000
16	1.0193	-16.9968	0.0350	0.0180	0.0000	0.0000
17	1.0045	-17.9545	0.0900	0.0580	0.0000	0.0000
18	0.9985	-17.7272	0.0320	0.0090	0.0000	0.0000
19	0.9926	-18.3091	0.0950	0.0340	0.0000	0.0000
20	0.9951	-18.3086	0.0220	0.0070	0.0000	0.0000
21	0.9779	-18.8932	0.1750	0.1120	0.0000	0.0000
22	0.9736	-18.9843	0.3500	0.2500	0.0000	0.0000
23	0.9961	-17.3943	0.0320	0.0160	0.0000	0.0000
24	0.9812	-18.3574	0.0870	0.0670	0.0000	0.0000
25	0.9995	-16.9780	0.0000	0.0000	0.0000	0.0000
26	0.9815	-17.4131	0.0350	0.0230	0.0000	0.0000
27	1.0195	-15.8592	0.0000	0.0000	0.0000	0.0000
28	1.0067	-12.5245	0.0000	0.0000	0.0000	0.0000
29	1.0110	-16.3129	0.0240	0.0090	0.0000	0.0000
30	1.0115	-16.3235	0.1060	0.0190	0.0000	0.0000
31	1.0100	-15.0438	0.0100	0.0075	0.1000	-0.2254
32	1.0100	-16.0333	0.0100	0.0075	0.1000	-0.1515
33	1.0100	-15.9733	0.0100	0.0075	0.1000	-0.1092

Table 4.16 shows the nodal report that shows, for each line, the complex current flow from node 1 to node 2 and the complex current flow from node 2 to node 1. There is an increase of power losses, 0.203821 p.u.

TABLE 4.16. LINES POWER FLOW REPORT FOR IEEE 30-BUS NETWORK WITH THREE WIND TURBINES

N1 - N2	Flow 1 -2 (P, Q)		Flow 2 – 1 (P, Q)	
1 - 2	1.853	-0.239	-1.794	0.358
1 - 3	0.864	0.075	-0.834	0.006
2 - 4	0.477	0.055	-0.465	-0.057
3 - 4	0.810	-0.018	-0.802	0.033
2 - 5	0.848	0.016	-0.816	0.071
2 - 6	0.652	0.013	-0.629	0.016
4 - 6	0.750	-0.198	-0.743	0.213
5 - 7	-0.126	0.126	0.127	-0.142
6 - 7	0.359	-0.040	-0.355	0.033
6 - 8	0.291	-0.162	-0.290	0.157
6 - 9	0.347	-0.104	-0.347	0.131
6 - 10	0.195	0.012	-0.195	0.009
9 - 11	0.000	-0.254	0.000	0.266
9 - 10	0.355	0.237	-0.355	-0.218
4 - 12	0.411	-0.119	-0.411	0.165
12 - 13	0.000	-0.211	0.000	0.217
12 - 14	0.022	0.088	-0.021	-0.086
12 - 15	0.165	0.146	-0.162	-0.140
12 - 16	0.141	0.057	-0.139	-0.053
14 - 15	0.049	-0.031	-0.048	0.032
16 - 17	0.104	0.035	-0.103	-0.032
15 - 18	0.114	0.017	-0.113	-0.015
18 - 19	0.081	0.006	-0.080	-0.005
19 - 20	-0.015	-0.029	0.015	0.029
10 - 20	0.037	0.037	-0.037	-0.036
10 - 17	-0.013	0.026	0.013	-0.026
10 - 21	0.303	0.242	-0.297	-0.230
10 - 22	0.171	0.137	-0.168	-0.130
21 - 22	0.122	0.118	-0.122	-0.118
15 - 23	0.104	0.039	-0.103	-0.037
22 - 24	-0.060	-0.002	0.060	0.003
23 - 24	0.071	0.021	-0.070	-0.019
24 - 25	-0.077	-0.009	0.078	0.012
25 - 26	0.035	0.024	-0.035	-0.023
25 - 27	-0.114	-0.035	0.115	0.038
28 - 27	0.151	-0.028	-0.151	0.037
27 - 29	0.024	0.008	-0.024	-0.008
27 - 30	0.016	0.005	-0.016	-0.005
29 - 30	-0.000	-0.001	0.000	0.001
8 - 28	-0.010	-0.002	0.010	-0.042
6 - 28	0.167	-0.110	-0.166	-0.020
14 - 31	-0.089	0.101	0.090	-0.233
15 - 32	-0.090	0.027	0.090	-0.159
30 - 33	-0.090	-0.015	0.090	-0.117

The harmonic propagation report is shown in Table 4.17. It shows the voltage and current in each node, the voltage rms, and the THD. Also, the harmonic voltage and angle for each harmonic calculated, 3rd, 5th, 7th, 11th, 13th, and 17th are shown.

TABLE 4.17. HARMONIC PROPAGATION REPORT FOR IEEE 30-BUS NETWORK WITH THREE WIND TURBINES

Nodal Voltages ----- Harmonic Voltages Magnitude --- Harmonic Voltage Angle

	V	A	Vrms	THD	1	3	5	7	11	13	17	1	3	5	7	11	13	17
1	1.060	0.000	1.060	0.000	1.060	0.000	0.000	0.000	0.000	0.000	0.000	0.000	174.449	15.789	-63.816	148.470	159.762	-63.153
2	1.043	-5.741	1.043	0.000	1.043	0.000	0.000	0.000	0.000	0.000	0.000	-5.741	172.536	11.072	-70.667	147.022	171.230	-45.622
3	1.017	-8.305	1.017	0.003	1.017	0.000	0.000	0.000	0.000	0.000	0.000	-8.305	174.267	16.139	-63.140	149.052	159.788	-63.065
4	1.007	-10.033	1.007	0.003	1.007	0.000	0.001	0.000	0.000	0.000	0.000	-10.033	174.373	16.390	-62.705	149.556	160.359	-62.422
5	1.010	-14.821	1.010	0.000	1.010	0.000	0.000	0.000	0.000	0.000	0.000	-14.821	165.451	0.451	-89.645	139.189	172.468	-28.377
6	1.007	-11.918	1.007	0.003	1.007	0.000	0.000	0.000	0.000	0.000	0.000	-11.918	167.778	4.413	-84.333	145.024	178.635	-21.819
7	1.000	-13.639	1.000	0.002	1.000	0.000	0.000	0.000	0.000	0.000	0.000	-13.639	163.803	-0.274	-89.754	139.427	172.897	-27.714
8	1.010	-12.713	1.010	0.000	1.010	0.000	0.000	0.000	0.000	0.000	0.000	-12.713	169.730	7.063	-77.237	144.908	-176.895	-10.741
9	1.031	-15.906	1.031	0.002	1.031	0.000	0.000	0.000	0.000	0.000	0.000	-15.906	158.795	-11.824	147.582	-16.850	122.475	-28.644
10	1.006	-18.063	1.006	0.005	1.006	0.000	0.000	0.000	0.000	0.000	0.000	-18.063	157.907	-13.176	145.187	-22.653	98.464	162.598
11	1.082	-15.906	1.082	0.000	1.082	0.000	0.000	0.000	0.000	0.000	0.000	-15.906	156.247	-13.978	145.863	-18.431	121.003	-30.027
12	1.043	-15.778	1.043	0.011	1.043	0.000	0.000	0.000	0.000	0.000	0.000	-15.778	-173.609	39.163	-44.789	174.077	35.031	-105.222
13	1.071	-15.778	1.071	0.000	1.071	0.000	0.000	0.000	0.000	0.000	0.000	-15.778	-176.152	37.014	-46.503	172.500	33.562	-106.601
14	1.018	-15.501	1.018	0.031	1.018	0.000	0.000	0.000	0.000	0.000	0.000	-15.501	-167.848	53.455	-38.805	-178.787	39.420	-105.226
15	1.014	-16.423	1.014	0.020	1.014	0.000	0.000	0.000	0.000	0.000	0.000	-16.423	-173.398	43.703	-45.861	172.387	25.678	-105.831
16	1.019	-16.997	1.019	0.006	1.019	0.000	0.000	0.000	0.000	0.000	0.000	-16.997	172.329	8.244	-75.197	-155.468	48.486	-109.576
17	1.005	-17.954	1.005	0.004	1.005	0.000	0.000	0.000	0.000	0.000	0.000	-17.954	160.695	-10.085	144.960	-29.475	78.859	-126.367
18	0.998	-17.727	0.998	0.012	0.998	0.000	0.000	0.000	0.000	0.000	0.000	-17.727	174.882	20.388	-53.098	173.878	28.196	-111.031
19	0.993	-18.309	0.993	0.008	0.993	0.000	0.000	0.000	0.000	0.000	0.000	-18.309	167.215	5.039	-78.371	-174.909	34.449	-116.450
20	0.995	-18.309	0.995	0.006	0.995	0.000	0.000	0.000	0.000	0.000	0.000	-18.309	164.939	-0.340	-165.110	-101.119	43.790	-118.742
21	0.978	-18.893	0.978	0.004	0.978	0.000	0.000	0.000	0.000	0.000	0.000	-18.893	154.685	-16.560	145.576	-8.950	-110.814	60.097
22	0.974	-18.984	0.974	0.005	0.974	0.000	0.000	0.000	0.000	0.000	0.000	-18.984	154.845	-16.248	147.800	12.338	-101.978	56.861
23	0.996	-17.394	0.996	0.010	0.996	0.000	0.000	0.000	0.000	0.000	0.000	-17.394	178.013	25.095	-54.755	154.521	-57.190	-86.497
24	0.981	-18.357	0.981	0.021	0.981	0.000	0.000	0.000	0.000	0.000	0.000	-18.357	165.656	1.062	-80.858	136.642	-91.015	54.496
25	0.999	-16.978	0.999	0.013	0.999	0.000	0.000	0.000	0.000	0.000	0.000	-16.978	173.580	16.120	-63.894	144.880	-78.077	124.513
26	0.981	-17.413	0.981	0.012	0.981	0.000	0.000	0.000	0.000	0.000	0.000	-17.413	170.052	11.824	-68.797	139.974	-82.880	119.872
27	1.019	-15.859	1.019	0.016	1.019	0.000	0.000	0.000	0.000	0.000	0.000	-15.859	-179.307	30.388	-56.463	152.341	-39.739	159.663
28	1.007	-12.524	1.007	0.007	1.007	0.000	0.000	0.000	0.000	0.000	0.000	-12.524	172.771	14.882	-67.321	145.718	-167.333	17.066
29	1.011	-16.313	1.011	0.028	1.011	0.000	0.000	0.000	0.000	0.000	0.000	-16.313	-176.964	38.725	-54.420	157.469	2.817	168.465
30	1.012	-16.323	1.012	0.046	1.012	0.000	0.000	0.000	0.000	0.000	0.000	-16.323	-172.525	47.489	-49.870	165.414	18.349	174.272
31	1.010	-15.044	1.010	0.010	1.010	0.000	0.000	0.000	0.000	0.000	0.000	-15.044	-163.651	60.240	-32.149	-168.852	53.913	-87.234
32	1.010	-16.033	1.010	0.010	1.010	0.000	0.000	0.000	0.000	0.000	0.000	-16.033	-168.606	53.236	-42.743	178.739	39.775	-98.946
33	1.010	-15.973	1.010	0.010	1.010	0.000	0.000	0.000	0.000	0.000	0.000	-15.973	-168.315	53.729	-42.512	178.407	38.491	-126.265

With the THD of each node, a logarithm average of harmonic distortion that is 0.0107% is calculated.

In Figure 4.25, the DPI of the system is shown, and Figure 4.26 shows the harmonic voltage for each node including fundamental frequency. Adding three wind turbines appears the 15th harmonics that causes resonances in the network, increasing the power losses.
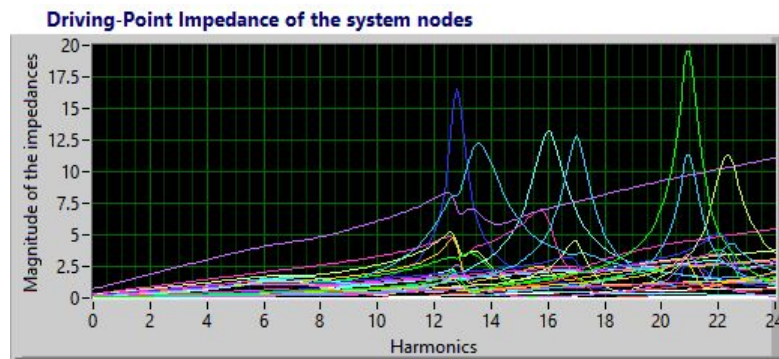
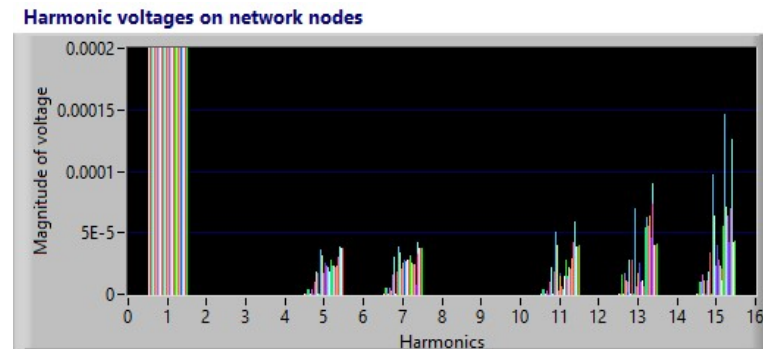**Figure 4.25. 30-Bus IEEE with three wind turbines DPI.**

Figure 4.26. Harmonic voltages on nodes of the 30-Bus IEEE with three wind turbines network.

4.6 Summary

A brief description of harmonics was presented. Furthermore, the international standards to mitigate harmonic effects help to understand and provide a basis of the solution to the problem accurately. Power flow at fundamental frequency, based on the Newton-Raphson method, and the current injection method were presented, and also, the frequency response of linear elements was introduced.

The algorithm can be modified to include different elements as the wind power clusters, and the algorithm can be implemented in any computer language. A network modified, where three wind turbines of 10 MW are included, is affected in the all the nodes, mainly around the nodes where the wind power clusters are connected. Depending of he connection, could appear some resonances generated by the harmonics generated.

Algorithms will be developed and programmed to obtain power flow and harmonic propagation. Additionally, data will be used in objective functions in an MOEA.

The next stage involves implementing the function as a subroutine of the genetic algorithm in order to obtain the desired results.

5 Multi-objective evolutionary algorithm to minimise harmonic propagation and power losses

5.1 Introduction

Interactions between network components affect the harmonic performance. Hence, it is essential to reduce the adverse effects of the harmonics in the network. Adverse effects, such as resonances that can cause instability and operating problems that could shut off one or more wind turbines, can cause a significant fault if they are not controlled quickly, and it is in this context that the proposed algorithm stands. The MOEA proposed to solve this problem consists of different stages.

- The algorithm starts with a network where the nodes and lines are fixed and will not be changed, as shown in Section 5.2.1. New nodes are proposed, with the restrictions to be connected only to specific nodes of the network, as shown in Section 5.2.3.

- First, it is necessary to develop the algorithm to calculate harmonic propagation and power flow in order to obtain the THD on each node and power losses on each line, as shown in Section 4.5. This stage is fundamental, because each generated chromosome must be evaluated. Once it is evaluated, different parameters are obtained. The THD of each node is used to obtain an average THD of the network configuration for each chromosome. The average THD and power losses are the main parameters considered and implemented in the algorithm.

- The next stage is to generate an initial population of chromosomes, after checking that these are valid chromosomes, as shown in Section 5.2.4. The criteria employed are that there are no isolated nodes, as shown in Section 5.2.2, and that the method to calculate power flow and harmonic propagation converges to a solution. In the case that a criterion is not satisfied, the chromosome is eliminated and a new one is generated. In Section 5.2.4.2, it is

assumed that the cable is fixed only to one size. Different sizes of cable can be implemented, but the algorithm must be modified to implement other sizes of cable. Also, the algorithm can be modified to choose the best cable according to the power flow in each line.

- Once the initial population is generated, results are shown, as shown in Section 5.2.5, and the next stage begins with an algorithm to reduce the number of lines, and consequently, the total distance of the cable, as shown in Section 5.2.6. This part of the algorithm checks for the longest distance between nodes and eliminates it. If the new average THD is higher than the previous or the new configuration result with an isolated node, then the eliminated line is restored, and it continues with the next longest line. This is repeated until the criterion is satisfied. In this case, the criterion is that all lines greater than a value of x kilometres will be eliminated. This x value allows multiple connections to nodes, mainly nodes that are closer or separated by a few kilometres. When x is zero, the algorithm obtains only one branch configuration.

- With the number of lines minimised, the average THD of the population changes. These chromosomes are ordered to obtain the best chromosomes using the Pareto front, as shown in Section 5.2.7.

- The final stage is a genetic algorithm as is proposed in Section 3.5.1. With the best individuals, obtained from the Pareto front, it generates a new population, as shown in Section 5.2.8. If the new Pareto front has at least one chromosome that is better, or if the maximum number of generations is not reached, then the algorithm creates another generation. Otherwise the algorithm stops and generates the final report, as shown in Section 5.2.9.

5.2 MOEA to minimise harmonic propagation and power losses in offshore wind power clusters

The algorithms described in Sections 3.5.1 and 4.5 are part of the evolutionary algorithm proposed in this section to solve the problem of minimising harmonic propagation and power losses in offshore wind power clusters.

The algorithms presented were complemented by the data necessary to obtain the objective functions and implemented to develop an MOEA in order to obtain the desired results.

The first objective function is the logarithmic average of THD that is calculated using the harmonic voltage vector, represented by Equation (4.22). The purpose of using a logarithm average instead of an arithmetic average is to consider a greater weight for the higher harmonic distortion. The THD index is calculated by the harmonic content of a specific node as follows:

$$THD_V = \frac{\sqrt{\sum_{h=2}^{H} V_h^2}}{V_1} \times 100\% \tag{5.1}$$

where the V_h is obtained from the solution of Equation (4.20).

The logarithmic average of THD can be represented as the following:

$$H_{THD} = \log \sum_{i=1}^{N} 10^{V_{THDi}} \tag{5.2}$$

And the function to minimise the logarithmic average of voltage THD can be represented as the following:

$$\text{Min } H_{THD} = \log \sum_{i=1}^{N} 10^{V_{THDi}} \tag{5.3}$$

Such that

$$V_h = Z_h I_h \tag{5.4}$$

$$V_{THDi\ min} \leq V_{THDi} \leq V_{THDi\ max} \tag{5.5}$$

$$H_{THDi\ min} \leq H_{THDi} \leq H_{THDi\ max} \tag{5.6}$$

where

V_h is the vector of nodal voltages for each harmonic h

Z_n is the nodal impedance matrix

I_h is the vector of the injected harmonic current by harmonic h

N is the number of nodes of the network

"*min*" and "*max*" are the lower and upper limits of the constraints

For Equation (5.2), subject to the penalty factor for constraint violations, the following is applicable

$$W_{V_{THDMi}} = V_{THDi} - V_{THDi\ max} \leq 0 \tag{5.7}$$

$$W_{V_{THDNi}} = V_{THDi} - V_{THDi\,min} \geq 0 \tag{5.8}$$

$$W_{H_{THDMi}} = H_{THDi} - H_{THDi\,max} \leq 0 \tag{5.9}$$

$$W_{H_{THDNi}} = H_{THDi} - H_{THDi\,min} \geq 0 \tag{5.10}$$

A new objective function with penalty factors is obtained when constraints are introduced into the objective function. The function for the logarithmic average of THD represented by Equation (5.2) is transformed in the following:

$$H = H_{THD} + \sum_{i=1}^{N} r_{Ii}\, W_{Ii}^2 + \sum_{i=1}^{N} r_{Hi}\, W_{Hi}^2 \tag{5.11}$$

where

H is the function for the logarithmic average of THD

W_{Ii} includes all constraints related to harmonic current vector

W_{Hi} includes all constraints related to the logarithmic average of THD

r_{Ii} is the penalty factor for violated constraints related to the harmonic current vector

r_{Hi} is the penalty factor for violated constraints related to the logarithmic average of THD

N is the total number of nodes

The second objective function is power losses. To obtain the function, the power flow problem with real and reactive power variables is used, and it can be represented as the following:

$$\text{Min } P_L = \sum_{i=1}^{N} P_{i(P_{Gi})} \tag{5.12}$$

Such that

$$P_i(V, \delta) = P_{Gi} - P_{Di} \tag{5.13}$$

$$Q_i(V, \delta) = Q_{Gi} - Q_{Di} \tag{5.14}$$

$$P_{Gi\,min} \leq P_{Gi}(V, \delta) \leq P_{Gi\,max} \tag{5.15}$$

$$Q_{Gi\,min} \leq Q_{Gi}(V, \delta) \leq Q_{Gi\,max} \tag{5.16}$$

$$V_{i\,min} \leq V_i \leq V_{i\,max} \tag{5.17}$$

where

P_{Gi} is the real power output of the generator connecting to bus i

Q_{Gi} is the reactive power output of the generator connecting to bus i

P_{Di} is the real power load connecting to bus i

Q_{Di} is the reactive power load connecting to bus i

P_i is the real power injection at bus i

Q_i is the reactive power injection at bus i

V_i is the voltage magnitude at bus i

P_i is the generator power flow function

"*min*" and "*max*" are the lower and upper limits of the constraints

Equations (5.13) and (5.14) are the power flow equations and can be written as the following:

$$P_i(V,\delta) = V_i \sum_{k=1}^{N} V_k \left(G_{ik} \cos \delta_{ik} + B_{ik} \sin \delta_{ik} \right) \tag{5.18}$$

$$Q_i(V,\delta) = V_i \sum_{k=1}^{N} V_k \left(G_{ik} \sin \delta_{ik} - B_{ik} \cos \delta_{ik} \right) \tag{5.19}$$

Substituting in Equation (5.12), it is then represented in terms of V and θ as the following:

$$\text{Min } P_L(V, \delta) \tag{5.20}$$

subject to

$$W_{Pi} = V_i \sum_{j=1}^{N} V_j \left(G_{ij} \cos \delta_{ij} + B_{ij} \sin \delta_{ij} \right) - P_{Gi} + P_{Di} = 0 \tag{5.21}$$

$$W_{Qi} = V_i \sum_{j=1}^{N} V_j \left(G_{ij} \sin \delta_{ij} - B_{ij} \cos \delta_{ij} \right) - Q_{Gi} + Q_{Di} = 0 \tag{5.22}$$

$$W_{PMi} = V_i \sum_{j=1}^{N} V_j \left(G_{ij} \cos \delta_{ij} + B_{ij} \sin \delta_{ij} \right) - P_{Gi\,max} \leq 0 \tag{5.23}$$

$$W_{PNi} = V_i \sum_{j=1}^{N} V_j \left(G_{ij} \cos \delta_{ij} + B_{ij} \sin \delta_{ij} \right) - P_{Gi\,min} \geq 0 \tag{5.24}$$

$$W_{QMi} = V_i \sum_{j=1}^{N} V_j \left(G_{ij} \sin \delta_{ij} - B_{ij} \cos \delta_{ij} \right) - Q_{Gi\,max} \leq 0 \qquad (5.25)$$

$$W_{QNi} = V_i \sum_{j=1}^{N} V_j \left(G_{ij} \sin \delta_{ij} - B_{ij} \cos \delta_{ij} \right) - Q_{Gi\,min} \geq 0 \qquad (5.26)$$

$$W_{VMi} = V_i - V_{i\,max} \leq 0 \qquad (5.27)$$

$$W_{VNi} = V_i - V_{i\,min} \geq 0 \qquad (5.28)$$

A new objective function with penalty factors is obtained when constraints are introduced into the objective function. The function for power losses represented by Equation (5.20) is transformed in the following:

$$L(X) = P_L(X) + \sum_{i=1}^{N} r_{Pi}\, W_{Pi}^2(X) + \sum_{i=1}^{N} r_{Qi}\, W_{Qi}^2(X) + \sum_{i=1}^{N} r_{Vi}\, W_{Vi}^2(X) \qquad (5.29)$$

where

X is the vector that depends on V and δ

W_{Pi} includes all constraints related to real power variables

W_{Qi} includes all constraints related to reactive power variables

W_{Vi} includes all constraints related to voltage variables

r_{Pi} is the penalty factor for violated constraints related to real power variables

r_{Qi} is the penalty factor for violated constraints related to reactive power variables

r_{Vi} is the penalty factor for violated constraints related to voltage

N is the total number of buses

The data is introduced to the objective function to calculate the power flow and the harmonic propagation.

The data requested are the highest harmonic and number of harmonics to consider, increase for the DPI frequency response, all the data of lines and transformers, the data for shut elements and impedances of the generators and nodes with harmonics injected, and the harmonics injected.

If there are no constraint violations, the penalty factors are zero, and the problem becomes an unconstrained optimisation problem.

The algorithm checks whether all constraints are met. If yes, then the results are saved. Otherwise the result is not considered.

With this information, the algorithm returns the information to evaluate the chromosomes.

The diagram of the proposed MOEA is shown in Figure 5.1. The developed MOEA is detailed in Appendix G.
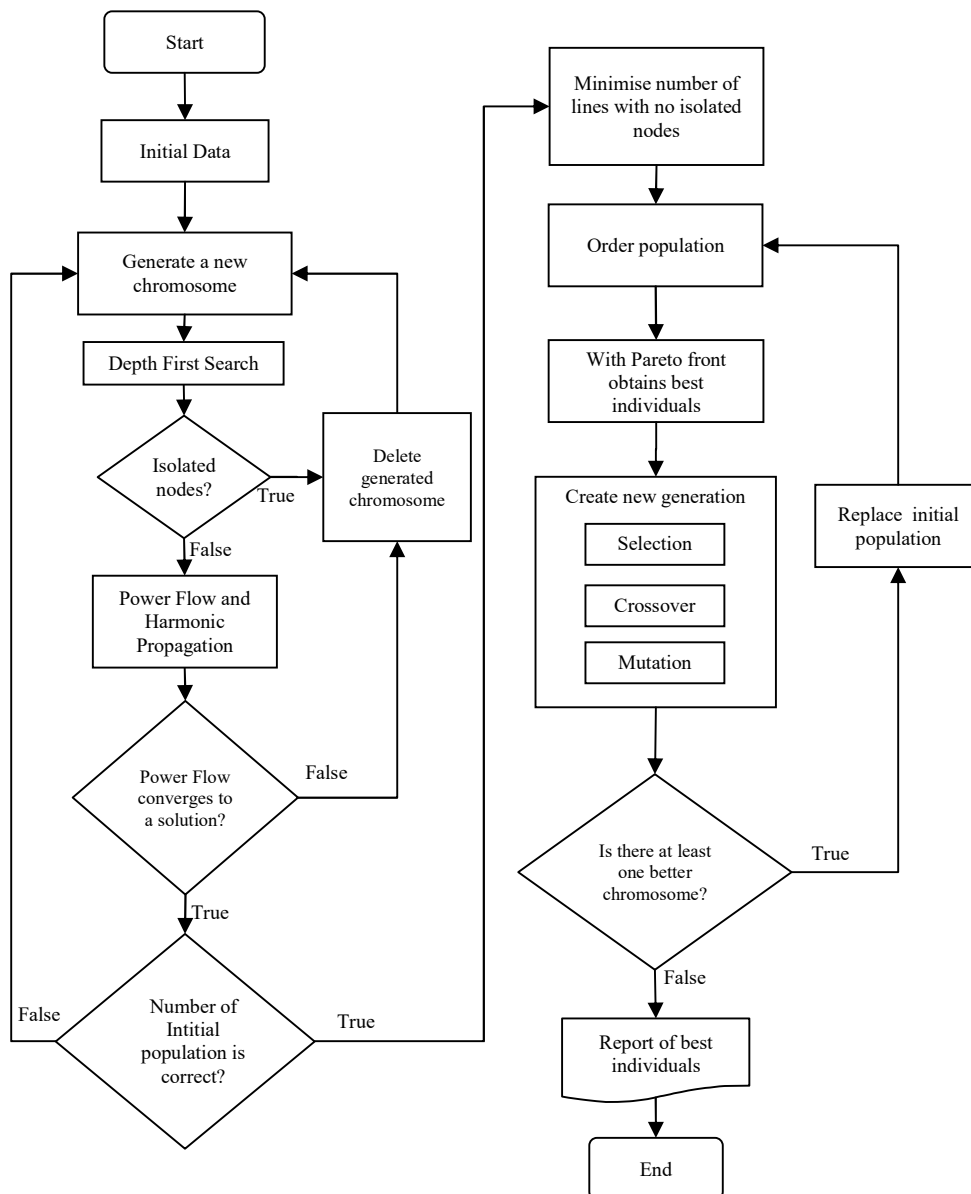
Figure 5.1. Diagram of the multi-objective evolutionary algorithm.

5.2.1   Basic network data

The proposed algorithm considers the existence of two electrical networks: one is a fixed grid which cannot change in its configuration (onshore AC grid), and the other is a network (offshore wind parks) in which the only factors known are the generation points

but not the interconnection between them and the onshore AC grid. The objective is to find the best grid that interconnects the offshore wind power clusters with the onshore AC grid, optimising the energy losses and THD within a steady operation point of the interconnected networks. The algorithm created starts using a basic network data with nodes and lines fixed, and this data will not change when the algorithm is running. A part of the initial data constants for the basic 30 nodes network used is shown in Figure 5.2.
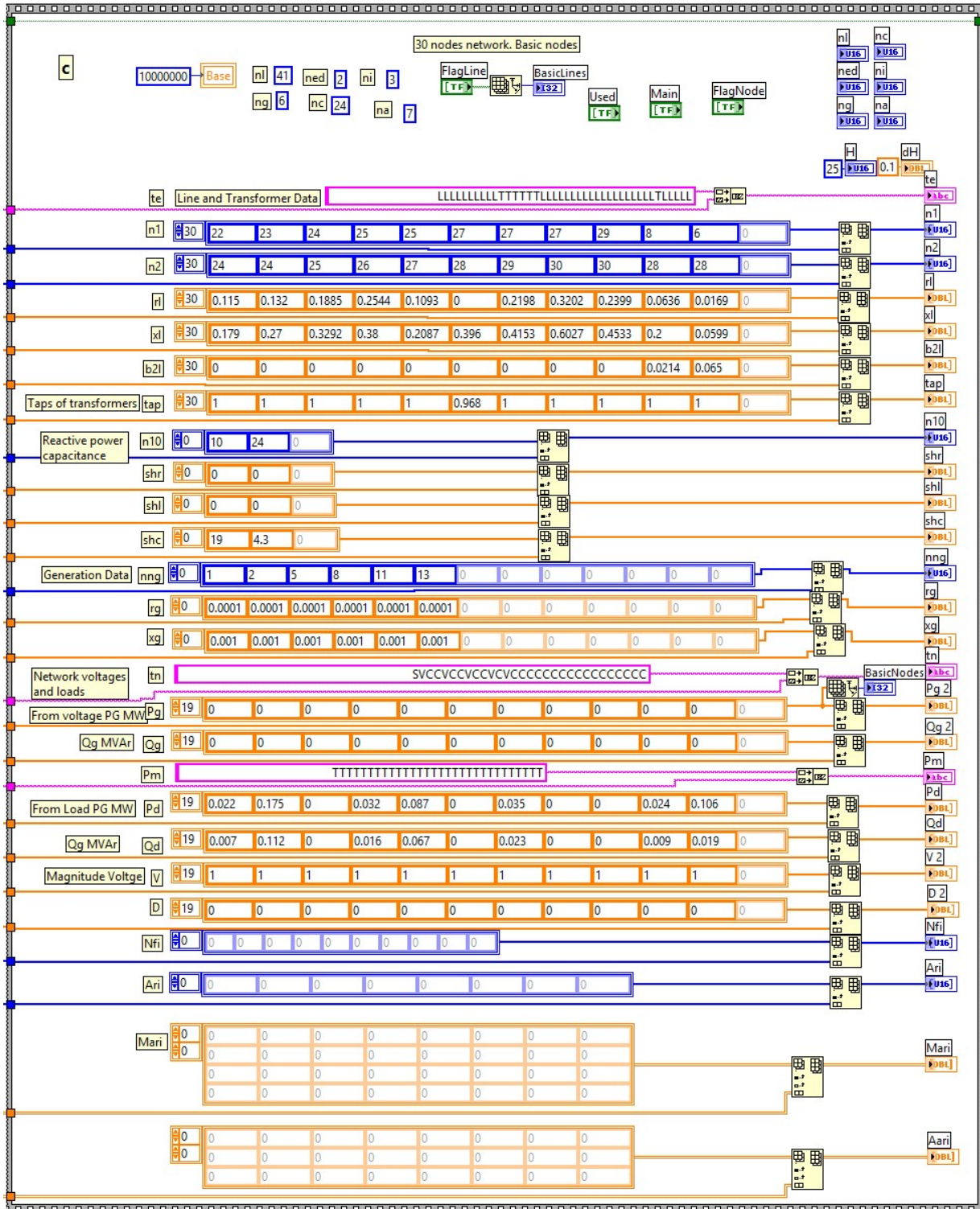

Figure 5.2. Initial data for 30-Bus IEEE network

The variables *n1* and *n2* are used to encode the chromosome using value encoding. These variables indicate the connection between nodes. Each connection represents a line between two nodes. Subsequently, for this problem, the length of each chromosome could be different.

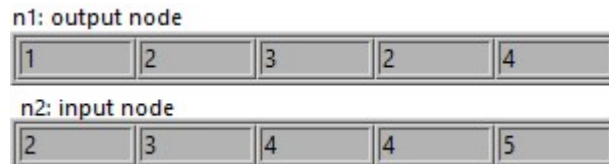The 5-bus network generated chromosome of Section 4.5.1 has five lines, and it is shown in Figure 5.3.

Figure 5.3. Lines of the 5-bus network.

The 30-bus IEEE network generated chromosome of Section 4.5.2 has 41 lines, and it is shown in Figure 5.4.

Figure 5.4. Lines of 30-bus IEEE network.

With the information of output and input nodes, a matrix of *N* by *N* is created, where *N* is the number of nodes. The matrix formed connects each node with one or more nodes. Furthermore, the possibility also exists that a node does not connect with any other node.

The 5x5 matrix formed for the 5-bus network shown before is presented in Figure 5.5. The fact that matrix connections are an identity matrix must be validated in order to check isolated nodes using the DFS algorithm.

Figure 5.5. Matrix formed for a network of five nodes.

The 41x41 matrix formed for the 30-bus IEEE network shown before is in Figure 5.6. Furthermore, the fact that matrix connections are an identity matrix must be validated in order to check isolated nodes using the DFS algorithm.

```
0 1 1 0 0 0 0 0 0 0 0 0 0 0 0 0 0 0 0 0 0 0 0 0 0 0 0 0 0 0
1 0 0 1 1 1 0 0 0 0 0 0 0 0 0 0 0 0 0 0 0 0 0 0 0 0 0 0 0 0
1 0 0 1 0 0 0 0 0 0 0 0 0 0 0 0 0 0 0 0 0 0 0 0 0 0 0 0 0 0
0 1 1 0 0 1 0 0 0 0 0 1 0 0 0 0 0 0 0 0 0 0 0 0 0 0 0 0 0 0
0 1 0 0 0 0 1 0 0 0 0 0 0 0 0 0 0 0 0 0 0 0 0 0 0 0 0 0 0 0
0 1 0 1 0 0 1 1 1 1 0 0 0 0 0 0 0 0 0 0 0 0 0 0 0 0 1 0 0 0
0 0 0 0 1 1 0 0 0 0 0 0 0 0 0 0 0 0 0 0 0 0 0 0 0 0 0 0 0 0
0 0 0 0 0 1 0 0 0 0 0 0 0 0 0 0 0 0 0 0 0 0 0 0 0 0 0 1 0 0
0 0 0 0 0 1 0 0 0 1 1 0 0 0 0 0 0 0 0 0 0 0 0 0 0 0 0 0 0 0
0 0 0 0 0 1 0 0 1 0 0 0 0 0 0 0 1 0 0 1 1 1 0 0 0 0 0 0 0 0
0 0 0 0 0 0 0 0 1 0 0 0 0 0 0 0 0 0 0 0 0 0 0 0 0 0 0 0 0 0
0 0 0 1 0 0 0 0 0 0 0 0 1 1 1 1 0 0 0 0 0 0 0 0 0 0 0 0 0 0
0 0 0 0 0 0 0 0 0 0 0 1 0 0 0 0 0 0 0 0 0 0 0 0 0 0 0 0 0 0
0 0 0 0 0 0 0 0 0 0 0 1 0 0 1 0 0 0 0 0 0 0 0 0 0 0 0 0 0 0
0 0 0 0 0 0 0 0 0 0 0 1 0 1 0 0 0 1 0 0 0 0 1 0 0 0 0 0 0 0
0 0 0 0 0 0 0 0 0 0 1 0 0 0 0 1 0 0 0 0 0 0 0 0 0 0 0 0 0 0
0 0 0 0 0 0 0 0 0 1 0 0 0 0 0 0 1 0 0 0 0 0 0 0 0 0 0 0 0 0
0 0 0 0 0 0 0 0 0 0 0 0 0 0 1 0 0 0 0 1 0 0 0 0 0 0 0 0 0 0
0 0 0 0 0 0 0 0 0 0 0 0 0 0 0 0 1 0 0 0 1 0 0 0 0 0 0 0 0 0
0 0 0 0 0 0 0 0 0 1 0 0 0 0 0 0 0 0 0 1 0 0 0 0 0 0 0 0 0 0
0 0 0 0 0 0 0 0 0 1 0 0 0 0 0 0 0 0 0 0 1 0 0 0 0 0 0 0 0 0
0 0 0 0 0 0 0 0 0 1 0 0 0 0 0 0 0 0 0 0 0 1 0 1 0 0 0 0 0 0
0 0 0 0 0 0 0 0 0 0 0 0 0 0 1 0 0 0 0 0 0 1 0 0 0 0 0 0 0 0
0 0 0 0 0 0 0 0 0 0 0 0 0 0 0 0 0 0 0 0 0 1 1 0 1 0 0 0 0 0
0 0 0 0 0 0 0 0 0 0 0 0 0 0 0 0 0 0 0 0 0 0 1 0 1 1 0 0 0 0
0 0 0 0 0 0 0 0 0 0 0 0 0 0 0 0 0 0 0 0 0 0 1 0 0 0 0 0 0 0
0 0 0 0 0 0 0 0 0 0 0 0 0 0 0 0 0 0 0 0 0 0 0 1 0 0 0 1 1
0 0 0 0 0 1 0 1 0 0 0 0 0 0 0 0 0 0 0 0 0 0 0 0 0 0 0 0 0 0
0 0 0 0 0 0 0 0 0 0 0 0 0 0 0 0 0 0 0 0 0 0 0 1 0 0 1
0 0 0 0 0 0 0 0 0 0 0 0 0 0 0 0 0 0 0 0 0 0 1 0 1 0
```

Figure 5.6. Matrix formed for a network of 30 nodes.

Each connection has associated variables, and these variables must be associated with the respective line to avoid calculation errors. Also, if there is a change in any line, a new parameter must be calculated to incorporate new data into the new configuration.

5.2.2 Elimination of isolated nodes

The offshore wind parks cannot contain isolated nodes. If the algorithm detects an isolated node, then this configuration is eliminated. The algorithm used to detect isolated nodes is DFS. DFS is a systematic algorithm to find all the vertices reachable from a source vertex. It traverses a connected component of a given graph and defines a spanning tree. The basic idea of the DFS is to explore every edge methodically. The DFS selects a source vertex s in the graph and marks it as "visited". Then, the vertex s becomes the

current vertex. Subsequently, it traverses the graph by considering an arbitrary edge (u, v) from the current vertex u. If the edge (u, v) leads to a marked vertex v, then it backs down to the vertex u. On the other hand, if the edge (u, v) leads to an unmarked vertex, then the vertex v is marked, and it is made the current vertex, and the process above is repeated until all the edges from the current vertex u lead to marked vertices.

To exit this process, the algorithm backs down along the edge that brought it to vertex u, and it returns to a previously marked vertex v. Again, this makes the vertex v the current vertex, and the aforementioned process is repeated for any edge that was missed earlier. If all of v's edges take to marked vertices, then again, it backs down to the vertex it came from to get to vertex v, and the search is repeated at that vertex [201]–[209].

Thus, it continues to go back down the path that it has traced until it finds a vertex that has unexplored edges, at which point, it takes one edge and continues exploring. When the DFS has backtracked all the way back to the source vertex, s, it has built a DFS tree of all the vertices reachable from that source.

If there are still undiscovered vertices in the graph, then it selects one of them as the source for another DFS tree. The result is a forest of DFS trees. The DFS algorithm consists of two parts: the first part marks all the nodes as False and then begins to analyse every node, and the second part is the recursive algorithm that is repeated until the last edge of the node is analysed [201]–[209]. The algorithm is shown below:

```
DFS(graph G)
  For every vertice u ∈ V[G] Do
      state[u] ← NO_VISITED
      father[u] ← NULL
  For every vertice u ∈ V[G] Do
    If state[u] = NO_VISITED Then
      DFS_Visited(u)


DFS_Visited(node u)
    state[u] ← VISITED
    For every v ∈ Edges[u] Do
    If state[v] = NO_VISITED Then
        father[v] ← u
        DFS_Visited(v)
      state[u] ← FINISHED
```

Note that the edges that lead to new vertices are called discovery or tree edges, and the edges that lead to already visited (marked) vertices are called back edges. Figure 5.7 shows the diagram of the DFS algorithm [201]–[209].
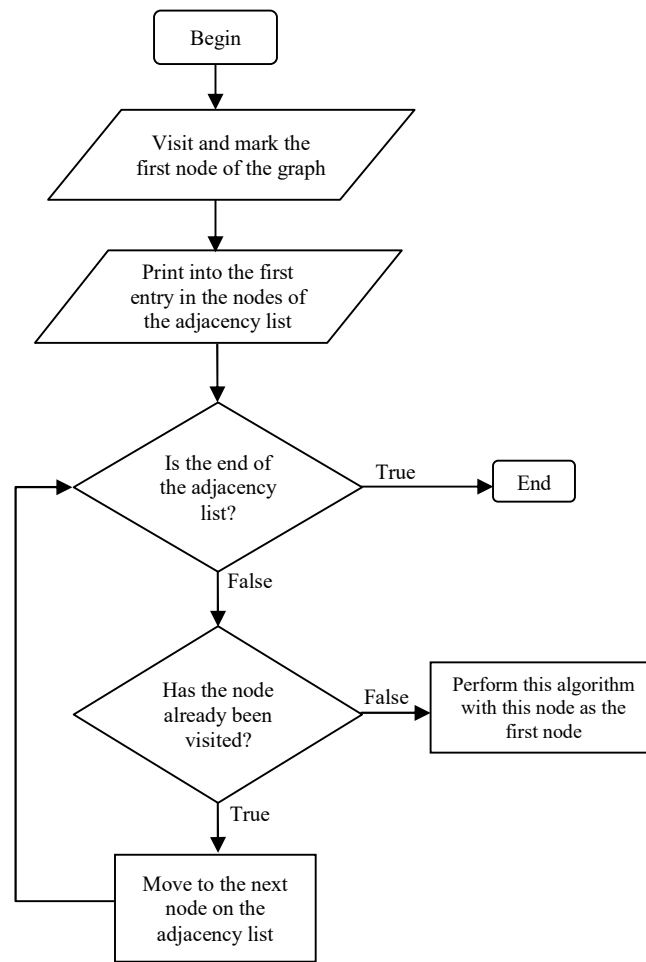
Figure 5.7. Diagram of the depth-first search algorithm.

This algorithm was implemented to locate the isolated nodes and eliminate them to ensure that all the nodes are connected to the network and to avoid configurations that have isolated nodes or islands. The algorithm requests the number of nodes and the network connections and returns a Boolean vector to know if the configuration has or does not have isolated nodes. The developed algorithm gives the final configuration of the network. The algorithm generates the matrix with all the nodes, and if all the components of the matrix are true, it means that all the nodes are connected to the network, and then, a graph is generated with the configuration. The algorithm implemented to eliminate isolated nodes is detailed in Appendix B.

5.2.3 Selection of nodes and lines used

With the network data, the algorithm creates new chromosomes. With Boolean constants, the algorithm determines which nodes will be used, which will be connected randomly, which will be connected to the main onshore AC grid, and which lines will be fixed. Figure 5.8 (a) shows the Boolean flags before the algorithm begins, (b) the constants used, and (c) the Boolean flags, after the algorithm begins.
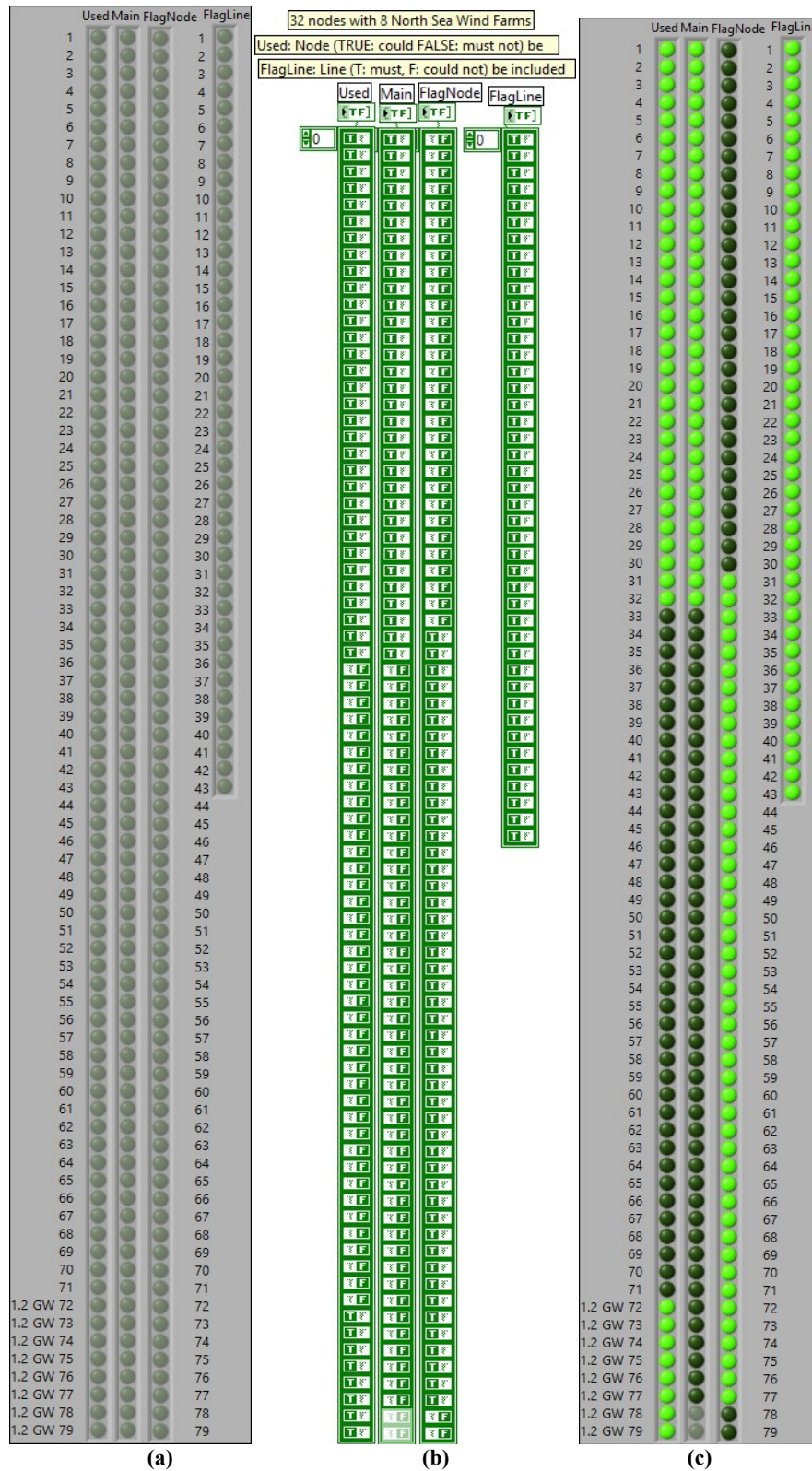
Figure 5.8. Boolean constants to determine elements to be used.

The Boolean constant "Used" determines all the nodes to be used, the Boolean constant "Main" determines which nodes are of the fixed network, and the Boolean constant "Flag Node" determines which nodes of the fixed network are allowed to connect to the proposed configuration. Additionally, "Flag Line" determines the lines of the network that are fixed and cannot be changed.

Figure 5.9 shows the total number of nodes captured and saved in a constant with latitude and longitude. The location on a map is shown in Figure 5.10. The selected nodes for the configuration generated are shown in Figure 5.11, and the location is shown in Figure 5.12.

Node	Latitude	Longitude	Name	Latitude	Longitude
Node 1	57.5420751	-2.1050387	Riffgat	53.69	6.4778113
Node 2	57.5708946	-3.4636165	Scroby Sands	52.633333	1.7811446
Node 3	56.7122835	-2.7356276	Sheringham Shoal	53.116667	1.1311446
Node 4	56.2761836	-2.8309193	Teesside	54.647222	-1.0966331
Node 5	55.9054419	-3.1517554	Thanet	51.433333	1.6311446
Node 6	55.9793974	-3.3656554	Thorntonbank	51.644167	2.9250335
Node 7	56.031978	-2.6122193	Trianel Windpark Borkum (phase 1)	54.041667	6.464478
Node 8	51.7658611	-2.7660055	Westermost Rough	53.805	0.1467002
Node 9	54.764767	-2.5189026	Amrumbank West	54.433333	7.6811446
Node 10	53.6410754	-2.7491387	Borkum Riffgrund I	53.966944	6.5517002
Node 11	53.4639199	-1.3571026	Butendiek	55.018889	7.7717002
Node 12	54.7083837	-1.2950748	Dudgeon	53.25	1.3811446
Node 13	55.6394308	-1.9436554	Eneco Luchterduinen	52.405	4.1597557
Node 14	53.8016222	-0.387347	Gemini	54.036111	5.9608669
Node 15	53.5518389	-0.2409915	Global Tech I	54.261944	6.4083669
Node 16	53.0738528	-0.9934109	Gode Wind 1 & 2	54.05	7.014478
Node 17	53.3368194	-2.0878998	Sandbank	55.191667	6.8561446
Node 18	52.7936972	0.3133835	Wind Farm 300 MW	53.985992	0.0478252
Node 19	52.1712553	0.1040475	Wind Farm 600 MW	53.3401921	0.5193446
Node 20	52.0667694	-1.3199609	Wind Farm 400 MW	52.9279056	1.7244252
Node 21	53.2741139	-2.6661387	Wind Farm 1	54.9492	-0.8998
Node 22	51.4153972	-1.5857193	Wind Farm 2	54.2534	0.3133
Node 23	52.1853333	1.4953278	Wind Farm 3	55.7579	-1.457
Node 24	51.7607778	0.864925	Wind Farm 125 km	55.6669	0.199
Node 25	51.4392306	-0.149072	1.2 GW 125 km	54.7093225	1.3209057
Node 26	50.9557645	-2.9741109	1.2 GW 144 km	54.4743475	1.864353
Node 27	51.3193889	1.017225	1.2 GW 160 km	54.7500031	1.914478
Node 28	51.9168778	-2.3952693	1.2 GW 170 km	55.0280225	1.738028
Node 29	50.7777222	-1.6272305	1.2 GW 179 km	54.7874225	2.3841613
Node 30	51.1144	1.1121723	1.2 GW 200 km	53.9573031	2.8309113
Alpha Ventus	54.016667	6.5978113	1.2 GW 210 km	54.4142281	2.9855002
BARD Offshore 1	54.355	5.9778113	1.2 GW 290 km	55.1797086	3.7846557
Beatrice	58.105556	-3.093056	Dogger Bank. Creyke Beck A. 1.2 GW	54.769	1.908
Belwind	51.66	2.7978113	Dogger Bank. Creyke Beck B. 1. 2GW	54.977	1.679
Blyth Offshore	55.135833	-1.490278	Dogger Bank. Teesside B. 1.2 GW	54.989	2.228
DanTysk	55.14	7.1978113	Dogger Bank. Teesside A. 1.2 GW	55.039	2.822
Egmond aan Zee (OWEZ)	52.606111	4.4167002	Dogger Bank. Teesside C Cancelled 1.2	55.245	1.858
Greater Gabbard	51.933333	1.8811446	Dogger Bank. Teesside D Cancelled 1.2	55.304	2.402
Gunfleet Sands 1 & Gunfleet Sands 1 & 2	51.716667	1.2117002	Dogger Bank. Tranche D Cancelled 2.4	55.429	2.982
Horns Rev I	55.529722	7.9039224	Hornsea Project Four. 1 GW	54.038	1.271
Horns Rev II	55.6	7.5878113	Hornsea Project Two. 1.8 GW	53.94	1.687
Humber Gateway	53.643889	0.2908669	Hornsea Project One. 1.2 GW	53.883	1.921
Hywind	59.14	5.0297557	Hornsea Project Three. 2 GW	53.873	2.537
Kentish Flats	51.46	1.0878113	Seagreen Alpha 525 MW	56.611	-1.821
Lincs	53.183333	0.4811446	Seagreen Bravo 525 MW	56.572	-1.658
London Array	51.643889	1.5514224	Seagreen Charlie 610 MW	56.471	-1.576
Lynn and Inner Dowsing	53.1275	0.4339224	Seagreen Delta 605 MW	56.368	-1.52
Meerwind Süd/Ost	54.383333	7.6811446	Seagreen Echo 605 MW	56.272	-1.467
Nordsee Ost	54.433333	7.6811446	Seagreen Foxtrot 565 MW	56.466	-1.795
Northwind	51.618889	2.8978113	Seagreen Golf 225 MW	56.263	-1.711
Princess Amalia	52.59	4.2178113			

Figure 5.9. Total number of nodes captured that could be used.

Figure 5.10. Nodes located in the map.

Node	Latitude	Longitude	Node	Latitude	Longitude
Node 1	57.5421	-2.10504	Node 21	53.2741	-2.66614
Node 2	57.5709	-3.46362	Node 22	51.4154	-1.58572
Node 3	56.7123	-2.73563	Node 23	52.1853	1.49533
Node 4	56.2762	-2.83092	Node 24	51.7608	0.864925
Node 5	55.9054	-3.15176	Node 25	51.4392	-0.149072
Node 6	55.9794	-3.36566	Node 26	50.9558	-2.97411
Node 7	56.032	-2.61222	Node 27	51.3194	1.01723
Node 8	51.7659	-2.76601	Node 28	51.9169	-2.39527
Node 9	54.7648	-2.5189	Node 29	50.7777	-1.62723
Node 10	53.6411	-2.74914	Node 30	51.1144	1.11217
Node 11	53.4639	-1.3571	Wind Farm 300 MW	53.986	0.0478252
Node 12	54.7084	-1.29507	Wind Farm 600 MW	53.3402	0.519345
Node 13	55.6394	-1.94366	1.2 GW 125 km	54.7093	1.32091
Node 14	53.8016	-0.387347	1.2 GW 144 km	54.4743	1.86435
Node 15	53.5518	-0.240991	1.2 GW 160 km	54.75	1.91448
Node 16	53.0739	-0.993411	1.2 GW 170 km	55.028	1.73803
Node 17	53.3368	-2.0879	1.2 GW 179 km	54.7874	2.38416
Node 18	52.7937	0.313383	1.2 GW 200 km	53.9573	2.83091
Node 19	52.1713	0.104048	1.2 GW 210 km	54.4142	2.9855
Node 20	52.0668	-1.31996	1.2 GW 290 km	55.1797	3.78466

Figure 5.11. Selected nodes.
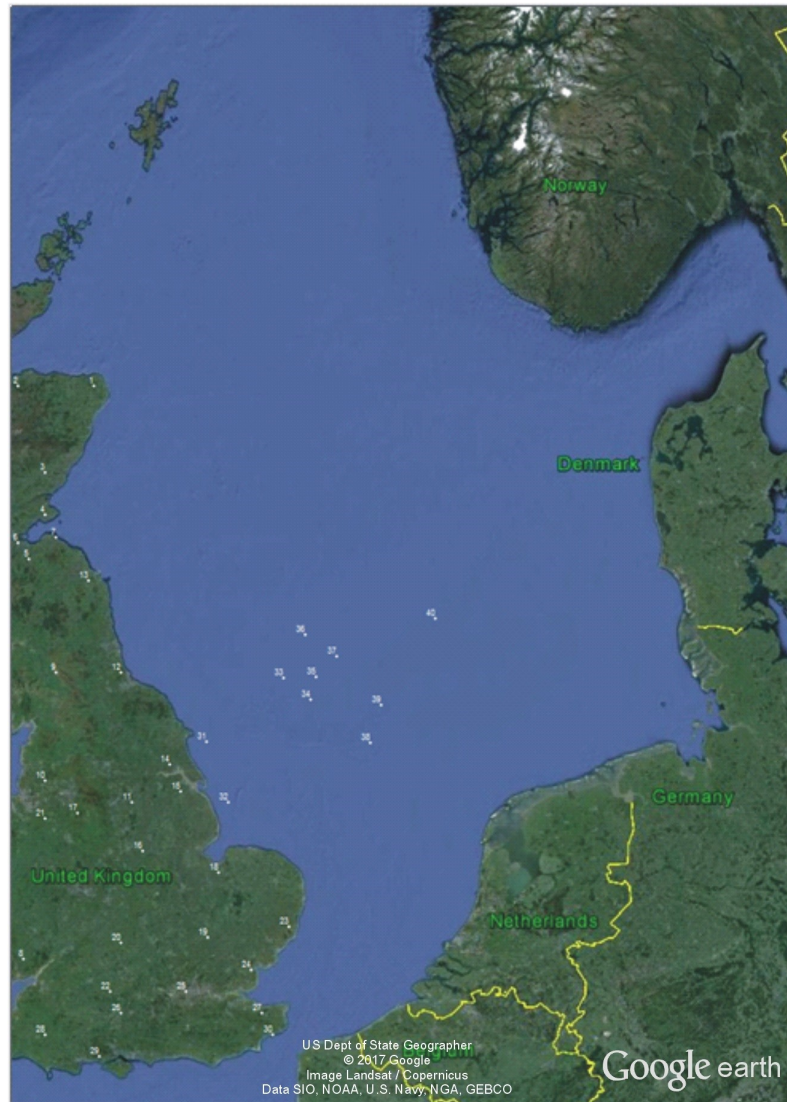
Figure 5.12. Selected nodes located in the map.

5.2.4   Generating a random population

The algorithm continues generating a random population with vectors of chromosomes. The length of chromosomes depends on the number of lines generated randomly. Each chromosome is checked with the DFS algorithm to avoid isolated nodes, and if there is an isolated node, the chromosome is deleted, and a new element is generated to replace it. If there are no isolated nodes, then the power flow and harmonic propagation algorithm converging to a solution is checked for. If there is no solution, the chromosome is deleted, and a new one is generated. The program creates a matrix with the data obtained, and this data is sent to the objective functions.

The chromosomes randomly generated use fixed nodes (onshore AC grid). The nodes are located on a map using latitude and longitude. With the latitude and longitude of each node, the distance between different nodes is calculated using the haversine formula.

5.2.4.1   *Haversine formula to calculate the distance between nodes*

With three points *u*, *v*, and *w*, a triangle is defined. If these points are on the surface of a sphere, as is shown in Figure 5.13, it is possible to calculate the distance between the two points. The three sides of the triangle are *a*, *b*, and *c* and the opposite angle is *C*. The haversine formula is an equation that uses latitudes and longitudes to calculate distances between two points on a sphere. The latitudes and longitudes are given in radians. The haversine formula is a particular case of the law of haversines that is derived from the spherical law of cosines and states *hav*(*c*) = *hav* (*a* – *b*) + sin(*a*) sin(*b*) *hav*(*C*).
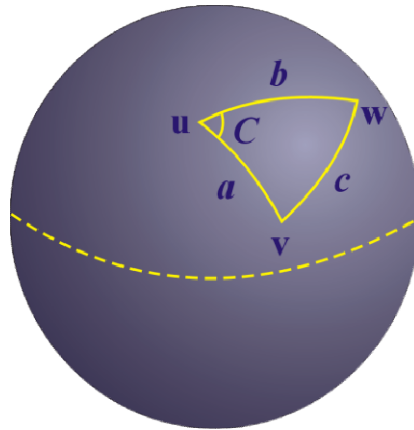
Figure 5.13. Spherical triangle solved by the law of haversines.

The haversine of the central angle for any two points is given by the following:

$$hav\left(\frac{d}{r}\right) = hav(\Delta\varphi) + \cos\varphi_1 \cos\varphi_2 hav(\Delta\lambda) \tag{5.30}$$

where *hav* is the haversine function and is given by the following:

$$hav(\theta) = \sin^2 \frac{\theta}{2} = \frac{(1 - \cos\theta)}{2} \tag{5.31}$$

where:

d is the distance between points A and B

r is the radius of the sphere

$\Delta\varphi$, is the difference of the latitudes of point A and B, in radians $(\varphi_2 - \varphi_1)$

$\Delta\lambda$, is the difference of the longitudes of point A and B, in radians $(\lambda_2 - \lambda_1)$

$\frac{d}{r}$ is the central angle in radians, $\left(\frac{d}{r}\right) \Rightarrow \left(\frac{d \cdot 180}{r\pi}\right)$

Applying inverse sine function, the following is arrived at:

$$d = rhav^{-1}(h) = 2r\arcsin(\sqrt{h}) \tag{5.32}$$

where *h* is $hav\left(\frac{d}{r}\right)$

$$d = 2r\arcsin\sqrt{hav(\Delta\varphi) + \cos\varphi_1\cos\varphi_2 hav(\Delta\lambda)} \tag{5.33}$$

$$d = 2r\arcsin\sqrt{\sin^2\left(\frac{\Delta\varphi}{2}\right) + \cos\varphi_1\cos\varphi_2\sin^2\left(\frac{\Delta\lambda}{2}\right)} \tag{5.34}$$

Finally, the equation implemented in the algorithm is the following:

$$d = 2r\arcsin\frac{\sqrt{(\sin\varphi_1 - \sin\varphi_2)^2 + (\cos\varphi_1\cos(\lambda_1 - \lambda_2) - \cos\varphi_2)^2 + (\cos\varphi_1\sin(\lambda_1 - \lambda_2))^2}}{2} \tag{5.35}$$

The radius of the Earth varies from 6,356.75 km at the poles to 6,378.16 km at the equator. The Earth's radius used in the algorithm is 6,372.8 km instead of the mean Earth radius of 6,371 km recommended by the International Union of Geodesy and Geophysics (IUGG). The reason for this is because it obtains more accurate results in calculating distances [210]–[213].

5.2.4.2 Calculating Resistance, Reactance, and Susceptance

With the distance between the nodes, the parameters of the line are calculated. These parameters are necessary to calculate power flow and harmonic propagation.

Resistance, reactance and susceptance for a typical line of a HVDC 115 kV, and 100 MW are calculated below.

$$kV_{LL} = 115 \text{ kV and } MVA_{base} = 100 \text{ MVA} \tag{5.36}$$

The base impedance is calculated by the following:

$$Z_{base} = \frac{kV_{LL}^{2}}{MVA_{base}} = \frac{115kV^{2}}{100MVA} = 132.25\Omega \tag{5.37}$$

The resistance, inductance, and capacitance of a typical cable are as follows:

$R_{km} = 0.0679 \ \Omega/\text{km}$

$L_{km} = 2.4217 \ \text{mH/km}$

$C_{km} = 0.4764 \ \mu\text{F/km}$

Considering a frequency

$f = 50 \text{ Hz}$

The resistance, inductance and susceptance values per unit are as follows:

$$R_{pu} = \frac{R_{km}}{Z_{base}} = \frac{0.0679^{\Omega}/_{km}}{132.25\Omega} = 0.00051342 \ {}^{pu}/_{km} \tag{5.38}$$

$$X_{Lpu} = \frac{2\pi fL_{km}}{1000Z_{base}} = \frac{2\pi(50)2.4217 \ {}^{mH}/_{km}}{1000(132.25\Omega)} = 0.00575274 \ {}^{pu}/_{km} \tag{5.39}$$

$$B/2_{pu} = \frac{2\pi fC_{km}Z_{base}}{2} = \frac{2\pi(50)0.4764 \ {}^{\mu F}/_{km}(132.25\Omega)}{2(1,000,000)} = 0.00989663 \ {}^{pu}/_{km} \tag{40}$$

These values were implemented in the algorithm to obtain the data of the lines. The resistance, inductance, and susceptance values per kilometre are as follows:

$$R = R_{pu} * km \tag{5.41}$$

$$X_{L} = X_{L \ pu} * km \tag{5.42}$$

$$B/2 = B/2_{pu} * km \tag{5.43}$$

With the distance calculated it is possible to obtain the values of the cable by kilometre in order to obtain the resistance, reactance, and susceptance for the different connections in the generated configurations of the offshore wind power clusters [134], [136]–[138].

The algorithm implemented to calculate the distance and impedance of the line is detailed in Appendix D.

All the chromosomes are evaluated with the objective function. Figure 5.14 shows a result that the function returns for just one chromosome. The function returns power losses and an average of THD as a result for each chromosome. Also, the function returns the number of lines, maximum distance and the total distance of the cable. With this data can be implemented a function of cost according to the cable, but it is necessary add information of the cost of the cables, depending their own characteristics.
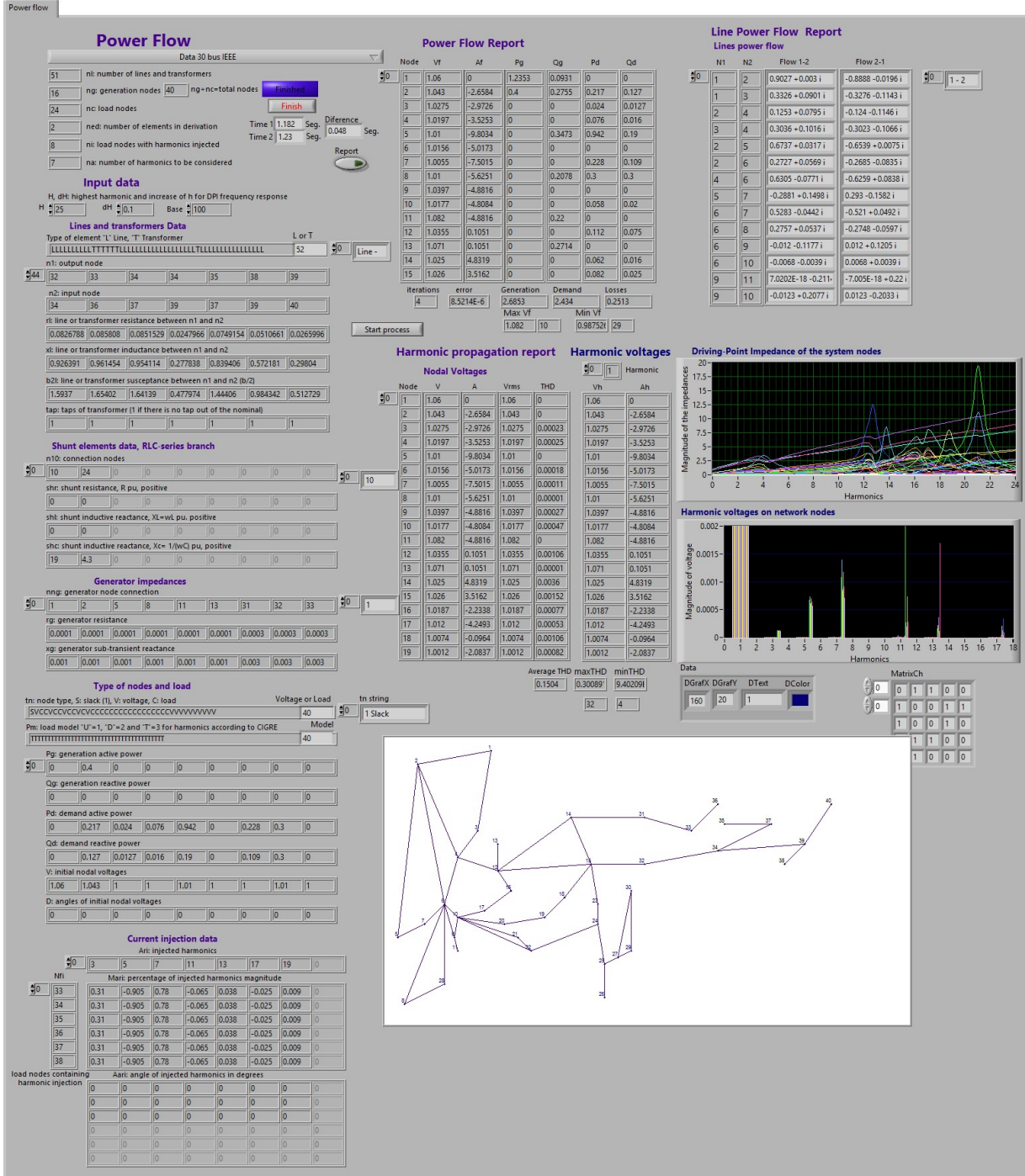
Figure 5.14 Example of the evaluation for each chromosome.

Figure 5.15 shows a generated chromosome with information regarding the THD and power losses. These parameters can be used to compare all chromosomes and make

decisions to obtain the best configurations. The connections for each node are generated randomly.
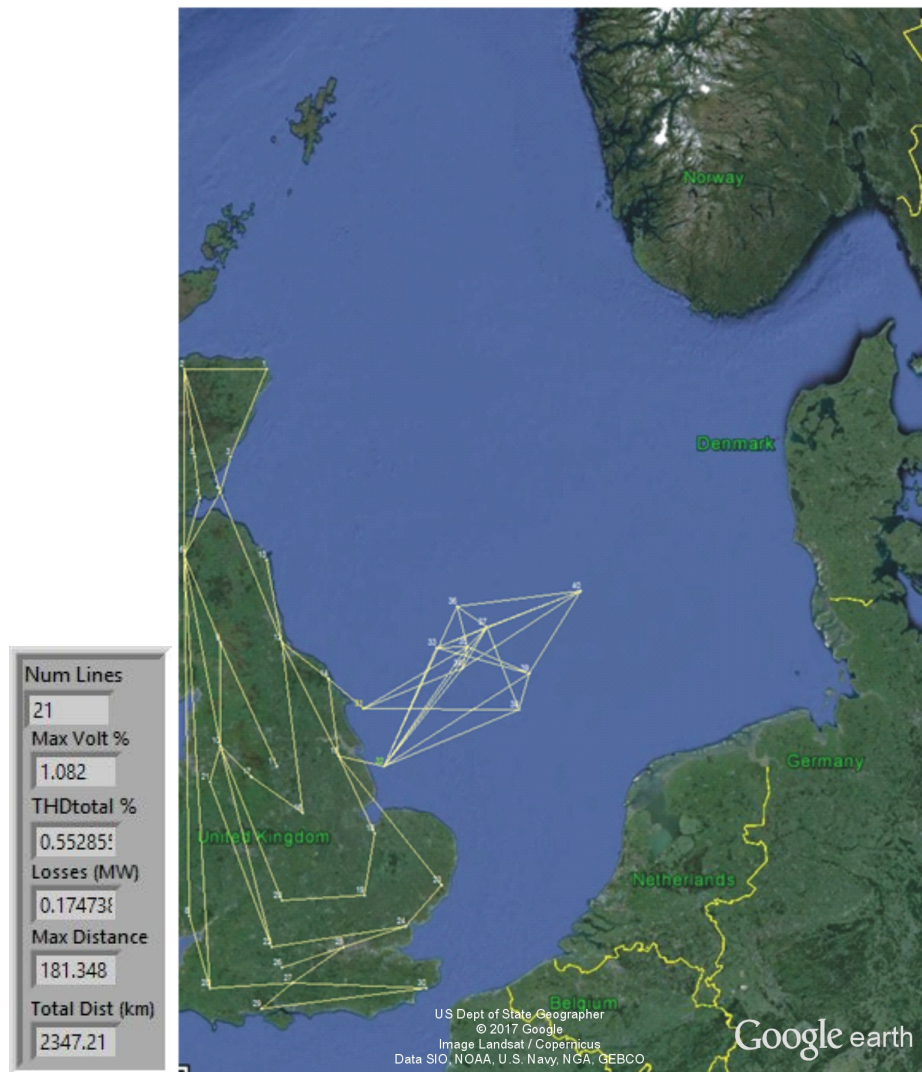
Figure 5.15 Random network generated for one chromosome.

The algorithm implemented to show the connections of the nodes on the map is detailed in Appendix C, and the algorithm implemented to generate and evaluate chromosomes randomly is detailed in Appendix E.

5.2.5 Randomly generated population

When all of the population is without isolated nodes, the algorithm returns for each chromosome, an average of THD as a function and power losses as another function. Furthermore, there are graphs shown for the number of lines, maximum distance, and the total distance of the cable. In Section 5.3, there is a comparison of generation times for different numbers of chromosomes.

Figure 5.16 shows an example of 1,500 chromosomes randomly generated in 31 minutes, 31.431 seconds. Figure 5.16(a) shows an XY graph with an average of THD in *x*-

axis and power losses in the *y*-axis. Figure 5.16(b) shows the number of lines of the network in the *z*-axis. Figure 5.16(c) shows the maximum distance of the generated nodes in the *z*-axis. Figure 5.16(d) shows the total length of the cable in the generated nodes in the *z*-axis.

Report:
Total of Chromosomes Generated in the First Generation: 1,500
Maximum Distance: 45 km
Pareto Fronts Considered: 30
Generation time: 00:31:31.431 = 1,891.431 seconds

(a)   (b)
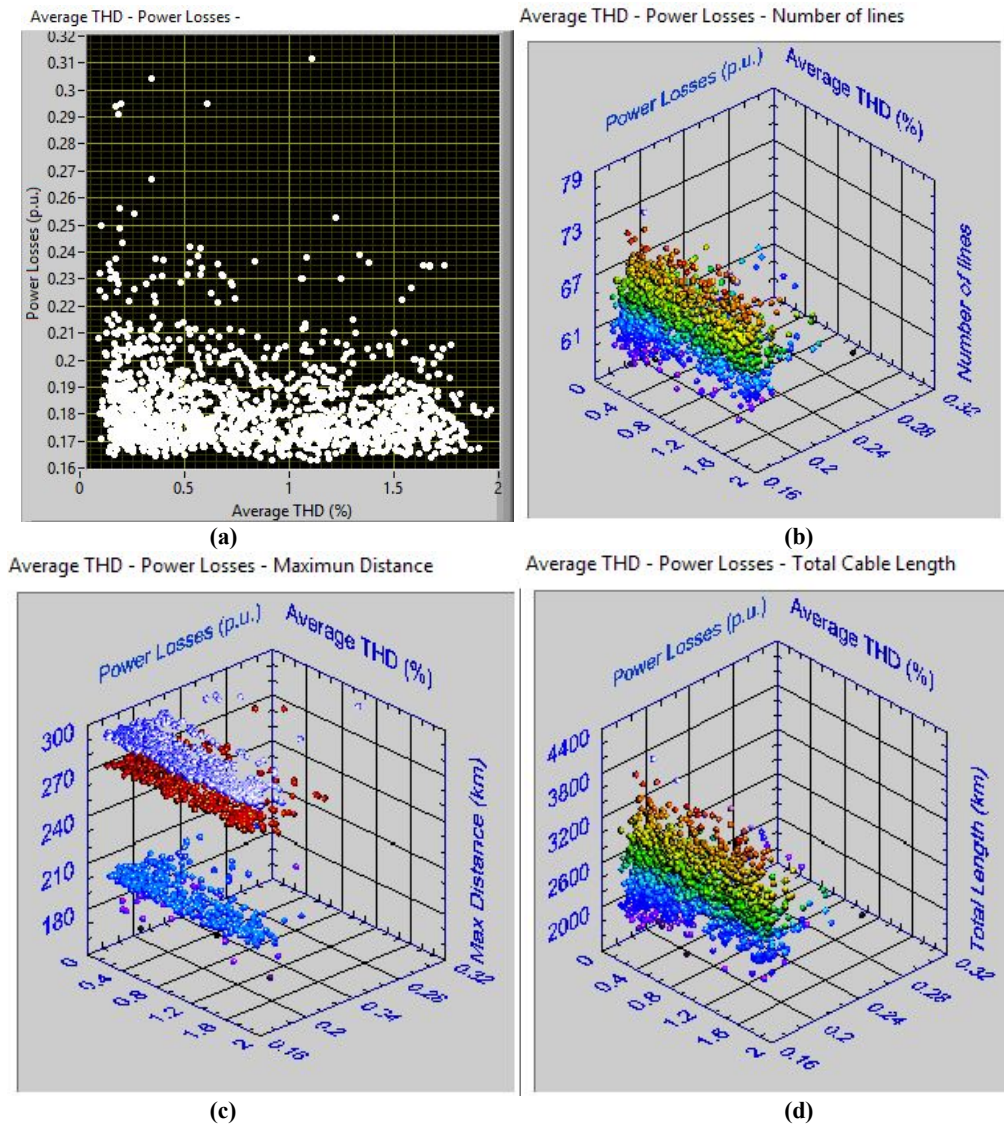
(c)   (d)
Figure 5.16. 1,500 random chromosomes generated.

5.2.6   Eliminating lines of the generated population

In the next stage, the algorithm checks for the longest distance between the nodes and eliminates it. If the new average THD is higher than the previous or the new configuration results with an isolated node, then the eliminated line is restored, and the algorithm continues with the next longest line. This is repeated until the criterion is

satisfied. In this case, the criterion is that all lines greater than a value of x kilometres will be eliminated. This x value allows multiple connections to nodes, mainly in the case of nodes that are closer. When x is zero, the algorithm obtains only a configuration of one branch. Figure 5.17 shows graphs for the 1,500 chromosomes generated after the number of lines is reduced by obtaining minimum distance tree for each chromosome and eliminating invalid chromosomes with a maximum distance of 45 km.

In Figure 5.17(a), it can be seen that when the number of lines decreases, the average THD decreases significantly but power losses increase at a lower rate. Additionally, in Figure 5.17(b), (c), and (d), it can be noted that the number of lines and max distance of the lines decrease significantly, consequently, the total length of the offshore network decrease too.
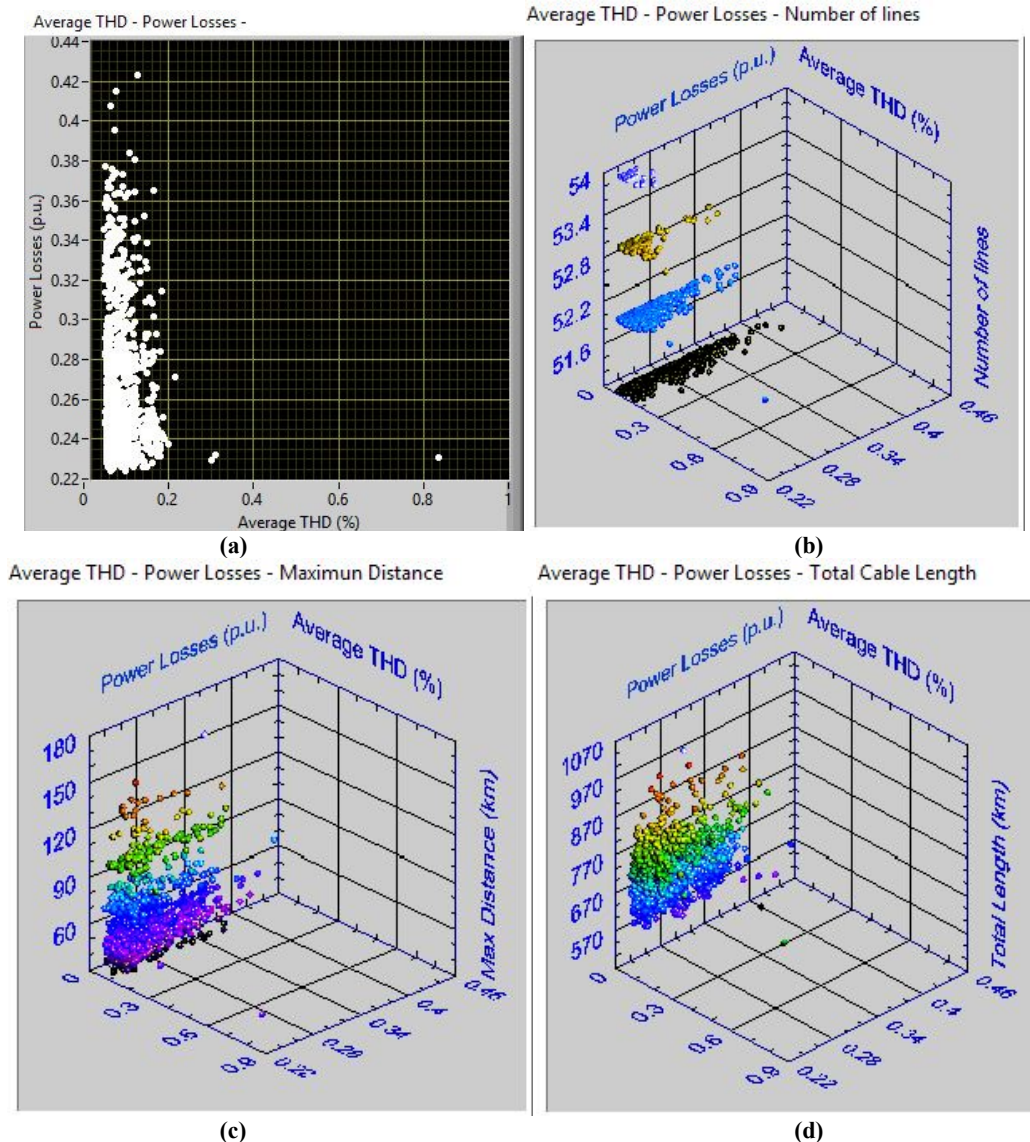
Figure 5.17. 1,500 random chromosomes generated after eliminating lines.

Figure 5.18 shows the configuration of a chromosome after the number of lines is reduced by obtaining minimum distance tree. This minimisation of lines is done for each generated chromosome.
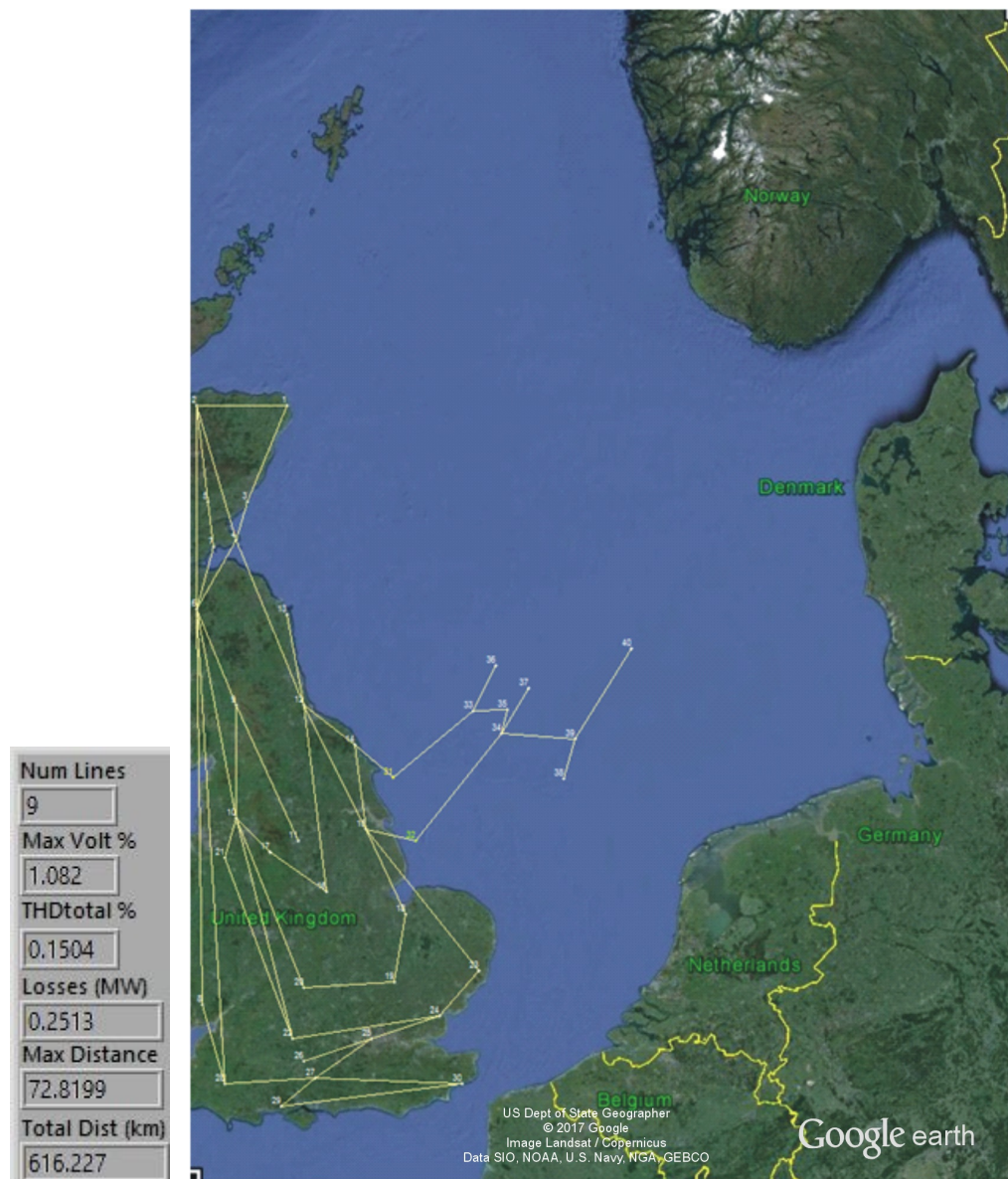
Figure 5.18 Network generated after eliminating lines.

It must be noted that the new chromosomes are very different from the initial population and the parameters are different as well. This is the first generation after the population was generated randomly, and with this generation, the process to obtain the best individuals will begin.

5.2.7   Obtaining the best individuals

With the number of lines minimised, the average THD of the population changes. These chromosomes are ordered from highest to lowest, and the best individuals are obtained using the Pareto front. This is the first generation of the best chromosomes. Each

chromosome is selected according to its fitness that is the comparison of the two functions to obtain the Pareto front. Figure 5.19 (a) and (b) shows 30 Pareto fronts, where only nine chromosomes are the best individuals of the first Pareto front. From Figure 5.19 (c), (d) and (e) other parameters can be evaluated to determine the best configuration using only the first Pareto front. Table 5.1 shows the data obtained for the first generation.

Generation of chromosomes number 1
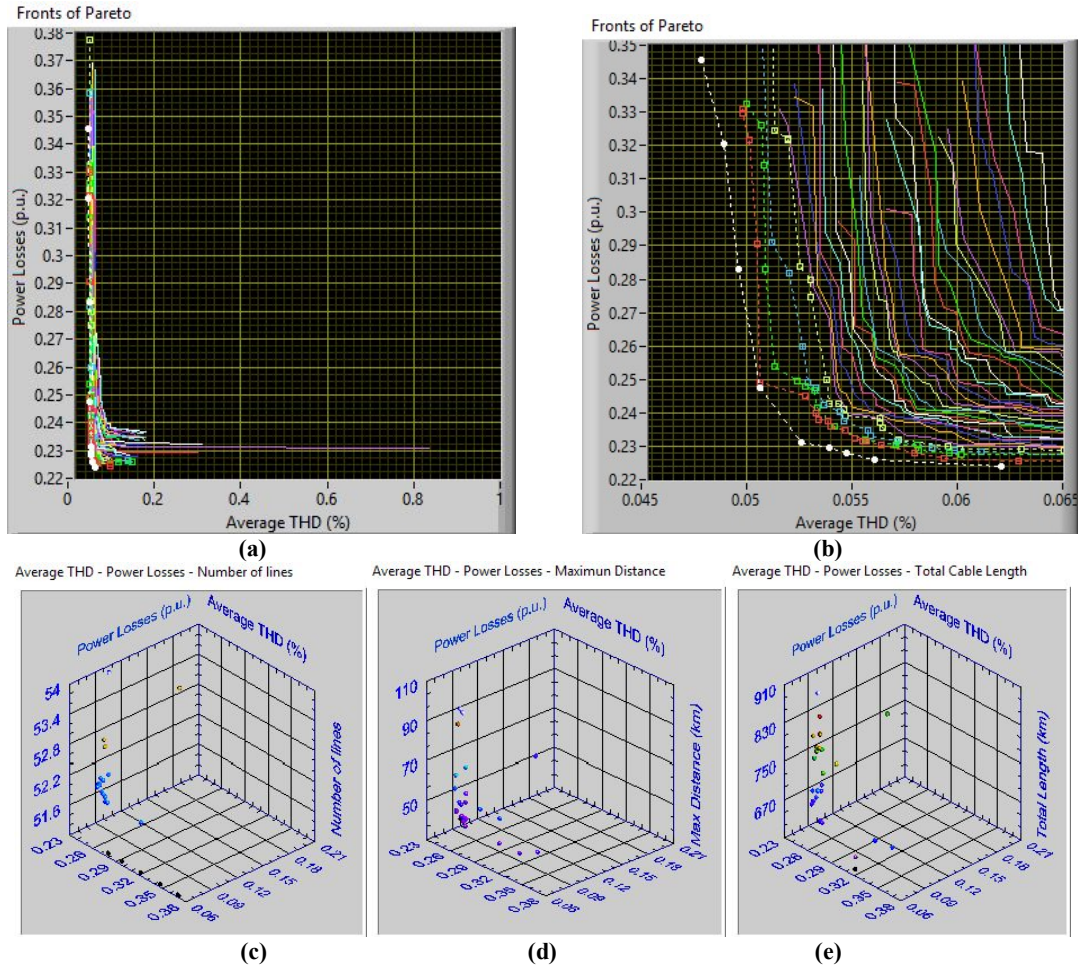
Figure 5.19. Pareto front is used to obtain the best individuals of first generation.

TABLE 5.1. DATA OBTAINED FOR THE FIRST GENERATION

	THD (%)	Power losses (p.u.)	Number of lines	Maximun distance (km)	Total cable length (km)
1	0.0478	0.3456	51	44.3771	604.6877
2	0.0489	0.3206	51	38.3902	609.1143
3	0.0496	0.2831	51	48.2967	590.0782
4	0.0506	0.2477	51	51.8084	603.3974
5	0.0526	0.2313	51	38.3902	594.8625
6	0.0539	0.2295	51	51.8084	667.8253
7	0.0547	0.2282	52	49.2254	677.8848
8	0.0561	0.2260	52	48.2967	688.7059
9	0.0621	0.2239	51	72.8199	731.8561

5.2.8   Generating new offspring with a genetic algorithm

The genetic algorithm proposed in Section 3.5.1 is implemented. With the best individuals obtained from all the Pareto fronts, a new population is generated. Each chromosome is selected according to its fitness, and the more suitable it is, the more chances it has to reproduce. Usually, a few chromosomes are the best, so all the chromosomes of the Pareto fronts are selected in pairs, and crossovers create two new individuals from each combination. These crossovers generate new offspring that will be part of the new generation.

After a crossover is conducted a mutation takes place to prevent the solutions from falling into a local optimum. The new offspring generated is processed to eliminate the longest lines according to the maximum distance allowed and, also to eliminate chromosomes that have isolated nodes or that which do not converge to a solution.

Figure 5.20 (a)-(e) shows the second generation of chromosomes. Table 5.2 shows the data obtained for the second generation of chromosomes.

Generation of chromosomes number 2
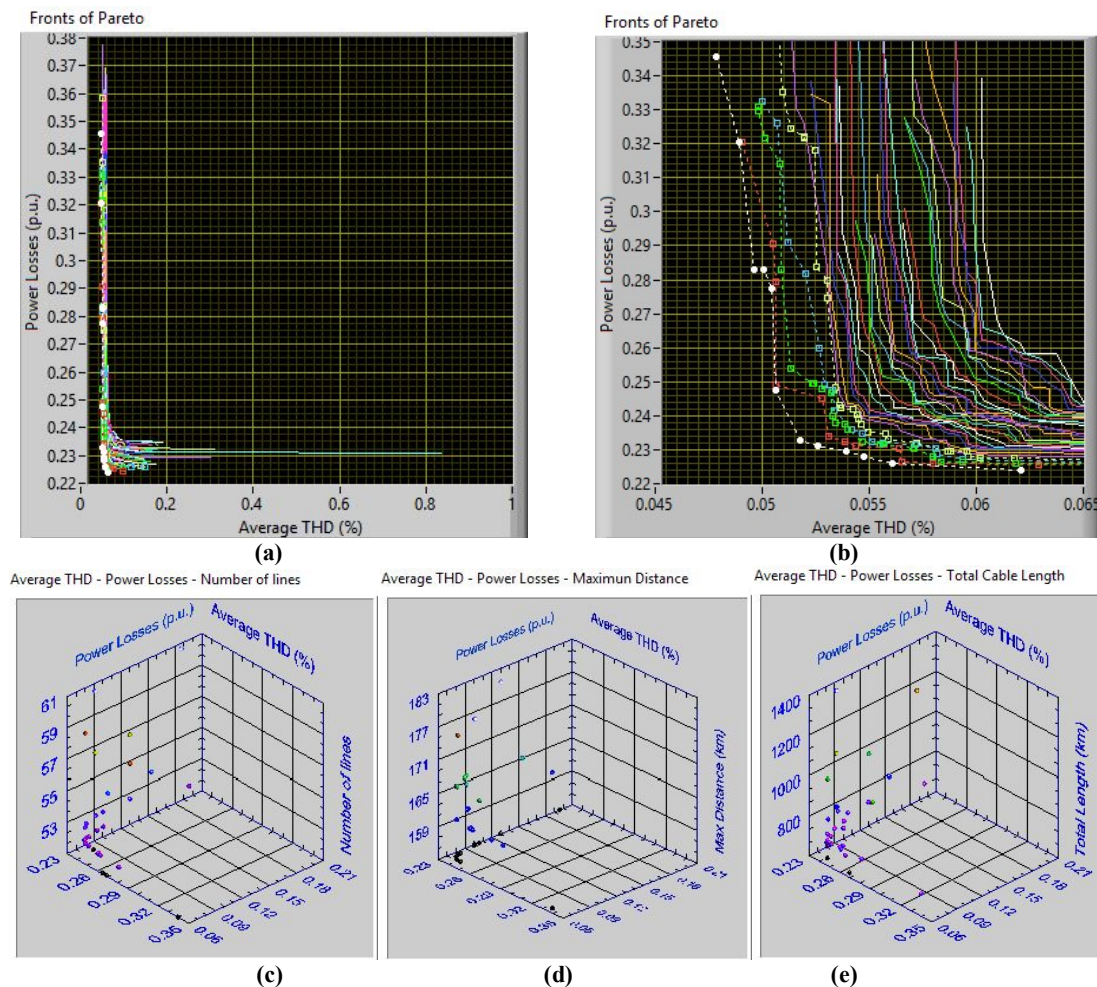
Figure 5.20. Use of Pareto front to obtain the best individuals of the second generation.

TABLE 5.2. DATA OBTAINED FOR THE SECOND GENERATION

	THD (%)	Power losses (p.u.)	Number of lines	Maximun distance (km)	Total cable length (km)
1	0.0478	0.3456	51	44.3771	604.6877
2	0.0489	0.3206	51	38.3902	609.1143
3	0.0496	0.2831	51	48.2967	590.0782
4	**0.0501**	**0.2831**	51	38.3902	618.2004
5	**0.0504**	**0.2774**	51	49.2254	617.7762
6	0.0506	0.2477	51	51.8084	603.3974
7	**0.0518**	**0.2328**	51	49.2254	623.0257
8	0.0526	0.2313	51	38.3902	594.8625
9	0.0539	0.2295	51	51.8084	667.8253
10	0.0547	0.2282	52	49.2254	677.8848
11	0.0561	0.2260	52	48.2967	688.7059
12	0.0621	0.2239	51	72.8199	731.8561

In the example, the second generation does not eliminate any individuals but obtains three new individuals that are integrated into the Pareto front. These new individuals (4, 5, and 7) are located in the middle part of the Pareto front. It is in this part of the algorithm that the analyst can use the data to make recommendations.

5.2.9   Report of the process

If the new Pareto front has at least one chromosome that is better, or if the required number of generations is not reached, then the algorithm creates another generation. Otherwise the algorithm stops and generates the final report in HTML, which could be exported to other formats. Another option to finish the process is when there is no new chromosome in a determined number of generations.

In this example, there are only two generations. The report includes the total processing time, data of the networks, data of the power flow and harmonic propagation, the DPI graph, harmonic voltages graph, and the configuration map for each chromosome.

In this case, the process to generate 1,500 chromosomes and evaluate and obtain the best individuals takes 13 hours and 20 minutes and this generates only two generations with 12 chromosomes or configurations as the best.

Total processing data time
13:20:37.361 = 48,037.361 seconds
12 chromosomes generated as the best options after 2 generations.

The report includes information for each configuration or chromosome that is included in the Pareto front. This information includes all data input of the network generated: generation data, network voltage and loads, reactive power, data for lines and transformers, shut elements, generator impedances, nodes with an injection of harmonics,

and percentage and angle of harmonics injected. In addition, the data output is included: power flow report, lines power flow, generation, demand and losses, and the harmonic propagation report.

In this example, only the DPI graph, harmonic voltages graph, and configuration map of the first and twelfth chromosomes are shown. Figure 5.21 shows the DPI graph and Figure 5.22 shows harmonic voltages on the network nodes including the fundamental frequency. Figure 5.23 shows only the harmonic graph without fundamental frequency and Figure 5.24 shows the network proposed for Configuration 1.

*** Results *** Configuration 1
Base: 10,000,000
Number of lines and Transformers: 51
Generation Nodes: 16
Load Nodes: 24
Total Nodes: 40
Number of elements in derivation: 2
Load nodes with harmonics injected: 8
Number of harmonics to be considered: 7
Processing time of Power Flow and Harmonic Propagation Study : 00:00:0.939 = 0.939 seconds
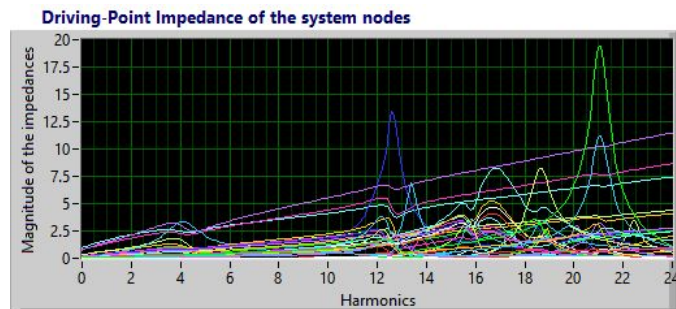
Figure 5.21. DPI graph for Configuration 1.
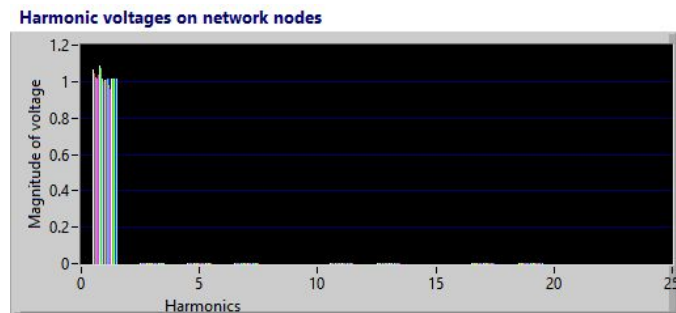
Figure 5.22. Harmonic graph including the fundamental frequency for Configuration 1.
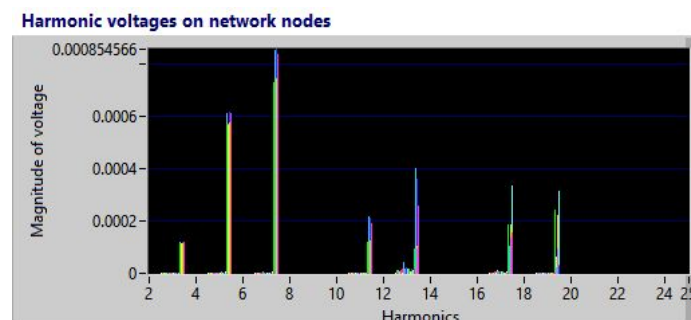
Figure 5.23. Harmonic graph for Configuration 1.

Map of the North Sea with connection option 1
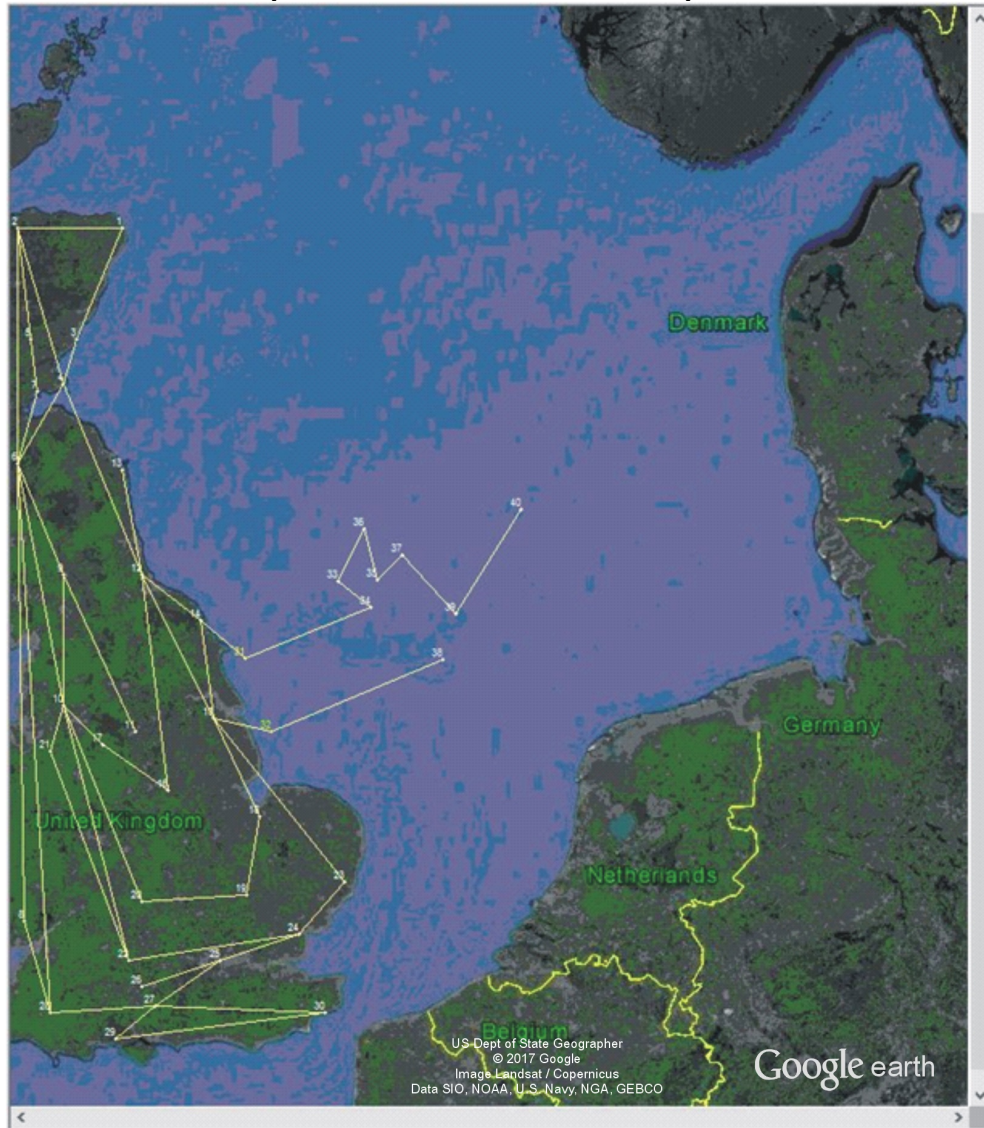
Figure 5.24. Configuration 1.

Number of iterations: 4
Error : 9.543471E-6
Generation : 2.779562 p.u.
Demand : 2.434000 p.u.
Power Losses: 0.345570 p.u..

Figure 5.25 shows the DPI graph. Figure 5.26 shows the harmonic graph without the fundamental frequency. Figure 5.27 shows the network proposed for Configuration 12.

*** Results *** Configuration 12
Base: 10000000
Number of lines and Transformers: 51
Generation Nodes: 16
Load Nodes: 24
Total Nodes: 40
Number of elements in derivation: 2
Load nodes with harmonics injected: 8
Number of harmonics to be considered: 7
Processing time of Power Flow and Harmonic Propagation Study : 00:00:1.001 = 1.001 seconds
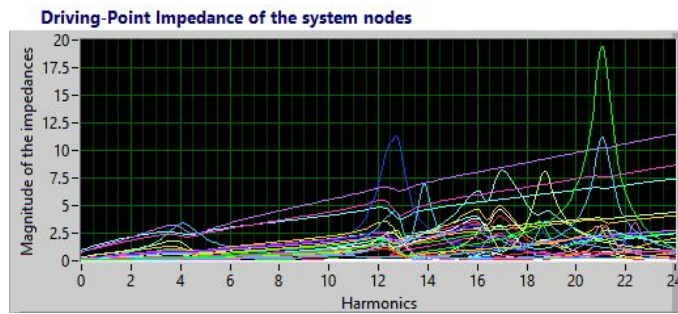
Figure 5.25. DPI graph for Configuration 12.
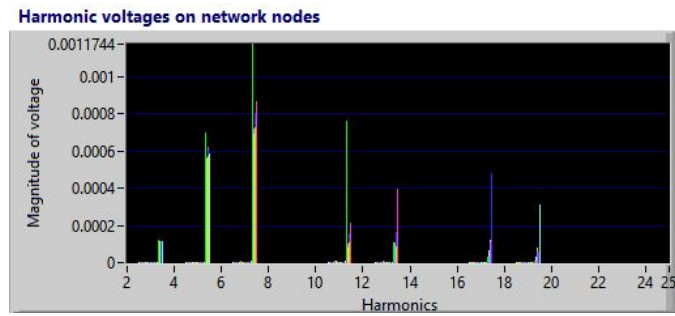
Figure 5.26. Harmonic graph for Configuration 12.

Map of the North Sea with connection option 12
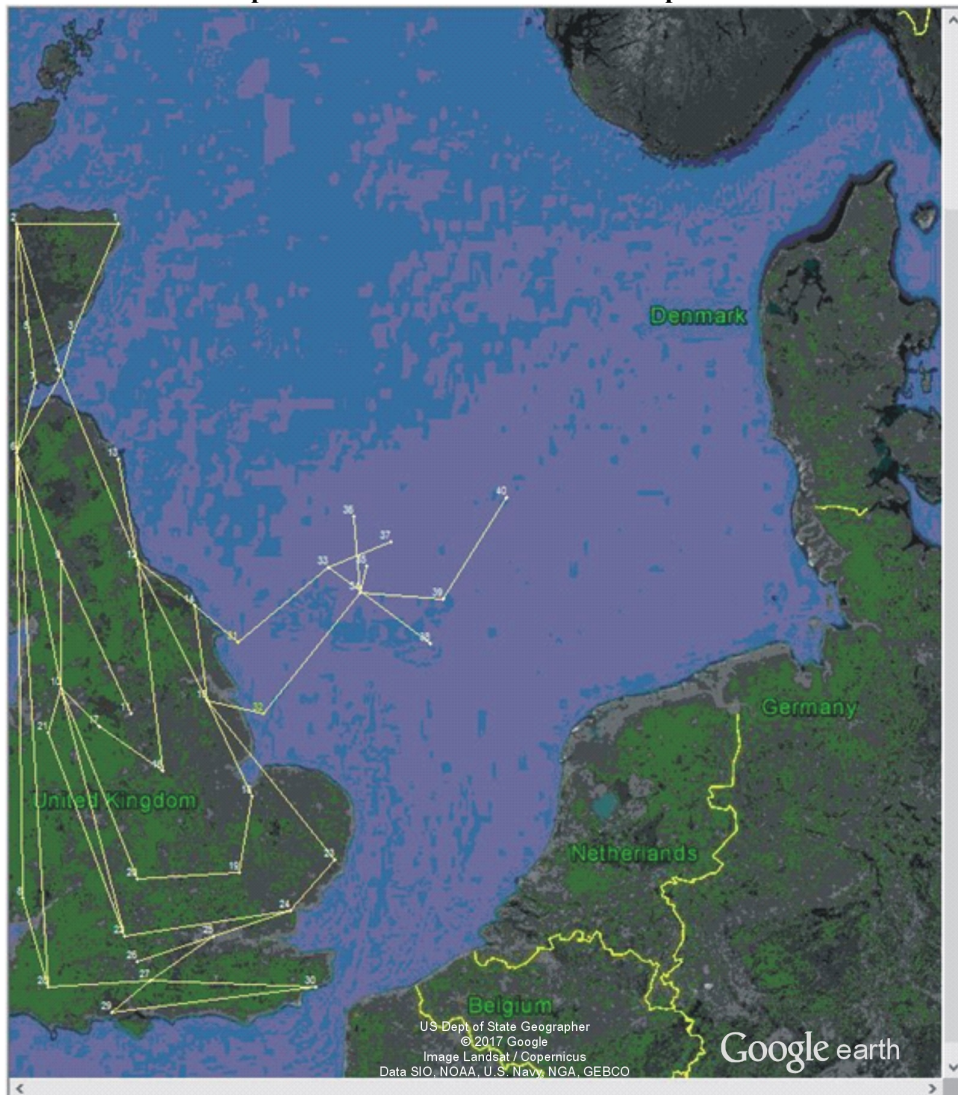
Figure 5.27. Configuration 12.

Number of iterations: 4
Error: 1.065607E-6
Generation: 2.657905 p.u.
Demand: 2.434000 p.u.
Power Losses: 0.223906 p.u.

5.3   Processing time to generate an initial population

The algorithm calculates and compares the average voltage THD and power losses of the complete network, and for the offshore wind power cluster, the maximum number of new lines, the maximum distance between wind power clusters, interconnections with the onshore grid, and total new cable length are calculated and compared. With this information, the algorithm will suggest the best configuration for the offshore network interconnected with the onshore AC grid. The processing time to obtain harmonic propagation and power flow depends on the number of nodes and lines generated. Furthermore, the processing time depends on the number of chromosomes generated in the initial population.

The number of chromosomes generated in the initial population is important because the algorithm could consume much time in eliminating lines to generate the first generation of chromosomes. If the number of the initial population is high, the algorithm will take too much time in the process, but if the number is low, the results could not be optimal.

5.3.1   Time to generate one chromosome

The next examples compare the time taken to generate a chromosome with different maximum distances. The algorithm runs under *Windows 10, 64 bits,* using an *Acer Aspire R14,* with a processor *Intel Celeron 3205U, 1.5GHz, 5.92 GB RAM.*

To generate 1 chromosome when maximum distance is 300 km, the generation time is 1.559 seconds. If the maximum distance is 250 km, then the generation time increases to 5.027 seconds and when the maximum distance is 200 km, the generation time increases to 47.782 seconds.

The time to generate each chromosome will depend on the distance allowed to connect the nodes. If the distance is too short, generating random chromosomes will be more difficult, because options for the random combination of nodes will be reduced drastically, and the consequence is that the generation of the population will take more time. It is better to allow a longer distance and then eliminate lines because the process to

eliminate lines takes almost the same time for each chromosome but is lower than the generation time with shorter lines.

It must be noted that if the distance allowed is shorter than the shorter line, the algorithm will not find a feasible configuration.

5.3.2   Time comparison in the generation of chromosomes

Time comparison is made in order to contrast the time between different numbers of chromosomes generated for the initial population when maximum distance is set to 45 km. Generating 10 chromosomes takes 14.573 seconds; 100 chromosomes takes 2 minutes, 30.401 seconds; 1,000 chromosomes takes 24 minutes, 22.411 seconds; and 31,536 chromosomes takes 15 hours, 55 minutes, and 7.558 seconds.

5.3.3   Time comparison with the elimination of lines

The process to eliminate lines will improve the overall process by avoiding a waste of time in the generation of the initial population when maximum distance is set to 45 km. Generating 10 chromosomes after eliminating the longest lines takes 4 minutes, 51.536 seconds; 100 chromosomes takes 46 minutes, 26.356 seconds; and 1,000 chromosomes take 7 hours, 41 minutes, and 47.67 seconds.

In the next Chapter there is the comparison when the algorithm is used as a mono-objective function and as a multi-objective function and how the use of multi-objective function improved the results.

5.4   Summary

In this chapter, an algorithm to reduce the adverse effects of the harmonic propagation in the network has been developed, specifically in the grid proposed for the North Sea wind power clusters. The algorithm developed was implemented to create an MOEA in order to obtain the desired results.

The implementation of the Newton-Raphson method to calculate power flow is the essential stage to obtain the functions that are to be implemented.

The chromosomes must be validated first in order to obtain reliable results. If the algorithm that calculates harmonic propagation and power flow does not converge to a valid solution, the chromosome must be eliminated. If there is at least one isolated node, the chromosome must be eliminated, because the algorithm to calculate power flow will not converge to a valid solution.

The chromosomes generated used fixed nodes to integrate the energy into the mainland. The nodes are located on a map, and each node is represented on the fixed network. The data of each line in the fixed network does not change, but, in the case of offshore wind power clusters, the proposed length and parameters of the cable are essential, because the data line changes depending on the nodes that are connected.

It is important to remark that in the proposed algorithm the study is done using wind power clusters, but could be implemented any type of power system.

Latitude and longitude are also necessary to calculate the distance between nodes. The parameters of the line can be calculated if the distance is known to generate the network and to obtain power flow and harmonic propagation. To calculate the distance between two points on a sphere the haversine formula is implemented. The haversine formula calculates an accurate result.

If the cable diameter changes, the harmonics will be affected, thicker diameters would decrease the harmonic propagation, but the cost will be increased considerably, in that way it is important to define the best cable diameter to reduce the cost, but this function it is not implemented in the algorithm. Also, it is not implemented the possibility to have two or more connection between two nodes, this option could reduce the cost of the cable and the harmonic propagation. To implement a subroutine to determine the best cable diameter it is necessary the information of the cable.

Time comparison it is done to select the best distance to connect each node. The processing time depends on the number of nodes and lines generated. Also, it depends on the number of chromosomes generated in the initial population. If the number of the initial population is high, the algorithm will take too much time to process, but if the number is low, the results could be less than optimal. To improve the performance of the algorithm, the initial population should not have restrictions on the number and length of lines.

After the initial population is generated, the algorithm eliminates the number of lines according to the restrictions of length. This stage improves the evolutionary algorithm to start the genetic algorithm having improved the first generation.

Pareto fronts help to minimise the number of chromosomes, eliminating all the chromosomes that do not comply with parameters according to the constraints implemented in the algorithm. The best chromosomes are kept for the next generation.

The crossover is done by pairs between all the chromosomes of the Pareto fronts selected. This is because, in this specific problem, the Pareto front does not generate too many valid chromosomes. Furthermore, many chromosomes are eliminated because there are isolated nodes, or the solution does not converge to any valid parameters. With the number of chromosomes, in the next generation, the probability of finding a better solution is low. Usually, only a few chromosomes are generated in this second generation.

The consequences of eliminating lines are the: decrease in the total length of the cable. In addition, the average THD decreases, but power losses increase.

The algorithm automatically generates the report to compare different options and has the possibility of suggesting the best configuration. These reports can be used to make recommendations for possible control strategies of wind power clusters planned for the near future in the North Sea. Also, the algorithm can be implemented in other locations for a variety of projects.

The MOEA developed performs well in reconfiguring the network proposed. Comparisons of time processing suggest that it is better to use all the possible connections and then go onto eliminating the most extended lines. This procedure efficiently improves processing time.

6   **Case studies, results, and discussion**

Different scenarios were proposed, and each scenario had a different number of wind power clusters located at different locations within an area. Latitudes and longitudes of each wind power cluster were used to calculate the distances and impedances of the lines. An onshore fixed 30 nodes AC grid was considered, and the 30 nodes grid is the IEEE-30 nodes modified in this research for harmonic analysis. The onshore and offshore grids are considered to be placed in the North Sea. Nodes for Scenario 1 are shown in Figure 6.1.

Figure 6.1. Nodes used for Scenario 1.

Scenario 1: This scenario has two nodes that can be connected to 8 offshore wind power clusters, each one of 1.2 GW. The whole network consists of 40 nodes; the first 30 nodes correspond to the onshore AC grid. Node 31 is connected to node 14 and node 32 is connected to node 15. The offshore wind power clusters are located near the Dogger Bank, ranging from 125 km to 290 km of the shore.

Scenario 2: This scenario has eight offshore wind power clusters corresponding to 4 of the Dogger Bank and 4 of the Hornsea. The whole network is of 38 nodes, and as per Scenario 1, the first 30 nodes correspond to the onshore AC grid. Nodes 12, 13, 14, and 15 can be connected to the offshore wind power clusters. The eight offshore wind power clusters are the following: Creyke Beck A and B and Teeside A and B, each one of 1.2 GW, Hornsea project One of 1.2 GW, Hornsea project Two of 1.8 GW, Hornsea project Three of 2 GW, and Hornsea project Four of 1 GW. Nodes for Scenario 2 are shown in Figure 6.2.

Figure 6.2. Nodes used for Scenario 2.

Scenario 3: This scenario has 15 offshore wind power clusters located at Dogger Bank, Hornsea, and Seagreen, The whole network is of 45 nodes, the first 30 nodes correspond to the onshore AC grid. Wind power clusters can be connected to nodes 3, 4, 12, 13, 14, and 15. The 15 offshore wind power clusters are the following: Creyke Beck A and B and Teeside A and B, each one of 1.2 GW, Hornsea project One of 1.2 GW, Hornsea project Two of 1.8 GW, Hornsea project Three of 2 GW and Hornsea project Four of 1 GW, Seagreen Alpha and Bravo of 525 MW, Charlie of 610 MW, Delta and Echo of 605 MW, Foxtrot of 565 MW, and Golf of 225 MW. Nodes for Scenario 3 are shown in Figure 6.3.

Figure 6.3. Nodes used for Scenario 3.

Scenario 1 is compared with 50, 100, 1,000, and 2,000 chromosomes generated. The purpose of comparing different numbers of generated chromosomes is to show that with 100 chromosomes, the results are adequate.

6.1   Time elapsed in generating chromosomes using Scenario 1

Using Scenario 1, the total time to generate and process 50 chromosomes is 30 minutes; 100 chromosomes is 46 minutes; 1,000 chromosomes is 8 hours 41 minutes, and 2,000 chromosomes is 17 hours 34 minutes. To compare the time elapsed, there are only two generations.

6.1.1   Scenario 1, time of chromosomes generated

To generate 100 chromosomes the time elapsed is 1 minute and 55 seconds, in comparison with 20 minutes and 53 seconds taken to generate 1,000 chromosomes and 43 minutes and 36 seconds to generate 2,000 chromosomes for Scenario 1.

The results are similar to the results obtained after processing chromosomes when 1,000 and 2,000 chromosomes are generated, but the generation time decreases significantly. Graphs are obtained automatically from the report generated by the algorithm. In Figure 6.4 graphs of chromosomes after the longest lines are eliminated are shown, and a minimal tree for each configuration is obtained. The graphs are for 100 chromosomes generated. In the XY graph, most of the chromosomes are between 0.225 and 0.3 per unit in the power losses in axe y and between 0.05 to 0.1 percent of average THD in axe x. Some chromosomes are excluded from this area.

It can be observed that power losses have increased, but the average THD has decreased, similar to in the generation of 1,000 and 2,000 chromosomes. To obtain minimum distance trees, the time elapsed is 44 minutes in comparison with the time elapsed of 8 hours 34 minutes taken to generate 1,000 and the time elapsed of 17 hours 10 minutes taken to generate 2,000 chromosomes.
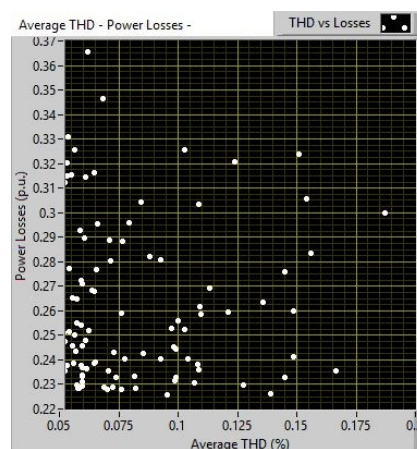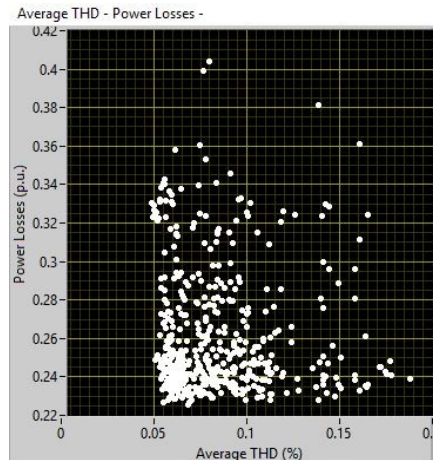

Figure 6.4. Longest lines eliminated of the 100 chromosomes generated.

Figure 6.5 shows the best chromosomes of the second generation after the crossover and mutation process. There are 5 Pareto fronts of the functions of average THD and power losses shown. To generate 100 chromosomes, to eliminate the longest distances, to eliminate chromosomes that do not converge to a solution, to obtain the best chromosomes using the Pareto front, and to use the best chromosomes to crossover and mutate to obtain a second generation, it entails an elapsed time of 46 minutes and 40 seconds that can be compared with 8 hours 41 minutes taken to generate 1,000 chromosomes and 17 hours 34 minutes taken to generate 2,000 chromosomes. After two generations, the algorithm generates 9 chromosomes or configurations as the best options.
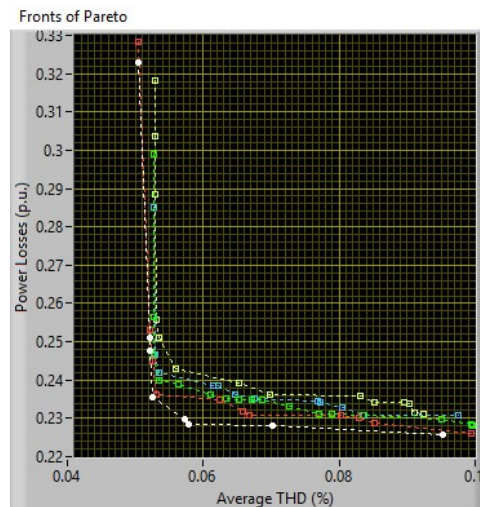
Figure 6.5. Pareto front obtained in the second generation of 100 chromosomes generated.

Table 6.1 shows the data obtained for the best chromosomes of the second generation after the crossover and mutation process. It must be noted that there is not necessarily a coincidence between the best options with the number of lines, the longest distance, or the total length of the cable.

TABLE 6.1. DATA OBTAINED FOR THE SECOND GENERATION OF 100 CHROMOSOMES

	THD (%)	Power losses (p.u.)	Number of lines	Maximun distance (km)	Total cable length (km)
1	0.0496	0.3311	51	72.8199	616.8069
2	0.0505	0.3228	51	56.7809	578.9156
3	0.0520	0.2465	51	56.7809	637.9391
4	0.0521	0.2424	52	51.8084	656.7756
5	0.0525	0.2356	52	44.3771	637.3500
6	0.0572	0.2298	53	48.2967	716.0741
7	0.0578	0.2283	52	72.8199	631.7711
8	0.0702	0.2280	51	44.3771	631.9523
9	0.0939	0.2251	53	48.2967	772.0124

6.1.2   Different number of chromosomes for Scenario 1

Figure 6.6 shows the Pareto front's comparison with the different number of chromosomes generated: 50, 100, 1,000, and 2,000 chromosomes. Figure 6.6 (a) shows the full range, and Figure 6.6 (b) shows a zoomed-in version of the results in a range of 0.049 to 0.066 of the average THD and 0.223 to 0.25 of power losses. Results indicate that the configurations of the network approach the average THD to 0.05 percent and power losses to 0.223 per unit as the best configuration of the network. This approach is independent of the number of chromosomes generated as part of the first generation. This criterion can be used to suggest a configuration for the offshore wind power clusters.

The time to generate only 100 chromosomes decreases significantly, and the results in comparison with a larger number of generated chromosomes are similar. So, it is a good approximation to start the first generation with ten times the nodes that are changing connections and then generate ten times the number of initially generated chromosomes.

(a)   (b)
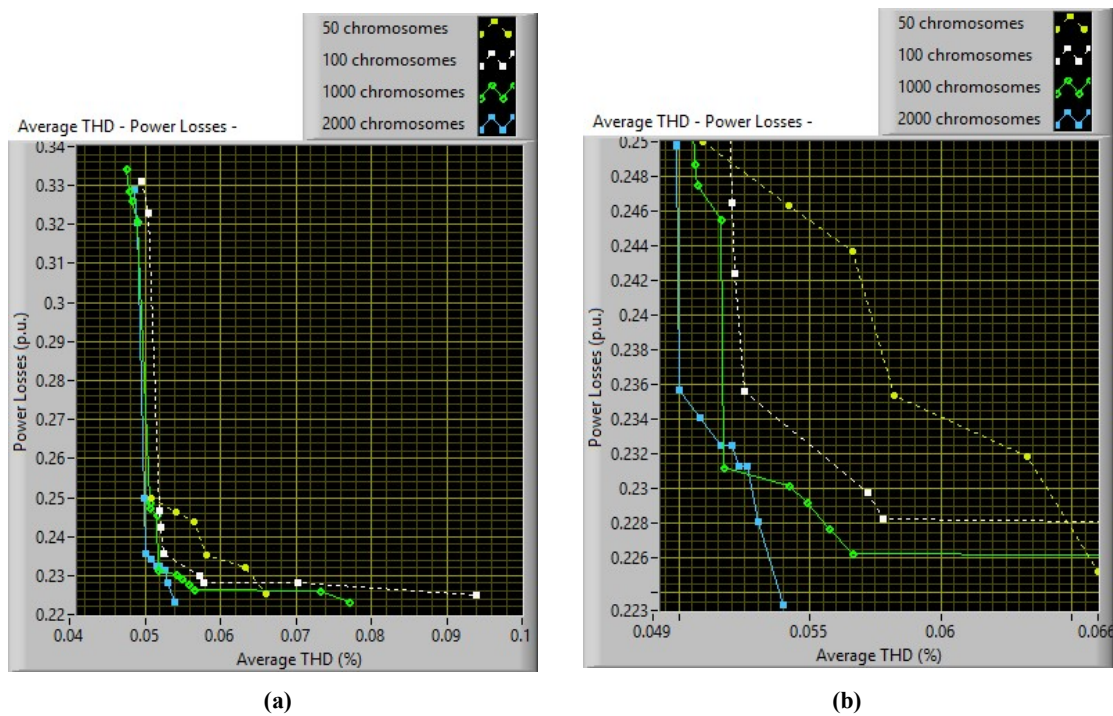
Figure 6.6. Comparison of results with a different number of chromosomes for Scenario 1.

6.2   Mono and multi-objective functions

An algorithm is used to create 500 chromosomes in order to compare results when only one function is used to obtain results and when multiple functions are used. For this purpose, Scenario 1 was used to obtain data.

6.2.1   Using mono-objective function

On first generation, 500 chromosomes are generated, and after 1,000 generations, 241 chromosomes are generated. Figure 6.7 shows the results ordered by the logarithmic average of THD, and the values are from 0.0478 to 0.1383 %.
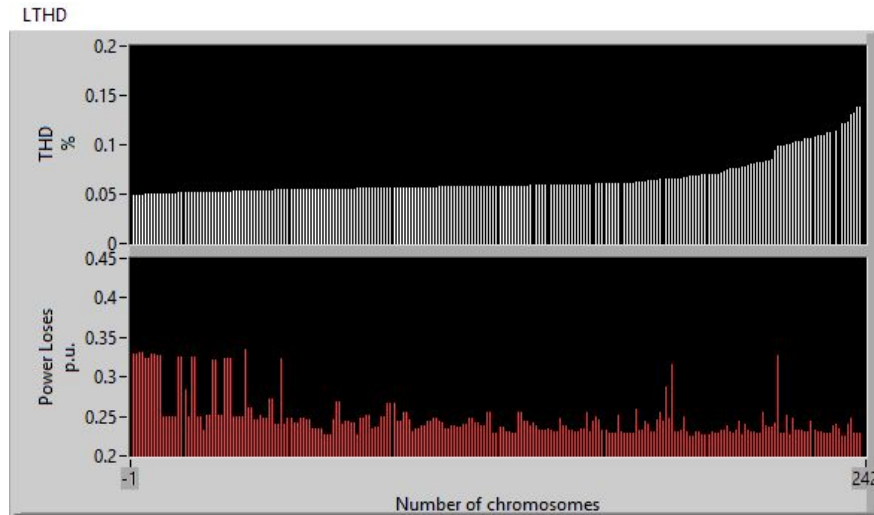
Figure 6.7. Functions ordered by logarithmic average of THD: 0.0478 % - 0.1383 %.

Table 6.2 shows the data ordered by the logarithmic average of THD. It is found that the logarithmic average of THD values are increasing, but all the other variables do not have a sequence. This could result in a low logarithmic average of THD, but the corresponding power losses are too high. The same results emerge for the other variables. Only the first ten chromosomes are shown.

TABLE 6.2. DATA ORDERED BY LOGARITHMIC AVERAGE OF THD

	THD (%)	Power losses (p.u.)	Number of lines	Maximun distance (km)	Total cable length (km)
1	0.0478	0.3287	51	167.1298	591.8186
2	0.0478	0.3293	51	167.1298	627.7066
3	0.0485	0.3304	51	167.1298	591.8186
4	0.0497	0.3228	51	167.1298	612.9728
5	0.0498	0.3290	51	167.1298	591.9106
6	0.0501	0.3267	51	167.1298	625.3344
7	0.0506	0.2487	51	167.1298	571.4340
8	0.0506	0.2490	51	167.1298	607.3220
9	0.0509	0.3252	51	167.1298	607.9495
10	0.0509	0.2832	51	153.8767	631.0162

Figure 6.8 shows the values ordered by power losses, with values from 0.2251 to 0.3354 p.u. The results are similar, as power losses are increasing, but the corresponding values of the logarithmic average of THD do not have a sequence similar to other functions.
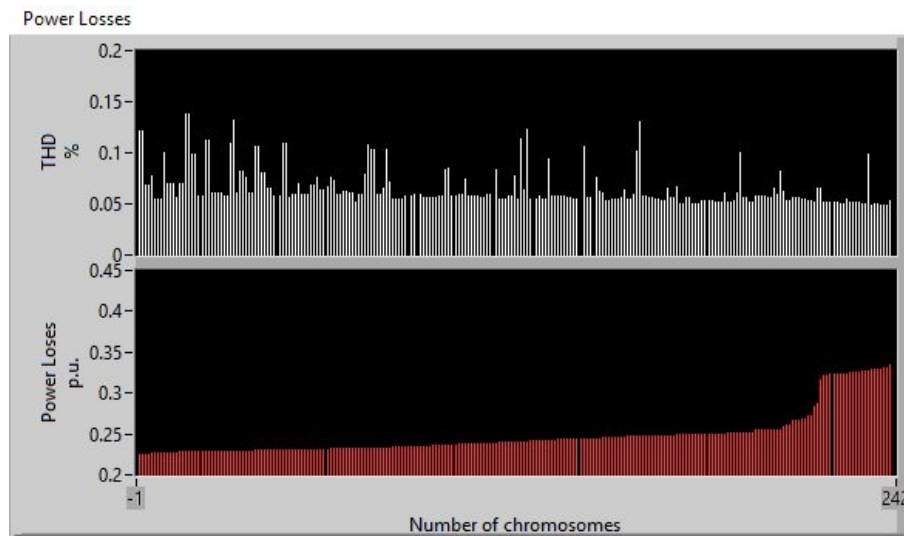
Figure 6.8. Functions ordered by power losses: 0.2251 p.u. – 0.3354 p.u.

Table 6.3 shows data ordered by power losses. It is found that power losses values are increasing, but all the other variables do not have a sequence. Only the first ten chromosomes are shown.

TABLE 6.3. DATA ORDERED BY POWER LOSSES

	THD (%)	Power losses (p.u.)	Number of lines	Maximun distance (km)	Total cable length (km)
1	0.1218	0.2251	53	153.8767	724.7720
2	0.0682	0.2253	53	153.8767	732.7091
3	0.0770	0.2258	53	153.8767	789.8820
4	0.0548	0.2266	52	153.8767	628.6891
5	0.1007	0.2267	53	153.8767	683.9423
6	0.0692	0.2267	54	153.8767	785.5422
7	0.0555	0.2269	52	153.8767	636.6262
8	0.0704	0.2277	52	153.8767	637.2424
9	0.1383	0.2278	51	153.8767	636.0743
10	0.0992	0.2279	53	153.8767	693.3438

6.2.2 Using multi-objective function

The same 500 generated chromosomes are used to compare results when the multi-objective algorithm is used, the maximum distance is 45 km, and 5 Pareto fronts are considered. The maximum distance of 45 km is considered to avoid distances too large, but the algorithm is allowed to interconnect with more than one line to each node. Figure 6.9

shows the chromosomes after the longest lines were eliminated. An XY graph with the logarithmic average of THD and power losses is shown. The time elapsed to obtain minimum distance trees and eliminate invalid chromosomes is 4 hours and 5 minutes.

Figure 6.9. Longest lines eliminated of the 500 chromosomes generated.

Figure 6.10 shows the best 7 chromosomes after the crossover and mutation process.
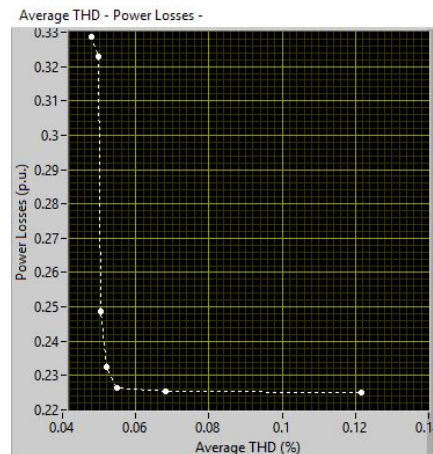
Figure 6.10. Pareto front obtained after 1,000 generations with the first generation of 500 chromosomes.

Table 6.4 shows the data of the best 7 chromosomes after 1,000 generations. First, the fifth and seventh chromosomes are highlighted to compare the results with the mono-objective function.

TABLE 6.4. DATA OBTAINED FOR 500 CHROMOSOMES GENERATED AFTER 1,000 GENERATIONS

	THD (%)	Power losses (p.u.)	Number of lines	Maximun distance (km)	Total cable length (km)
1	**0.0478**	**0.3287**	**51**	**167.1298**	**591.8186**
2	0.0497	0.3228	51	167.1298	612.9728
3	0.0506	0.2487	51	167.1298	571.4340
4	0.0519	0.2324	51	153.8767	625.0930
5	**0.0548**	**0.2266**	**52**	**153.8767**	**628.6891**
6	0.0682	0.2253	53	153.8767	732.7091
7	**0.1218**	**0.2251**	**53**	**153.8767**	**724.7720**

From Table 6.2, the best chromosome generated for the logarithmic average of THD is the first option in Table 6.4 that shows results when it is used in the multi-objective algorithm. The logarithmic average of THD is 0.0478%, and the power losses value is 0.3287 p.u. Furthermore, using additional information, this configuration has 51 lines, and the total cable length is 591.81 km. Figure 6.11 shows the first configuration proposed by the algorithm.
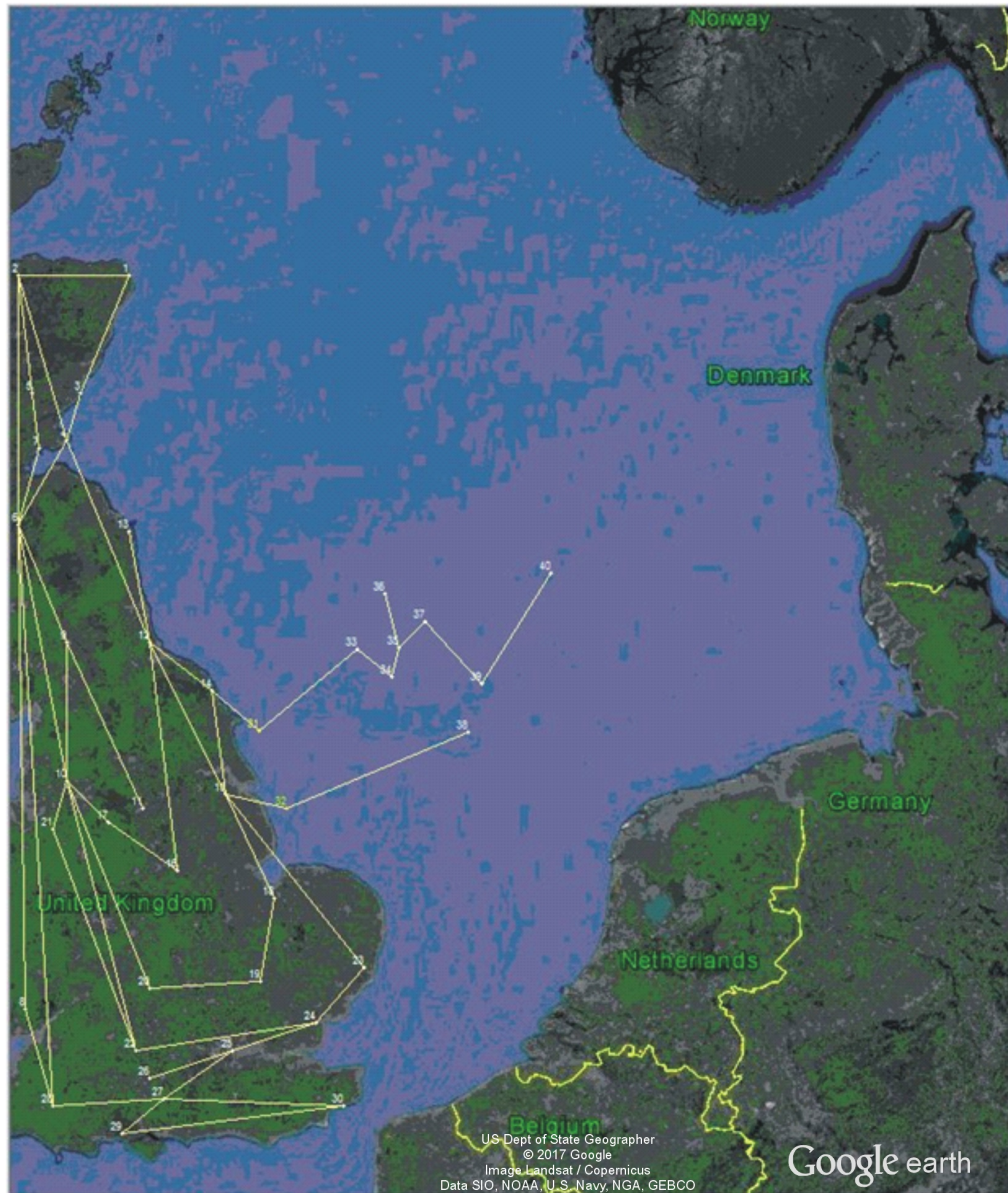
Figure 6.11. Configuration 1 for Scenario 1.

From Table 6.3, the best chromosome generated for power losses is the last option in Table 6.4 that shows results when it is used the multi-objective algorithm. The logarithmic average of THD is higher than the first option at 0.1218%, and the power losses value is lower at 0.2251 p.u. Also, using additional information, this configuration

has two more lines, 53 lines, and the total cable length is longer at 724.77 km. Figure 6.12 shows the last configuration proposed by the algorithm.
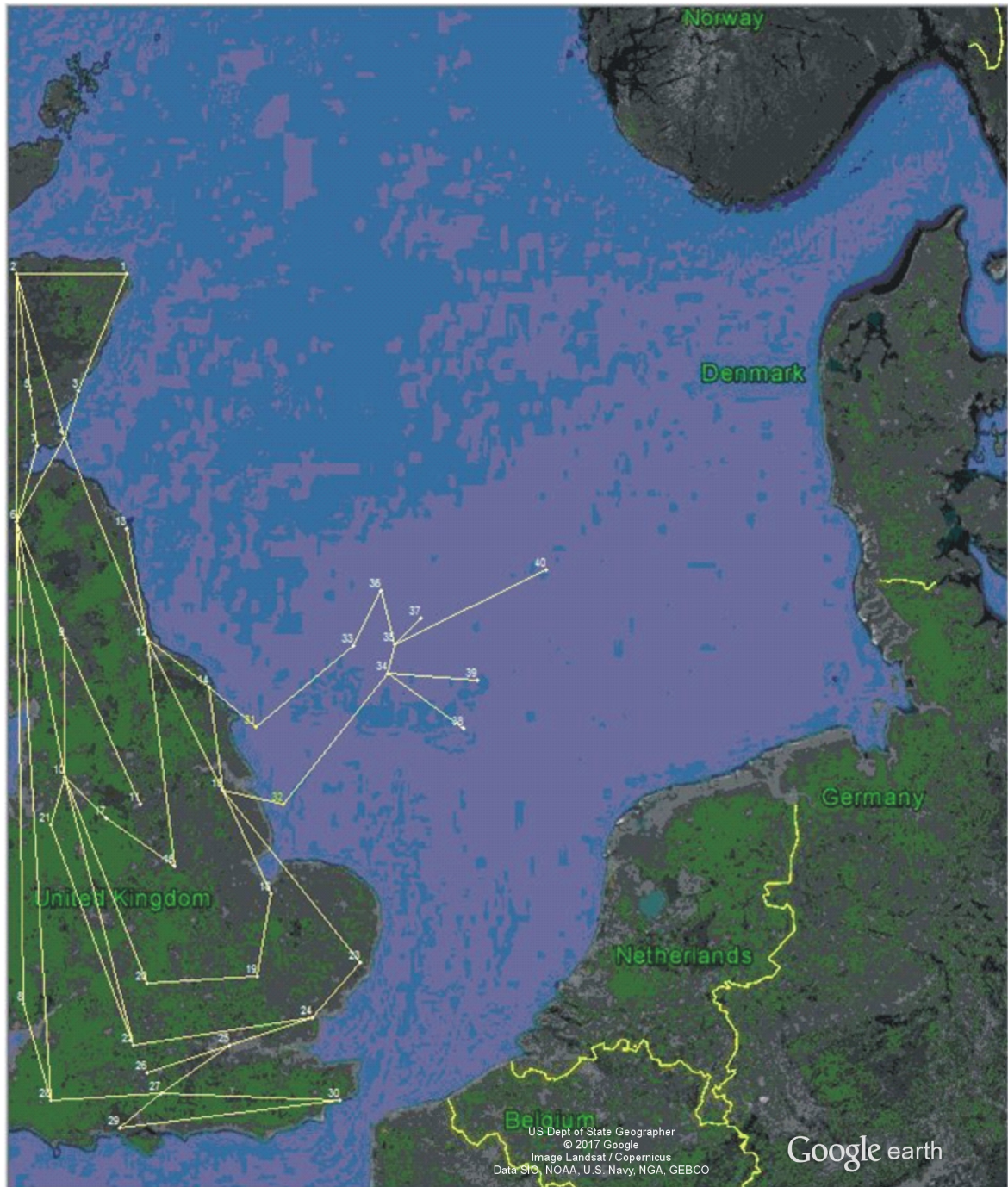
Figure 6.12. Configuration 7 for Scenario 1.

Choosing the fifth chromosome from Table 6.4, there is an interaction between the two objective functions. The logarithmic average of THD is higher than the first option, but it is lower than last option at 0.0548%, and the power losses value is also lower than the first option but higher than last option at 0.2266 p.u. Also, using additional information,

this configuration has 52 lines, and the total cable length is 628.68 km. Figure 6.13 shows the fifth configuration proposed by the algorithm.
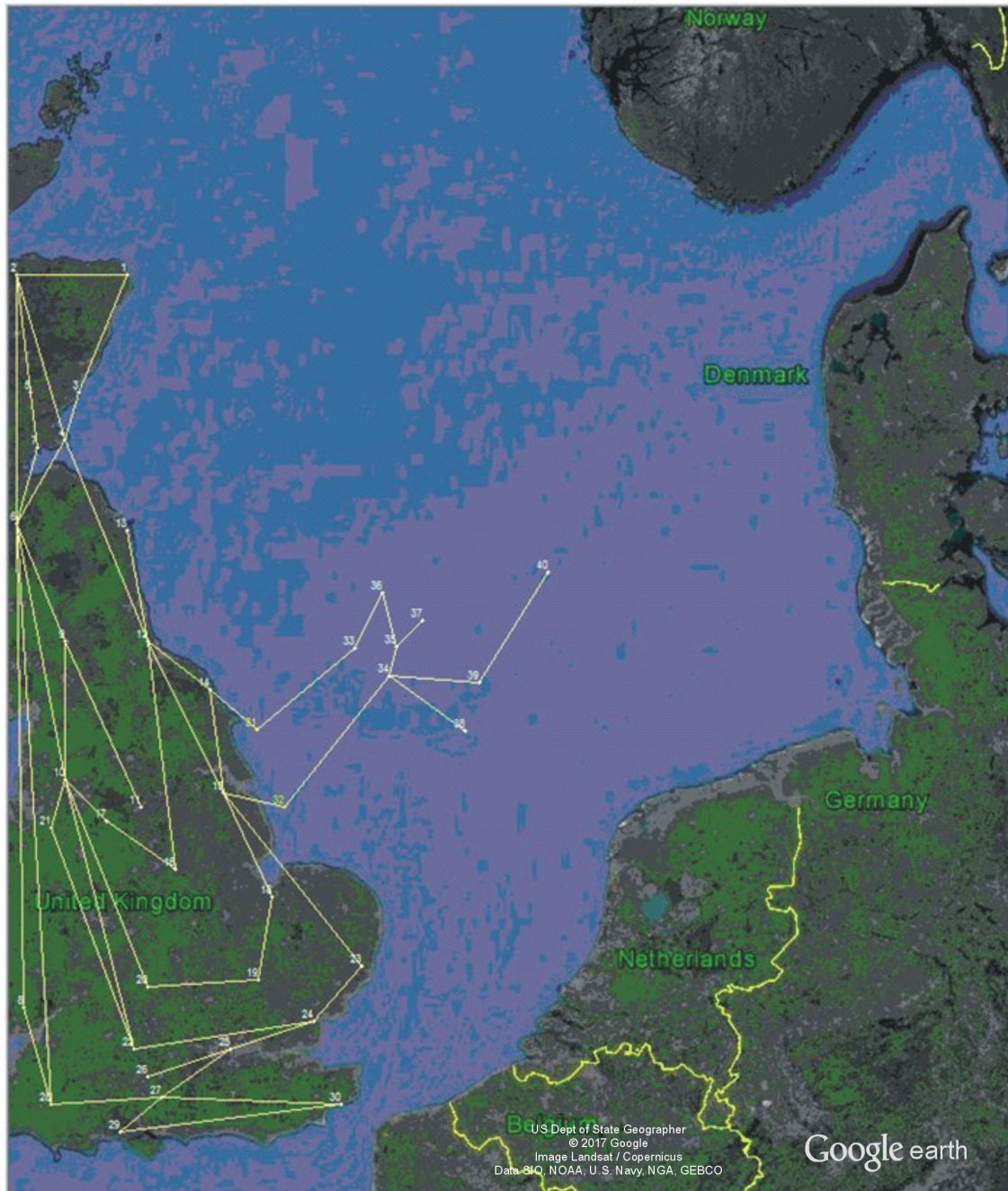
Figure 6.13. Configuration 5 for Scenario 1.

The total processing time for data is 49 hours, 23 minutes, and 14.322 seconds and after 1000 generations, seven chromosomes are generated as the best options. The number of lines and transformers is 52, with 16 generation nodes and 24 load nodes, and with a total of 40 nodes. There are eight load nodes with harmonics injected, and seven harmonics are considered. The processing time for the power flow and harmonic propagation study for this configuration is 0.904 seconds in 4 iterations.

In Figure 6.14, the DPI of the system nodes is shown, and Figure 6.15 shows the harmonic voltages on the network for the proposed configuration, Configuration 5.
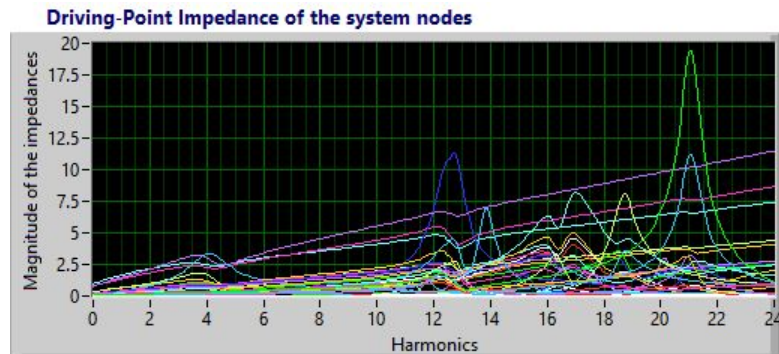
Figure 6.14. DPI graph for Configuration 5.
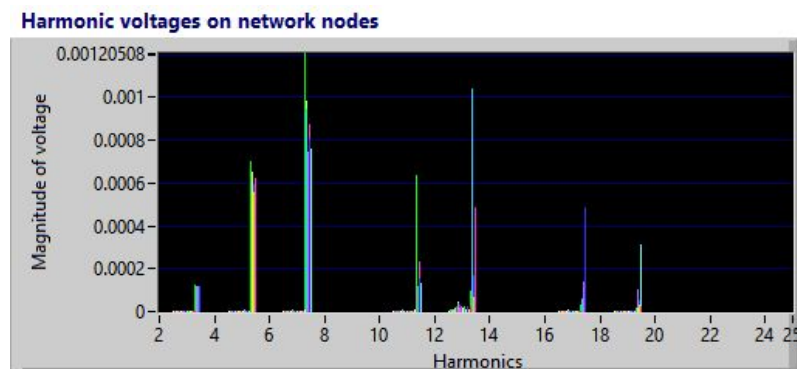
Figure 6.15. Harmonic voltages graph.

6.3   Results for Scenario 1

Scenario 1 has 32 fixed nodes and eight nodes that are randomly connected. Node 31 is connected to node 14 and node 32 is connected to node 15. The eight nodes generated represent offshore wind power clusters of 1.2 GW each, and these can be connected between them or to nodes 31 and 32.

For Scenario 1, to generate 100 chromosomes the time elapsed is 2 minutes and 25 seconds. In the XY graph, most of the chromosomes are between 0.16 and 0.24 per unit in the power losses in axe y and between 0.1 to 2 percent of the average THD in axe x.

The data shown is solely for comparison with the data obtained when the longest lines are eliminated, and a minimal tree is obtained for each configuration. Graphs are obtained from the report generated by the algorithm.

In Figure 6.16, graphs of chromosomes are shown after the longest lines are eliminated, and a minimal tree for each configuration is obtained.

The graphs are for 100 chromosomes generated. In the XY graph, most of the chromosomes are between 0.22 and 0.34 per unit in the power losses in axe *y* and between 0.05 to 0.16 percent of average THD in axe *x*. Some chromosomes are excluded from this area. It can be observed that power losses have decreased significantly and that the average THD has decreased too.
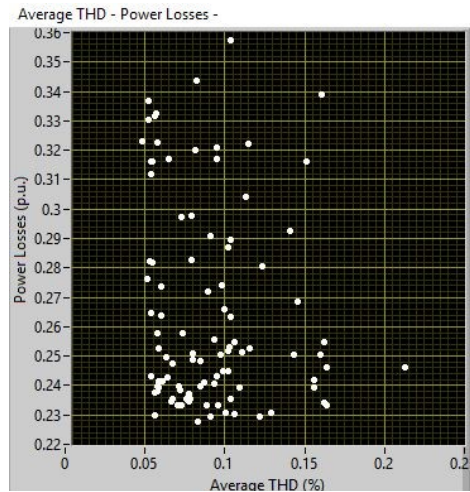
Figure 6.16. Longest lines eliminated of the 100 chromosomes generated, Scenario 1.

Figure 6.17 shows the best chromosomes of the first generation after the crossover and mutation process. The Pareto fronts of the functions of average THD and power losses are shown.

To generate 100 chromosomes, to eliminate the longest distances, to eliminate chromosomes that do not converge to a solution, to obtain the best chromosomes using the Pareto front, and to use the best chromosomes to crossover and mutate to obtain the first generation it was involved an elapsed time of 50 minutes.
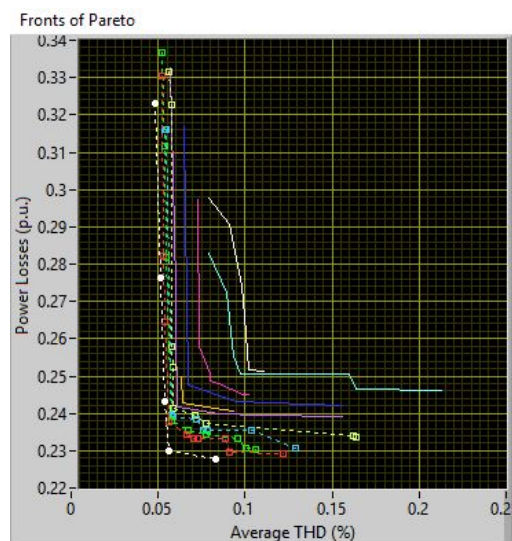
Figure 6.17. Pareto front obtained in the first generation of 100 chromosomes generated, Scenario 1.

Figure 6.18 shows the best chromosomes after 1,000 generations and after the crossover and mutation process. To generate 1,000 generations, the time elapsed is 19 hours, 32 minutes, and the algorithm generates eight chromosomes or configurations as the best options.
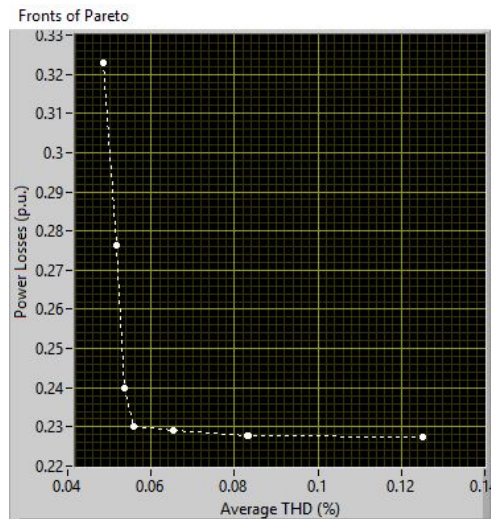
Figure 6.18. Pareto front obtained after 1,000 generations for Scenario 1.

Table 6.5 shows the data obtained for the best chromosomes. It must be noted that there is not necessarily a coincidence between the best options with the number of lines, the longest distance, or the total length of the cable.

TABLE 6.5. DATA OBTAINED AFTER 1,000 GENERATIONS FOR SCENARIO 1

	THD (%)	Power losses (p.u.)	Number of lines	Maximun distance (km)	Total cable length (km)
1	0.0485	0.3229	51	167.1298	588.5649
2	0.0517	0.2762	51	153.8767	616.6151
3	0.0535	0.2398	52	153.8767	665.8188
4	0.0560	0.2300	52	153.8767	744.8725
5	0.0653	0.2291	54	153.8767	745.2685
6	0.0832	0.2279	53	153.8767	716.6702
7	0.0833	0.2278	53	153.8767	711.6977
8	0.1252	0.2276	53	153.8767	687.8610

The results indicate that the configurations of the network approach the average THD to 0.056 percent and power losses to 0.23 per unit as the best configuration of the network. This criterion can be used to suggest a configuration of the offshore wind power clusters. A complete report is available on Appendix H, Section H.2.

6.4   Results for Scenario 2

Scenario 2 has eight offshore wind power clusters corresponding to 4 clusters of the Dogger Bank and 4 clusters of the Hornsea. Nodes 12, 13, 14 and 15 can be connected to the offshore wind power clusters. The eight offshore wind power clusters are the following: Creyke Beck A and B and Teeside A and B, each one of 1.2 GW, Hornsea project One of 1.2 GW, Hornsea project Two of 1.8 GW, Hornsea project Three of 2 GW, and Hornsea project Four of 1 GW.

For Scenario 2, to generate 100 chromosomes, the time elapsed is 17 minutes and 36 seconds. In the XY graph, most of the chromosomes are between 3 and 13 per unit in the power losses in axe y and between 0.2 to 2 percent of the average THD in axe x.

The data shown is solely for comparison with the data obtained when the longest lines are eliminated, and a minimal tree for each configuration is obtained. The graphs are obtained from the report generated by the algorithm.

In Figure 6.19, graphs of chromosomes after the longest lines are eliminated are shown, and a minimal tree for each configuration is obtained.

The graphs are for 100 chromosomes generated. In the XY graph, most of the chromosomes are between 0.22 and 0.65 per unit in the power losses in axe y and between 0.04 to 0.12 percent of the average THD in axe x. Some chromosomes are excluded from this area. It can be observed that the power losses have decreased significantly and the average THD has decreased as well.
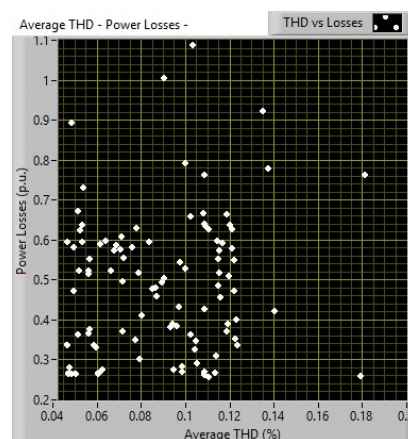
Figure 6.19. Longest lines eliminated of the 100 chromosomes generated, Scenario 2

Figure 6.20 shows the best chromosomes of the first generation after the crossover and mutation process. The Pareto fronts of the functions of the average THD and power losses are shown.

To generate 100 chromosomes, to eliminate the longest distances, to eliminate chromosomes that do not converge to a solution, to obtain the best chromosomes using the Pareto front and, to use the best chromosomes to crossover and mutate to obtain the first generation it was involved an elapsed time of 1 hour and 24 minutes.
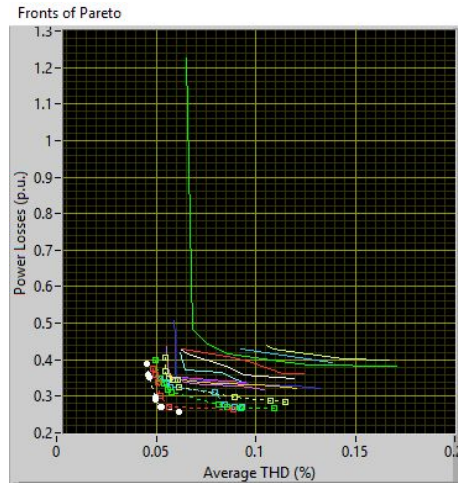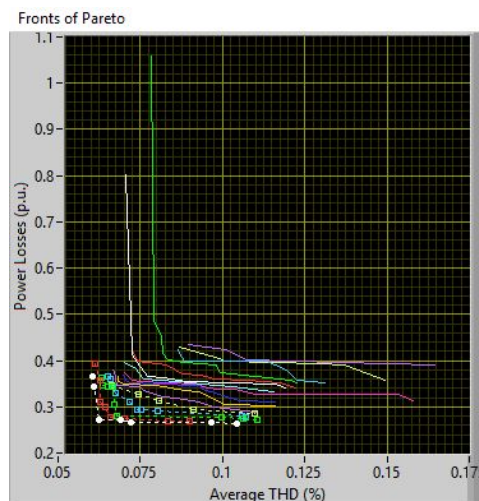

Figure 6.20. Pareto front obtained in the first generation, Scenario 2.

Figure 6.21 shows the best chromosomes after 1,000 generations and after the crossover and mutation process. To generate 1,000 generations, the time elapsed is 35 hours and 7 minutes, and the algorithm generates 13 chromosomes or configurations as the best options.
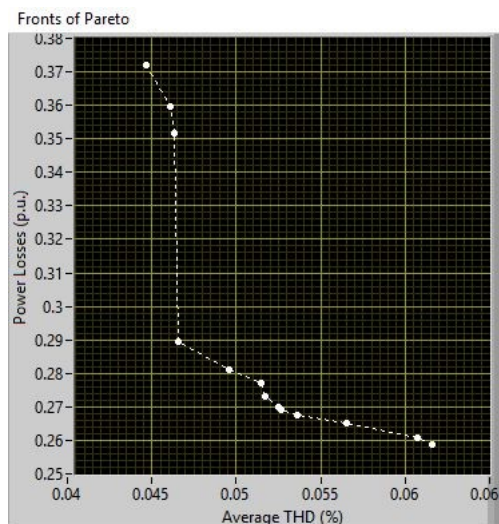
Figure 6.21. Pareto front obtained after 1,000 generations for Scenario 2.

Table 6.6 shows the data obtained for the best chromosomes. It must be noted that as in the first generation, there is not necessarily a coincidence between the best options with the number of lines, the longest distance, or the total length of the cable.

TABLE 6.6. DATA OBTAINED AFTER 1,000 GENERATIONS FOR SCENARIO 2

	THD (%)	Power losses (p.u.)	Number of lines	Maximun distance (km)	Total cable length (km)
1	0.0447	0.3722	49	111.7604	418.4618
2	0.0461	0.3597	49	111.7604	401.8721
3	0.0463	0.3515	50	111.7604	424.0210
4	0.0466	0.2893	49	111.7604	440.0372
5	0.0496	0.2811	50	111.7604	432.7067
6	0.0515	0.2772	50	111.7604	398.1801
7	0.0517	0.2731	49	133.9574	499.9185
8	0.0525	0.2700	49	113.0968	438.5422
9	0.0526	0.2693	49	113.0968	454.3281
10	0.0536	0.2674	49	113.0968	433.9902
11	0.0565	0.2653	50	111.7604	467.6053
12	0.0607	0.2609	49	133.9574	534.8170
13	0.0616	0.2589	49	113.0968	503.4154

The results indicate that the configurations of the network approach the average THD to 0.055 percent and power losses to 0.26 per unit as the best configuration of the network. This criterion can be used to suggest a configuration of the offshore wind power clusters. A complete report is provided in Appendix H, Section H.3.

6.5   Results for Scenario 3

Scenario 3 has 15 offshore wind power clusters located at the Dogger Bank, Hornsea, and Seagreen. Wind power clusters can be connected to nodes 3, 4, 12, 13, 14, and 15. The 15 offshore wind power clusters are as follows: Creyke Beck A and B and Teeside A and B, each one of 1.2 GW, Hornsea project One of 1.2 GW, Hornsea project Two of 1.8 GW, Hornsea project Three of 2 GW and Hornsea project Four of 1 GW, Seagreen Alpha and Bravo of 525 MW, Charlie of 610 MW, Delta and Echo of 605 MW, Foxtrot of 565 MW, and Golf of 225 MW.

For Scenario 3, to generate 150 chromosomes, the time elapsed is 5 minutes and 42 seconds. In the XY graph, only one chromosome is shown, because, with the long distances, the algorithm does not converge to a solution. The chromosomes are generated to be processed and to eliminate the longest lines in order to obtain a solution. For only one generated chromosome, power losses in axe y are 18 per unit, and the average THD in axe x is 0.87 percent.

The data shown is solely for comparison with the data obtained when the longest lines are eliminated, and a minimal tree for each configuration is obtained. The graphs are obtained from the report generated by the algorithm.

In Figure 6.22, chromosomes, after the longest lines are eliminated, are shown, and a minimal tree for each configuration is obtained. The graphs are for 100 chromosomes generated. In the XY graph, most of the chromosomes are between 0.25 and 0.55 per unit in the power losses in axe *y* and between 0.06 to 0.12 percent of the average THD in axe *x*. Some chromosomes are excluded from this area. It can be observed that power losses have decreased significantly compared with the only chromosome shown in the first generation, and also, the average THD has decreased.
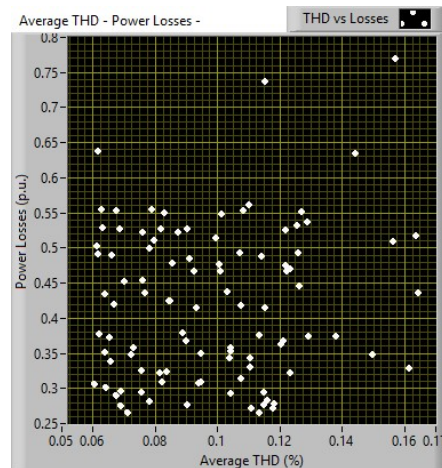
Figure 6.22. Chromosomes after longest lines are eliminated of the 150 chromosomes, Scenario 3.

Figure 6.23 shows the best chromosomes of the first generation after the crossover and mutation process. It is the Pareto front of the functions of the average THD and power losses. To generate 150 chromosomes, to eliminate the longest distances, to eliminate chromosomes that do not converge to a solution, to obtain the best chromosomes using the Pareto front, and to use the best chromosomes to crossover and mutate to obtain the first generation it was involved an elapsed time of 9 hours and 23 minutes.

Figure 6.23. Pareto front obtained in the first generation of 150 chromosomes generated, Scenario 3.

Figure 6.24 shows the best chromosomes after 500 generations and after the crossover and mutation process. To generate 500 generations, the time elapsed is 61 hours, and the algorithm generates eight chromosomes or configurations as the best options.
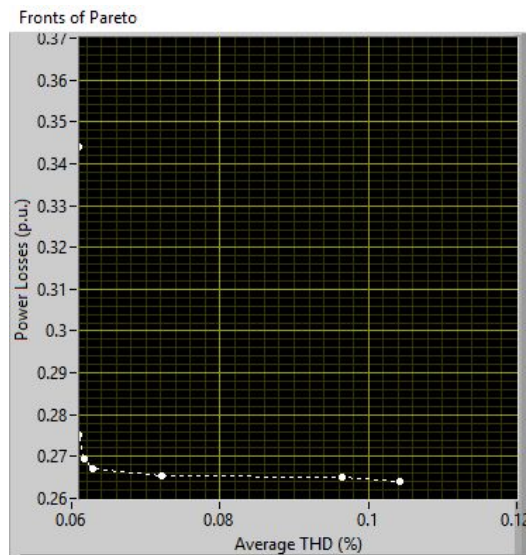
Figure 6.24. Pareto front obtained after 500 generations for Scenario 3.

Table 6.7 shows the data obtained for the best chromosomes. It must be noted that as in the first generation, there is not necessarily a coincidence between the best options with the number of lines, the longest distance, or the total length of the cable.

TABLE 6.7. DATA OBTAINED AFTER 500 GENERATIONS FOR SCENARIO 3

	THD (%)	Power losses (p.u.)	Number of lines	Maximun distance (km)	Total cable length (km)
1	0.0605	0.3655	60	115.3429	761.8323
2	0.0609	0.3440	57	111.7604	614.8928
3	0.0610	0.2753	57	111.7604	645.4751
4	0.0617	0.2694	57	111.7604	611.6694
5	0.0629	0.2669	60	113.0968	681.3083
6	0.0722	0.2655	77	411.0729	4456.0700
7	0.0965	0.2650	75	385.0543	3666.7357
8	0.1043	0.2639	79	411.0729	5082.5616

The results indicate that the configurations of the network approach the average THD to 0.0629 percent and power losses to 0.2699 per unit as the best configuration of the network.

This criterion can be used to suggest a configuration of the offshore wind power clusters. A complete report is on Appendix H, Section H.4.

6.6 Summary

As an example and explanation, three scenarios were proposed as case studies to prove the performance of the algorithm.

Scenario 1 was proposed regarding Dogger Bank with eight offshore wind power clusters generating 9.6 GW. The distances between offshore wind power clusters and the shore range from 125 km to 290 km. Furthermore, two nodes were proposed near the shore to connect the offshore wind power clusters. The purpose of this scenario is to show the algorithm results, with distances between nodes that show the different configurations in detail.

Scenario 2 was proposed using the Dogger Bank and Hornsea offshore wind power projects with a total capacity of 10.8 GW.

Scenario 3 was proposed by adding to Scenario 2 with the Seagreen offshore wind power project, adding 3.66 GW, generating a total of 14.46 GW.

All of this offshore capacity will be delivered to the mainland, so the study of the potential impact that the integration of this energy could cause is required.

In the case of Scenario 3, the distances of the lines are very long, so the algorithm that calculates the power flow and harmonic propagation does not converge to a valid solution, and as a consequence, only a few valid chromosomes are generated. In this scenario, the algorithm does not eliminate the generated chromosomes. The chromosomes are processed, and then, the longest lines are eliminated, with this process, the algorithm converges to a valid solution, and then, the information can be used.

The MOEA performs well in reconfiguring and demonstrating different solutions. The comparisons of time processing suggest that when processing between 50 and 100 chromosomes, the algorithm converges to reasonable solutions and improves time.

Additionally, comparing process time using only one objective function, it is seen that it is very similar to the time required in using multi-objective functions, and the result is improved using at least two functions.

It should be noted that the topology affects power losses and harmonics. If the topology is defined based on a single objective, other parameters may become worse, but it is possible to obtain solutions that satisfy two or more objectives that can be considered in the process of design.

With the implementation of the algorithm, it is possible to suggest the best configuration in large offshore power clusters to maintain harmonics at levels that let the offshore wind power clusters work without problems of operation and avoid instabilities in the network. This suggestion must be considered with other parameters to obtain the best configuration to integrate the energy into the mainland successfully.

7   Conclusion and future work

7.1   Conclusions

It was found that the interaction of different offshore wind power clusters will generate harmonics, and with the long distances between offshore wind power clusters, the subsea cables could generate resonances that may cause instabilities when generated power is connected to the grid. Such instability could shut off one or more wind turbines, causing a significant fault if not controlled quickly.

This research helps determine that it is possible to reduce the harmonics propagation by changing the configuration of the offshore wind power clusters, decreasing the adverse effects into the onshore AC grid

The research is focused on developing an MOEA applied to harmonic propagation studies and the optimisation of large offshore wind power clusters considered in the future projects that will take place in the North Sea. This is the main reason to understand the context of the problem of harmonic propagation and a general description of the electrical components of an offshore wind farm. It is essential to include the components of the offshore substation or substations, and furthermore, the problems related to cable layout is necessary to avoid resonance problems.

It is essential to know the necessary components in order to implement data and obtain a better execution of the algorithm proposed to optimise the network because it is possible that the generation of harmonics could be present in the network, as previously mentioned, the network includes different components.

Comprehensive research work on power flow, harmonic propagation, and methods to solve them has been carried out, and it was noted that the harmonics generated in a wind farm could be treated as one unit to connect with other offshore wind farms in order to create a sole sizeable offshore wind power cluster that will interact with other offshore wind power clusters as well.

These are appropriate reasons to optimise the connection between offshore wind power clusters in order to minimise harmonic propagation and avoid resonance problems using only the configuration of the wind power clusters.

Based on the general review, a suitable power flow method was chosen. The algorithm to obtain power flow is based on the Newton-Raphson method that allows for the solving of the mismatched equations. The algorithm can be implemented in any language, and it can work with optimal results.

Furthermore, the theory to obtain harmonic propagation has been presented, and it was found that the current injection method used for harmonic propagation study and it facilitates the implementation of any device that generates distortion by harmonics. Such devices could be a single turbine, a wind farm, or a wind power cluster. Subsequently, this is the main reason to implement the current injection method in the power flow algorithm in order to calculate harmonic propagation.

Based on what was mentioned above, the algorithm was developed and programmed in order to obtain power flow and harmonic propagation, and the data was also used in the objective functions in the MOEA developed.

Another topic that was reviewed was the evolutionary algorithms theory. A comprehensive overview of recent research of this topic has been carried out, and it was found that evolutionary algorithms are different from the conventional optimisation methods and converge to the global optimum solutions.

Additionally, it was found that an advantage of genetic algorithms is their parallelism because genetic algorithms travel in a search space with more individuals, so they are less likely to get stuck in a local extreme as in other methods.

It is complicated to consider all the possible variables in the optimisation of electrical networks. When harmonic distortion and power losses are used as functions, the problem is not linear, and it could be solved with evolutionary algorithms. Because evolutionary algorithms are generally used to solve specific difficult problems and are quite easy to implement, a genetic algorithm was proposed to solve the problem.

On the other hand, choosing encoding and fitness functions can be quite tricky. However, if the functions and encoding are identified and defined, the genetic algorithms generate highly effective results.

After the review of the literature, one can conclude that the best genetic algorithm to be implemented for the task is the NSGA. The reason for this is because it is possible to classify Pareto fronts, and although this algorithm adopts a stochastic remainder of proportional selection, it is possible to get more copies of the first front because its chromosomes are the strongest and most capable of overcoming it. Furthermore, it is possible to explore other possibilities with weaker chromosomes to avoid falling into a local optimum solution.

Based on this, the work presents an MOEA to reconfigure electrical systems by minimising harmonics and power losses. The algorithm calculates the power flow and the harmonic propagation, and then, it uses an evolutionary algorithm to obtain the maximum current flow. Data is saved from each configuration, and with all the data compiled, the algorithm suggests the best configuration with less THD and fewer power losses.

Finally, in this research, an algorithm to reduce the adverse effects of the propagation of harmonics in the network has been developed, specifically for the grid proposed for the North Sea wind power clusters.

Extensive simulation results were presented to verify all the proposed algorithms. Simulations were carried out using LabVIEW software, and the results are included in this thesis.

The proposed algorithm considers the fact that two electrical networks exist: one is a fixed grid which cannot change in its configuration (onshore AC grid), and the other is a network (offshore wind parks) in which the only factors known are the generation points but not the interconnection between them and the onshore AC grid. The onshore fixed 30 nodes grid is based on the IEEE-30 nodes modified. As the algorithm starts with a network with fixed nodes and lines, it is critical to know the initial values to avoid mistakes when the power flow is calculated.

In this research wind power cluster were implemented, but any type of power systems can be implemented in the algorithm.

The chromosomes generated to use those fixed nodes to integrate their energy into mainland. The nodes are located on a map. The data of each line in the fixed network does not change but, in case of offshore wind power clusters, the proposed length and parameters of the cable are essential because the data line changes depending on the nodes that are connected.

Latitude and longitude are also necessary to calculate the distance between nodes. The parameters of the line can be calculated if the distance is known to generate the network and to obtain power flow and harmonic propagation. To calculate the distance between two points on a sphere, the haversine formula is implemented. The haversine formula calculates an accurate distance.

The validation includes the use of DFS to check that there are no isolated nodes. If there is at least one isolated node, the chromosome must be eliminated, because the algorithm to calculate power flow will not converge to a valid solution.

The processing time depends on the number of nodes and lines generated. In addition, it depends on the number of chromosomes generated in the initial population. If the number of the initial population is high, the algorithm will take too much time to process, but if the number is low, the results could not be the desired ones.

The number of chromosomes generated in the initial population is important because the algorithm could consume much time in eliminating lines to create the first generation of chromosomes. To improve the performance of the algorithm, there are two different stages.

The time that is taken to generate each chromosome will depend on the distance that is allowed to connect the nodes. If the distance is too short, generating random chromosomes will be more difficult, because options for the random combination of nodes will be reduced drastically, and the consequence is that that generation of the population will take more time.

It is better that in the first stage, the initial population does not have restrictions on the number and length of lines. So, the algorithm allows a longer distance, and then, it eliminates lines. This is because the process to eliminate lines takes almost the same time for each chromosome but is lower than the generation time for shorter lines.

It must be noted that if the distance allowed is shorter than the shorter line between nodes, the algorithm will not find a feasible configuration because isolated nodes will be generated. Comparisons in time processing suggest that it is better to use all the possible connections and then go further regarding eliminating long lines. This procedure efficiently improves processing time.

After the initial population is generated, a second stage starts. This stage eliminates the number of lines according to the restrictions of length. This stage improves the evolutionary algorithm to start the genetic algorithm having improved the first generation.

It must be considered that a generated chromosome in the initial stage is entirely different from the same chromosome after eliminating the longest lines. This is the main reason to obtain the first Pareto front after eliminating the longest lines.

The Pareto fronts help in minimising the number of chromosomes, eliminating all the chromosomes that do not adapt to the required parameters according to the constraints implemented in the algorithm. The best chromosomes are kept for the next generation.

The crossover is by pairs between all the chromosomes of the Pareto fronts selected. This is because, in this specific problem, the Pareto front does not generate too many valid chromosomes. Also, many chromosomes are eliminated, because there are isolated nodes or the solution does not converge to any valid parameters.

The consequence of eliminating lines is the decrease in the total length of the cable. In addition, the average THD decreases, but power losses increase, amongst other factors.

With the THD of each node, a logarithmic average of THD is calculated. The reason for this is to avoid a low distortion value if there is only one high THD and the others THDs are low. This is important in order to obtain a better performance of the algorithm.

Furthermore, the longer the length of lines, the higher the capacitive effect is, and power losses can be more significant too. Power losses depend on cable resistance and the current line. This is $P=I^2R$, and the current depends on the voltage in the nodes of the line. This is why its behaviour cannot be predicted.

In the thesis it is used a single type of cable, but the voltage of the cables is relevant for harmonic propagation. A change of the type of cable, affects the whole network. A function that can be implemented is the cost of the cable, information of each type of cable can be implemented, and furthermore, thicker diameter of cables will decrease the effect of the harmonic propagation, and power losses, but will increase the cost of the cable. With the cable information, a function that calculates the diameter of the cable and the relationship with the harmonic propagation and power losses can be implemented to minimise the total cost. If the power exceeds the cable capacity, the function can include

the possibility of redundancies between nodes, to connect a parallel line, or even more lines.

The THD increases due to resonance phenomena and with the change in the configuration of the network, the response in the THD can be very drastic. Harmonic impedance generated by long transmission cable causes parallel resonances that have a frequency shift depending on the number of cables connected.

When the number of cables is reduced, there is a shift to lower frequencies. Also, harmonics produced by the wind turbines have a frequency shift according to the wind speed, the number of turbines, and cables in operation.

Additionally, when a parallel resonance occurs at the same frequency as one of the harmonics produced by the wind turbines, a situation can be presented in the grid, causing a major fault, as network instabilities can cause the turbines to remain out of service, or even worse, they can cause a cascading effect in other turbines that may overheat and damage the equipment.

A high THD is mainly due to parallel resonance problems at this specific node of the network.

Significant power losses are mainly due to very considerable differences in voltage between the end nodes of the lines and cables.

The harmonic propagation and power flow algorithm were presented, developed and programmed, and they were used as objective functions in a genetic algorithm. The algorithm was implemented as a subroutine within the genetic algorithm.

Also, an evolutionary algorithm has been developed, programmed, and implemented. Algorithms developed were implemented, and an MOEA was created in order to obtain the desired results.

Topology affects power losses and harmonics. If the topology is defined based on a single objective, other parameters may become worse, but it is possible to obtain solutions that satisfy two or more objectives that can be considered in the process of design.

The MOEA developed performs well in reconfiguring and minimising power losses and THD in the network proposed. The polymorphism of LabVIEW was very useful to obtain the results that are necessary to implement the algorithm and use it within another algorithm.

The algorithm that was implemented is quite simple and easy, and it is also advantageous. This is the reason for nature using genetic algorithms, and although it takes a long time, nature has enough time to process such complex aspects and does so efficiently. However, when the same processes have to be carried out using a computer, the computer has to be forced to be faster to obtain the best results.

7.2   Contributions

This thesis contributes to developing an optimisation algorithm to minimising power losses and THD by implementing an MOEA to suggest the best interconnection options for the projects of the near future in the North Sea.

The advantage of optimisation using an evolutionary algorithm is that it offers high-performance global search ability. This means that chromosomes can find feasible solutions in all possible search areas.

Therefore, an optimisation method based on an evolutionary and genetic algorithm is proposed to solve the optimal configuration problem in this research, using power flow and harmonic propagation as the primary functions.

The algorithm automatically generates the report to compare different options and has the possibility of suggesting the best configuration. These reports can be used to make recommendations for possible control strategies of wind power clusters planned for the near future in the North Sea.

Furthermore, the algorithm can be implemented in other locations with a variety of projects and scenarios.

Using the average THD and power losses improves the configuration, but the total value of the length of the cable could be used to suggest a better configuration. Also, the DPI could help avoid a configuration with resonance or improve the network.

7.3   Future work

Further research is required to optimise some parts of the algorithm in order to improve processing time, as the use of subroutines to send and receive information and optimise the main algorithm is important.

Also, different kinds of encoding, selection, crossover, and mutation could be implemented.

Instead of the Newton-Raphson method, another method could be implemented to calculate power flow and harmonic propagation and prove performance.

The THD and the power losses are the primary objective functions, but other function can be implemented, and not only electrical, cost functions could also be implemented to minimise economic factors.

The network can be increased to include all the nodes of the North Sea and for the future projects to deliver all generated energy to the main onshore AC grid.

Each component can be modelled to use better approximations of data, specifically the harmonic models.

Develop a function to let the connection of two or more lines between nodes with in order to minimise the cost of the cable using cables of less diameter. This function can optimise the cost of the cable, the harmonic propagation and the power losses.

The algorithm could be implemented with different type of elements to be used with multi-technology offshore wind turbines, only it is necessary to include the node with the harmonic injected currents of each element according to the harmonic model.

References

[1]   J. Zhu, *Optimization of Power System Operation*. John Wiley & Sons, 2009.

[2]   M. V. Chavez-Baez, O. Anaya-Lara, K. L. Lo, and J. McDonald, "Review of harmonics in offshore wind farms," in *2013 48th International Universities' Power Engineering Conference (UPEC)*, 2013, pp. 1–5.

[3]   "European Wind Energy Association," 2011. [Online]. Available: http://www.ewea.org/.

[4]   B. Fox, L. Bryans, D. Flynn, N. Jenkins, D. Millborrow, M. O'Malley, R. Watson, and O. Anaya-Lara, *Wind Power Integration : Connection and System Operational Aspects*. UK: IET Power and Energy Series, 2007.

[5]   "POWER cluster. Offshore Wind Energy," 2017. [Online]. Available: http://www.power-cluster.net/.

[6]   J. F. Herbert-Acero, O. Probst, P.-E. Réthore, G. C. Larsen, and K. K. Castillo-villar, "A Review of Methodological Approaches for the Design and Optimization of Wind Farms," *energies*, no. 1, pp. 6930–7016, 2014.

[7]   B. Pérez, R. Mínguez, and R. Guanche, "Offshore wind farm layout optimization using mathematical programming techniques," *Renew. Energy*, vol. 53, pp. 389–399, 2013.

[8]   B. C. Neagu and G. Georgescu, "Wind Farm Cable Route Optimization Using a Simple Approach," *Electr. Power Eng. (EPE), 2014 Int. Conf. Expo. on, Iasi*, no. Epe, pp. 1004–1009, 2014.

[9]   S. F. Rodrigues, R. Teixeira Pinto, M. Soleimanzadeh, P. A. N. Bosman, and P. Bauer, "Wake losses optimization of offshore wind farms with moveable floating wind turbines," *Energy Convers. Manag.*, vol. 89, pp. 933–941, 2015.

[10]   S. Salcedo-Sanz, D. Gallo-Marazuela, A. Pastor-Sánchez, L. Carro-Calvo, A. Portilla-Figueras, and L. Prieto, "Evolutionary computation approaches for real offshore wind farm layout: A case study in northern Europe," *Expert Syst. Appl.*, vol. 40, no. 16, pp. 6292–6297, 2013.

[11]   A. Kusiak and Z. Song, "Design of wind farm layout for maximum wind energy capture," *Renew. Energy*, vol. 35, no. 1, pp. 685–694, 2010.

[12]   J. S. González, Á. G. G. Rodríguez, J. C. Mora, M. Burgos Payán, and J. R. Santos, "Overall design optimization of wind farms," *Renew. Energy*, vol. 36, no. 7, pp. 1973–1982, 2011.

[13]   J. S. González, A. G. Gonzalez Rodriguez, J. C. Mora, J. R. Santos, and M. B. Payan, "Optimization of wind farm turbines layout using an evolutive algorithm," *Renew. Energy*, vol. 35, no. 8, pp. 1671–1681, 2010.

[14]   B. Saavedra-Moreno, S. Salcedo-Sanz, A. Paniagua-Tineo, L. Prieto, and A. Portilla-Figueras, "Seeding evolutionary algorithms with heuristics for optimal wind turbines positioning in wind farms," *Renew. Energy*, vol. 36, no. 11, pp. 2838–2844, 2011.

[15]   S. A. Grady, M. Y. Hussaini, and M. M. Abdullah, "Placement of wind turbines using genetic algorithms," *Renew. Energy*, vol. 30, no. 2, pp. 259–270, 2005.

[16]   A. Emami and P. Noghreh, "New approach on optimization in placement of wind turbines within wind farm by genetic algorithms," *Renew. Energy*, vol. 35, no. 7, pp. 1559–1564, 2010.

[17]   M. Zhao, Z. Chen, and J. Hjerrild, "Analysis of the behaviour of genetic algorithm applied in optimization of electrical system design for offshore wind farms," *IECON 2006 - 32nd Annu. Conf. IEEE Ind. Electron.*, vol. 1–11, no. 1, pp. 304–309, 2006.

[18]   M. Zhao, Z. Chen, and F. Blaabjerg, "Optimisation of electrical system for offshore wind farms via genetic algorithm," *Renew. Power Gener. IET*, vol. 1, no. 1, pp. 10–16, 2007.

[19]   F. M. González-Longatt, P. Wall, P. Regulski, and V. Terzija, "Optimal electric network design for a large offshore wind farm based on a modified genetic algorithm approach," *IEEE Syst. J.*, vol. 6, no. 1, pp. 164–172, 2012.

[20]   F. Gonzalez-Longatt, "Optimal offshore wind farms' collector design based on the multiple travelling salesman problem and genetic algorithm," *PowerTech (POWERTECH), 2013 IEEE Grenoble*, 2013.

[21]   O. Dahmani, S. Bourguet, P. Guerin, M. Machmoum, P. Rhein, and L. Josse, "Optimization of the internal grid of an offshore wind farm using Genetic algorithm," *2013 IEEE Grenoble Conf. PowerTech, POWERTECH 2013*, 2013.

[22]   A. M. Jenkins, M. Scutariu, and K. S. Smith, "Offshore wind farm inter-array cable layout," *2013 IEEE Grenoble Conf. PowerTech, POWERTECH 2013*, pp. 2–7, 2013.

[23]   O. Dahmani, S. Bourguet, M. Machmoum, P. Guerin, P. Rhein, and L. Josse, "Optimization of the

Connection Topology of an Offshore Wind Farm Network," *IEEE Syst. J.*, vol. 9, no. 4, pp. 1519–1528, 2015.

[24]   W. S. Moon, J. C. Kim, A. Jo, and J. N. Won, "Grid optimization for offshore wind farm layout and substation location," *IEEE Transp. Electrif. Conf. Expo, ITEC Asia-Pacific 2014 - Conf. Proc.*, pp. 14–19, 2014.

[25]   Y. Chen, H. Li, K. Jin, and Q. Song, "Wind farm layout optimization using genetic algorithm with different hub height wind turbines," *Energy Convers. Manag.*, vol. 70, pp. 56–65, 2013.

[26]   S. Pookpunt and W. Ongsakul, "Optimal placement of wind turbines within wind farm using binary particle swarm optimization with time-varying acceleration coefficients," *Renew. Energy*, vol. 55, pp. 266–276, 2013.

[27]   P. Hou, S. Member, W. Hu, and M. Soltani, "Optimized Placement of Wind Turbines in Large-Scale Offshore Wind Farm Using Particle Swarm Optimization Algorithm," *IEEE Trans. Sustain. Energy*, vol. 6, no. 4, pp. 1272–1282, 2015.

[28]   P. Y. Yin and T. Y. Wang, "A GRASP-VNS algorithm for optimal wind-turbine placement in wind farms," *Renew. Energy*, vol. 48, pp. 489–498, 2012.

[29]   P. Hou, W. Hu, and Z. Chen, "Offshore Substation Locating in Wind Farms Based on Prim Algorithm," *2015 IEEE Power Energy Soc. Gen. Meet. Denver, CO*, pp. 1–5, 2015.

[30]   S. Salcedo-Sanz, D. Gallo-Marazuela, A. Pastor-Sánchez, L. Carro-Calvo, A. Portilla-Figueras, and L. Prieto, "Offshore wind farm design with the Coral Reefs Optimization algorithm," *Renew. Energy*, vol. 63, pp. 109–115, 2014.

[31]   Y. Eroĝlu and S. U. Seçkiner, "Design of wind farm layout using ant colony algorithm," *Renew. Energy*, vol. 44, pp. 53–62, 2012.

[32]   C. M. Ituarte-Villarreal and J. F. Espiritu, "Optimization of wind turbine placement using a viral based optimization algorithm," *Procedia Comput. Sci.*, vol. 6, pp. 469–474, 2011.

[33]   G. Marmidis, S. Lazarou, and E. Pyrgioti, "Optimal placement of wind turbines in a wind park using Monte Carlo simulation," *Renew. Energy*, vol. 33, no. 7, pp. 1455–1460, 2008.

[34]   S. Lumbreras and A. Ramos, "A Benders' decomposition approach for optimizing the electric system of offshore wind farms," *2011 IEEE Trondheim PowerTech*, pp. 1–8, 2011.

[35]   S. Lumbreras and A. Ramos, "Optimal design of the electrical layout of an offshore wind farm applying decomposition strategies," *IEEE Trans. Power Syst.*, vol. 28, no. 2, pp. 1434–1441, 2013.

[36]   M. Wagner, J. Day, and F. Neumann, "A fast and effective local search algorithm for optimizing the placement of wind turbines," *Renew. Energy*, vol. 51, pp. 64–70, 2013.

[37]   P. Hou, W. Hu, and Z. Chen, "Offshore Wind Farm Cable Connection Configuration Optimization using Dynamic Minimum Spanning Tree Algorithm," *IET Renew. Power Gener.*, 2015.

[38]   P. Hou, W. Hu, C. Chen, and Z. Chen, "Optimisation of offshore wind farm cable connection layout considering levelised production cost using dynamic minimum spanning tree algorithm," *IET Renew. Power Gener.*, vol. 10, no. 2, pp. 175–183, 2016.

[39]   P. D. Hopewell, F. Castro-Sayas, and D. I. Bailey, "Optimising the design of offshore wind farm collection networks," *41st Int. Univ. Power Eng. Conf. UPEC 2006, Conf. Proc.*, vol. 1, no. l, pp. 84–88, 2006.

[40]   C. Meyer, M. Höing, A. Peterson, and R. W. De Doncker, "Control and design of DC grids for offshore wind farms," *IEEE Trans. Ind. Appl.*, vol. 43, no. 6, pp. 1475–1482, 2007.

[41]   M. Nandigam and S. K. Dhali, "Optimal design of an offshore wind farm layout," *2008 Int. Symp. Power Electron. Electr. Drives, Autom. Motion*, pp. 1470–1474, 2008.

[42]   D. W. Elliott, S. J. Finney, and C. E. Jones, "Offshore wind farm cluster based DC collection network - operation and design considerations," *10th IET Int. Conf. AC DC Power Transm. (ACDC 2012)*, p. 6, 2012.

[43]   W. Wiechowski and P. B. Eriksen, "Selected studies on offshore wind farm cable connections - challenges and experience of the Danish TSO," *IEEE Power Energy Soc. 2008 Gen. Meet. Convers. Deliv. Electr. Energy 21st Century, PES*, pp. 1–8, 2008.

[44]   M. Banzo and A. Ramos, "Stochastic Optimization Model for Electric Power System Planning of Offshore Wind Farms," *IEEE Trans. Power Syst.*, vol. 26, no. 3, pp. 1338–1348, 2011.

[45]   D. A. Pierre, *Optimization theory with applications*. New York: Courier Corporation, 1986.

[46]   G. P. Rangaiah, *Multi-Objective Optimization: Techniques and Applications in Chemical Engineering*. World Scientific, 2008.

[47]   D. Shirmohammadi and H. W. Hong, "Reconfiguration of electric distribution networks for resistive line losses reduction," *IEEE Trans. Power Deliv.*, vol. 4, no. 2, pp. 1492–1498, Apr. 1989.

[48]   S. Kalambe and G. Agnihotri, "Loss minimization techniques used in distribution network: Bibliographical survey," *Renew. Sustain. Energy Rev.*, vol. 29, pp. 184–200, 2014.

[49]   H.-D. Chiang and R. Jean-Jumeau, "Optimal network reconfigurations in distribution systems. I. A

new formulation and a solution methodology," *IEEE Trans. Power Deliv.*, vol. 5, no. 4, pp. 1902–1909, 1990.

[50]   H.-D. Chiang and R. Jean-Jumeau, "Optimal network reconfigurations in distribution systems. II. Solution algorithms and numerical results," *IEEE Trans. Power Deliv.*, vol. 5, no. 3, pp. 1568–1574, Jul. 1990.

[51]   J. Z. Zhu, "Optimal reconfiguration of electrical distribution network using the refined genetic algorithm," *Electr. Power Syst. Res.*, vol. 62, no. 1, pp. 37–42, May 2002.

[52]   E. Lopez, H. Opazo, L. Garcia, and P. Bastard, "Online Reconfiguration Considering Variability Demand: Applications to Real Networks," *IEEE Trans. Power Syst.*, vol. 19, no. 1, pp. 549–553, Feb. 2004.

[53]   E. Romero Ramos, A. Gomez Exposito, J. Riquelme Santos, and F. Llorens Iborra, "Path-Based Distribution Network Modeling: Application to Reconfiguration for Loss Reduction," *IEEE Trans. Power Syst.*, vol. 20, no. 2, pp. 556–564, May 2005.

[54]   F. V. Gomes, S. Carneiro, J. L. R. Pereira, M. P. Vinagre, P. A. N. Garcia, and L. R. Araujo, "A New Heuristic Reconfiguration Algorithm for Large Distribution Systems," *IEEE Trans. Power Syst.*, vol. 20, no. 3, pp. 1373–1378, Aug. 2005.

[55]   W.-S. Tan, M. Y. Hassan, M. S. Majid, and H. Abdul Rahman, "Optimal distributed renewable generation planning: A review of different approaches," *Renew. Sustain. Energy Rev.*, vol. 18, pp. 626–645, Feb. 2013.

[56]   T. Ackermann, *Wind Power in Power Systems*, vol. 140, no. February. England: John Wiley & Sons Ltd, 2005.

[57]   E. Acha, V. G. Agelidis, O. Anaya-Lara, and T. J. E. Miller, *Power Electronic Control in Electrical Systems*. Great Britain: Newnes Power Engineering Series, 2002.

[58]   Y. H. Song and A. T. Johns, *Flexible AC Transmission Systems (FACTS)*. England: The Institution of Electrical Engineers, 1999.

[59]   H. Wang, "A unified model for the analysis of FACTS devices in damping power system oscillations. III. Unified power flow controller," *IEEE Trans. Power Deliv.*, vol. 15, no. 3, pp. 978–983, Jul. 2000.

[60]   T. J. Hammons, D. Woodford, J. Loughtan, M. Chamia, J. Donahoe, D. Povh, B. Bisewski, and W. Long, "Role of HVDC transmission in future energy development," *IEEE Power Eng. Rev.*, vol. 20, no. 2, pp. 10–25, Feb. 2000.

[61]   C. H. Chien and R. W. G. Bucknall, "Harmonic calculations of proximity effect on impedance characteristics in subsea power transmission cables," *IEEE Trans. Power Deliv.*, vol. 24, no. 4, pp. 2150–2158, 2009.

[62]   A. Beddard and M. Barnes, "VSC-HVDC availability analysis," Manchester, UK, 2011.

[63]   J. S. Contreras-Jimenez and F. Rivas-Davalos, "Reliability and Availability of VSC-HVDC links : A State of the Art," *2015 IEEE Int. Autumn Meet. Power, Electron. Comput. (ROPEC), Ixtapa*, pp. 1–8, 2015.

[64]   "B4-60 Designing HVDC Grids for Optimal Reliability and Availability Performance - Cigre," 2016. [Online]. Available: http://b4.cigre.org/WG-Area/B4-60-Designing-HVDC-Grids-for-Optimal-Reliability-and-Availability-Performance.

[65]   "Global Wind Energy Council," 2011. [Online]. Available: http://www.gwec.net/.

[66]   "International Energy Agency," 2011. [Online]. Available: http://www.iea.org/.

[67]   J. B. Glasdam, *Harmonics in offshore wind power plants : application of power electronic devices in transmission systems*, 1st ed. Springer, 2016.

[68]   L. Monjo, L. Sainz, J. Liang, and J. Pedra, "Study of resonance in wind parks," *Electr. Power Syst. Res.*, vol. 128, pp. 30–38, 2015.

[69]   F. Fuchs and A. Mertens, "Prediction and avoidance of grid-connected converter's instability caused by wind Park typical, load-varying grid resonance," *2014 IEEE Energy Convers. Congr. Expo. ECCE 2014*, pp. 2633–2640, 2014.

[70]   S. Zhang, S. Jiang, X. Lu, B. Ge, and F. Z. Peng, "Resonance issues and damping techniques for grid-connected inverters with long transmission cable," *IEEE Trans. Power Electron.*, vol. 29, no. 1, pp. 110–120, 2014.

[71]   H. A. Pérez, *Flexible AC Transmission Systems Modelling in Optimal Power Flows Using Newton's Method*. University of Glasgow, 1998.

[72]   R. Ellis and P. Eng, "Power System Harmonics–A Reference Guide to Causes, Effects and Corrective Measures," Rockwell International Corporation, 2001.

[73]   J. Arrillaga, Y. H. Liu, and N. R. Watson, *Flexible Power Transmission: The HVDC Options*. England: John Wiley and Sons, 2007.

[74]   B. Badrzadeh, M. Gupta, N. Singh, A. Petersson, L. Max, and M. Hogdahl, "Power system harmonic analysis in wind power plants — Part I: Study methodology and techniques," *2012 IEEE Ind. Appl.*

References

Soc. Annu. Meet., pp. 1–11, 2012.

[75]   B. Badrzadeh and M. Gupta, "Power system harmonic analysis in wind power plants — Part II: Practical experiences and mitigation methods," *2012 IEEE Ind. Appl. Soc. Annu. Meet.*, pp. 1–8, 2012.

[76]   R. King and J. B. Ekanayake, "Harmonic modelling of offshore wind farms," in *IEEE PES General Meeting*, 2010, pp. 1–6.

[77]   L. H. Kocewiak, J. Hjerrild, and C. L. Bak, "The impact of harmonics calculation methods on power quality assessment in wind farms," *Proc. 14th Int. Conf. Harmon. Qual. Power - ICHQP 2010*, pp. 1–9, 2010.

[78]   A. Shafiu, A. Hernandez, F. Schettler, J. Finn, and E. Jørgensen, "Harmonic studies for offshore windfarms," *9th IET Int. Conf. AC DC Power Transm. (ACDC 2010)*, pp. O41–O41, 2010.

[79]   H. Dong, S. E. Vocational, and M. Yuan, "The Study of Control Strategy for VSC-HVDC applied in offshore wind farm and grid connection," pp. 3–6, 2011.

[80]   R. Blasco-Gimenez, N. Aparicio, S. Añó-Villalba, and S. Bernal-Perez, "LCC-HVDC connection of offshore wind farms with reduced filter banks," *IEEE Trans. Ind. Electron.*, vol. 60, no. 6, pp. 2372–2380, 2013.

[81]   Z. Emin, F. Fernandez, M. Poeller, and G. E. Williamson, "Harmonic Distortion Specification and Compliance of an Offshore Wind Generation," pp. 1–6.

[82]   K. Nisak, B. Hasan, K. Rauma, A. Luna, J. I. Candela, P. Rodríguez, and S. Member, "Harmonic Compensation Analysis in Offshore Wind Power Plants Using Hybrid Filters," *IEEE Trans. Ind. Appl.*, vol. 50, no. 3, pp. 2050–2060, 2014.

[83]   A. Holm and K. Yang, "Propagation of harmonic emission from the turbines through the collection grid to the public grid," *22nd Int. Conf. Electr. Distrib.*, vol. 53, no. 9, pp. 1689–1699, 2013.

[84]   T. Liu, J. Wen, X. Fu, C. Ji, and M. Han, "Harmonic Analysis of the Grid-connected Wind Farm by Simulation and Calculation," pp. 1342–1345, 2014.

[85]   N. G. M. Thao, K. Uchida, K. Kofuji, T. Jintsugawa, and C. Nakazawa, "A comprehensive analysis study about harmonic resonances in megawatt grid-connected wind farms," *3rd Int. Conf. Renew. Energy Res. Appl. ICRERA 2014*, pp. 387–394, 2015.

[86]   K. Yang, M. H. J. Bollen, and E. O. A. Larsson, "Aggregation and Amplification of Wind-Turbine Harmonic Emission in a Wind Park," *IEEE Trans. Power Deliv.*, vol. 30, no. 2, pp. 791–799, 2015.

[87]   W. Zhao, C. Xie, and Y. Liu, "Resonance Analysis of DFIG-Based Offshore Wind Farm," *TENCON 2015 - 2015 IEEE Reg. 10 Conf. Macao*, pp. 1–4, 2015.

[88]   C. Buchhagen, C. Rauscher, A. Menze, and J. Jung, "BorWin1 – First Experiences with harmonic interactions in converter dominated grids," *Int. ETG Congr. 2015; Die Energiewende - Blueprints new energy age; Proc. of, Bonn, Ger.*, pp. 27–33, 2015.

[89]   G. L. Xie, B. H. Zhang, Y. Li, and C. X. Mao, "Harmonic propagation and interaction evaluation between small-scale wind farms and nonlinear loads," *Energies*, vol. 6, no. 7, pp. 3297–3322, 2013.

[90]   N. G. Hingorani and L. Gyugyi, *Understanding FACTS: Concepts and Technology of Flexible AC Transmission Systems*. New York: The Institute of Electrical and Electronics Engineering, Inc., 2000.

[91]   C. Barker and B. Andersen, "A new era in HVDC?," *IEE Rev.*, vol. 46, no. 2, pp. 33–39, Mar. 2000.

[92]   S. Nilsson, "Special application considerations for custom power systems," in *IEEE Power Engineering Society. 1999 Winter Meeting (Cat. No.99CH36233)*, 1999, vol. 2, pp. 1127–1131 vol.2.

[93]   O. Anaya-Lara and E. Acha, "Modeling and analysis of custom power systems by PSCAD/EMTDC," *IEEE Trans. Power Deliv.*, vol. 17, no. 1, pp. 266–272, 2002.

[94]   M. V. Chavez-Baez, O. Anaya-Lara, K. L. Lo, and J. McDonald, "Harmonics and power loss reduction in multi-technology offshore wind farms using simplex method," in *2013 48th International Universities' Power Engineering Conference (UPEC)*, 2013, pp. 1–5.

[95]   "Offshore wind in Europe grew 25% in 2017 | WindEurope." [Online]. Available: https://windeurope.org/newsroom/press-releases/offshore-wind-europe-grew-25-2017/. [Accessed: 22-May-2018].

[96]   Published on behalf of The Crown Estate, "A Guide to an Offshore Wind Farm," 2010. [Online]. Available: http://www.thecrownestate.co.uk.

[97]   "The Crown Estate," 2012. [Online]. Available: http://www.thecrownestate.co.uk/.

[98]   "Renewable UK | Offshore Wind," 2014. [Online]. Available: http://www.renewableuk.com/.

[99]   European Wind Energy Association, "2050 : Facilitating 50 % Wind Energy - Recommendations on transmission infrastructure, system operation and electricity market integration," pp. 1–11, 2011.

[100] Sustainable Energy Authority of Ireland, "Introduction to the Wind Energy Roadmap to 2050: The development of renewable energy, including both offshore and onshore wind, is central to our energy policy.," pp. 1–10, 2011.

[101] G. Corbetta, "Wind energy scenarios for 2030," *EWEA*, no. July, pp. 1–8, 2015.

References

[102] "WindEurope." [Online]. Available: https://windeurope.org/about-us/new-identity/#.

[103] ABB Group, "Technical Application Papers No.13 : Wind power plants," Bergamo, Italy, 2011.

[104] W. Zhixin, J. Chuanwen, A. Qian, and W. Chengmin, "The key technology of offshore wind farm and its new development in China," *Renew. Sustain. Energy Rev.*, vol. 13, no. 1, pp. 216–222, 2009.

[105] D. Shen, Xu Liang, and Yingduo Han, "A modified per-unit STATCOM model and analysis of open loop response time," in *2000 IEEE Power Engineering Society Winter Meeting. Conference Proceedings (Cat. No.00CH37077)*, 2000, vol. 4, pp. 2624–2629.

[106] O. Anaya-Lara, N. Jenkins, J. Ekanayake, P. Cartwright, and M. Hughes, *Wind energy generation : modelling and control*, vol. 54, no. 2. Great Britain: John Wiley and Sons Ltd, 2009.

[107] Z. Chen and F. Blaabjerg, "Wind farm-A power source in future power systems," *Renew. Sustain. Energy Rev.*, vol. 13, no. 6–7, pp. 1288–1300, 2009.

[108] "Development of the cost of offshore wind power up to 2015," 2017. [Online]. Available: https://www.wind-energy-the-facts.org/development-of-the-cost-of-offshore-wind-power-up-to-2015.html.

[109] Siemens, "What is the real cost of offshore wind? Wind in the cost debate," 2014.

[110] "10 big wind turbines - Windpower Monthly," 2015. [Online]. Available: http://www.windpowermonthly.com/10-biggest-turbines.

[111] "A History of Offshore Wind Power - Offshore Wind Works," 2015. [Online]. Available: http://offshorewind.works/inform/a-history-of-offshore-wind-power/.

[112] "South Baltic Offshore Wind Energy Regions," 2015. [Online]. Available: http://www.southbaltic-offshore.eu/regions-denmark.html.

[113] A. Ellis, E. Muljadi, J. Sanchez-Gasca, and Y. Kazachkov, "Generic models for simulation of wind power plants in bulk system planning studies," *Power Energy Soc. Gen. Meet. 2011 IEEE*, pp. 1–8, 2011.

[114] S. T. Tentzerakis and S. A. Papathanassiou, "An investigation of the harmonic emissions of wind turbines," *IEEE Trans. Energy Convers.*, vol. 22, no. 1, pp. 150–158, 2007.

[115] O. Anaya-Lara, D. Campos-Gaona, E. L. Moreno-Goytia, and G. P. Adam, *Offshore wind energy generation : control, protection, and integration to electrical systems*, First. UK: John Wiley and Sons Ltd, 2014.

[116] S. Khanum and K. Ratnakar, "Evaluation of reactances and time constants of synchronous generator," *NCRIET-2014*, vol. 3, no. Special, 2014.

[117] E. Muljadi, C. P. Butterfield, H. Romanowitz, and R. Yinger, "Self-Excitation and Harmonics in Wind Power Generation," *J. Sol. Energy Eng.*, vol. 127, no. 4, p. 581, 2005.

[118] R. Singh, A. K. Singh, and A. K. Singh, "Transient Stability Improvement of a FSIG Based Grid Connected wind Farm with the help of a SVC and a STATCOM: A Comparison," *Int. J. Comput. Electr. Eng.*, vol. 4, no. 1, 2012.

[119] M. Bradt, B. Badrzadeh, E. Camm, D. Mueller, J. Schoene, T. Siebert, T. Smith, M. Starke, and R. Walling, "Harmonics and resonance issues in wind power plants," *Proc. IEEE Power Eng. Soc. Transm. Distrib. Conf.*, pp. 1–8, 2012.

[120] E. Hernandez Mayoral and M. Madrigal Martinez, "A step forward in the modeling of the doubly-fed induction machine for harmonic analysis," in *2013 IEEE International Autumn Meeting on Power Electronics and Computing (ROPEC)*, 2013, pp. 1–7.

[121] S. Tentzerakis, S. Papathanassiou, and P. Papadopoulos, "Evaluation of Wind Farm Harmonic Current Emissions," *Proc. EWEC*, no. 1, 2007.

[122] L. H. Kocewiak, J. Hjerrild, and C. L. Bak, "Harmonic models of a back-to-back converter in large offshore wind farms compared with measurement data," *Proc. Nord. Wind Power Conf. 2009*, 2009.

[123] S. Liang, Q. Hu, and W. Lee, "A Survey of Harmonic Emissions of a Commercially Operated Wind Farm," *IEEE Trans. Ind. Appl.*, vol. 48, no. 3, pp. 1115–1123, 2012.

[124] A. A. Romero-Quete, G. O. Suvire, H. C. Zini, and G. Rattá, "Time-varying harmonic analysis in electric power systems with wind farms, through the possibility theory," *DYNA*, vol. 82, no. 192. pp. 185–194, 25-Aug-2015.

[125] M. J. Kaiser and B. Snyder, "Offshore Wind Energy Installation and Decommissioning Cost Estimation in the U.S. Outer Continental Shelf," Herndon, VA, 2011.

[126] M. J. Kaiser and B. Snyder, *Offshore Wind Energy Cost Modeling: Installation and Decommissioning*. London: Springer, 2012.

[127] A. Reidy and R. Watson, "Comparison of VSC based HVDC and HVAC interconnections to a large offshore wind farm," *IEEE Power Eng. Soc. Gen. Meet. 2005*, pp. 1–8, 2005.

[128] "PSCAD Home," 2016. [Online]. Available: https://hvdc.ca/pscad.

[129] C. H. Chien and R. W. G. Bucknall, "Analysis of Harmonics in Subsea Power Transmission Cables Used in VSC–HVDC Transmission Systems Operating Under Steady-State Conditions," *IEEE Trans.*

Power Deliv., vol. 22, no. 4, pp. 2489–2497, Oct. 2007.

[130] J. Finn, "Designing Substations for Offshore Wind Farm Connections," *CIGRE NGN NAREC*. 2008.

[131] M. Zubiaga, G. Abad, J. A. Barrena, S. Aurtenetxea, and A. Carcar, "Spectral analysis of a transmission system based on AC submarine cables for an offshore wind farm," in *2009 35th Annual Conference of IEEE Industrial Electronics*, 2009, pp. 871–876.

[132] F. Santjer, "Influence of transmission lines on grid connection," *DEWI - Global Wind Energy Services*, 2011. [Online]. Available: http://www.dewi.de/dewi_res/fileadmin/pdf/publications/Publikations/15_4_Santjer.pdf.

[133] "NSW Government Departments & Services." [Online]. Available: https://www.nsw.gov.au/.

[134] M. Zubiaga, *Energy Transmission and Grid Integration of AC Offshore Wind Farms*. InTech, 2012.

[135] I. NEPSI - Northeast Power System, "Per-Unit And Base Impedance Calculation." [Online]. Available: http://nepsi.com/resources/calculators/per-unit-impedance-calculator.htm. [Accessed: 14-Apr-2016].

[136] Nexans, "Submarine Power Cables," Nexans, 2013.

[137] A. M. MacNeill, "Submarine power cable transmission line parameters and performance," Dalhousie University, Halifax, Nova Scotia, 2012.

[138] R. Stølan, "Losses and Inductive Parameters in Subsea Power Cables," Norwegian University of Science and Technology, 2009.

[139] "Offshore | EWEA," 2016. [Online]. Available: http://www.ewea.org/policy-issues/offshore/.

[140] "European Network of Transmission System Operators for Electricity," 2016. [Online]. Available: https://www.entsoe.eu/Pages/default.aspx.

[141] J. De Decker, "Offshore Electricity Grid Implementation in the North Sea: A regulatory-economic assessment - Intelligent Energy Europe - European Commission," 2016. [Online]. Available: https://ec.europa.eu/energy/intelligent/projects/en/projects/northseagrid.

[142] "Europe's North Sea Offshore Wind Potential | Revolve Media," 2017. [Online]. Available: http://revolve.media/europes-north-sea-offshore-wind-potential/.

[143] J. Momoh, *Smart Grid: Fundamentals of Design and Analysis*. John Wiley & Sons, 2012.

[144] J. Orlin, "A polynomial time primal network simplex algorithm for minimum cost flows," *Math. Program. 78*, pp. 109–129, 1997.

[145] D. B. Fogel, "An introduction to simulated evolutionary optimization.," *IEEE Trans. Neural Netw.*, vol. 5, no. 1, pp. 3–14, Jan. 1994.

[146] C.-L. Chen and J.-L. Chen, "A neural network approach for evaluating distribution system reliability," *Electr. Power Syst. Res.*, vol. 26, no. 3, pp. 225–229, Apr. 1993.

[147] I. Roytelman, V. Melnik, S. S. H. Lee, and R. L. Lugtu, "Multi-objective feeder reconfiguration by distribution management system," *IEEE Trans. Power Syst.*, vol. 11, no. 2, pp. 661–667, May 1996.

[148] V. Borozan, D. Rajicic, and R. Ackovski, "Improved method for loss minimization in distribution networks," *IEEE Trans. Power Syst.*, vol. 10, no. 3, pp. 1420–1425, 1995.

[149] R. Taleski and D. Rajicic, "Distribution network reconfiguration for energy loss reduction," *IEEE Trans. Power Syst.*, vol. 12, no. 1, pp. 398–406, 1997.

[150] D. Shirmohammadi and W.-H. E. Liu, "Distribution feeder reconfiguration for operation cost reduction," *IEEE Trans. Power Syst.*, vol. 12, no. 2, pp. 730–735, May 1997.

[151] T. E. DcDermott, I. Drezga, and R. P. Broadwater, "A heuristic nonlinear constructive method for distribution system reconfiguration," *IEEE Trans. Power Syst.*, vol. 14, no. 2, pp. 478–483, May 1999.

[152] Y.-T. Hsiao, "Multiobjective Evolution Programming Method for Feeder Reconfiguration," *IEEE Trans. Power Syst.*, vol. 19, no. 1, pp. 594–599, Feb. 2004.

[153] Y.-Y. Hong and S.-Y. Ho, "Determination of Network Configuration Considering Multiobjective in Distribution Systems Using Genetic Algorithms," *IEEE Trans. Power Syst.*, vol. 20, no. 2, pp. 1062–1069, May 2005.

[154] D. Das, "A Fuzzy Multiobjective Approach for Network Reconfiguration of Distribution Systems," *IEEE Trans. Power Deliv.*, vol. 21, no. 1, pp. 202–209, Jan. 2006.

[155] J. Mendoza, R. Lopez, D. Morales, E. Lopez, P. Dessante, and R. Moraga, "Minimal Loss Reconfiguration Using Genetic Algorithms With Restricted Population and Addressed Operators: Real Application," *IEEE Trans. Power Syst.*, vol. 21, no. 2, pp. 948–954, May 2006.

[156] D. Zhang, Z. Fu, and L. Zhang, "An improved TS algorithm for loss-minimum reconfiguration in large-scale distribution systems," *Electr. Power Syst. Res.*, vol. 77, no. 5–6, pp. 685–694, Apr. 2007.

[157] J. A. Martín and A. J. Gil, "A new heuristic approach for distribution systems loss reduction," *Electr. Power Syst. Res.*, vol. 78, no. 11, pp. 1953–1958, Nov. 2008.

[158] D. P. Bernardon, V. J. Garcia, A. S. Q. Ferreira, and L. N. Canha, "Electric distribution network reconfiguration based on a fuzzy multi-criteria decision making algorithm," *Electr. Power Syst. Res.*,

vol. 79, no. 10, pp. 1400–1407, Oct. 2009.

[159] G. Vulasala, S. Sirigiri, and R. Thiruveedula, "Feeder Reconfiguration for Loss Reduction in Unbalanced Distribution System Using Genetic Algorithm," *Int. J. Electr. Electron. Eng.*, vol. 3, no. 12, pp. 754–762, 2009.

[160] Badali S, "Distribution feeder reconfiguration for deviation bus voltage minimization based on modified honey bee mating optimization algorithm," *Eur. J. Sci. Res.*, vol. 71, no. 3, pp. 338–346, 2012.

[161] K. Nagaraju, S. Sivanagaraju, T. Ramana, and V. Ganesh, "Heuristic Approach for Distribution Systems Feeder Reconfiguration to Line Maximum Loadability," *Int. J. Electr. Eng. Informatics*, vol. 4, no. 1, Mar. 2012.

[162] L. S. M. Guedes, A. C. Lisboa, D. A. G. Vieira, and R. R. Saldanha, "A Multiobjective Heuristic for Reconfiguration of the Electrical Radial Network," *IEEE Trans. Power Deliv.*, vol. 28, no. 1, pp. 311–319, Jan. 2013.

[163] J. Torres, J. L. Guardado, F. Rivas-Dávalos, S. Maximov, and E. Melgoza, "A genetic algorithm based on the edge window decoder technique to optimize power distribution systems reconfiguration," *Int. J. Electr. Power Energy Syst.*, vol. 45, no. 1, pp. 28–34, Feb. 2013.

[164] R. M. Vitorino, H. M. Jorge, and L. P. Neves, "Loss and reliability optimization for power distribution system operation," *Electr. Power Syst. Res.*, vol. 96, pp. 177–184, Mar. 2013.

[165] Lee and M. A. El-Sharkawi, *Modern Heuristic Optimization Techniques: Theory and Applications to Power Systems*. John Wiley & Sons, 2008.

[166] A. Zhou, B.-Y. Qu, H. Li, S.-Z. Zhao, P. N. Suganthan, and Q. Zhang, "Multiobjective evolutionary algorithms: A survey of the state of the art," *Swarm Evol. Comput.*, vol. 1, no. 1, pp. 32–49, Mar. 2011.

[167] T. T. Nguyen, S. Yang, and J. Branke, "Evolutionary dynamic optimization: A survey of the state of the art," *Swarm Evol. Comput.*, vol. 6, pp. 1–24, Oct. 2012.

[168] S. M. Elsayed, R. A. Sarker, and D. L. Essam, "A new genetic algorithm for solving optimization problems," *Eng. Appl. Artif. Intell.*, vol. 27, pp. 57–69, Jan. 2014.

[169] M. H. Ali, *Wind energy systems : solutions for power quality and stabilization*. CRC Press, 2012.

[170] M. Madrigal and E. Acha, "A new harmonic power flow method based on the instantaneous power balance," in *10th International Conference on Harmonics and Quality of Power. Proceedings (Cat. No.02EX630)*, 2002, vol. 2, pp. 655–662.

[171] V. Preciado, M. Madrigal, E. Muljadi, and V. Gevorgian, "Harmonics in a wind power plant," in *2015 IEEE Power & Energy Society General Meeting*, 2015, pp. 1–5.

[172] P. Haigh, J. McCullagh, and D. M. Joseph, "Ensuring grid code harmonic compliance of wind farms," *10th IET Int. Conf. AC DC Power Transm. (ACDC 2012)*, pp. 61–61, 2012.

[173] "ENA - G5 CoP WG," 2016. [Online]. Available: http://www.energynetworks.org/electricity/engineering/network-equipment-and-system-issues/g5-code-of-practice-working-group.html.

[174] Engineering directorate of the energy networks Association, *Engineering Recommendation G5/4-1*, no. 4. 2005.

[175] National Grid Transmission Electricity, *The Grid Code*, no. 5. 2012, pp. 1–606.

[176] National Grid, *The serviced grid code – 11 Revision*, no. 4. 2012, pp. 1–3.

[177] Ofgen, *System Operator – Transmission Owner Code*. 2016.

[178] National Grid, *System Operator Transmission Owner Code*. 2016.

[179] T. M. Blooming and D. J. Carnovale, "Application of IEEE Std 519-1992 Harmonic Limits," *Conf. Rec. 2006 IEEE IAS Pulp Pap. Conf. Eat. Electr.*, 2006.

[180] Ofgen, *Standard EN 50160*. 2016.

[181] Schneider electric, *European Standard EN 50160*. 2016.

[182] M. Scheidiger, "Power System Harmonics Analysis of High Power Variable Speed Drives Power System Harmonics Analysis of High Power Variable Speed Drives," Royal Institute of Technology, Sweden, 2013.

[183] B. Badrzadeh and M. Gupta, "Practical experiences and mitigation methods of harmonics in wind power plants," *IEEE Trans. Ind. Appl.*, vol. 49, no. 5, pp. 2279–2289, 2013.

[184] H. Markiewicz and A. Klajn, "Voltage Disturbances Standard EN 50160: Voltage characteristics in public distribution systems," *Power Qual. Appl. Guid.*, vol. 5.4.2, pp. 4–11, 2004.

[185] J. Arrillaga and N. R. Watson, *Power System Harmonics*, 2nd ed. West Sussex: Wiley, 2003.

[186] D. Xia and G. Heydt, "Harmonic Power Flow Studies Part I - Formulation and Solution," *IEEE Trans. Power Appar. Syst.*, vol. PAS-101, no. 6, pp. 1257–1265, Jun. 1982.

[187] D. Xia and G. Heydt, "Harmonic Power Flow Studies - Part II Implementation and Practical Application," *IEEE Trans. Power Appar. Syst.*, vol. PAS-101, no. 6, pp. 1266–1270, Jun. 1982.

References

[188] M. Valcarel and J. G. Mayordomo, "Harmonic power flow for unbalanced systems," *IEEE Trans. Power Deliv.*, vol. 8, no. 4, pp. 2052–2059, 1993.

[189] J. G. Mayordomo, L. F. Beites, R. Asensi, F. Orzaez, M. Izzeddine, and L. Zabala, "A contribution for modeling controlled and uncontrolled AC/DC converters in harmonic power flows," *IEEE Trans. Power Deliv.*, vol. 13, no. 4, pp. 1501–1508, 1998.

[190] "Modeling and simulation of the propagation of harmonics in electric power networks. I. Concepts, models, and simulation techniques," *IEEE Trans. Power Deliv.*, vol. 11, no. 1, pp. 452–465, 1996.

[191] J. Arrillaga, B. C. Smith, N. R. Watson, and A. R. Wood, *Power System Harmonic Analysis*. Chichester: John Wiley & Sons, 1997.

[192] E. Acha and M. Madrigal, *Power Systems Harmonics: Computer Modelling and Analysis*. Chichester: John Wiley & Sons, 2001.

[193] G. Heydt, *Electric Power Quality*. Scottsdale: Stars in a Circle Publications, 1991.

[194] S. Frank and S. Rebennack, "A Primer on Optimal Power Flow: Theory, Formulation, and Practical Examples," no. 14, pp. 18–20, 2012.

[195] J. D. Glover, M. Sarma, and T. Overbye, *Power System Analysis and Design*. Cengage Learning, 2011.

[196] A. J. Wood, B. F. Wollenberg, and G. B. Sheblé, *Power Generation, Operation and Control*. Wiley, 2013.

[197] M. M. Martinez, "Modelling of power electronics controllers for harmonic analysis in power systems," University of Glasgow, 2001.

[198] N. R. Watson and J. Arrillaga, "Harmonics in large systems," *Electric Power Systems Research*, vol. 66, no. 1. pp. 15–29, 2003.

[199] J. C. Das, *Power system analysis : short-circuit load flow and harmonics*. Marcel Dekker, 2002.

[200] S. A. Papathanassiou and M. P. Papadopoulos, "Harmonic Analysis in a Power System with Wind Generation," *IEEE Trans. Power Deliv.*, vol. 21, no. 4, pp. 2006–2016, Oct. 2006.

[201] A. J. Bondy and U. S. R. Murty, *Graph Theory with Applications*. Wiley, 1991.

[202] R. J. Wilson, *Introduction to Graph Theory*. Longman, 2010.

[203] F. S. Roberts, *Graph Theory and Its Applications to Problems of Society*. Philadelphia: SIAM, 1978.

[204] C. Vasudev, *Graph Theory with Applications*. New Delhi: New Age International Ltd Publishers, 2006.

[205] A. Bondy and U. S. R. Murty, *Graph Theory: Graduate text in mathematics*. London: Springer, 2010.

[206] L. Lin, Z. Tie, and X. Cunxi, "The Intelligence System of Failures Diagnosis for Robot Base on the Knowledge Decision-Making," in *2008 International Workshop on Education Technology and Training & 2008 International Workshop on Geoscience and Remote Sensing*, 2008, vol. 2, pp. 820–822.

[207] J. Hualong, W. Hongqi, and T. Yonghong, "Design and realization of a maze robot," in *2011 International Conference on Consumer Electronics, Communications and Networks (CECNet)*, 2011, pp. 201–204.

[208] J. Heng, "A Design Model for Multi-objective Optimization of Photovoltaic Battery Configuration Problem," in *2013 5th International Conference on Intelligent Human-Machine Systems and Cybernetics*, 2013, vol. 2, pp. 226–229.

[209] S. Sabharwal, D. Sabharwal, S. K. Singh, and A. Gabrani, "An event-based approach to generate test scenarios," in *2010 International Conference on Computer and Communication Technology (ICCCT)*, 2010, pp. 551–556.

[210] "Resolutions of the Union and of the Associations," 1967.

[211] I. Todhunter, *Spherical Trigonometry For the use of colleges and schools*. 2006.

[212] G. Van Brummelen, *Heavenly mathematics the forgotten art of spherical trigonometry*. Princeton University Press, 2013.

[213] "Haversine formula - Rosetta Code." [Online]. Available: https://rosettacode.org/wiki/Haversine_formula.

Appendices

The algorithms were implemented in LabVIEW and the virtual instruments developed are as follows:

- *00 Main Genetic.vi* (Main virtual instrument **- Appendix G**)

- *1 PF and HP For Genetic.vi* (Randomly generates chromosomes **- Appendix F**)

- *1 PF and HP only calculate.vi* (Evaluate chromosomes **- Appendix E**)

- *2 Power Flow and Harmonic Propagation.vi* (Calculate the harmonic propagation and power flow of the network **- Appendix A**)

- *0 DFS Algorithm.vi* (Implement the DFS algorithm **- Appendix B**)

- *0 DFS VI Recursivity.vi* (Calls the DFS algorithm to be used recursively **- Appendix B**)

- *3 Graph.vi* (Draw in the North Sea map the connections of the nodes **- Appendix C**)

- *3 Zin.vi* (Obtain distance and Impedance of the lines **- Appendix D**)

- *4map768x1320tif.jpg* (Map of the North Sea used to show the network)

Because LabVIEW is a visual program, the algorithms can be extensive to be clearly displayed on an A4 sheet size, so for the algorithms "*2 Power Flow and Harmonic Propagation.vi*", "*1 PF and HP For Genetic.vi*" and "*00 Main Genetic.vi*" an A1 sheet size is attached where the complete algorithm can be reviewed clearly.

A. Power flow and harmonic propagation. Program code.

Algorithm "*2 Power Flow and Harmonic Propagation.vi*" was implemented in LabVIEW to calculate the power flow and the harmonic propagation on an electrical network. The algorithm requests the data of network and returns a cluster containing all the information. The icon of the algorithm is shown in Figure A.1; it shows the input and output cluster data.
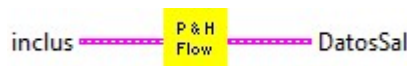
Figure A.1. Icon of the power flow and harmonic propagation data in and out algorithm developed in LabVIEW.

The front panel of the algorithm is shown in Figure A.2; the front panel shows all data that is necessary to calculate the power flow and harmonic propagation. The operation of this algorithm was explained in detail in Chapter 4 and examples were implemented in Chapter 5.
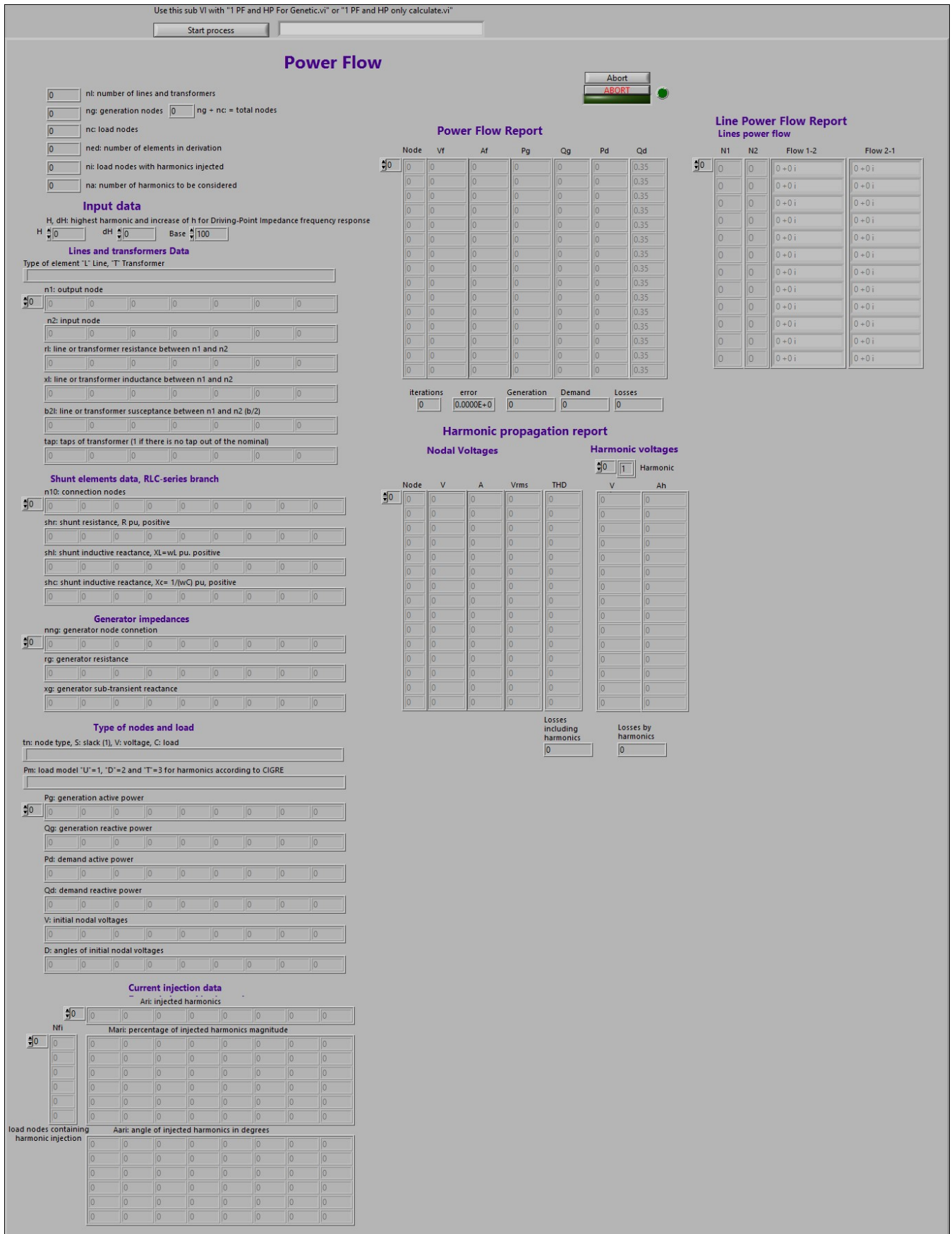
Figure A.2. Front panel of the harmonic propagation and power flow algorithm.

Figure A.19 shows the algorithm implemented; it is printed on an A1 sheet size on page 157. Figure A.19 (a) shows the input cluster and data is assigned to the input variables (b). The number of lines and transformers is obtained from *n1*, a vector of the output node. With the length of *n10* is gotten the number of elements in derivation. Load nodes with harmonics injected are obtained from the length of *nfi*, load nodes containing harmonic injection. *Ari* has the injected harmonics, and its length is the number of harmonic to be considered.

In Figure A.19 (c) there is the initialisation of variables, and the vectors are synchronized to show the same element number for each vector.

In Figure A.19 (d) is shown the process to obtain the number of generation and load nodes. *tn* has the information of node type: Slack node is *S,* and it is node 1, generation node is *V,* and load node is *C*. It is checked each element of *tn*. In (d1) is shown the default option, if there is a load node, *C*, then *nc* is increased. If there is a generation node or the slack node, then *ng* is increased, Figure A.3 (d2) and (d4). The result is the number of total nodes *N*.
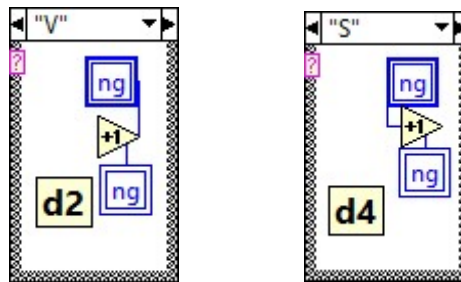
Figure A.3. Options for generation node and slack node.

In Figure A.19 (e) starts the power flow study, first is the variable initialisation. In (f) it is created the nodal admittance matrix of the network, *Ybu*s, for power flow study. In (g) elements in derivation are considered in *Ybus*, if there is an element in derivation, then it is added to *Ybus*, (g1).

In Figure A.19 (h) it is calculated the total power and angles are initialised with zero in nodes *PQ* and *PV*. If the element is a load node, *C*, then is used the option in (h3). In case that element is a generation node then is used the function shown in Figure A.4 (h2).
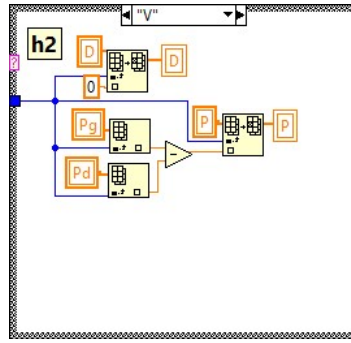
Figure A.4. Option to calculate total power when is a generation node.

In Figure A.19 (i) it is calculated the active and reactive power using *Ybus*. Also, the Jacobian is initialised with *0*s. The matrix is of *NxN*. The Jacobian is calculated in (j). To calculate the Jacobian, different options are depending on the output node type and the input node type.

One option is that the output node is a load node, *C*, Figure A.19 (j2) and the input node be a load node too, *C*, (j2b). If the index of row and column are different then functions to calculate generation active power is in (j2b1a), demand active power in (j2b2a), reactive generation power in (j2b3a) and demand reactive power in (j2b4a).

If the index of row and column are equal then functions to calculate generation active power is in Figure A.5 (j2b1b), demand active power in (j2b2b), reactive generation power in (j2b3b) and demand reactive power in (j2b4b).
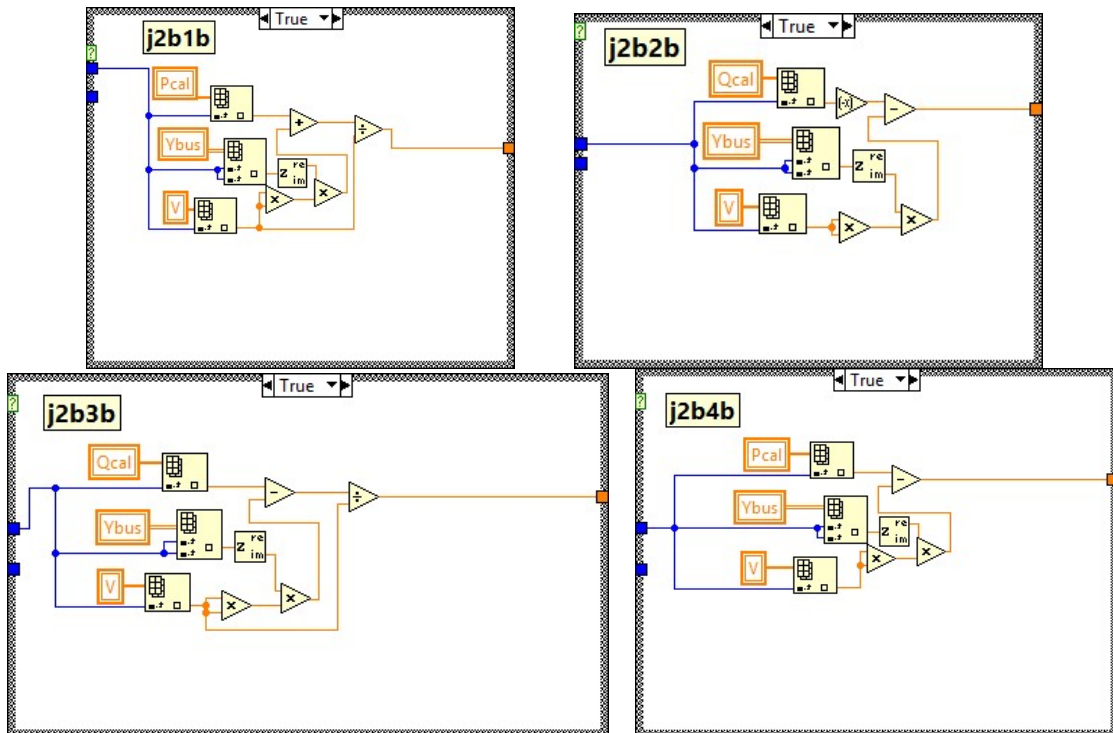
Figure A.5. Functions to calculate Jacobian if the index of column and row is equal.

A second option is that the output node is a load node, *C*, Figure A.19 (j2) and the input node be a generation node, *V*, Figure A.6 (j2c). If the index of row and column are different then only it is calculated demanded power and the functions to calculate active power demanded is in (j2c1a) and reactive power demanded in (j2c2a).
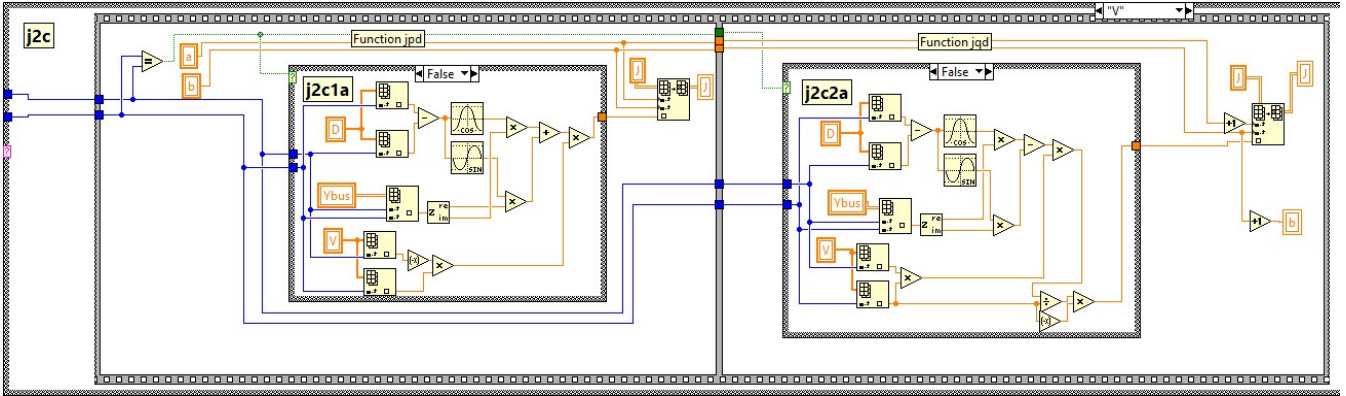
Figure A.6. Functions for connection from load node to generation node.

If the index of row and column are equal then functions to calculate active power demanded is in Figure A.7 (j2c1b) and reactive power demanded in (j2c2b).
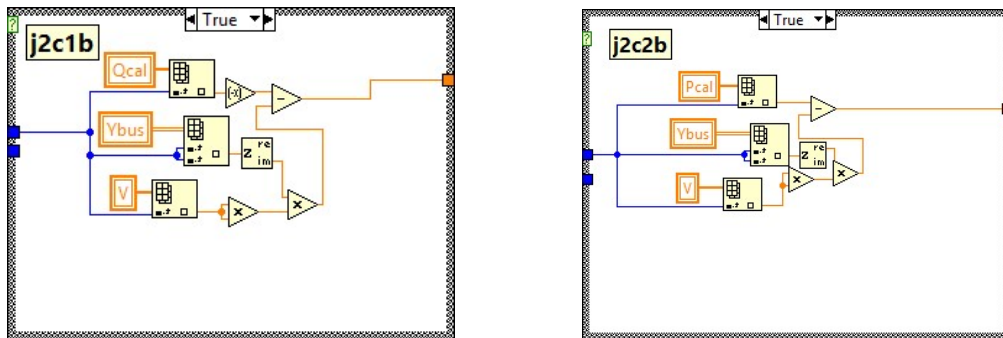
Figure A.7. Functions when index row and column are equal.

A third option is that the output node is a generation node, *V*, Figure A.8 (j3) and the input node be a load node, *C*, (j3b). If the index of row and column are different then only is calculated demanded power, the functions to calculate active power demanded is in (j3b1a), and reactive power demanded in (j3b2a).
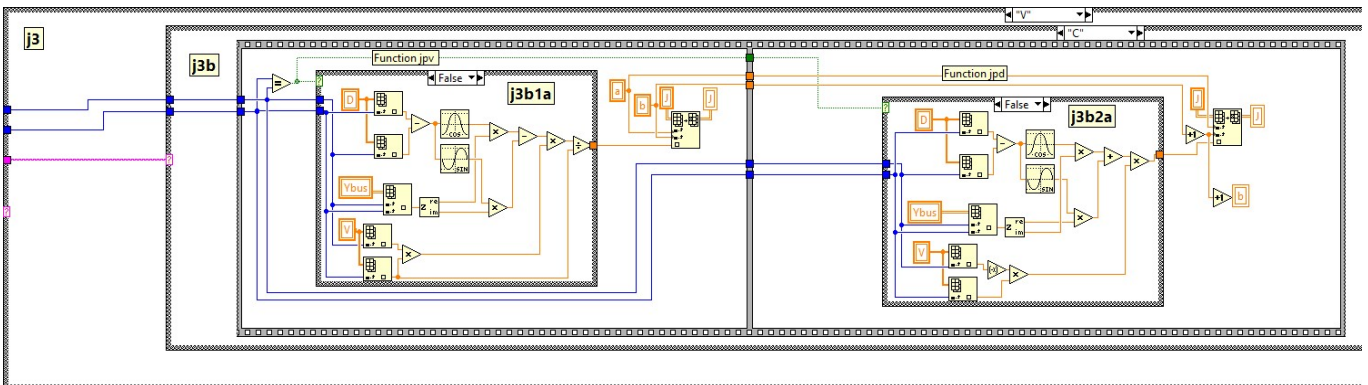
Figure A.8. Functions for connection from generation node to load node.

If the index of row and column are equal then functions to calculate active power demanded is in Figure A.9 (j2c1b) and reactive power demanded in (j2c2b).
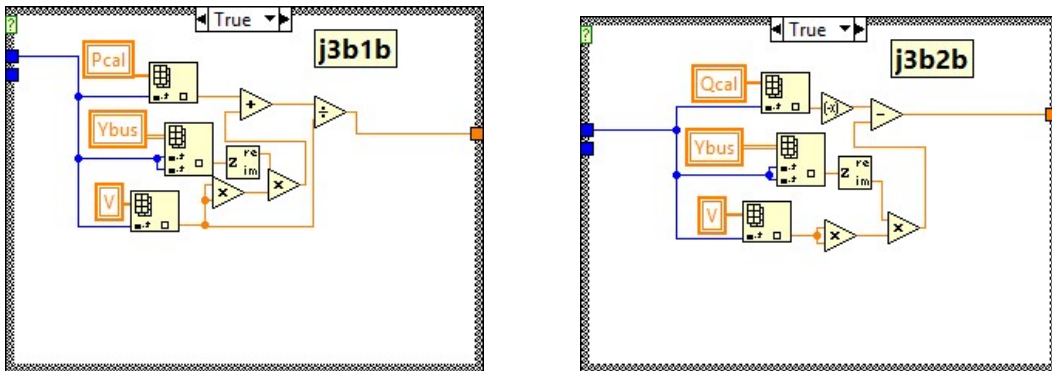
Figure A.9. Functions when index row and column are equal.

Moreover, last option is that the output node is a generation node, *V*, Figure A.8 (j3) and the input node be a generation node too, *V*, Figure A.10 (j3c). If the index of row and column are different then only is calculated active demanded power with the function in (j3c1a).
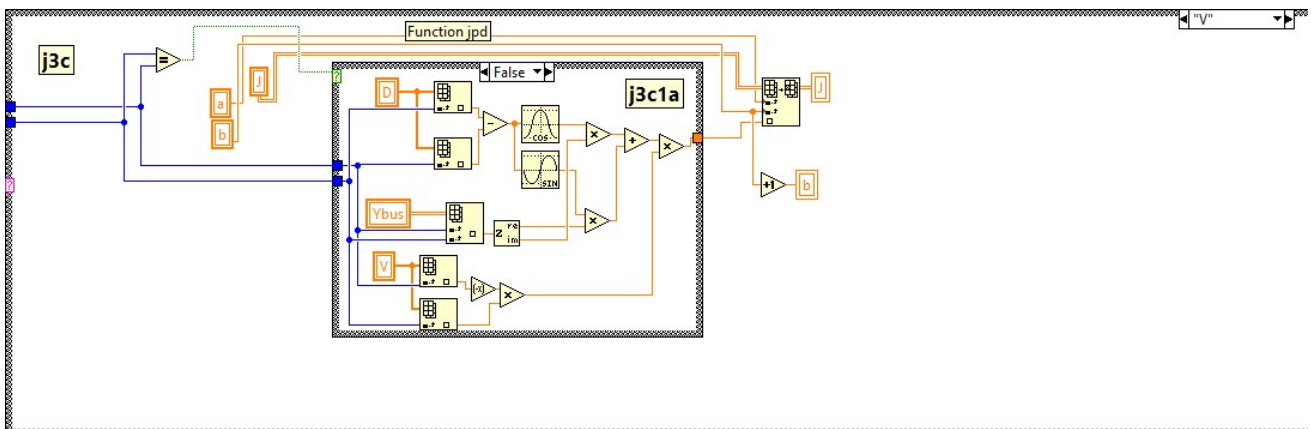
Figure A.10. Functions for connection from generation node to generation node.

If the index of row and column are equal then functions to calculate active power demanded is in Figure A.11 (j3c1b).
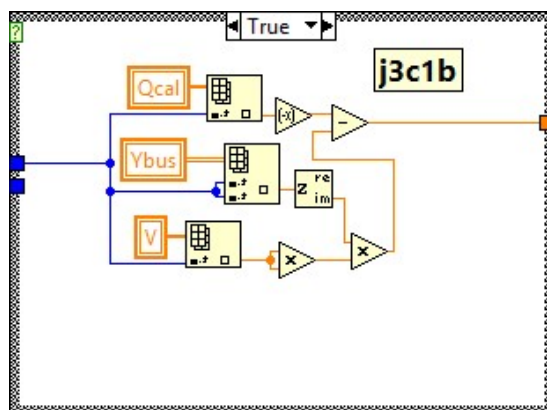
Figure A.11. Functions when index row and column are equal.

Finally, if node analyzed is not a load node, the function used is in Figure A.19 (k1), else is used the function of Figure A.12 (k2).
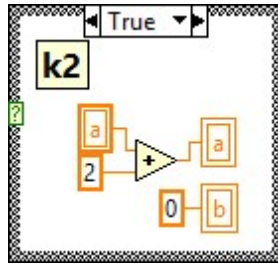
Figure A.12. Function used when is not load node.

Using the spare matrix, Zeros are eliminated from the Jacobian Figure A.19 (l). Then it is calculated deviation in power (m). If the node is load node the function used is in (m1), else the function used is in Figure A.13 (m2).
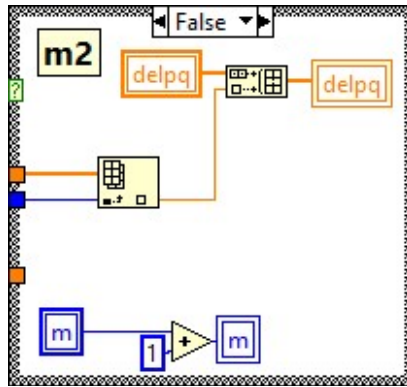
Figure A.13. Function used for not load nodes.

In Figure A.19 (n) deviation of voltage and angle are calculated finding the inverse matrix of the Jacobian and then multiplying by the deviation in power vector. Then it is updated voltage and angle (o). If the node is load node the function used is in (o1), else the function used is in Figure A.14 (o2).
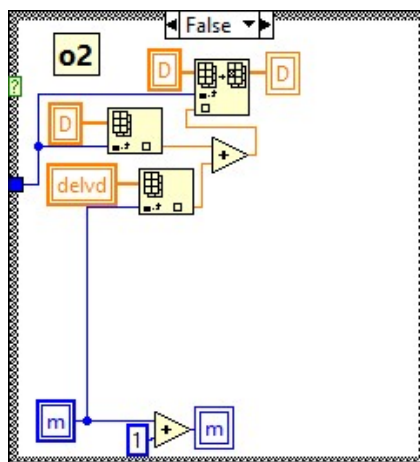
Figure A.14. Function used for not load nodes.

In Figure A.19 (p) is calculated power error between iterations. If one element is more significant than previous error, then this value is the new error (p1). Finally, in Figure A.19 (q) the algorithm checks if the error is smaller than 0.0001 or iterations are not higher than 20 to finish the loop. Iterations usually are less than 5, so if there are more than 20 the system does not converge to a solution.

In Figure A.19 (r) power flow in lines, frequency response and harmonic voltages are calculated.

In Figure A.19 (ra) it is calculated power flow in lines. In (r1) it is initialised active and reactive power generated. In (r2), it is checked all nodes, if any element is of generation, then is used the function (r2a). In (r3), it is calculated the power flow in lines using the load nodes angles and initial voltages. Finally, in (r4), it is calculated total demand, total generation and total losses.

In Figure A.19 (s), it is calculated frequency response. In (s1), admittance and impedance matrices are initialised with *0*s. In (s2) is compared the input, if the input is a transformer, *T*, then is used the function in (s2a), if input line, *L*, is used the function in Figure A.15. (s2b).
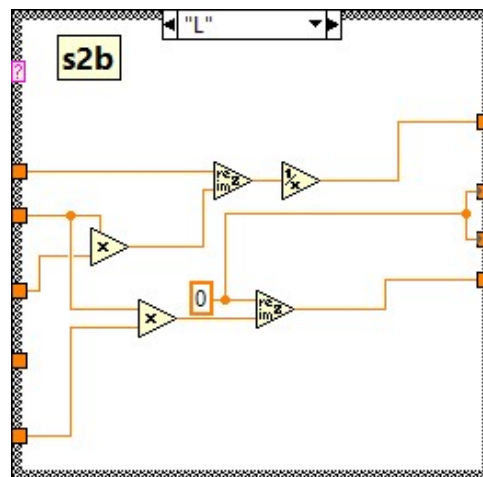
Figure A.15. Function used if the input is a line.

In Figure A.19 (s3) it is calculated admittance matrix. In (s4) generator impedances and in (s5), shunt elements are considered to calculate the admittance matrix, if at least one element is different of zero, then it is used the function in (s5a).

In Figure A.19 (s6), if active demand power is different from zero, then it is selected CIGRE load input, the default option is model One, *U*, (s6a1). Figure A.16 (s6a2) shows model Two, *D*, and (s6a3) shows model Three, *T*.
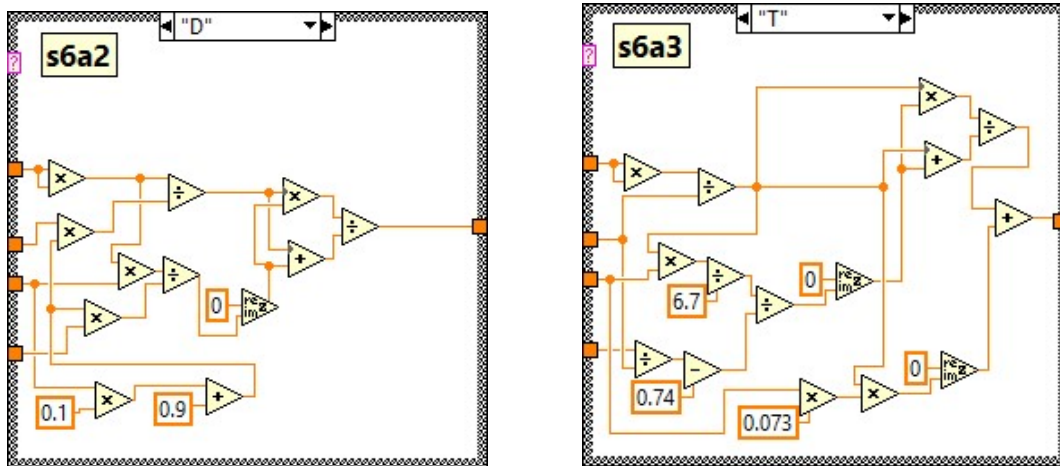
Figure A.16. CIGRE load model Two and Three.

In Figure A.19 (s7) it is calculated the impedance matrix using the complex inverse matrix function. In (s8), it is calculated the diagonal of the admittance matrix, and it is joined to the impedance matrix. In (s9), if it was calculated the highest harmonic for driving point impedance frequency response, then it is used the function to transpose impedance matrix.

In Figure A.19 (t), it is calculated harmonic voltages. In (t1), it is created the injection vector at the fundamental frequency. In (t2), it is a loop with the number of harmonics to be considered. In (t3), it is created the injection vector at *h* harmonics. In (t4), it is a loop with the number of lines of the network. If the element is a transformer, *T*, then it is used the function in (t4a), if the element is a line, *L*, it is used function in Figure A.17 (t4b).
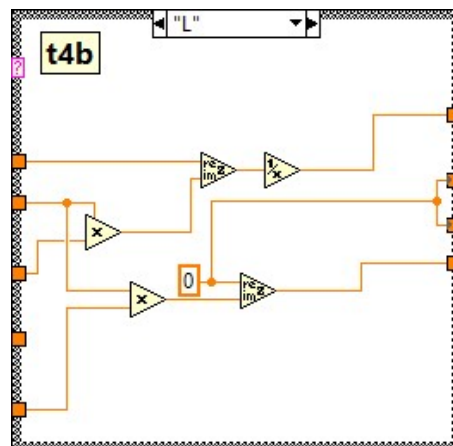
Figure A.17. Function used if the element is a line.

In Figure A.19 (t5), it is calculated admittance matrix including line and transformer inputs. In (t6), generator inputs and in (t7), shunt elements are considered, If at least one element is different from zero, then it is used the function in (t7a).

In Figure A.19 (t6), if active demand power is different from zero, then it is selected CIGRE input load, the default option is model One, *U*, (t8a1). Figure A.18 (t8a2) shows model Two, *D*, and (t8a3) shows model Three, *T*.
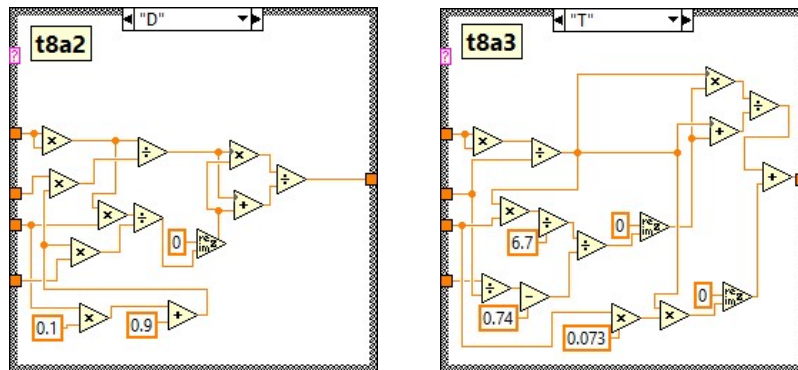
Figure A.18. CIGRE input load model Two and Three.

In Figure A.19 (t9), it is calculated the harmonic line voltage finding the inverse matrix of the Admittance matrix and then multiplying by the line power flow.

In Figure A.19 (u), power flow, line power flow and harmonic propagation reports are displayed. In (v), harmonic voltages are converted from complex to polar. In (w), total fundamental and harmonic voltages are calculated. In (x), the information is assigned to its respective output variable.

In Figure A.19 (y), line power flow generated by harmonics is calculated. In (y1), it is initialised active and reactive power generated. In (y), it is checked all nodes; if any element is of generation, then it is used the function (y2a). In (y3), it is calculated the power flow in lines using the load nodes angles and initial voltages. Finally, in (y4), it is calculated total demand, total generation and total losses including harmonics.

Finally, in Figure A.19 (z), all the information is transferred to the output cluster to be used in the evolutionary algorithm.

On the next page, there is attached the expanded diagram.
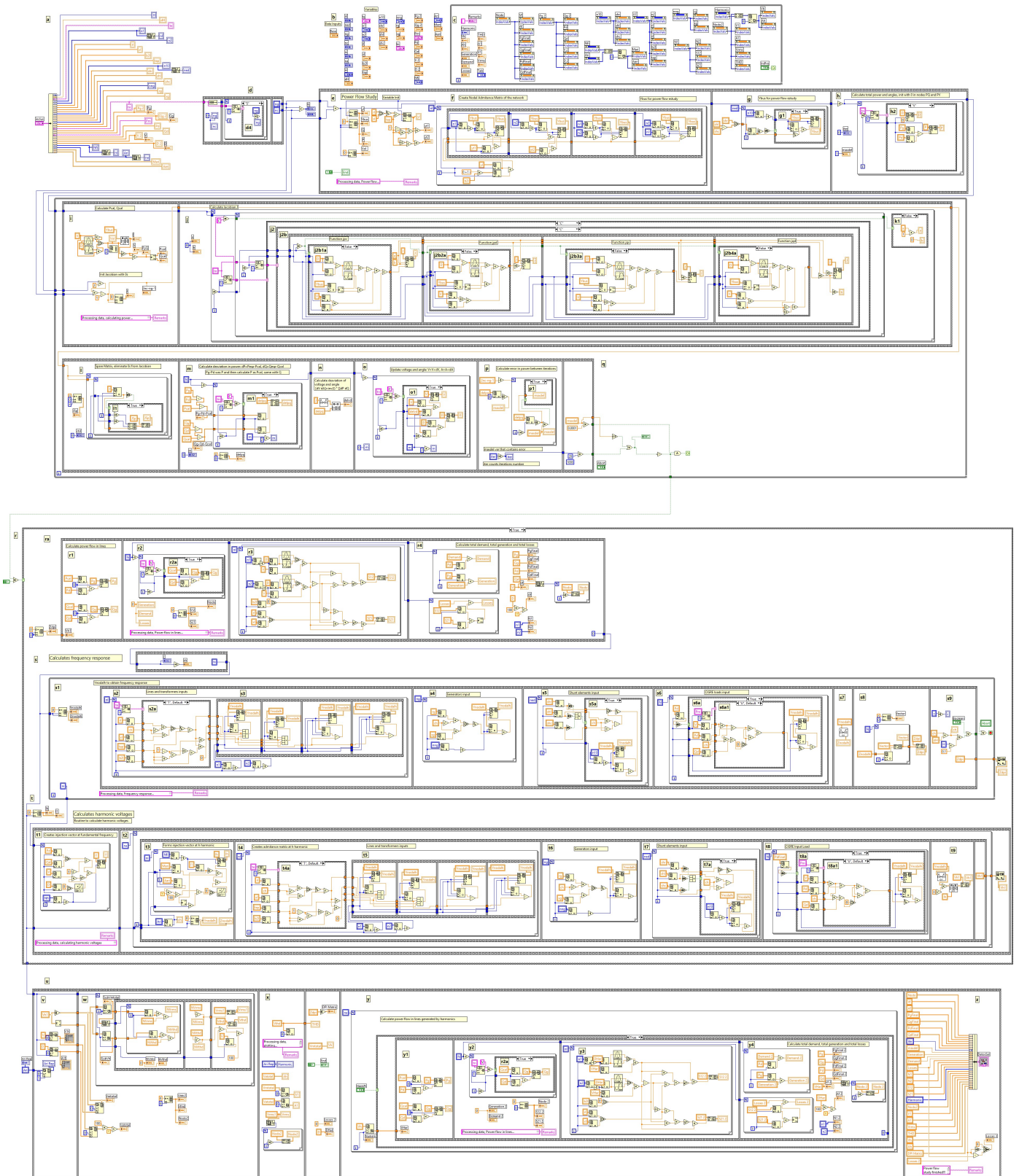
Figure A.19. Algorithm to calculate power flow and harmonic propagation.
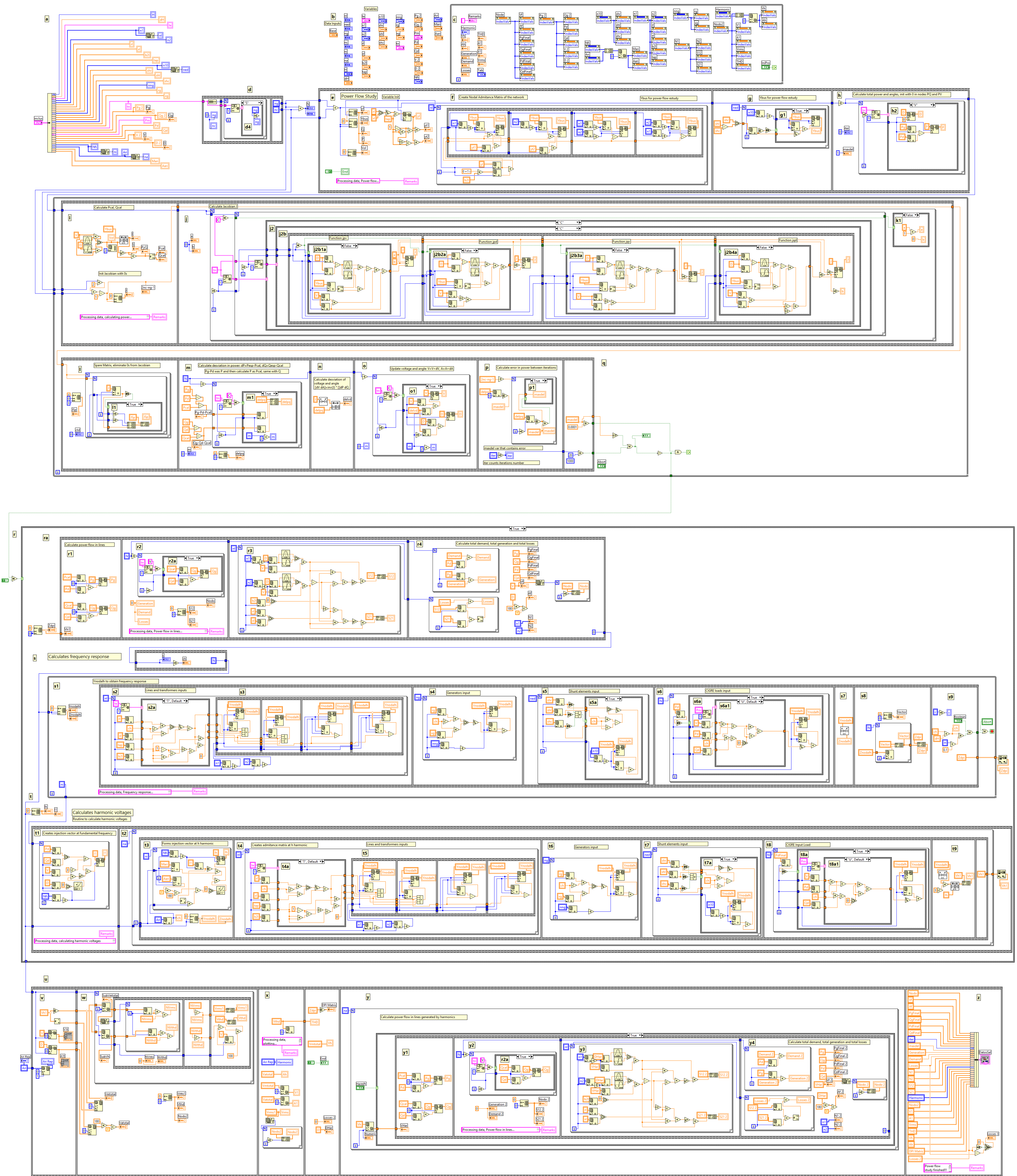
Figure A.19. Algorithm to calculate power flow and harmonic propagation.

B. Elimination of isolated nodes. Program code.

Algorithms "*0 DFS Algorithm.vi*" and "*0 DFS VI Recursivity.vi*" were implemented in LabVIEW to locate the isolated nodes and eliminate them from being sure that all the nodes are connected to the network and avoid configurations that have isolated nodes or islands. The algorithm requests the number of nodes and the matrix of network connections and returns the matrix of connections and a Boolean vector to know if the configuration has or has not isolated nodes. The icon of DFS is shown in Figure B.1; it shows the input and output data.

Figure B.1. Icon of DFS algorithm.

The front panel of the algorithm is shown in Figure B.2, the front panel shows the number of nodes and starts with the vertex *1*. The algorithm returns a TRUE if all the nodes are connected, else returns a FALSE.

Figure B.2. DFS Front panel.

Figure B.3 shows the DFS algorithm. The DFS algorithm consists of two parts; the first part read matrix and number of nodes, (a), marks all nodes with zero as is shown in (b) and then start to analyse every node. All the nodes are marked as not visited, and the algorithm starts with vertex 1. Then the algorithm starts the second part of the algorithm (c). Finally send the information of the matrix of connection to the output, (d).
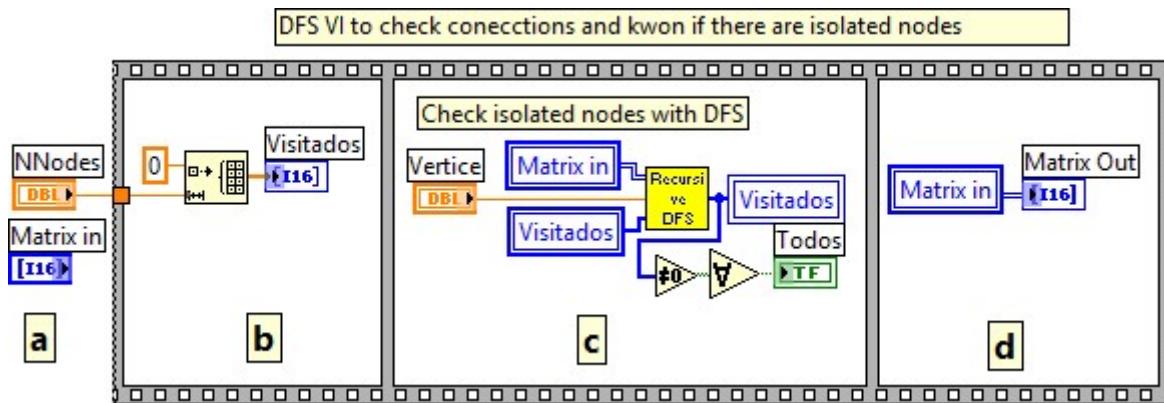
Figure B.3. DFS algorithm.

The second part it is the recursive algorithm used in DFS. Figure B.4 shows the icon of the recursive algorithm used for depth-first search. Input data are the matrix of reviewed nodes, number of vertex that is analyzed and the vector of visited vertices.
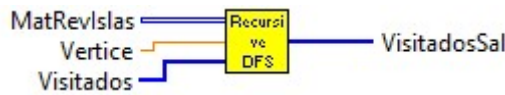
Figure B.4. Icon of the recursive DFS algorithm.

Figure B.5 shows the front panel of the recursive DFS, Front panel has the vertex number, neighbour list and the list of the visited neighbours.

Figure B.5. Recursive DFS front panel.

The recursive algorithm code is shown in Figure B.6. The algorithm starts with the initial input data, Figure B.6 (a). The algorithm checks the visited nodes that are marked with *1*; if there is a *1* in the visited node, then it is marked the node as a neighbour, (b).

If the list of neighbours is empty and the vertex is number 1, Figure B.6 (c), the algorithm restarts the number of visited nodes, Figure B.7 (d2), else the algorithm calls itself until the last edge of the node is analysed, Figure B.6 (d1) and (e).

The algorithm generates the matrix with all the nodes, and if all the components of the matrix are TRUE means that all the nodes are connected.
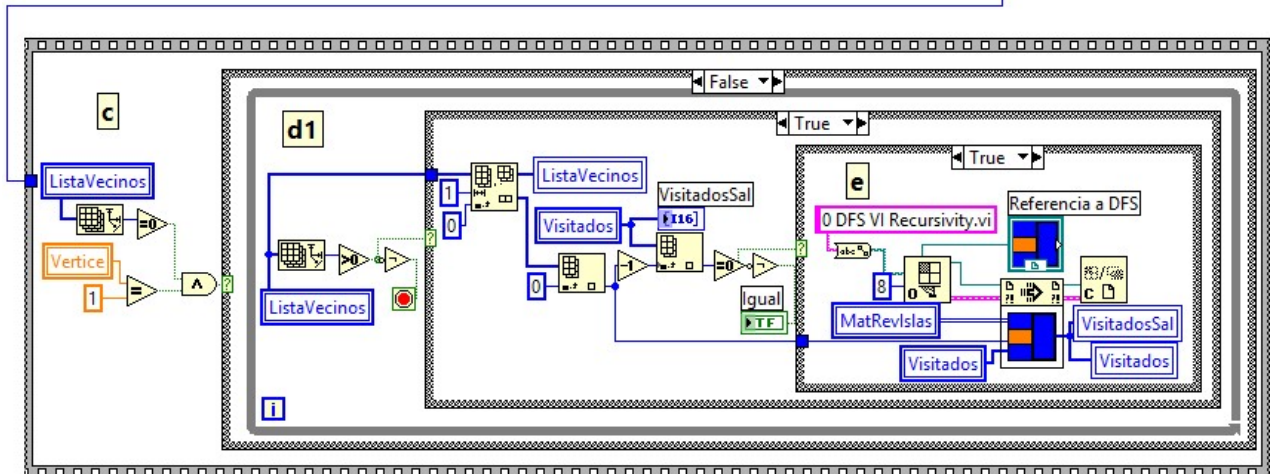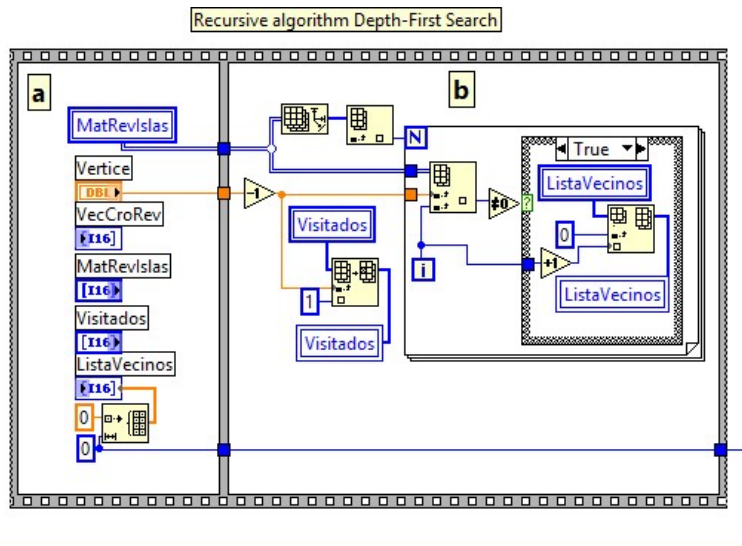
Figure B.6. Recursive DFS algorithm.
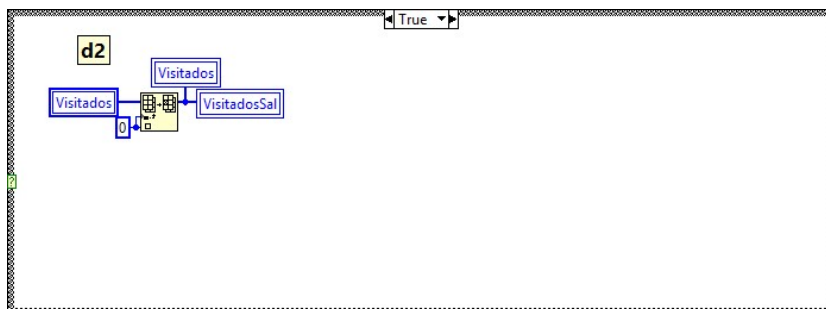
Figure B.7. Algorithm restores visited nodes.

C. Graph nodes on the map. Program code.

Algorithm "*3 Graph.vi*" was implemented in LabVIEW to locate the nodes in a map of the North Sea and graph the connections between nodes. The icon of the graph algorithm is shown in Figure C.1. Input data requested are the coordinates in the map, name of the node and colour of the text. Output data is the map with the nodes and connections.
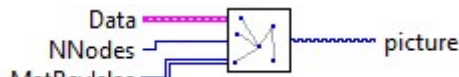
Figure C.1. Icon of the graph algorithm.

Figure C.2 shows the front panel of the algorithm that is used to graph the nodes and lines. The map of the North Sea is gotten from the file "*4map768x1320tif.jpg*".
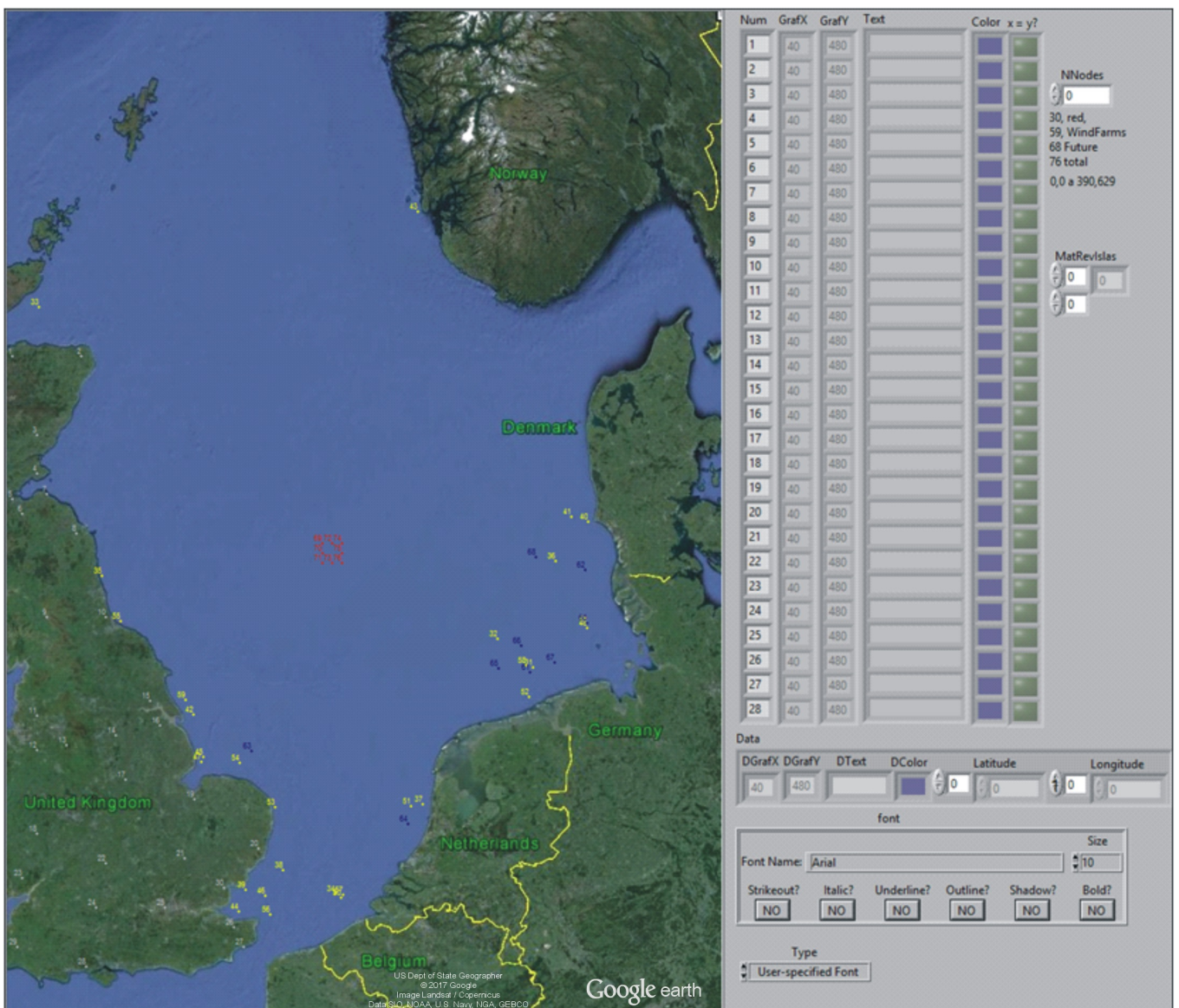
Figure C.2. Graph algorithm Front panel.

Figure C.3 show the algorithm to graph nodes and lines. In (a) the algorithm obtains the vector of coordinates to locate the node in the map, the name of the node and the colour of the text. In Figure C.3(b) is getting the picture of the map. In (c) there is a loop to draw the node and text of each node. Finally, (d) is a loop to draw the lines to connect the nodes from point A to point B according to the matrix of connections.
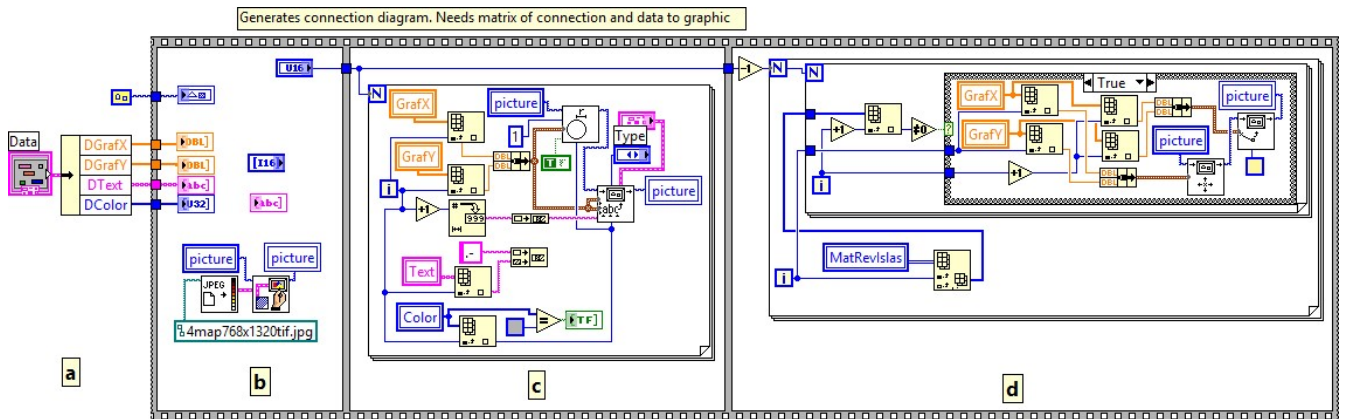
Figure C.3. Graph algorithm.

D. Calculate distance and impedance of the line. Program code.

The algorithm "*3 Zin.vi*" was implemented in LabVIEW to obtain the distance between nodes and with the distance obtain data of resistance, reactance and susceptance of each line of the configuration. Figure D.1 shows the icon. Input data are latitude and longitude of the start point and end point; the other parameter is the cable type. Output data are resistance, reactance, susceptance and distance between the two points.
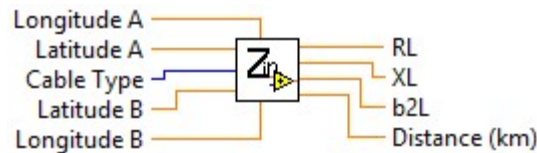
Figure D.1. Icon of distance and impedance algorithm.

Figure D.2 shows the front panel with the cable type and latitudes and longitudes as inputs and resistance, reactance, susceptance and distance as outputs.
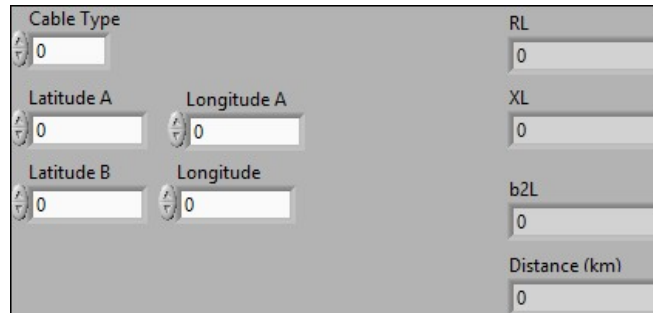
Figure D.2. Distance and Impedance front panel.

In Figure D.3 is shown the algorithm to obtain data. (a) shows latitudes and longitudes that are converted to radians to implement the haversine formula in (b). With the distance between the two points, it is chosen the type of conductor. The default type is shown in (c1). Finally, (d) multiplies values per kilometre by the distance to obtain the data that will be used in the algorithm.
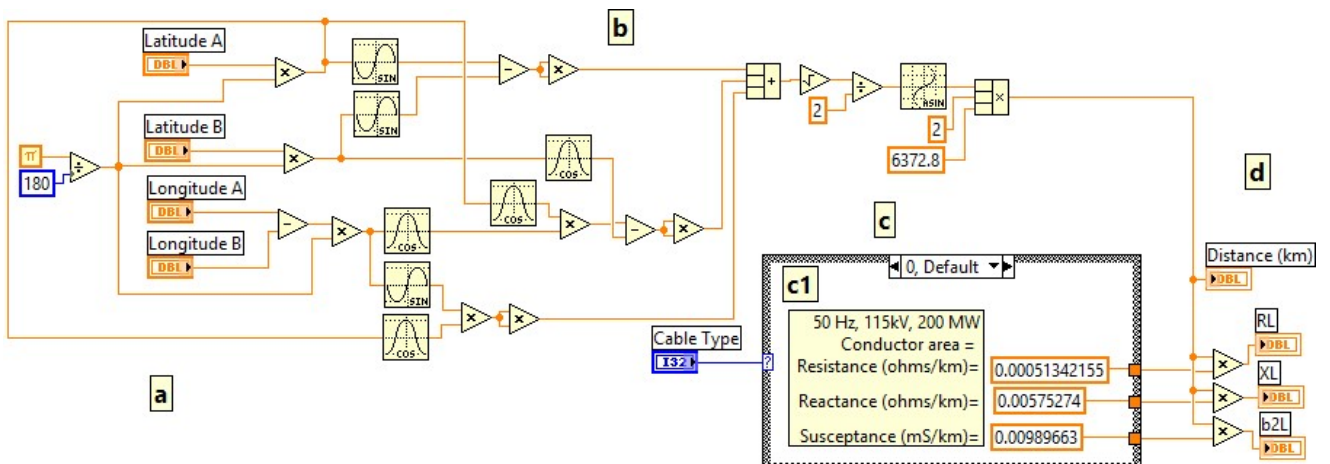
Figure D.3. Distance and impedance algorithm.

Figure D.4 shows another five cable types that can be used in the algorithm implemented. The default type is the used for 50 Hz, 115 kV and 200 MW.
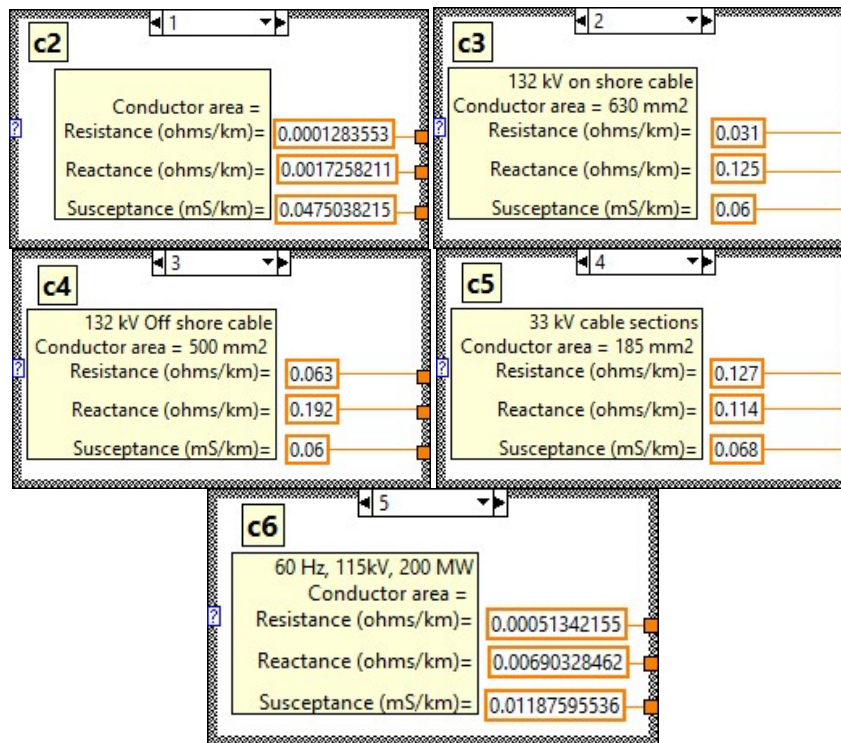
Figure D.4. Different cables values.

E. Evaluate chromosomes. Program code.

Algorithm "*1 PF and HP only calculate.vi*", was implemented in LabVIEW to evaluate the chromosomes. This algorithm calculates the power flow and harmonic propagation on an electrical network. The algorithm requests a cluster with data of network and returns a cluster with all the information. The icon of the algorithm is shown in Figure E.1; it shows the input data cluster and output are three clusters.
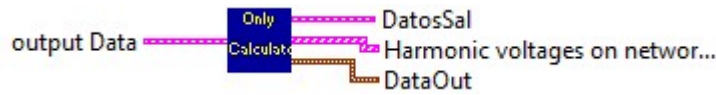
Figure E.1. Icon of the algorithm to evaluate the chromosomes.

The front panel is shown in Figure E.2; the front panel shows the cluster with all data that is necessary to calculate power flow and harmonic propagation. The output is power flow, line power flow and harmonic propagation reports.
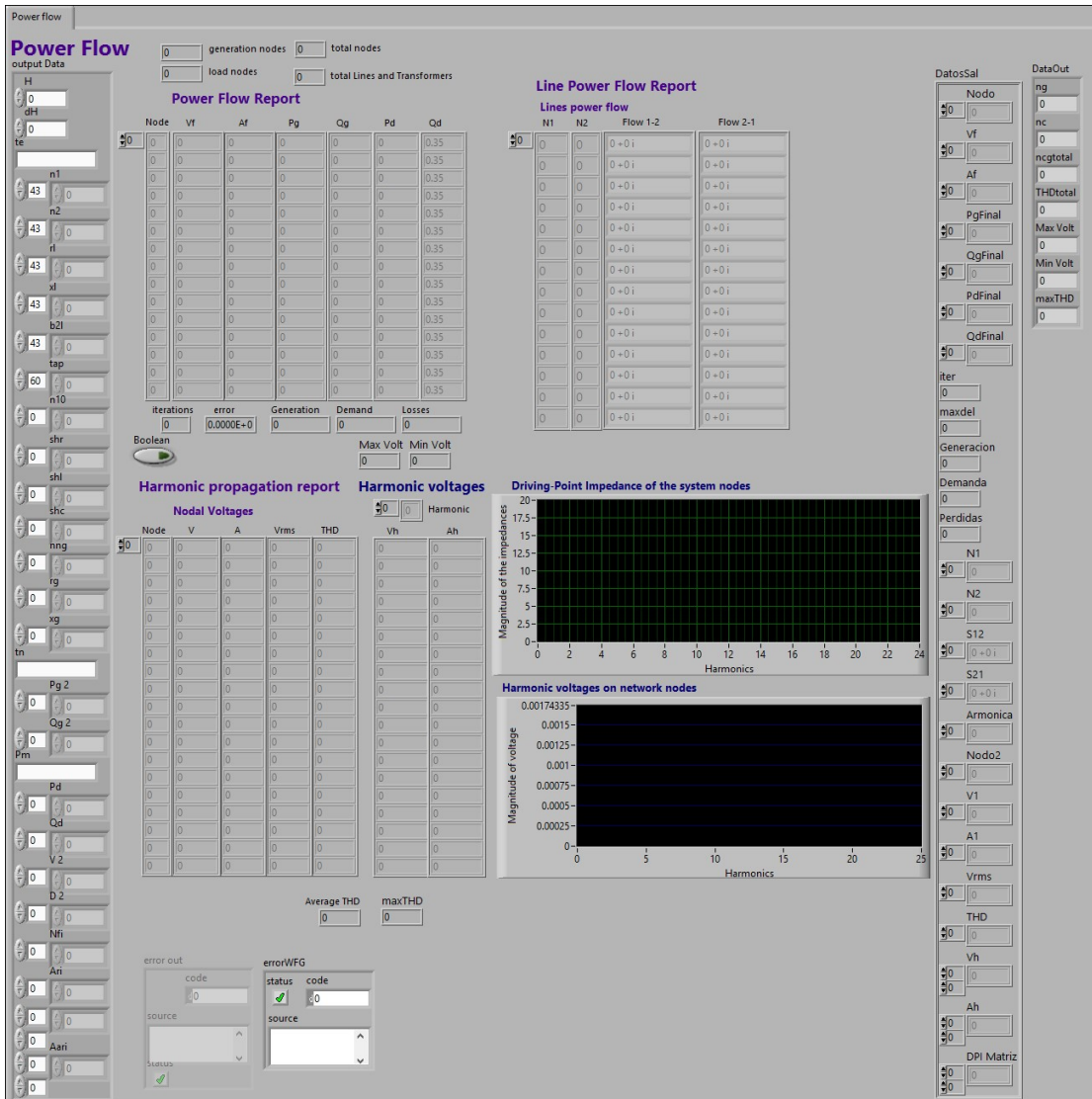
Figure E.2. Front panel of the algorithm to evaluate chromosomes.

Figure E.4 shows the algorithm implemented. Figure E.4 (a), it is shown the synchronization of the vector to show the same element calculated flows.

In Figure E.4 (b), it is called sub-routine or sub-vi to calculate power flow and harmonic propagation. All information is shown in the front panel and also, it is sent to the output cluster.

In Figure E.4 (c), it is shown the process to obtain the number of generation and load nodes. *tn* has the information of node type: Slack node is *S,* and it is node 1, generation node is *V,* and load node is *C*. It is checked each element of *tn*. In (c1), it is shown the default option, if there is a load node, *C*, then *nc* is increased. If there is a generation node or the slack node, then *ng* is increased, Figure E.3 (c2) and (c4). The result is the number of total nodes *N*.
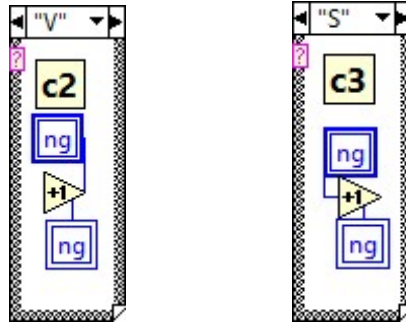
Figure E.3. Options for generation node and slack node.

In Figure E.4 (d), it is calculated the logarithmic average of THD, and it is configured the graph to show harmonic voltages of the system in each node.

In Figure E.4 (e), it is gotten the logarithm of the sum of each THD, to obtain a logarithmic average of THD. In (f), it is formed a cluster with the logarithmic average to be used in the main program. Finally, in Figure E.4 (g) the loop is finished.
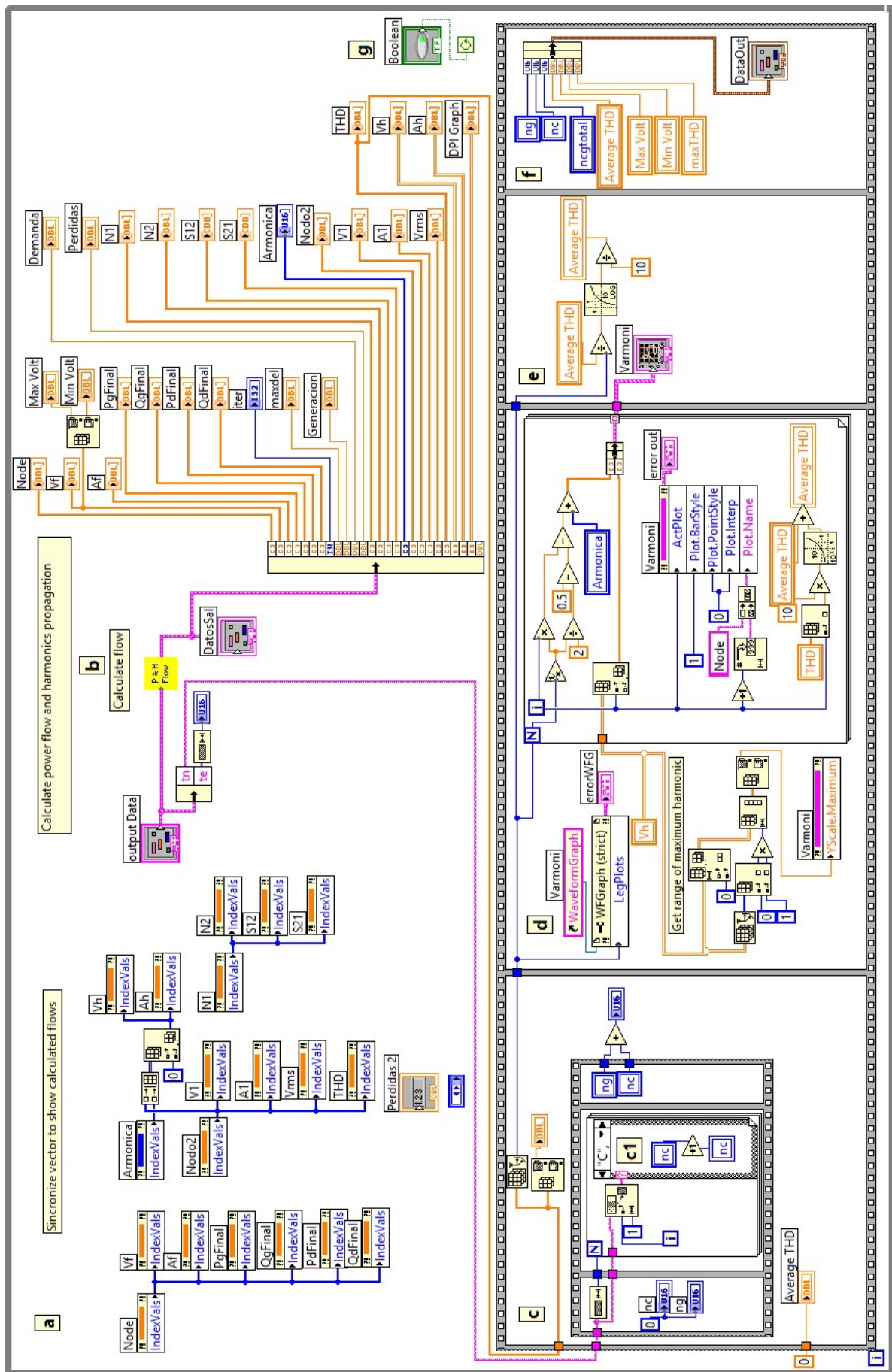
Figure E.4. Algorithm to evaluate chromosomes.

F. Randomly generate and evaluate chromosomes. Program code.

The algorithm "*1 PF and HP For Genetic.vi*", was implemented in LabVIEW to generate the chromosomes. The algorithm requests the number of chromosomes to be generated, the maximum distance that will be allowed and scenario to be considered, and returns a cluster with all the information of power flow and harmonic propagation. The icon of the algorithm is shown in Figure F.1; it shows the input data cluster and output data.
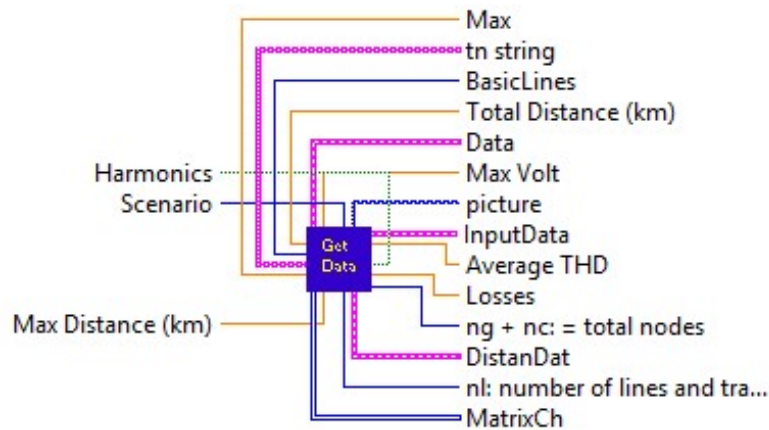
Figure F.1. Icon of the algorithm that generates initial population randomly.

The front panel of the algorithm is shown in Figure F.2.
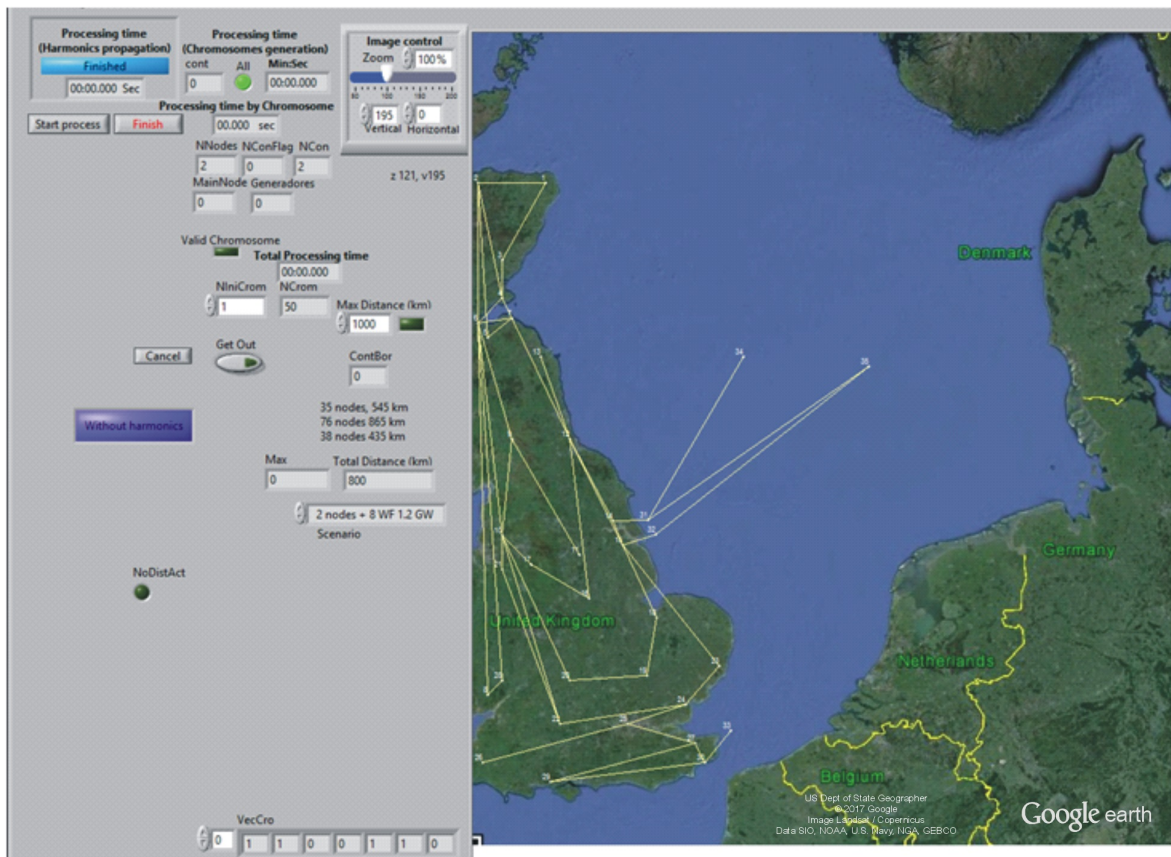
Figure F.2. Front panel of the algorithm that generates an initial population randomly.

Figure F.9 shows the algorithm implemented; it is printed on an A1 sheet size on page 175.

In Figure F.9 (a), it is the information of each node. First two columns are the location of the node in the map. The third column is the name of each node. Next two columns are the coordinates of each node on the earth, latitude and longitude are used to calculate the distance between nodes and obtain resistance, reactance and susceptance for each line.

In Figure F.9 (b), it is shown data for different scenarios. In (b1) it is data for Scenario 1, that is the default scenario.

Figure F.3 (b2) shows data for Scenario 2 and Figure F.4 (b3) shows data for Scenario 3.

Boolean constant *Used* determines which node will be used.

Constant *Main* will determine if the node is part of the fixed grid or if it is of the proposed nodes.

Constant *FlagNode* determines if the node can be connected randomly to another node.

Constant *FlagLine* determines if the line that connects two nodes can be eliminated.

The other variables are data that will be used to calculate power flow and harmonic propagation.

Variable *nng* determines which nodes are proposed as wind power cluster and variable *Pg* determines the generated power by each one.

Variable *Nfi* indicates which nodes will inject harmonics.

Variable *Ari* determines which harmonics will be injected.

Variable *Mari* determines the percentage of the fundamental and angle that is injected.

Used	Main	FlagNode	FlagLine

b8

8 wind farms, 2 Wind Cluster at Dogger Bank and Hornsea

nl	41	ned	2	ni	3
ng	6	nc	24	na	7

te — Line and Transformer Data

n1	0	0	0	0	0	0	0	0	0	0
n2	0	0	0	0	0	0	0	0	0	0
rl	0	0	0	0	0	0	0	0	0	0
xl	0	0	0	0	0	0	0	0	0	0
b2l	0	0	0	0	0	0	0	0	0	0

Taps of transformers — tap

tap	0	0	0	0	0	0	0	0	0	0

Reactive power capacitance

n10	0	0	0	0
shr	0	0	0	0
shl	0	0	0	0
shc	0	0	0	0

Generation Data — nng

nng	31	32	33	34	35	36	37	38	0	0	0
rg	0.0003	0.0003	0.0003	0.0003	0.0003	0.0003	0.0003	0.0003	0	0	0
xg	0.003	0.003	0.003	0.003	0.003	0.003	0.003	0.003	0	0	0

Network voltages and loads — tn VVVVVVV

From voltage PG MW — Pg

Pg	0.12	0.12	0.12	0.12	0.1	0.18	0.12	0.2	0	0	0

Qg MVAr

Qg	0	0	0	0	0	0	0	0	0	0	0

Pm TTTTTTT

From Load PG MW — Pd

Pd	-0.04	-0.04	-0.04	-0.04	-0.04	-0.04	-0.04	-0.04	0	0	0

Qg MVAr

Qd	0.001	0.001	0.001	0.001	0.001	0.001	0.001	0.001	0	0	0

Magnitude Voltge

V	1.01	1.01	1.01	1.01	1.01	1.01	1.01	1.01	0	0	0
D	0	0	0	0	0	0	0	0	0	0	0
Nfi	31	32	33	34	35	36	37	38	0	0	0
Ari	3	5	7	11	13	17	19	0	0	0	

Mari

0.31	-0.905	0.78	-0.065	0.038	-0.025	0.009	0	0	0
0.31	-0.905	0.78	-0.065	0.038	-0.025	0.009	0	0	0
0.31	-0.905	0.78	-0.065	0.038	-0.025	0.009	0	0	0
0.31	-0.905	0.78	-0.065	0.038	-0.025	0.009	0	0	0
0.31	-0.905	0.78	-0.065	0.038	-0.025	0.009	0	0	0
0.31	-0.905	0.78	-0.065	0.038	-0.025	0.009	0	0	0
0.31	-0.905	0.78	-0.065	0.038	-0.025	0.009	0	0	0
0.31	-0.905	0.78	-0.065	0.038	-0.025	0.009	0	0	0
0	0	0	0	0	0	0	0	0	0
0	0	0	0	0	0	0	0	0	0

0	0	0	0	0	0	0	0	0	0
0	0	0	0	0	0	0	0	0	0
0	0	0	0	0	0	0	0	0	0
0	0	0	0	0	0	0	0	0	0
0	0	0	0	0	0	0	0	0	0
0	0	0	0	0	0	0	0	0	0
0	0	0	0	0	0	0	0	0	0
0	0	0	0	0	0	0	0	0	0
0	0	0	0	0	0	0	0	0	0

WF 300, WF 600, WF 400, WF, WF, WF, 1.2 GW, Dogger, Hornsea, Seagreen

Figure F.3. Data for Scenario 2.

Used | Main | FlagNode | FlagLine

b9

2 nodes 15 wind farms, 3 Wind Cluster at Dogger Bank, Hornsea and Seagreen

nl 41   ned 2   ni 3
ng 6   nc 24   na 7

te   Line and Transformer Data

n1   0 0 0 0 0 0 0 0 0 0 0

n2   0 0 0 0 0 0 0 0 0 0 0

rl   0 0 0 0 0 0 0 0 0 0 0

xl   0 0 0 0 0 0 0 0 0 0 0

b2l   0 0 0 0 0 0 0 0 0 0 0

Taps of transformers   tap   0 0 0 0 0 0 0 0 0 0 0

Reactive power capacitance   n10   0 0 0 0

shr   0 0 0 0

shl   0 0 0 0

shc   0 0 0 0

Generation Data   nng   7   38 39 40 41 42 43 44 45 46 47 48

rg   0   0.0003 0.0003 0.0003 0.0003 0.0003 0.0003 0.0003 0.0003 0.0003 0.0003 0.0003

xg   0   0.003 0.003 0.003 0.003 0.003 0.003 0.003 0.003 0.003 0.003 0.003

Network voltages and loads   tn   VVVVVVVVVVVVVVV

From voltage PG MW   Pg   0   0.01 0.01 0.01 0.12 0.12 0.12 0.12 0.1 0.18 0.12 0.2

Qg MVAr   Qg   0   0 0 0 0 0 0 0 0 0 0

Pm   TTTTTTTTTTTTTTT

From Load PG MW   Pd   0   -0.004 -0.004 -0.004 -0.04 -0.04 -0.04 -0.04 -0.04 -0.04 -0.04 -0.04

Qg MVAr   Qd   0   0.0001 0.0001 0.0001 0.001 0.001 0.001 0.001 0.001 0.001 0.001 0.001

Magnitude Voltge   V   0   1.01 1.01 1.01 1.01 1.01 1.01 1.01 1.01 1.01 1.01 1.01

D   0   0 0 0 0 0 0 0 0 0 0 0

Nfi   7   38 39 40 41 42 43 44 45 46 47 48

Ari   0   3 5 7 11 13 17 19 0 0 0

Mari   14 / 0

0.31	-0.905	0.78	-0.065	0.038	-0.025	0.009	0	0	0
0.31	-0.905	0.78	-0.065	0.038	-0.025	0.009	0	0	0
0.31	-0.905	0.78	-0.065	0.038	-0.025	0.009	0	0	0
0.31	-0.905	0.78	-0.065	0.038	-0.025	0.009	0	0	0
0	0	0	0	0	0	0	0	0	0
0	0	0	0	0	0	0	0	0	0
0	0	0	0	0	0	0	0	0	0
0	0	0	0	0	0	0	0	0	0
0	0	0	0	0	0	0	0	0	0

14 / 0

0	0	0	0	0	0	0	0	0
0	0	0	0	0	0	0	0	0
0	0	0	0	0	0	0	0	0
0	0	0	0	0	0	0	0	0
0	0	0	0	0	0	0	0	0
0	0	0	0	0	0	0	0	0
0	0	0	0	0	0	0	0	0
0	0	0	0	0	0	0	0	0
0	0	0	0	0	0	0	0	0

WF 300
WF 600
WF 400
WF
WF
WF
WF
1.2 GW

Dogger

Hornsea

Seagreen

Figure F.4. Data for Scenario 3.

In Figure F.9 (c), it is shown data of the fixed network. Data of the selected scenario is added to obtain the network that will be used. In (d), it is assigned vectors that indicate outline node and in line node. In (e) starts a loop to create a matrix to be analyzed by DFS.

In Figure F.9 (f1), the coordinates of each node are assigned to a cluster. In (f2), it is a loop to select only nodes that are used in the scenario selected (g1). In (f3), it is checked the nodes to be used. If the element is TRUE, then it is calculated the number of generators and number of nodes (f3a); else in Figure F.5 (f3b), it is shown option to add a new node.
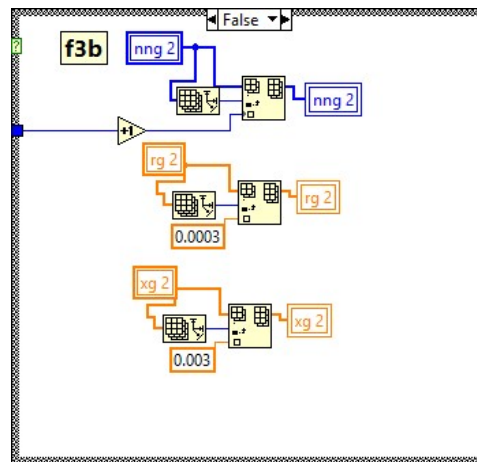
Figure F.5. Add a new node.

In Figure F.9 (g1), it is obtained node type, in (g1), it is a case of a Slack node, *S*. In Figure F.6 (g2), it is generation option, *V*, and (g3), it is load option, *C*.

Figure F.6. Options for generator and load node.

In Figure F.9 (f4), it is formed assigned the wind option according to constant *MainNode*. (f5) Initialise variables according to the number of nodes.

In Figure F.9 (f5), it is created the connection matrix according to constant *FlagNode*. If the element is TRUE then in (f5a) it is selected an element from *Constant Main*, if the element is not of the fixed networks, then it is selected to form part of the network, if the random number is 1, then it is selected to be connected (f5b). If the new line was selected, then is gotten resistance, reactance and susceptance using latitude and

longitude of both nodes and if the line is not longer than the maximum distance then this line is selected (f5c).

In Figure F.9 (f6), the algorithm ensures that the primary nodes are connected, and in (f7), it is created the identity matrix that will be used to check isolated nodes. In (f8), connection matrix is checked to verify that all nodes are connected. In (f9), are assigned all necessary parameters to use the line.

In Figure F.9 (h) starts a loop to calculate power flow and harmonic propagation in each chromosome. In (h1), the vector is synchronized to show the same element. In (h2), it is calculated the number of generation and load nodes. *tn* has the information of node type: Slack node is *S,* and it is node 1, generation node is *V,* and load node is *C.* It is checked each element of *tn*. In (h2), it is shown the default option, if there is a load node, *C*, then *nc* is increased. If there is a generation node or the slack node, then *ng* is increased, Figure F.7. The result is the number of total nodes *N*.
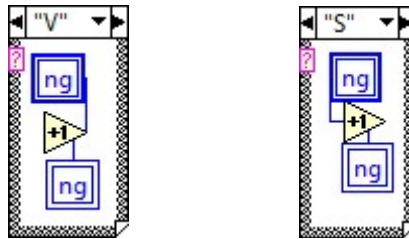
Figure F.7. Options for generation node and slack node.

In Figure F.9 (h3), it is calculated voltage range, if it is out of range, (0.9-1.1p.u.), the chromosome is deleted. In (h4), it is calculated the logarithmic average of THD, and it is configured the graph to show harmonic voltages of the system in each node and in (h5) it is gotten the logarithm of the sum of each THD, in order to obtain a logarithmic average of THD. The equation used to obtain the logarithmic average of THD is:

$$\text{logarithmic average of THD} = \log\sum_{i=1}^{N} 10^{V_{THDi}} \qquad (\text{F.1})$$

In Figure F.8 (i1) starts the process to generate the report *Print Report* is TRUE. In (i2), there are loops to generate a string of nodes type, generation nodes and shunt elements nodes. Also, outline nodes and in line nodes are generated. In (i3), it is the process to generate an html file with all the information of each configuration generated. Finally, in Figure F.9 (j), it is shown the process to finish this algorithm.
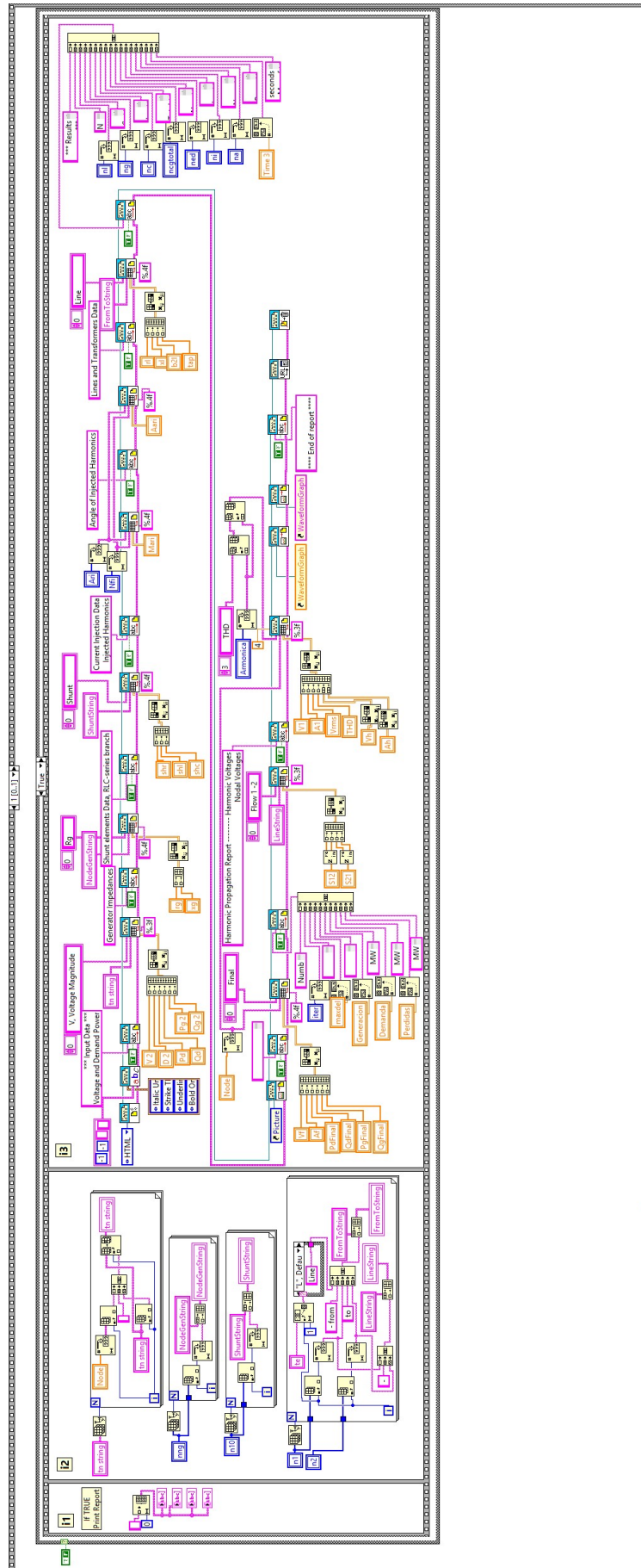
Figure F.8. Process to generate a report.

On the next page, there is attached the expanded diagram.
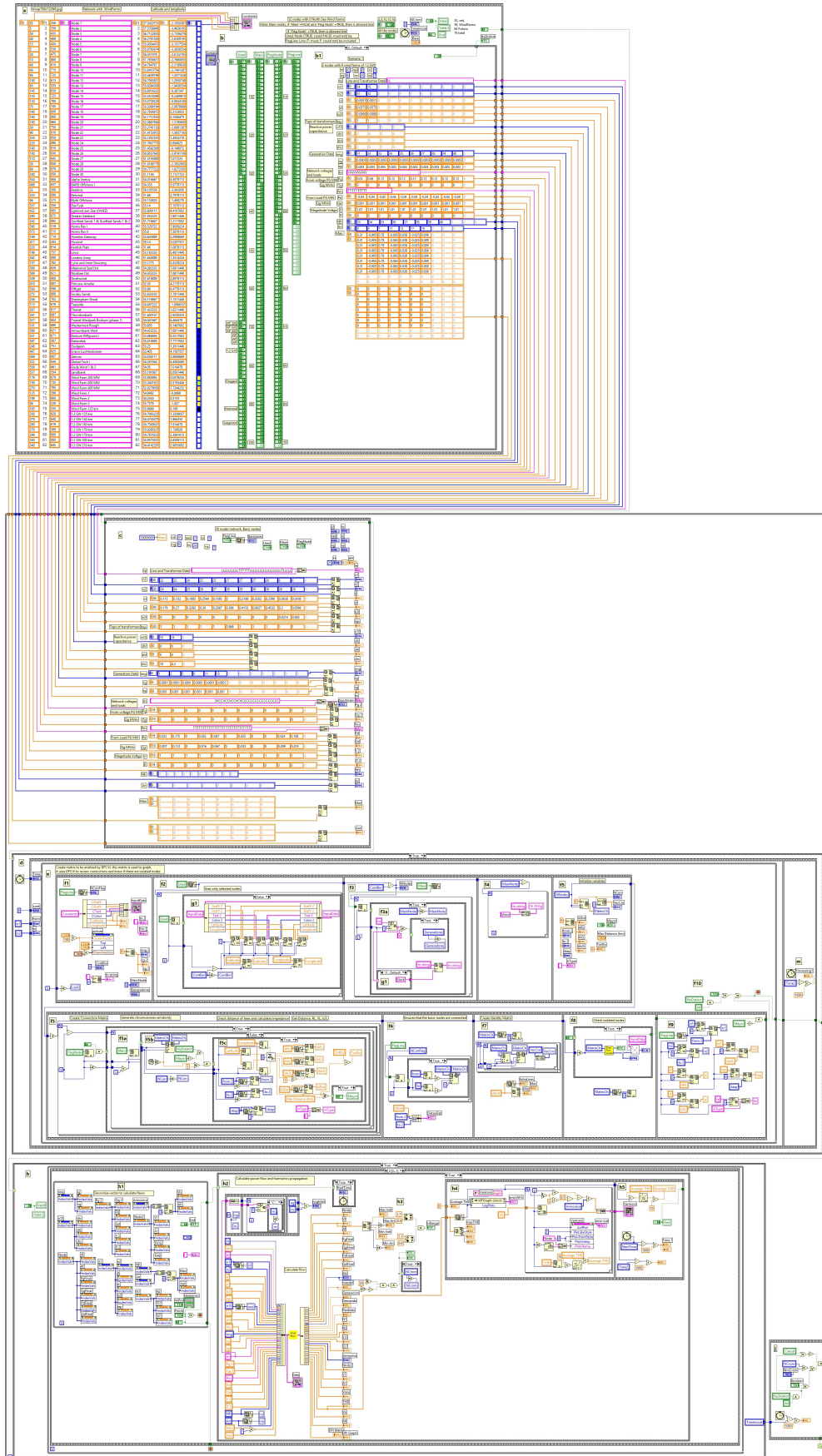
Figure F.9. Algorithm to randomly generate and evaluate initial population.
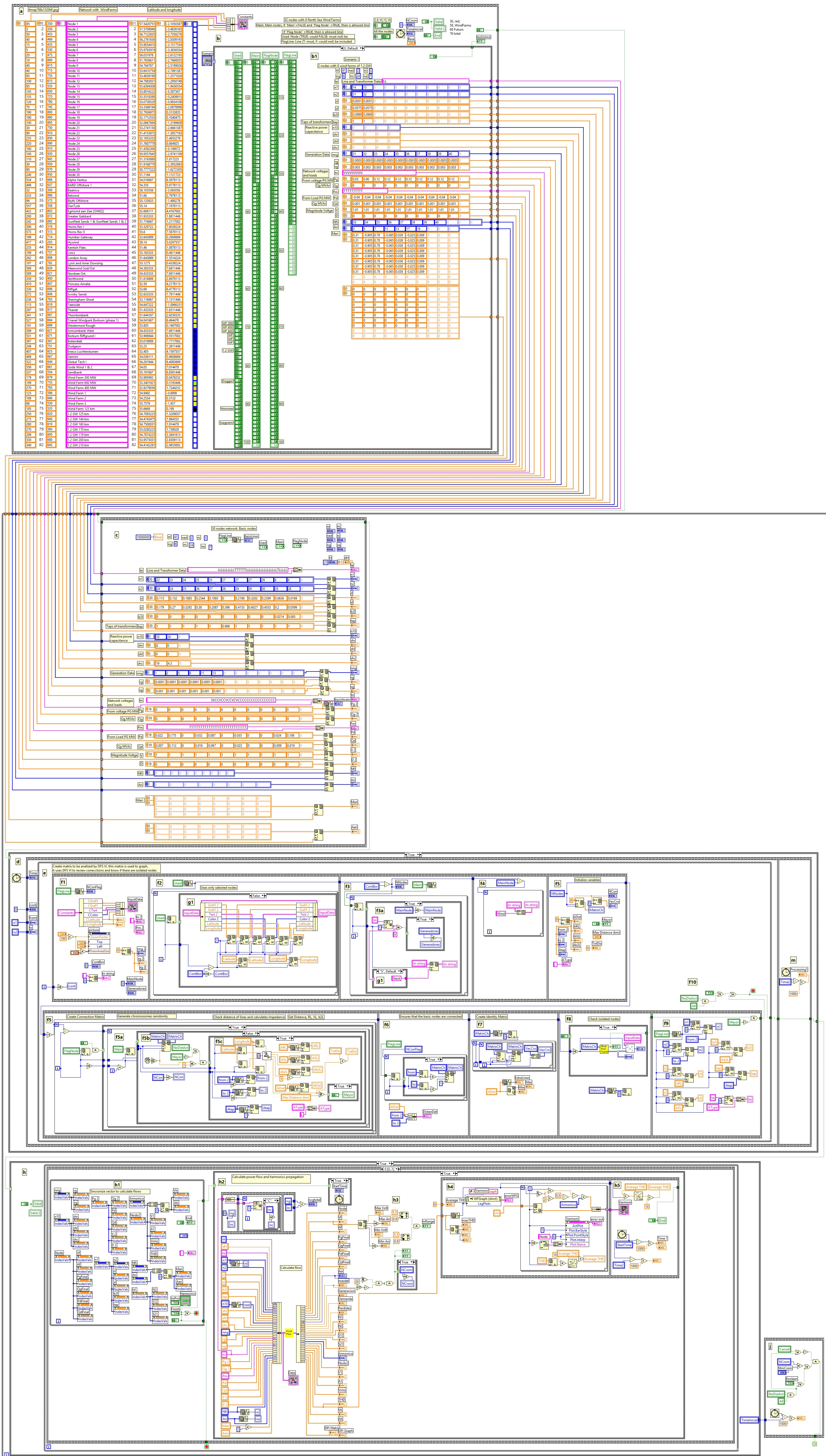
Figure F.9. Algorithm to generate initial population randomly.

G. Evolutionary algorithm. Program code.

A genetic algorithm, called *"00 Main Genetic.vi"*, was implemented in LabVIEW. This algorithm is the multi-objective evolutionary algorithm to minimise harmonics and reduce power losses in offshore wind farms.

The icon of the algorithm is shown in Figure G.1; it does not have any input or output, because this is the main program used to generate all the process.

Figure G.1 Icon of the evolutionary algorithm

Figure G.2 shows the front panel of the algorithm. It shows the map where all the nodes of the network will be located. There are graphics to show the chromosomes generated and Pareto fronts, and there are comparisons with other functions. The front panel contains data from the nodes and lines of the networks and power flow and line flow reports. Also, it is shown the harmonic propagation report, DPI graph and harmonic voltages in each node.
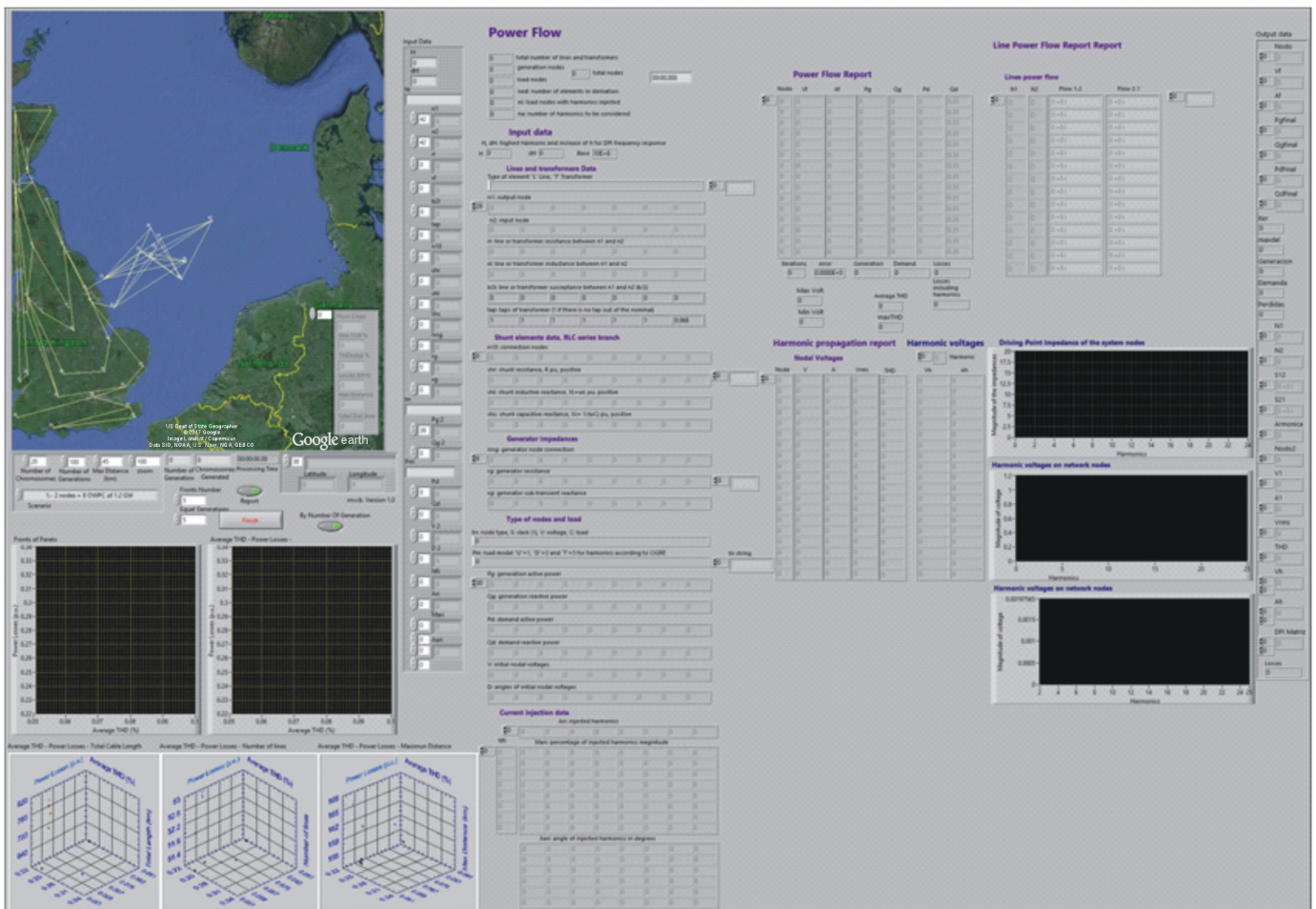
Figure G.2 Front panel of the evolutionary algorithm developed.

Figure G.9 shows the algorithm implemented; it is printed on an A1 sheet size on page 181. Before the algorithm starts, must be selected number of chromosomes that will be generated in the first generation, maximum distance allowed to connect between nodes, scenario, there are ten possible scenarios, a number of Pareto fronts to be considered and if a report of the process want to be generated, then Boolean variable *Report* must be TRUE. After select initial values, the algorithm can be started.

Figure G.9 (a1) starts the time counter and (a2) shows variable initialisation. In (a3), it is a loop to generate the first generation of chromosomes. In (a4) starts the timer. In (a5), it is called the subroutine "*1 PF and HP For Genetic.vi*", in order o generate the first generation of chromosomes according to the scenario selected. In (a6), it is reading the timer to obtain the generation time of each chromosome. In (a7), it is compared the number of chromosomes generated with the number to generate, if the number is equal, then the process finishes. In (a8) arrays with all the information for each configuration are formed. In (a9) the chromosomes generated are displayed. In (a10), it is gotten total generation time. In (a11), it is prepared the first stage of the report.

Figure G.9 (b) shows the start of the evolutionary algorithm. In (c), it is a loop to eliminate the longest lines. In (c1), it is selected data for only one configuration. In (c2), it is calculated the total length of the network, without the length of the fixed network.

In Figure G.9 (d1), it is gotten the maximum line length index. In (d2) the index is used to obtain data of the connection matrix. If it is Scenario 0, 1, 2 or 3 and there are not more lines, then the algorithm is not allowed to eliminate this connection, this is in order to generate chromosomes because on these scenarios there are very long lines and the power flow algorithm does not converge to a solution. In (d3), it is called subroutine "*0 DFS Algorithm.vi*", if all nodes are connected, and maximum distance allowed is in range, then the connection is eliminated (e1), else the connection is restored, Figure G.3 (e2). Loop continues until there are not more lines that can be deleted.
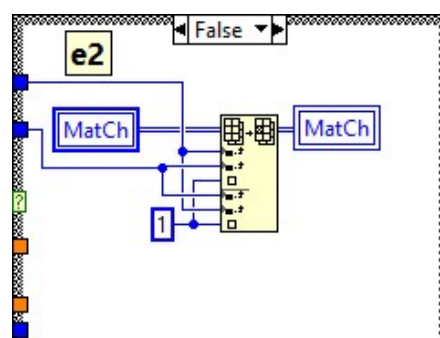
Figure G.3 Restore connection line.

In Figure G.9 (d4) data from deleted connections are eliminated. In (d5), it is calculated power flow and harmonic propagation. In (d6), if average THD in less than Average of the previous configuration then lines that were not deleted are restored. In (d7), there are displayed the nodes with lines in the map. In (d8) distance is multiplied by -1 to make the value negative and that for the next iteration the value does not be the longest. In (d9) data is saved in the vector. In (d10), it is checked if the loop is finished. In (d11), it is gotten total time to eliminate the longest lines. In (f) data is displayed.

In Figure G.9 (g1) vectors are assigned with the elements of the last loop. In (g2) there is a loop to delete all nodes that were marked with zeros. If node selected contains a zero, then is deleted in (g3a), else a node counter is increased, Figure G.4 (g3b).
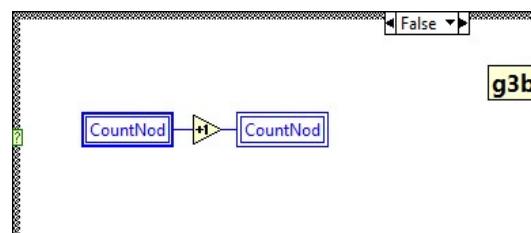
Figure G.4 Increasing the number of nodes.

In Figure G.9 (g4), it is prepared the information to generate the second stage of the report. In (g5) functions are initialised to obtain Pareto fronts.

In Figure G.9 (h1) all variables used to obtain Pareto fronts are initialised. In (h2) starts a loop to obtain Pareto fronts, all variables used to obtain one Pareto front are initialised. In (h3), it is the process to obtain the non-dependant chromosomes that will be the Pareto front. In (h4), if the chromosome is non-dependant, then it is added to the Pareto front. In (h5) the chromosome is deleted from the population. In (h6) vectors are ordered from lowest to highest.

In Figure G.9 (h7), it is a process to check that there are not two identical consecutive chromosomes. If it is TRUE then the chromosome is deleted, (i1), else it is increased a counter, Figure G.5 (i2). Finally, in Figure G.9 (h9), information is displayed, and variables are assigned to obtain the next Pareto front.
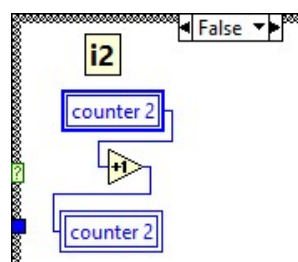
Figure G.5 Counter of number of chromosomes.

In Figure G.9 (h10), it is shown the results of each chromosome; vectors are synchronized to show the same element. If another configuration is chosen, then the new configuration is displayed, and power flow and harmonic propagation are recalculated. In (h11), it is validated that there are not another possibilities of new better chromosomes. In (h12), it is prepared the information of the Pareto front to send to the report. In (h13), it is checked if another better option was or was not.

If there is another possibility, then the genetic algorithm starts again, Figure G.9 (j1). First in (j2), there is a crossover by pairs with all the chromosomes of the first front. In (j3) starts a mutation of all the chromosomes. In (j4) two elements are taken, and data is exchanged. In (j5) for each chromosome is generated a new one changing a line randomly.

Reason to use all the chromosomes is that too many generated chromosomes are not valid. In Figure G.9 (j6), it is created the new data of the chromosomes.

In Figure G.9 (j7), starts a loop to eliminate configurations with no connected nodes. In (j8), it is used the total number of nodes to create a matrix with 0s. In (j9), it is formed the connection matrix. In (j10), it is called the subroutine "*0 DFS Algorithm.vi*", if it does not have isolated nodes then the configuration is added to the vector of valid elements, (k2), if it has at least one isolated node, then it is deleted, Figure G.6 (k1).
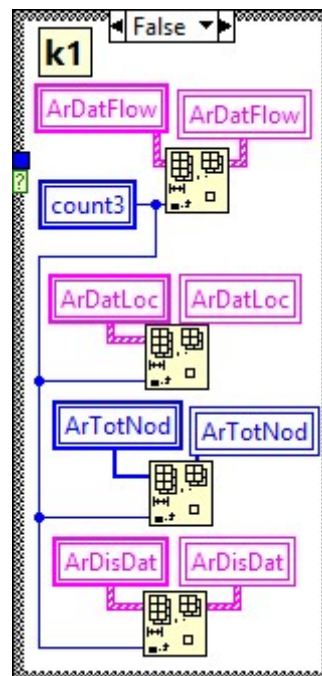
Figure G.6 Chromosome is deleted from the vector.

In Figure G.9 (j11), it is checked that there are not more elements to finish the loop. In (j12) starts a loop and data is displayed. In (j13), it is recalculated power flow and

harmonic propagation. In (j14), it is recalculated the total cable length. In (j15), it is displayed new output data. In (j16), it is formed a vector with all the information. In (j17), it is increased the number of generation.

In Figure G.9 (l1), if *Print Report* is TRUE, then information is prepared to display report stage 4, else the report is closed, Figure G.7 (l2).

Figure G.7 Report is closed without being generated.

In Figure G.9 (m1), it is a loop to generate the final report. In (m2), it is calculated the power flow and harmonic propagation for each generated chromosome as the best, also, it is displayed the configuration in the map.

In Figure G.9 (n), if variable *Print Report* is TRUE, then there are generated all string to show in the report (n1). There are generated strings node types, connection nodes with shut elements, generator connection nodes, connection type. The connection can be a line, *L*, or a transformer, *T*, Figure G.8.
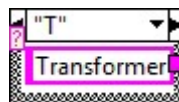
Figure G.8 Option when the connection is a transformer.

In Figure G.9 (n2), the report is generated. Finally, in (n3), the report is sending to the internet explorer, and it is closed.

On the next page, there is attached the expanded diagram.
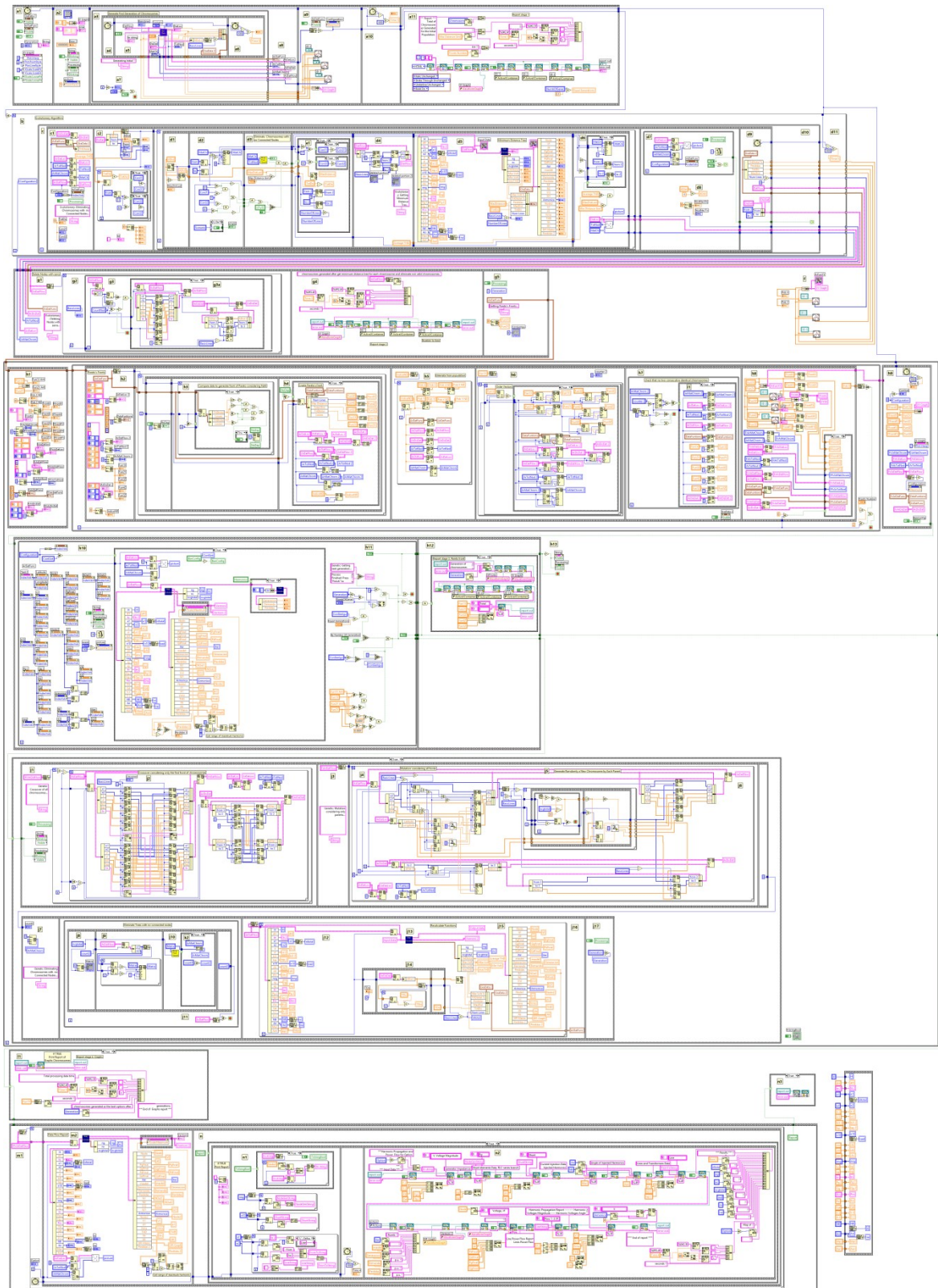
Figure G.9 Evolutionary algorithm.
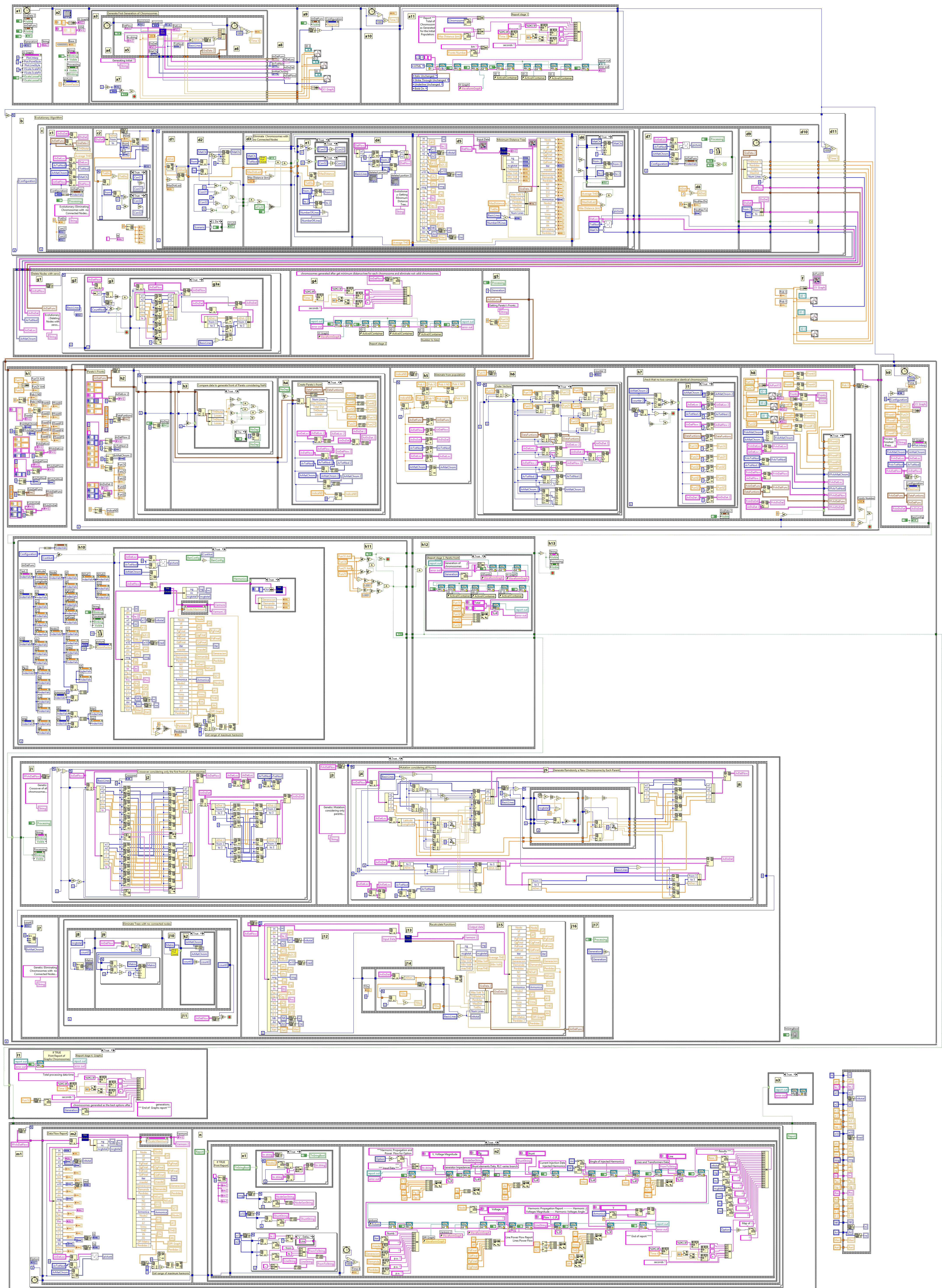
Figure G.9. Evolutionary algorithm.

H. Results.

This Appendix shows the results of the algorithm to calculate power flow and harmonic propagation for 33-bus network when 3 wind turbines are added as nodes 31, 32 and 33, Section H.1.

Also, results obtained by the evolutionary algorithm are presented. Results are from the report generated by the algorithm. Data of the power flow, line flow and harmonic propagation are not including because there is too much information. Results for Scenario 1, Section H.2, results for Scenario 2, Section H.3 and results for Scenario 3, section H.4.

H.1   33 -bus network with 3 Wind Turbines

Figure H.1 shows a network modified from the 30-bus of IEEE to include 3 non-linear loads to represent wind turbines.
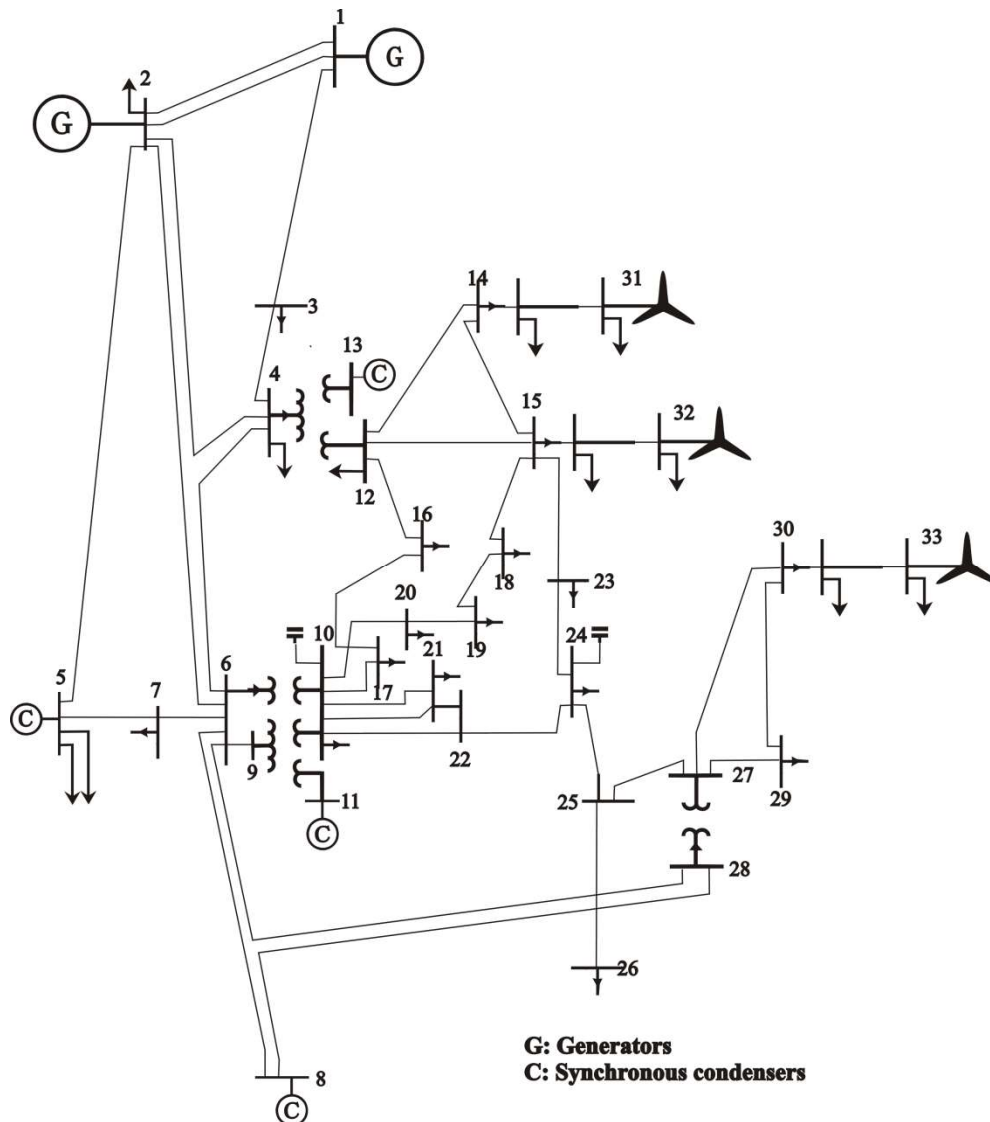
Figure H.1 IEEE 30-Bus network with three wind turbines.

Below is the data network. Base power is 100 MW. Generation data is shown in Table H.1. Table H.2 shows data of reactive power of capacitance bank. Voltages and loads of the network are shown in Table H.3. Table H.4 shows data of the lines and transformers. Table H.5 shows data of the taps of transformers and Table H.6 shows data of the harmonic current injection.

TABLE H.1. GENERATION DATA

Node	P_g (MW)	V (pu)	X_g (pu)	R_g (pu)
1	0	1.06	0.001	0.0001
2	40	1.043	0.001	0.0001
5	0	1.010	0.001	0.0001
8	0	1.010	0.001	0.0001
11	0	1.082	0.001	0.0001
13	0	1.071	0.001	0.0001
31	10	1.01	0.003	0.0003
32	10	1.01	0.003	0.0003
33	10	1.01	0.003	0.0003

TABLE H.2. REACTIVE POWER OF CAPACITANCE BANK

N	MVAr	V (pu)
10	19	1.0
24	4.3	1.0

TABLE H.3. NETWORK VOLTAGES AND LOADS

Node	Type	Magnitude	Angle	MW	MVAr
1	Slack	1.06	0	0	0
2	Voltage	1.043	0	21.7	12.7
3	Load	1	0	2.4	1.2
4	Load	1	0	7.6	1.6
5	Voltage	1.01	0	94.2	19
6	Load	1	0	0	0
7	Load	1	0	22.8	10.9
8	Voltage	1.01	0	30	30
9	Load	1	0	0	0
10	Load	1	0	5.8	2
11	Voltage	1.082	0	0	0
12	Load	1	0	11.2	7.5
13	Voltage	1.071	0	0	0
14	Load	1	0	6.2	1.6
15	Load	1	0	8.2	2.5
16	Load	1	0	3.5	1.8
17	Load	1	0	9	5.8
18	Load	1	0	3.2	0.9
19	Load	1	0	9.5	3.4
20	Load	1	0	2.2	0.7
21	Load	1	0	17.5	11.2
22	Load	1	0	0	0
23	Load	1	0	3.2	1.6
24	Load	1	0	8.7	6.7
25	Load	1	0	0	0
26	Load	1	0	3.5	2.3

27	Load	1	0	0	0
28	Load	1	0	0	0
29	Load	1	0	2.4	0.9
30	Load	1	0	10.6	1.9
31	Voltage	1.01	0	1.0	0.75
32	Voltage	1.01	0	1.0	0.75
33	Voltage	1.01	0	1.0	0.75

TABLE H.4. LINES AND TRANSFORMERS DATA

N1	N2	R	X	B/2
1	2	0.0192	0.0575	0.02640
1	3	0.0452	0.1852	0.02040
2	4	0.0570	0.1737	0.01840
3	4	0.0132	0.0379	0.00420
2	5	0.0472	0.1983	0.02090
2	6	0.0581	0.1763	0.01870
4	6	0.0119	0.0414	0.00450
5	7	0.0460	0.1160	0.01020
6	7	0.0267	0.0820	0.00850
6	8	0.0120	0.0420	0.00450
6	9	0	0.2080	0
6	10	0	0.5560	0
9	11	0	0.2080	0
9	10	0	0.1100	0
4	12	0	0.2560	0
12	13	0	0.1400	0
12	14	0.1231	0.2559	0
12	15	0.0662	0.1304	0
12	16	0.0945	0.1987	0
14	15	0.2210	0.1997	0
16	17	0.0824	0.1923	0
15	18	0.1073	0.2185	0
18	19	0.0639	0.1292	0
19	20	0.0340	0.0680	0
10	20	0.0936	0.2090	0
10	17	0.0324	0.0845	0
10	21	0.0348	0.0749	0
10	22	0.0727	0.1499	0
21	22	0.0116	0.0236	0
15	23	0.1000	0.2020	0
22	24	0.1150	0.1790	0
23	24	0.1320	0.2700	0
24	25	0.1885	0.3292	0
25	26	0.2544	0.3800	0
25	27	0.1093	0.2087	0
28	27	0	0.3960	0
27	29	0.2198	0.4153	0
27	30	0.3202	0.6027	0
29	30	0.2399	0.4533	0
8	28	0.0636	0.2000	0.0214
6	28	0.0169	0.0599	0.065
14	31	0.0169	0.0599	0.065
15	32	0.0169	0.0599	0.065
30	33	0.0169	0.0599	0.065

Connection Nodes	Tap (pu)
6-9	0.978
6-10	0.969
9-11	1
9-10	1
4-12	0.932
12-13	1
28-27	0.968

TABLE H.6. CURRENT INJECTION DATA

harmonic	Node 31		Node 32		Node 33	
	Magnitude %	Angle (grades)	Magnitude %	Angle (grades)	Magnitude %	Angle (grades)
3	20%	15	0%	-15	0%	30
5	15%	25	25%	45	17%	45
7	10%	-40	18%	10	12%	18
11	4%	20	10%	65	9%	-32
13	0%	0	7%	-12	6%	18
17	0%	0	0%	0	5%	14
19	0%	0	0%	0	2%	10

Report of this example generated by the algorithm is shown below.

Main Power Flow and Harmonics Propagation
*** Input Data ***
Voltage and Demand Power

33 nodes with 3 wind turbines

	V, Voltage Magnitude	D, Angle	Demand Active Power Pd (MW)	Demand Reactive Power Qd	Generation Active Power Pg (MW)	Generation Reactive Power Qg
1 Slack	1.060	0.000	0.000	0.000	0.000	0.000
2 Voltage	1.043	0.000	0.217	0.127	0.400	0.000
3 Load	1.000	0.000	0.024	0.012	0.000	0.000
4 Load	1.000	0.000	0.076	0.016	0.000	0.000
5 Voltage	1.010	0.000	0.942	0.190	0.000	0.000
6 Load	1.000	0.000	0.000	0.000	0.000	0.000
7 Load	1.000	0.000	0.228	0.109	0.000	0.000
8 Voltage	1.010	0.000	0.300	0.300	0.000	0.000
9 Load	1.000	0.000	0.000	0.000	0.000	0.000
10 Load	1.000	0.000	0.058	0.020	0.000	0.000
11 Voltage	1.082	0.000	0.000	0.000	0.000	0.000
12 Load	1.000	0.000	0.112	0.075	0.000	0.000
13 Voltage	1.071	0.000	0.000	0.000	0.000	0.000
14 Load	1.000	0.000	0.062	0.016	0.000	0.000
15 Load	1.000	0.000	0.082	0.025	0.000	0.000
16 Load	1.000	0.000	0.035	0.018	0.000	0.000
17 Load	1.000	0.000	0.090	0.058	0.000	0.000
18 Load	1.000	0.000	0.032	0.009	0.000	0.000
19 Load	1.000	0.000	0.095	0.034	0.000	0.000
20 Load	1.000	0.000	0.022	0.007	0.000	0.000
21 Load	1.000	0.000	0.175	0.112	0.000	0.000

22 Load	1.000	0.000	0.350	0.250	0.000	0.000
23 Load	1.000	0.000	0.032	0.016	0.000	0.000
24 Load	1.000	0.000	0.087	0.067	0.000	0.000
25 Load	1.000	0.000	0.000	0.000	0.000	0.000
26 Load	1.000	0.000	0.035	0.023	0.000	0.000
27 Load	1.000	0.000	0.000	0.000	0.000	0.000
28 Load	1.000	0.000	0.000	0.000	0.000	0.000
29 Load	1.000	0.000	0.024	0.009	0.000	0.000
30 Load	1.000	0.000	0.106	0.019	0.000	0.000
31 Voltage	1.010	0.000	0.010	0.007	0.100	0.000
32 Voltage	1.010	0.000	0.010	0.007	0.100	0.000
33 Voltage	1.010	0.000	0.010	0.007	0.100	0.000

Generator Impedances

	Rg	**Xg**
1	0.0001	0.0010
2	0.0001	0.0010
5	0.0001	0.0010
8	0.0001	0.0010
11	0.0001	0.0010
13	0.0001	0.0010
31	0.0003	0.0030
32	0.0003	0.0030
33	0.0003	0.0030

Shunt elements Data, RLC-series branch

	Shunt Resistance	**Shunt Inductive Reactance**	**Shunt Capacitive Reactance**
10	0.0000	0.0000	5.2632
24	0.0000	0.0000	23.2558

Current Injection Data
Injected Harmonics

	5	**7**	**11**	**13**	**15**	**17**
31	0.2000	-0.1429	0.0909	-0.0769	0.0667	-0.0588
32	0.2000	-0.1429	0.0909	-0.0769	0.0667	-0.0588
33	0.2000	-0.1429	0.0909	-0.0769	0.0667	-0.0588

Angle of Injected Harmonics

	5	**7**	**11**	**13**	**15**	**17**
31	0.0000	0.0000	0.0000	0.0000	0.0000	0.0000
32	0.0000	0.0000	0.0000	0.0000	0.0000	0.0000
33	0.0000	0.0000	0.0000	0.0000	0.0000	0.0000

Lines and Transformers Data

	Line resistance n1-n2	**Line Inductance n1-n2**	**Line susceptance n1-n2**	**Taps of transformers**
Line - from 1 to 2	0.0192	0.0575	0.0264	1.0000
Line - from 1 to 3	0.0452	0.1852	0.0204	1.0000

Line - from 2 to 4	0.0570	0.1737	0.0184	1.0000
Line - from 3 to 4	0.0132	0.0379	0.0042	1.0000
Line - from 2 to 5	0.0472	0.1983	0.0209	1.0000
Line - from 2 to 6	0.0581	0.1763	0.0187	1.0000
Line - from 4 to 6	0.0119	0.0414	0.0045	1.0000
Line - from 5 to 7	0.0460	0.1160	0.0102	1.0000
Line - from 6 to 7	0.0267	0.0820	0.0085	1.0000
Line - from 6 to 8	0.0120	0.0420	0.0045	1.0000
Transformer - from 6 to 9	0.0000	0.2080	0.0000	0.9780
Transformer - from 6 to 10	0.0000	0.5560	0.0000	0.9690
Transformer - from 9 to 11	0.0000	0.2080	0.0000	1.0000
Transformer - from 9 to 10	0.0000	0.1100	0.0000	1.0000
Transformer - from 4 to 12	0.0000	0.2560	0.0000	0.9320
Transformer - from 12 to 13	0.0000	0.1400	0.0000	1.0000
Line - from 12 to 14	0.1231	0.2559	0.0000	1.0000
Line - from 12 to 15	0.0662	0.1304	0.0000	1.0000
Line - from 12 to 16	0.0945	0.1987	0.0000	1.0000
Line - from 14 to 15	0.2210	0.1997	0.0000	1.0000
Line - from 16 to 17	0.0824	0.1923	0.0000	1.0000
Line - from 15 to 18	0.1073	0.2185	0.0000	1.0000
Line - from 18 to 19	0.0639	0.1292	0.0000	1.0000
Line - from 19 to 20	0.0340	0.0680	0.0000	1.0000
Line - from 10 to 20	0.0936	0.2090	0.0000	1.0000
Line - from 10 to 17	0.0324	0.0845	0.0000	1.0000
Line - from 10 to 21	0.0348	0.0749	0.0000	1.0000
Line - from 10 to 22	0.0727	0.1499	0.0000	1.0000
Line - from 21 to 22	0.0116	0.0236	0.0000	1.0000
Line - from 15 to 23	0.1000	0.2020	0.0000	1.0000
Line - from 22 to 24	0.1150	0.1790	0.0000	1.0000
Line - from 23 to 24	0.1320	0.2700	0.0000	1.0000
Line - from 24 to 25	0.1885	0.3292	0.0000	1.0000
Line - from 25 to 26	0.2544	0.3800	0.0000	1.0000
Line - from 25 to 27	0.1093	0.2087	0.0000	1.0000
Transformer - from 28 to 27	0.0000	0.3960	0.0000	0.9680
Line - from 27 to 29	0.2198	0.4153	0.0000	1.0000
Line - from 27 to 30	0.3202	0.6027	0.0000	1.0000
Line - from 29 to 30	0.2399	0.4533	0.0000	1.0000
Line - from 8 to 28	0.0636	0.2000	0.0214	1.0000
Line - from 6 to 28	0.0169	0.0599	0.0650	1.0000
Line - from 14 to 31	0.0169	0.0599	0.0650	1.0000
Line - from 15 to 32	0.0169	0.0599	0.0650	1.0000
Line - from 30 to 33	0.0169	0.0599	0.0650	1.0000

*** Results ***
Number of lines and Transformers: 44
Generation Nodes: 9
Load Nodes: 24
Total Nodes: 33
Number of elements in derivation: 2

Load nodes with harmonics injected: 3
Number of harmonics to be considered: 6
Processing time of Power Flow and Harmonics Propagation Study: 0.079000 seconds
Connected Nodes
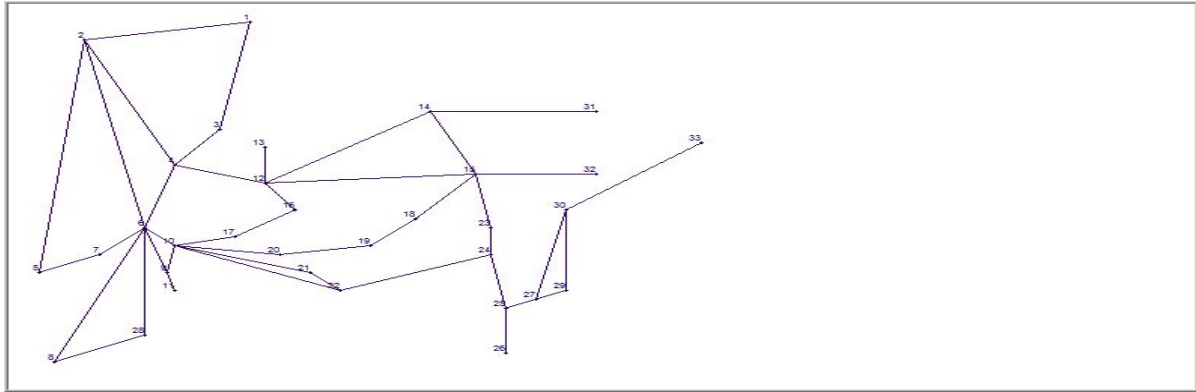
Power Flow Report

|	Final Voltage, Vf	Final Angle, Af	Demand Active Power Pd (p.u.)	Demand Reactive Power Qd	Generation Active Power Pg (p.u.)	Generation Reactive Power Qg
1	1.0600	0.0000	0.0000	0.0000	2.7178	-0.1640
2	1.0430	-5.7406	0.2170	0.1270	0.4000	0.5697
3	1.0167	-8.3051	0.0240	0.0120	0.0000	0.0000
4	1.0072	-10.0330	0.0760	0.0160	0.0000	0.0000
5	1.0100	-14.8209	0.9420	0.1900	0.0000	0.3871
6	1.0068	-11.9180	0.0000	0.0000	0.0000	0.0000
7	1.0003	-13.6390	0.2280	0.1090	0.0000	0.0000
8	1.0100	-12.7126	0.3000	0.3000	0.0000	0.4551
9	1.0308	-15.9065	0.0000	0.0000	0.0000	0.0000
10	1.0062	-18.0632	0.0580	0.0200	0.0000	0.0000
11	1.0820	-15.9065	0.0000	0.0000	0.0000	0.2662
12	1.0427	-15.7777	0.1120	0.0750	0.0000	0.0000
13	1.0710	-15.7777	0.0000	0.0000	0.0000	0.2165
14	1.0184	-15.5009	0.0620	0.0160	0.0000	0.0000
15	1.0140	-16.4226	0.0820	0.0250	0.0000	0.0000
16	1.0193	-16.9968	0.0350	0.0180	0.0000	0.0000
17	1.0045	-17.9545	0.0900	0.0580	0.0000	0.0000
18	0.9985	-17.7272	0.0320	0.0090	0.0000	0.0000
19	0.9926	-18.3091	0.0950	0.0340	0.0000	0.0000
20	0.9951	-18.3086	0.0220	0.0070	0.0000	0.0000
21	0.9779	-18.8932	0.1750	0.1120	0.0000	0.0000
22	0.9736	-18.9843	0.3500	0.2500	0.0000	0.0000
23	0.9961	-17.3943	0.0320	0.0160	0.0000	0.0000
24	0.9812	-18.3574	0.0870	0.0670	0.0000	0.0000
25	0.9995	-16.9780	0.0000	0.0000	0.0000	0.0000
26	0.9815	-17.4131	0.0350	0.0230	0.0000	0.0000
27	1.0195	-15.8592	0.0000	0.0000	0.0000	0.0000
28	1.0067	-12.5245	0.0000	0.0000	0.0000	0.0000
29	1.0110	-16.3129	0.0240	0.0090	0.0000	0.0000
30	1.0115	-16.3235	0.1060	0.0190	0.0000	0.0000

31 1.0100	-15.0438	0.0100	0.0075	0.1000	-0.2254
32 1.0100	-16.0333	0.0100	0.0075	0.1000	-0.1515
33 1.0100	-15.9733	0.0100	0.0075	0.1000	-0.1092

Number of iterations: 4
Error: 6.675232E-8
Generation: 3.417821 p.u.
Demand: 3.214000 p.u.
Power Losses: 0.203821 p.u.

Nodal Report
Lines flow

	Flow 1 -2		**Flow 2 - 1**	
1 - 2	1.853	-0.239	-1.794	0.358
1 - 3	0.864	0.075	-0.834	0.006
2 - 4	0.477	0.055	-0.465	-0.057
3 - 4	0.810	-0.018	-0.802	0.033
2 - 5	0.848	0.016	-0.816	0.071
2 - 6	0.652	0.013	-0.629	0.016
4 - 6	0.750	-0.198	-0.743	0.213
5 - 7	-0.126	0.126	0.127	-0.142
6 - 7	0.359	-0.040	-0.355	0.033
6 - 8	0.291	-0.162	-0.290	0.157
6 - 9	0.347	-0.104	-0.347	0.131
6 - 10	0.195	0.012	-0.195	0.009
9 - 11	0.000	-0.254	0.000	0.266
9 - 10	0.355	0.237	-0.355	-0.218
4 - 12	0.411	-0.119	-0.411	0.165
12 - 13	0.000	-0.211	0.000	0.217
12 - 14	0.022	0.088	-0.021	-0.086
12 - 15	0.165	0.146	-0.162	-0.140
12 - 16	0.141	0.057	-0.139	-0.053
14 - 15	0.049	-0.031	-0.048	0.032
16 - 17	0.104	0.035	-0.103	-0.032
15 - 18	0.114	0.017	-0.113	-0.015
18 - 19	0.081	0.006	-0.080	-0.005
19 - 20	-0.015	-0.029	0.015	0.029
10 - 20	0.037	0.037	-0.037	-0.036
10 - 17	-0.013	0.026	0.013	-0.026
10 - 21	0.303	0.242	-0.297	-0.230
10 - 22	0.171	0.137	-0.168	-0.130
21 - 22	0.122	0.118	-0.122	-0.118
15 - 23	0.104	0.039	-0.103	-0.037
22 - 24	-0.060	-0.002	0.060	0.003
23 - 24	0.071	0.021	-0.070	-0.019
24 - 25	-0.077	-0.009	0.078	0.012
25 - 26	0.035	0.024	-0.035	-0.023
25 - 27	-0.114	-0.035	0.115	0.038
28 - 27	0.151	-0.028	-0.151	0.037
27 - 29	0.024	0.008	-0.024	-0.008

27 - 30	0.016	0.005	-0.016	-0.005
29 - 30	-0.000	-0.001	0.000	0.001
8 - 28	-0.010	-0.002	0.010	-0.042
6 - 28	0.167	-0.110	-0.166	-0.020
14 - 31	-0.089	0.101	0.090	-0.233
15 - 32	-0.090	0.027	0.090	-0.159
30 - 33	-0.090	-0.015	0.090	-0.117

Harmonic Propagation Report
Nodal Voltages ----- Harmonic Magnitude Voltages ---------------- Harmonic Voltage Angle

	V	A	Vrms	THD	1	5	7	11	13	15	17	1	5	7	11	13	15	17
1	1.060	0.000	1.060	0.000	1.060	0.000	0.000	0.000	0.000	0.000	0.000	0.000	174.449	15.789	-63.816	148.470	159.762	-63.153
2	1.043	-5.741	1.043	0.000	1.043	0.000	0.000	0.000	0.000	0.000	0.000	-5.741	172.536	11.072	-70.667	147.022	171.230	-45.622
3	1.017	-8.305	1.017	0.003	1.017	0.000	0.000	0.000	0.000	0.000	0.000	-8.305	174.267	16.139	-63.140	149.052	159.788	-63.065
4	1.007	-10.033	1.007	0.003	1.007	0.000	0.000	0.000	0.000	0.000	0.000	-10.033	174.373	16.390	-62.705	149.556	160.359	-62.422
5	1.010	-14.821	1.010	0.000	1.010	0.000	0.000	0.000	0.000	0.000	0.000	-14.821	165.451	0.451	-89.645	139.189	172.468	-28.377
6	1.007	-11.918	1.007	0.003	1.007	0.000	0.000	0.000	0.000	0.000	0.000	-11.918	167.778	4.413	-84.333	145.024	178.635	-21.819
7	1.000	-13.639	1.000	0.002	1.000	0.000	0.000	0.000	0.000	0.000	0.000	-13.639	163.803	-0.274	-89.754	139.427	172.897	-27.714
8	1.010	-12.713	1.010	0.000	1.010	0.000	0.000	0.000	0.000	0.000	0.000	-12.713	169.730	7.063	-77.237	144.908	-176.895	-10.741
9	1.031	-15.906	1.031	0.002	1.031	0.000	0.000	0.000	0.000	0.000	0.000	-15.906	158.795	-11.824	147.582	-16.850	122.475	-28.644
10	1.006	-18.063	1.006	0.005	1.006	0.000	0.000	0.000	0.000	0.000	0.000	-18.063	157.907	-13.176	145.187	-22.653	98.464	162.598
11	1.082	-15.906	1.082	0.000	1.082	0.000	0.000	0.000	0.000	0.000	0.000	-15.906	156.247	-13.978	145.863	-18.431	121.003	-30.027
12	1.043	-15.778	1.043	0.011	1.043	0.000	0.000	0.000	0.000	0.000	0.000	-15.778	-173.609	39.163	-44.789	174.077	35.031	-105.222
13	1.071	-15.778	1.071	0.000	1.071	0.000	0.000	0.000	0.000	0.000	0.000	-15.778	-176.152	37.014	-46.503	172.500	33.562	-106.601
14	1.018	-15.501	1.018	0.031	1.018	0.000	0.000	0.000	0.000	0.000	0.000	-15.501	-167.848	53.455	-38.805	-178.787	39.420	-105.226
15	1.014	-16.423	1.014	0.020	1.014	0.000	0.000	0.000	0.000	0.000	0.000	-16.423	-173.398	43.703	-45.861	172.387	25.678	-105.831
16	1.019	-16.997	1.019	0.006	1.019	0.000	0.000	0.000	0.000	0.000	0.000	-16.997	172.329	8.244	-75.197	-155.468	48.486	-109.576
17	1.005	-17.954	1.005	0.004	1.005	0.000	0.000	0.000	0.000	0.000	0.000	-17.954	160.695	-10.085	144.960	-29.475	78.859	-126.367
18	0.998	-17.727	0.998	0.012	0.998	0.000	0.000	0.000	0.000	0.000	0.000	-17.727	174.882	20.388	-53.098	173.878	28.196	-111.031
19	0.993	-18.309	0.993	0.008	0.993	0.000	0.000	0.000	0.000	0.000	0.000	-18.309	167.215	5.039	-78.371	-174.909	34.449	-116.450
20	0.995	-18.309	0.995	0.006	0.995	0.000	0.000	0.000	0.000	0.000	0.000	-18.309	164.939	-0.340	-165.110	-101.119	43.790	-118.742
21	0.978	-18.893	0.978	0.004	0.978	0.000	0.000	0.000	0.000	0.000	0.000	-18.893	154.685	-16.560	145.576	-8.950	-110.814	60.097
22	0.974	-18.984	0.974	0.005	0.974	0.000	0.000	0.000	0.000	0.000	0.000	-18.984	154.845	-16.248	147.800	12.338	-101.978	56.861
23	0.996	-17.394	0.996	0.010	0.996	0.000	0.000	0.000	0.000	0.000	0.000	-17.394	178.013	25.095	-54.755	154.521	-57.190	-86.497
24	0.981	-18.357	0.981	0.021	0.981	0.000	0.000	0.000	0.000	0.000	0.000	-18.357	165.656	1.062	-80.858	136.642	-91.015	54.496
25	0.999	-16.978	0.999	0.013	0.999	0.000	0.000	0.000	0.000	0.000	0.000	-16.978	173.580	16.120	-63.894	144.880	-78.077	124.513
26	0.981	-17.413	0.981	0.012	0.981	0.000	0.000	0.000	0.000	0.000	0.000	-17.413	170.052	11.824	-68.797	139.974	-82.880	119.872
27	1.019	-15.859	1.019	0.016	1.019	0.000	0.000	0.000	0.000	0.000	0.000	-15.859	-179.307	30.388	-56.463	152.341	-39.739	159.663
28	1.007	-12.524	1.007	0.007	1.007	0.000	0.000	0.000	0.000	0.000	0.000	-12.524	172.771	14.882	-67.321	145.718	-167.333	17.066
29	1.011	-16.313	1.011	0.028	1.011	0.000	0.000	0.000	0.000	0.000	0.000	-16.313	-176.964	38.725	-54.420	157.469	2.817	168.465
30	1.012	-16.323	1.012	0.046	1.012	0.000	0.000	0.000	0.000	0.000	0.000	-16.323	-172.525	47.489	-49.870	165.414	18.349	174.272
31	1.010	-15.044	1.010	0.010	1.010	0.000	0.000	0.000	0.000	0.000	0.000	-15.044	-163.651	60.240	-32.149	-168.852	53.913	-87.234
32	1.010	-16.033	1.010	0.010	1.010	0.000	0.000	0.000	0.000	0.000	0.000	-16.033	-168.606	53.236	-42.743	178.739	39.775	-98.946
33	1.010	-15.973	1.010	0.010	1.010	0.000	0.000	0.000	0.000	0.000	0.000	-15.973	-168.315	53.729	-42.512	178.407	38.491	-126.265

Driving-Point Impedance of the system nodes
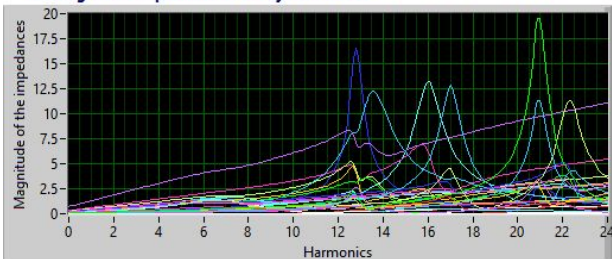
Harmonic voltages on network nodes
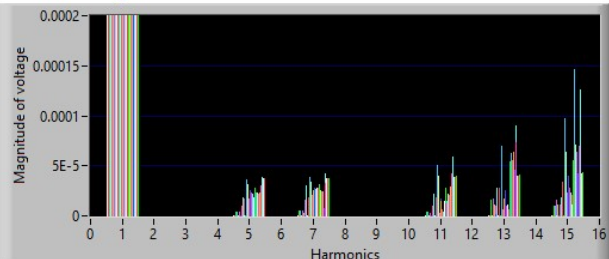
Power flow

Power Flow

33 nodes with 3 wind turbines

44	nl: number of lines and transformers
9	ng: generation nodes	33	ng+nc=total nodes	Finished
24	nc: load nodes
2	ned: number of elements in derivation
3	ni: load nodes with harmonics injected
6	na: number of harmonics to be considered

Start process

Time 1 0.648 Seg. Diference
Time 2 0.85 Seg. 0.202 Seg.

Finish

Report

Input data

H, dH: highest harmonic and increase of h for DPI frequency response

H 25 dH 0.1 Base 100

Lines and transformers Data

Type of element 'L' Line, 'T' Transformer

LLLLLLLLLLLTTTTTTLLLLLLLLLLLLLLLLTLLLLLLLL

n1: output node

| 1 | 1 | 2 | 3 | 2 | 2 | 4 |

n2: input node

| 2 | 3 | 4 | 4 | 5 | 6 | 6 |

rl: line or transformer resistance between n1 and n2

| 0.0192 | 0.0452 | 0.057 | 0.0132 | 0.0472 | 0.0581 | 0.0119 |

xl: line or transformer inductance between n1 and n2

| 0.0575 | 0.1852 | 0.1737 | 0.0379 | 0.1983 | 0.1763 | 0.0414 |

b2l: line or transformer susceptance between n1 and n2 (b/2)

| 0.0264 | 0.0204 | 0.0184 | 0.0042 | 0.0209 | 0.0187 | 0.0045 |

tap: taps of transformer (1 if there is no tap out of the nominal)

| 1 | 1 | 1 | 1 | 1 | 1 | 1 |

Shunt elements data, RLC-series branch

n10: connection nodes

| 10 | 24 | 0 | 0 | 0 | 0 | 0 | 0 | 0 |

shr: shunt resistance, R pu, positive

| 0 | 0 | 0 | 0 | 0 | 0 | 0 | 0 | 0 |

shl: shunt inductive reactance, XL=wL pu. positive

| 0 | 0 | 0 | 0 | 0 | 0 | 0 | 0 | 0 |

shc: shunt inductive reactance, Xc= 1/(wC) pu, positive

| 5.26316 | 23.2558 | 0 | 0 | 0 | 0 | 0 | 0 | 0 |

Generator impedances

nng: generator node connection

| 1 | 2 | 5 | 8 | 11 | 13 | 31 | 32 | 33 |

rg: generator resistance

| 0.0001 | 0.0001 | 0.0001 | 0.0001 | 0.0001 | 0.0001 | 0.0003 | 0.0003 | 0.0003 |

xg: generator sub-transient reactance

| 0.001 | 0.001 | 0.001 | 0.001 | 0.001 | 0.001 | 0.003 | 0.003 | 0.003 |

Type of nodes and load

tn: node type, S: slack (1), V: voltage, C: load   tn string

SVCCVCCVCCVCVCVCCCCCCCCCCCCCCCCVVV

Pm: load model 'U'=1, 'D'=2 and 'T'=3 for harmonics according to CIGRE

Pg: generation active power

| 0 | 0.4 | 0 | 0 | 0 | 0 | 0 | 0 |

Qg: generation reactive power

| 0 | 0 | 0 | 0 | 0 | 0 | 0 | 0 |

Pd: demand active power

| 0 | 0.217 | 0.024 | 0.076 | 0.942 | 0 | 0.228 | 0.3 | 0 |

Qd: demand reactive power

| 0 | 0.127 | 0.012 | 0.016 | 0.19 | 0 | 0.109 | 0.3 | 0 |

V: initial nodal voltages

| 1.06 | 1.043 | 1 | 1 | 1.01 | 1 | 1 | 1.01 | 1 |

D: angles of initial nodal voltages

| 0 | 0 | 0 | 0 | 0 | 0 | 0 | 0 |

Current injection data

Ari: injected harmonics

| 5 | 7 | 11 | 13 | 15 | 17 | 0 | 0 |

Nfi   Mari: percentage of injected harmonics magnitude

31	0.2	-0.1428	0.09090	-0.0769	0.06666	-0.0588	0	0
32	0.2	-0.1428	0.09090	-0.0769	0.06666	-0.0588	0	0
33	0.2	-0.1428	0.09090	-0.0769	0.06666	-0.0588	0	0
0	0	0	0	0	0	0	0	0
0	0	0	0	0	0	0	0	0

load nodes containing   Aari: angle of injected harmonics in degrees
harmonic injection

0	0	0	0	0	0	0
0	0	0	0	0	0	0
0	0	0	0	0	0	0

Power Flow Report

Node	Vf	Af	Pg	Qg	Pd	Qd
1	1.06	0	2.7178	-0.164	0	0
2	1.043	-5.7406	0.4	0.5697	0.217	0.127
3	1.0167	-8.3051	0	0	0.024	0.012
4	1.0072	-10.033	0	0	0.076	0.016
5	1.01	-14.8209	0	0.3871	0.942	0.19
6	1.0068	-11.918	0	0	0	0
7	1.0003	-13.639	0	0	0.228	0.109
8	1.01	-12.7126	0	0.4551	0.3	0.3
9	1.0308	-15.9065	0	0	0	0
10	1.0062	-18.0632	0	0	0.058	0.02
11	1.082	-15.9065	0	0.2662	0	0
12	1.0427	-15.7777	0	0	0.112	0.075
13	1.071	-15.7777	0	0.2165	0	0
14	1.0184	-15.5009	0	0	0.062	0.016
15	1.014	-16.4226	0	0	0.082	0.025

iterations	error	Generation	Demand	Losses	with harmonics	by harmonics
4	6.6752E-8	3.4178	3.214	0.2038	0.2038	0

Max Vf   Min Vf

| 1.082 | 10 | | 0.97359 | 21 |

Harmonic propagation report   Harmonic voltages

Nodal Voltages   Harmonic

Node	V	A	Vrms	THD
1	1.06	-5.7406	1.06	0.00002
2	1.043	-5.7406	1.043	0.00003
3	1.0167	-8.3051	1.0167	0.00325
4	1.0072	-10.033	1.0072	0.00321
5	1.01	-14.8209	1.01	0.00002
6	1.0068	-11.918	1.0068	0.00305
7	1.0003	-13.639	1.0003	0.00205
8	1.01	-12.7126	1.01	0.0001
9	1.0308	-15.9065	1.0308	0.00242
10	1.0062	-18.0632	1.0062	0.0052
11	1.082	-15.9065	1.082	0.00001
12	1.0427	-15.7777	1.0427	0.0106
13	1.071	-15.7777	1.071	0.00007
14	1.0184	-15.5009	1.0184	0.03051
15	1.014	-16.4226	1.014	0.01982
16	1.0193	-16.9968	1.0193	0.00632
17	1.0045	-17.9545	1.0045	0.00445
18	0.9985	-17.7272	0.9985	0.01192
19	0.9926	-18.3091	0.9926	0.00787

Vh	Ah
1.06	0
1.043	-5.7406
1.0167	-8.3051
1.0072	-10.033
1.01	-14.8209
1.0068	-11.918
1.0003	-13.639
1.01	-12.7126
1.0308	-15.9065
1.0062	-18.0632
1.082	-15.9065
1.0427	-15.7777
1.071	-15.7777
1.0184	-15.5009
1.014	-16.4226
1.0193	-16.9968
1.0045	-17.9545
0.9985	-17.7272
0.9926	-18.3091

Average THD   maxTHD   minTHD

| 0.0107 | | 0.04580 | 1.10406 |
| | | 29 | 10 |

Line Power Flow Report

Lines Power Flow

N1	N2	Flow 1-2	Flow 2-1
1	2	1.8534 -0.2387 i	-1.794 +0.3584 i
1	3	0.8644 +0.0747 i	-0.834 +0.006 i
2	4	0.4774 +0.0553 i	-0.4651 -0.0567 i
3	4	0.81 -0.018 i	-0.8016 +0.0334 i
2	5	0.8475 +0.0157 i	-0.8163 +0.0715 i
2	6	0.6521 +0.0134 i	-0.6293 +0.0164 i
4	6	0.7501 -0.1978 i	-0.7431 +0.2132 i
5	7	-0.1257 +0.1256 i	0.1273 -0.1423 i
6	7	0.3587 -0.04 i	-0.3553 +0.0333 i
6	8	0.2909 -0.1616 i	-0.2896 +0.157 i
6	9	0.3471 -0.1041 i	-0.3471 +0.1311 i
6	10	0.1951 +0.0115 i	-0.1951 +0.0094 i
9	11	8.4026E-19 -0.2536 i	-1.0774E-18 +0.26
9	10	0.3549 +0.2371 i	-0.3549 -0.2182 i

Driving-Point Impedance of the system nodes

Harmonic voltages on network nodes

MatrixCh

0	1	1	0	0
1	0	0	1	1
1	0	0	1	0
0	1	1	0	0
0	1	0	0	0

Data

DGrafX DGrafY DText DColor

| 160 | 20 | 1 | |

H.2   Results for Scenario 1

Results were obtained from the report generated by the algorithm, only are presented the Pareto front of the first and last generation and the best configurations that the algorithm generates. Network data and reports are not attached because reports include generation data, network voltages and loads, lines and transformers data, harmonic current injection data, power flow report, line power flow report and harmonic propagation report for each configuration, and it is much information to be presented in the appendix.

For Scenario 1 were proposed 100 chromosomes as the first generation and were generated 1,000 offsprings.

H.2.1   100 chromosomes

*** Report ***
Total of Chromosomes Generated for the Initial Population: 100
Maximum Distance: 45 km
Pareto Fronts Considered: 10
Generation time: 00:02:25.058 = 145.058 seconds
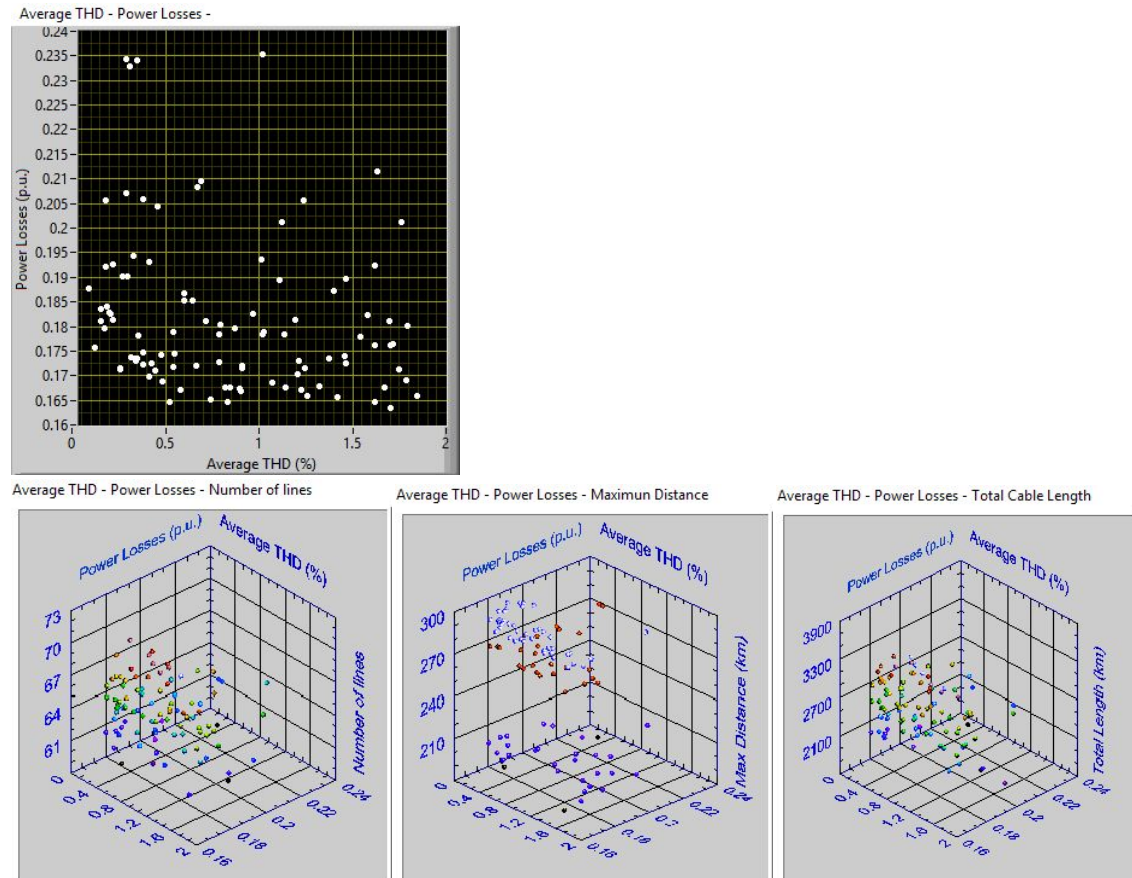
100 chromosomes generated after obtain minimum distance tree for each chromosome and eliminate not valid chromosomes. 00:50:14.837 = 3014.837 seconds
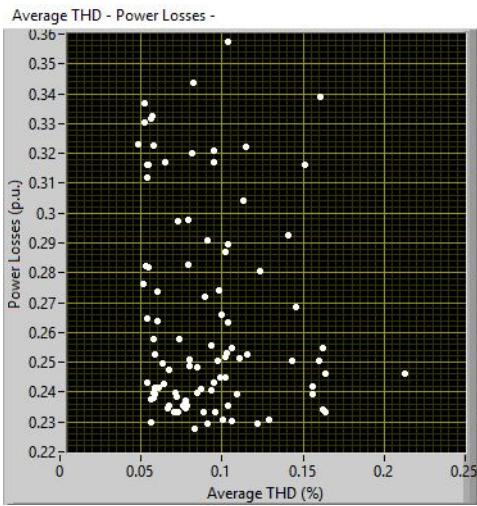
Average THD - Power Losses -

Average THD - Power Losses - Number of lines

Average THD - Power Losses - Maximun Distance

Average THD - Power Losses - Total Cable Length

Generation of chromosomes number 1

Fronts of Pareto
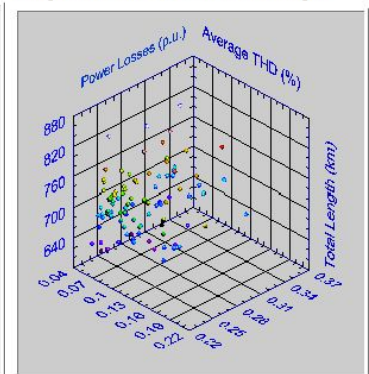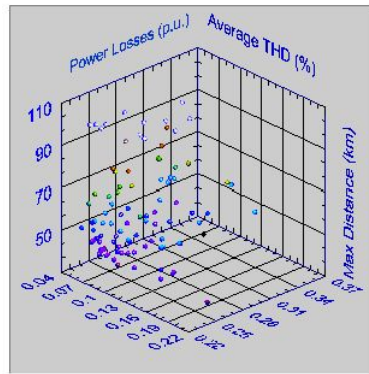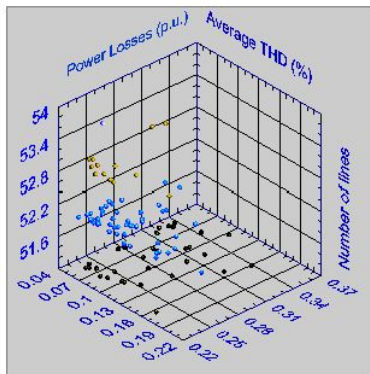
Average THD - Power Losses -
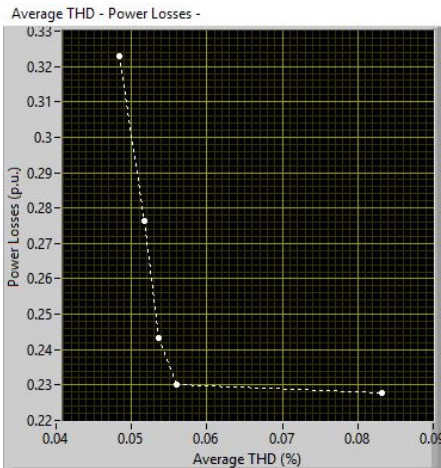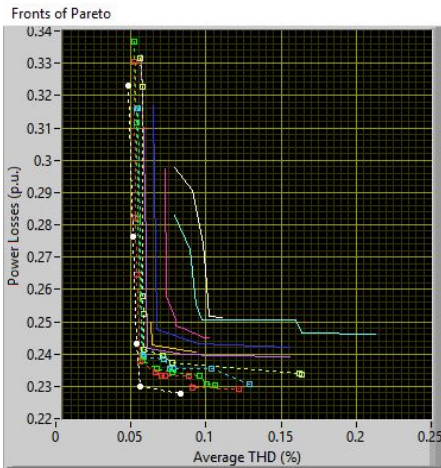
Average THD - Power Losses - Number of lines

Average THD - Power Losses - Maximun Distance

Average THD - Power Losses - Total Cable Length
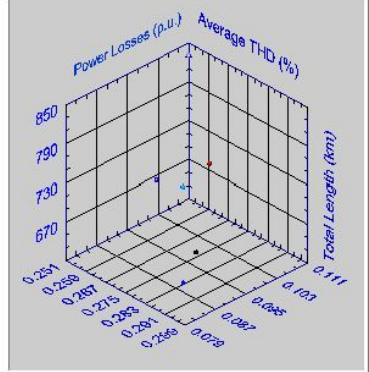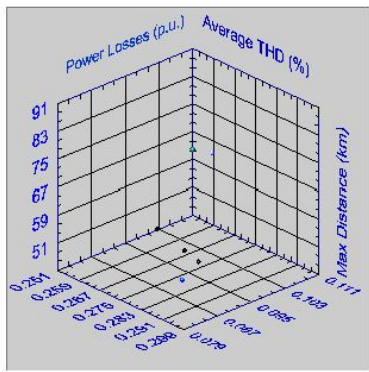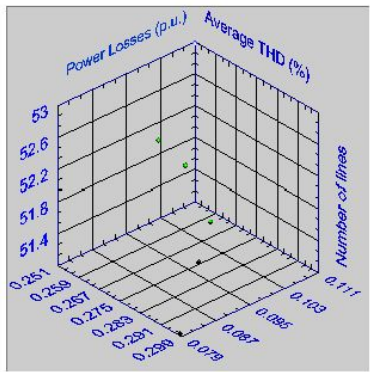
	THD (%)	Power losses (p.u.)	Number of lines	Maximun distance (km)	Total cable length (km)
1	0.0485	0.3229	51	56.7809	588.5649
2	0.0517	0.2762	51	49.2254	650.3220
3	0.0536	0.2433	51	51.8084	604.5096
4	0.0560	0.2300	52	51.8084	631.6790
5	0.0832	0.2279	53	44.3771	716.6702
6	0.0833	0.2278	53	44.3771	711.6977

Generation of chromosomes number 1000

Fronts of Pareto

Average THD - Power Losses - Number of lines

Average THD - Power Losses - Maximun Distance

Average THD - Power Losses - Total Cable Length
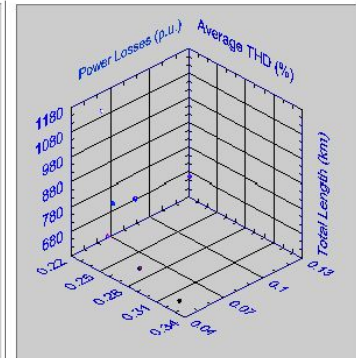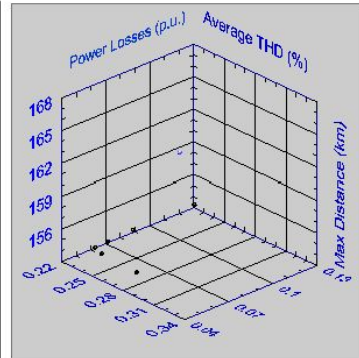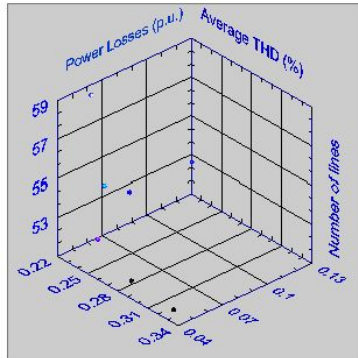
	THD (%)	Power losses (p.u.)	Number of lines	Maximun distance (km)	Total cable length (km)
1	0.0485	0.3229	51	167.1298	588.5649
2	0.0517	0.2762	51	153.8767	616.6151
3	0.0535	0.2398	52	153.8767	665.8188
4	0.0560	0.2300	59	153.8767	1144.8725
5	0.0653	0.2291	54	153.8767	745.2685
6	0.0832	0.2279	53	153.8767	716.6702
7	0.0833	0.2278	53	153.8767	711.6977
8	0.1252	0.2276	53	153.8767	687.8610

Total processing data time
19:32:1.644 = 70321.644 seconds
8 chromosomes generated as the best options after 1000 generations.
*** End of Graphs report ***

*** Results ***
Base: 10000000
Number of lines and Transformers: 51
Generation Nodes: 16
Load Nodes: 24
Total Nodes: 40
Number of elements in derivation: 2
Load nodes with harmonics injected: 8
Number of harmonics to be considered: 7
Processing time of Power Flow and Harmonic Propagation Study : 00:00:0.845 = 0.845 seconds
**Map of the North Sea with connection option 1**

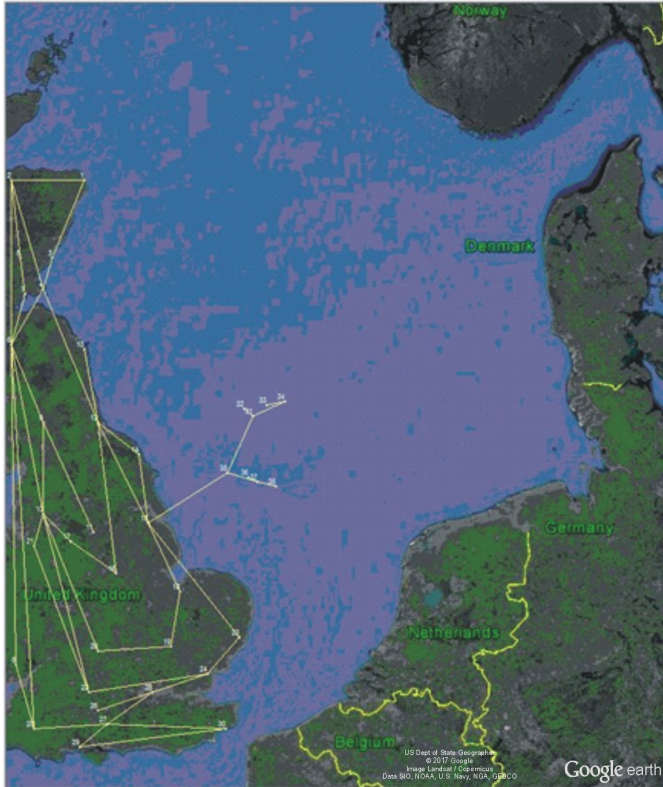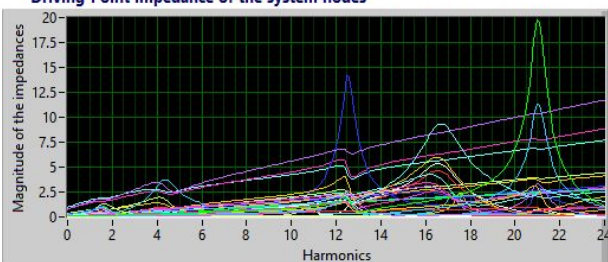**Number of iterations: 4**
Error : 7.131746E-6
Generation : 2.756900 p.u.
Demand : 2.434000 p.u.
Power Losses: 0.322906 p.u.
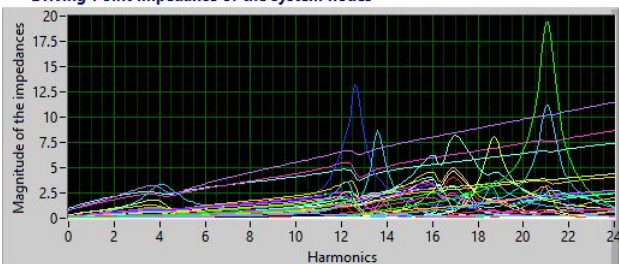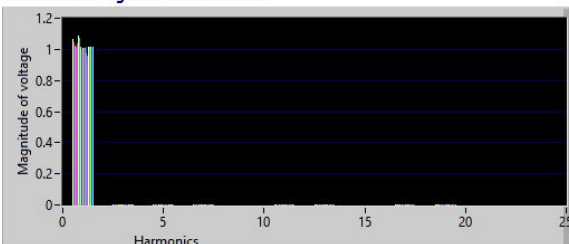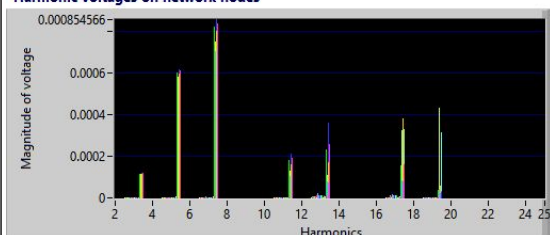
*** Results ***
Base: 10000000
Number of lines and Transformers: 51
Generation Nodes: 16
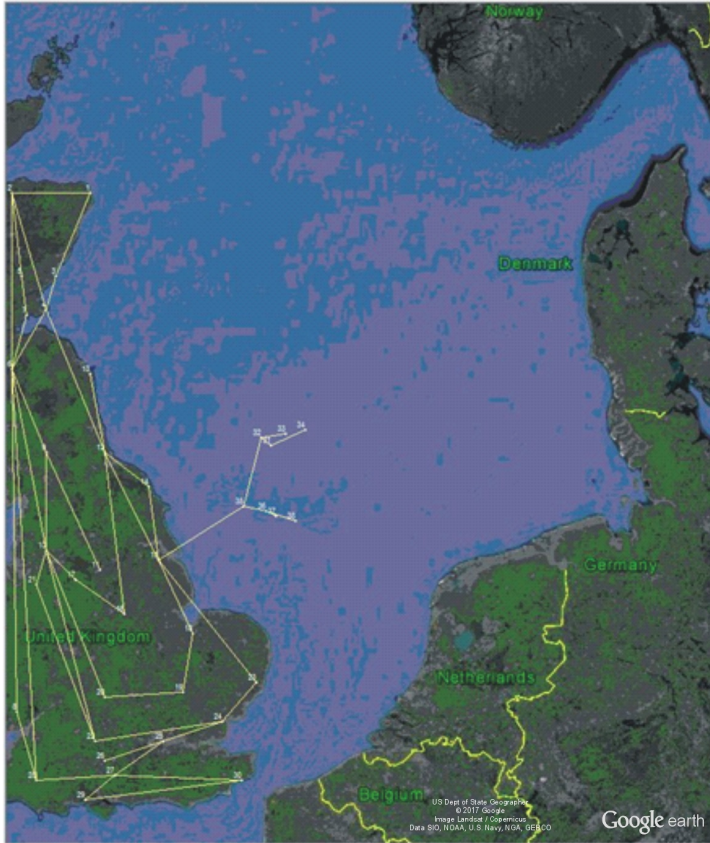**Load Nodes: 24**
Total Nodes: 40
Number of elements in derivation: 2
Load nodes with harmonics injected: 8
Number of harmonics to be considered: 7
Processing time of Power Flow and Harmonic Propagation Study : 00:00:0.885 = 0.885 seconds
Map of the North Sea with connection option 2
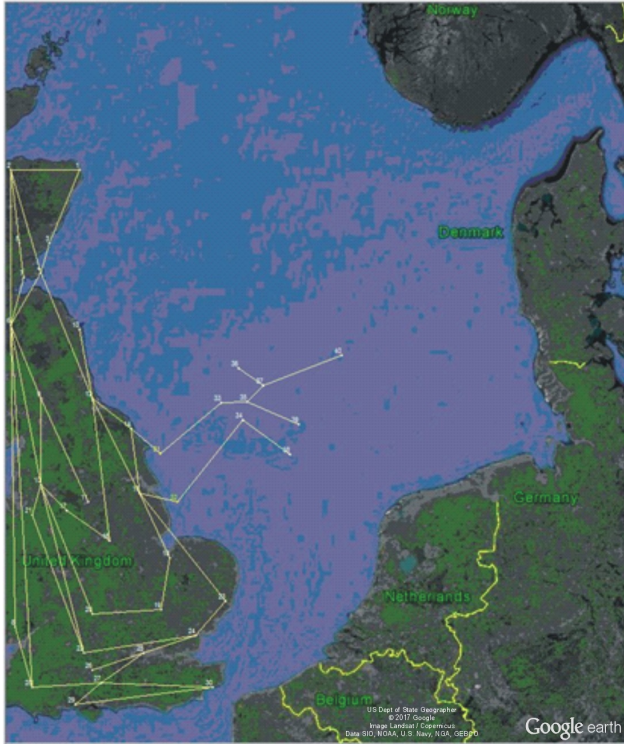
Number of iterations: 4
Error : 3.520948E-6
Generation : 2.710215 p.u.
Demand : 2.434000 p.u.
Power Losses: 0.276218 p.u.
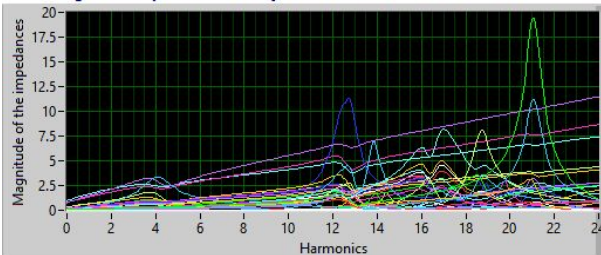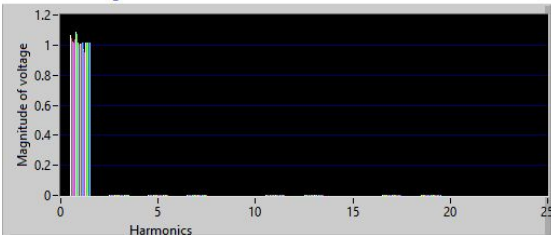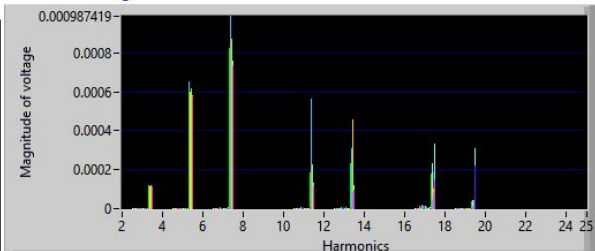
*** Results ***
Base: 10000000
Number of lines and Transformers: 52
Generation Nodes: 16
Load Nodes: 24
Total Nodes: 40
Number of elements in derivation: 2
Load nodes with harmonics injected: 8
Number of harmonics to be considered: 7
Processing time of Power Flow and Harmonic Propagation Study : 00:00:0.891 = 0.891 seconds
Map of the North Sea with connection option 3
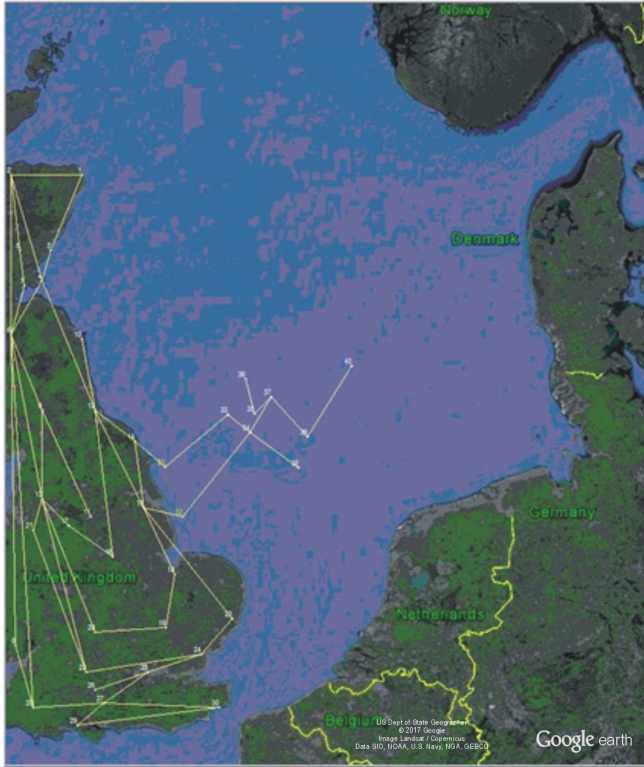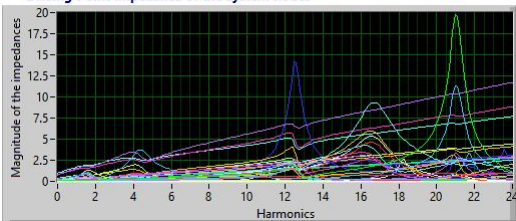

Number of iterations: 4
Error : 1.331043E-6
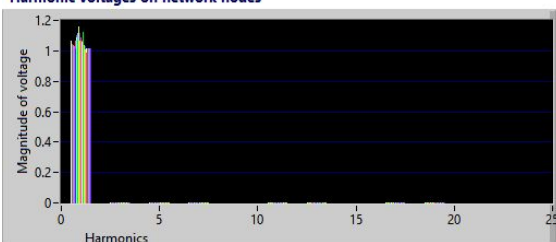**Generation : 2.673837 p.u.**
Demand : 2.434000 p.u.
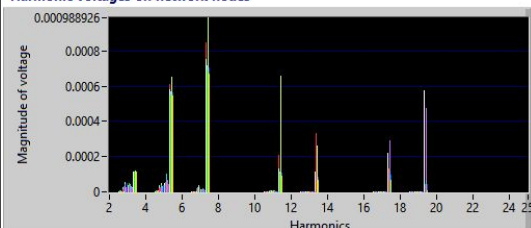**Power Losses: 0.239838 p.u.**
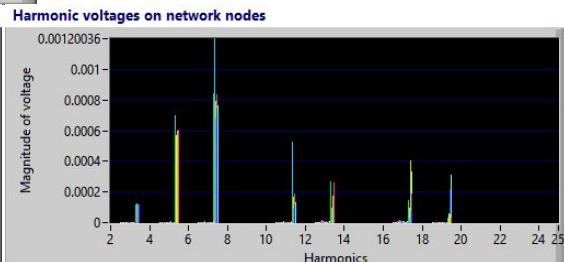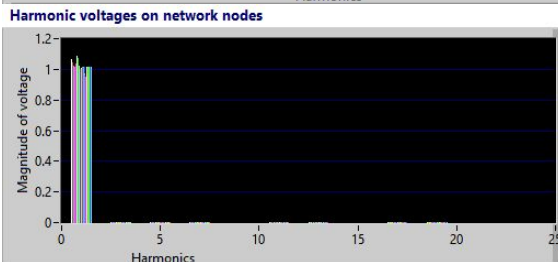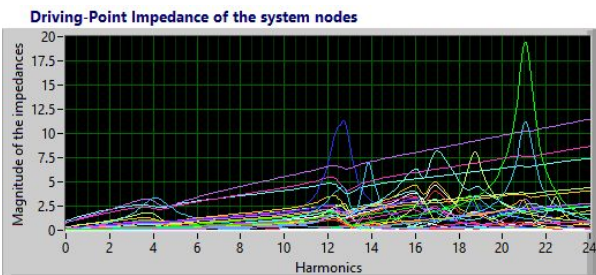
*** Results ***
Base: 10000000
Number of lines and Transformers: 52
Generation Nodes: 16
Load Nodes: 24
Total Nodes: 40
Number of elements in derivation: 2
Load nodes with harmonics injected: 8
Number of harmonics to be considered: 7
Processing time of Power Flow and Harmonic Propagation Study : 00:00:0.89 = 0.89 seconds
Map of the North Sea with connection option 4

Number of iterations: 4
Error : 1.151683E-6
Generation : 2.664036 p.u.
Demand : 2.434000 p.u.
Power Losses: 0.230036 p.u.
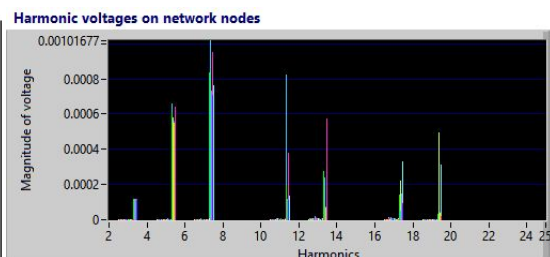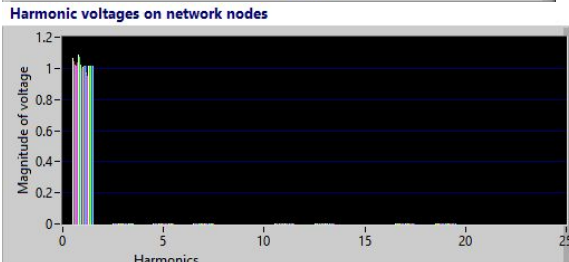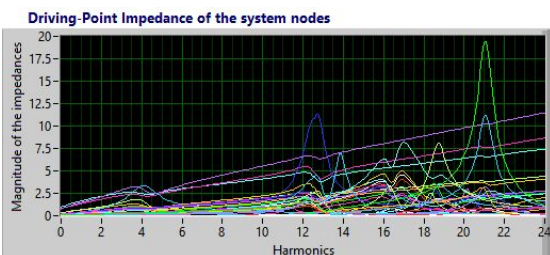
*** Results ***
Base: 10000000
Number of lines and Transformers: 54
Generation Nodes: 16
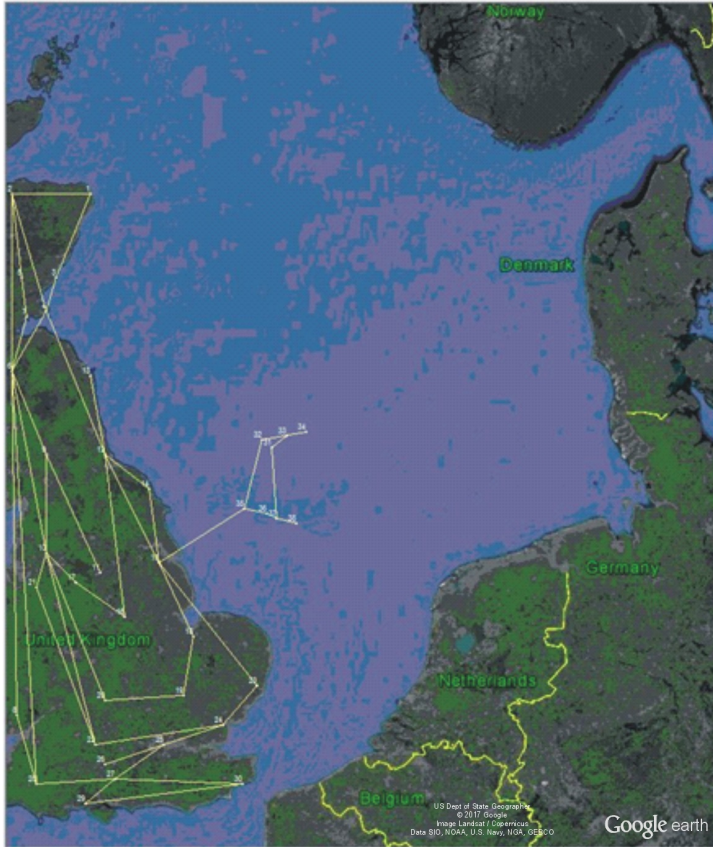**Load Nodes: 24**
Total Nodes: 40
Number of elements in derivation: 2
Load nodes with harmonics injected: 8
Number of harmonics to be considered: 7
Processing time of Power Flow and Harmonic Propagation Study : 00:00:0.904 = 0.904 seconds
Map of the North Sea with connection option 5
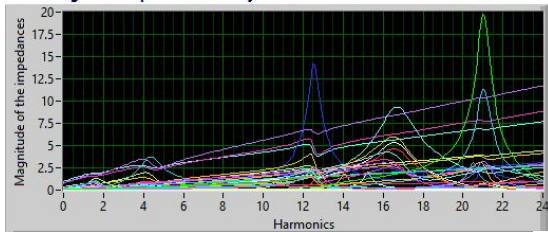

Number of iterations: 4
Error : 1.232946E-6
Generation : 2.663142 p.u.
Demand : 2.434000 p.u.
Power Losses: 0.229143 p.u.
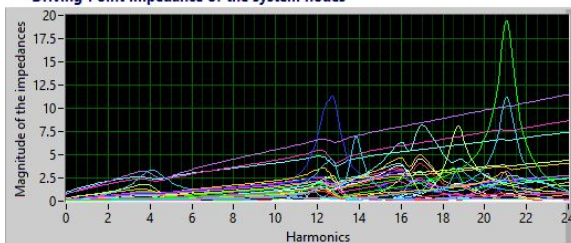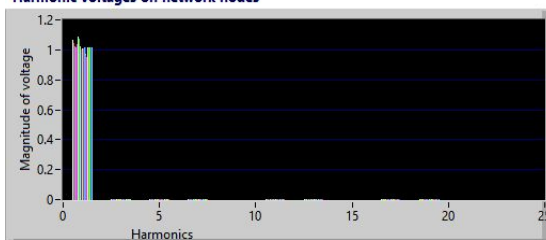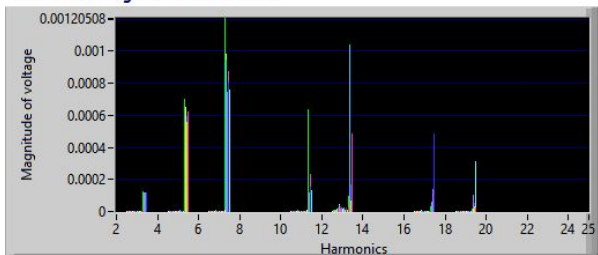
*** Results ***
Base: 10000000
Number of lines and Transformers: 53
Generation Nodes: 16
Load Nodes: 24
Total Nodes: 40
Number of elements in derivation: 2
Load nodes with harmonics injected: 8
Number of harmonics to be considered: 7
Processing time of Power Flow and Harmonic Propagation Study : 00:00:0.898 = 0.898 seconds
Map of the North Sea with connection option 6

Number of iterations: 4
Error : 1.205781E-6
Generation : 2.661854 p.u.
Demand : 2.434000 p.u.
Power Losses: 0.227855 p.u.
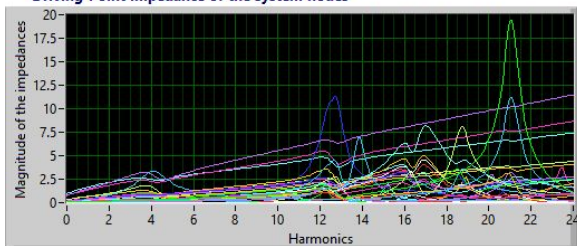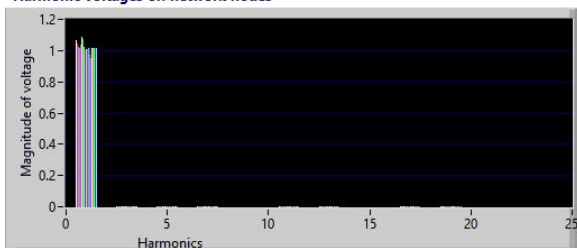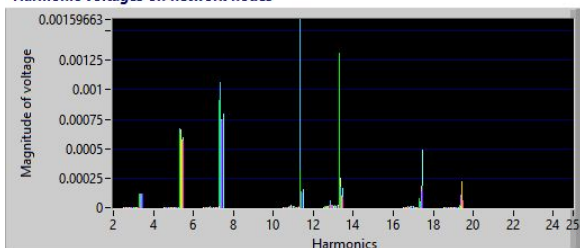
*** Results ***
Base: 10000000
Number of lines and Transformers: 53
Generation Nodes: 16
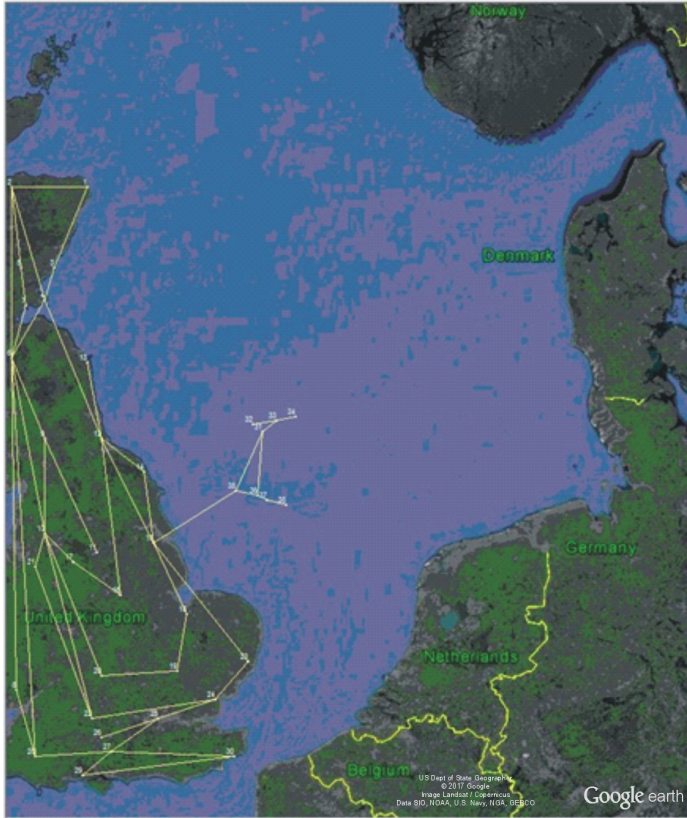**Load Nodes: 24**
Total Nodes: 40
Number of elements in derivation: 2
Load nodes with harmonics injected: 8
Number of harmonics to be considered: 7
Processing time of Power Flow and Harmonic Propagation Study : 00:00:0.931 = 0.931 seconds
Map of the North Sea with connection option 7


Number of iterations: 4
Error : 1.185159E-6
Generation : 2.661792 p.u.
Demand : 2.434000 p.u.
Power Losses: 0.227793 p.u.
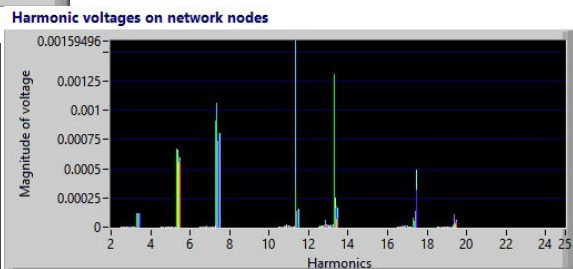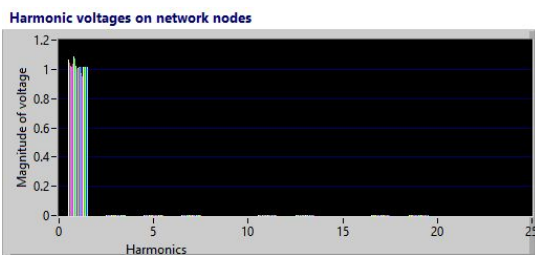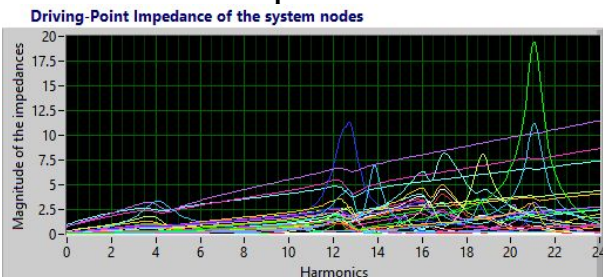
*** Results ***
Base: 10000000
Number of lines and Transformers: 53
Generation Nodes: 16
Load Nodes: 24
Total Nodes: 40
Number of elements in derivation: 2
Load nodes with harmonics injected: 8
Number of harmonics to be considered: 7
Processing time of Power Flow and Harmonic Propagation Study : 00:00:0.915 = 0.915 seconds
Map of the North Sea with connection option 8

Number of iterations: 4
Error : 1.151016E-6
Generation : 2.661590 p.u.
**Demand : 2.434000 p.u.**
Power Losses: 0.227591 p.u.
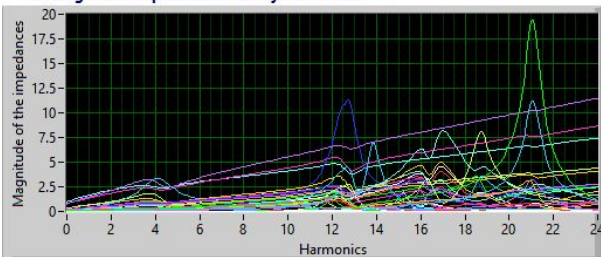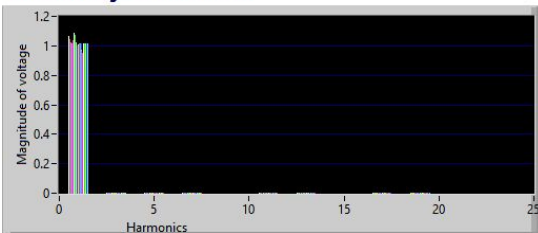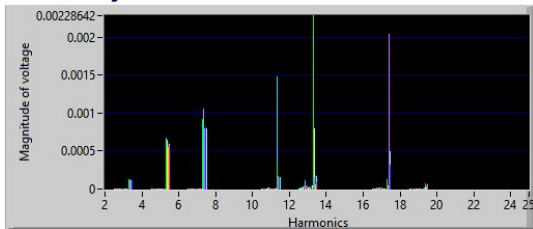
H.3 Results for Scenario 2

As in Scenario 1, results were obtained from the report generated by the algorithm, only are presented the Pareto front of the first and last generation and the best configurations that the algorithm generates. Network data and reports are not attached because if it is included for each configuration, it is much information.

For Scenario 2 were proposed 100 chromosomes as the first generation and were generated 1,000 offsprings. If new geneartions are generated, time is increased significantly.

H.3.1 100 chromosomes

*** Report ***
Total of Chromosomes Generated for the Initial Population: 100
Maximum Distance: 45 km
Pareto Fronts Considered: 15
Generation time: 00:17:36.239 = 1056.239 seconds
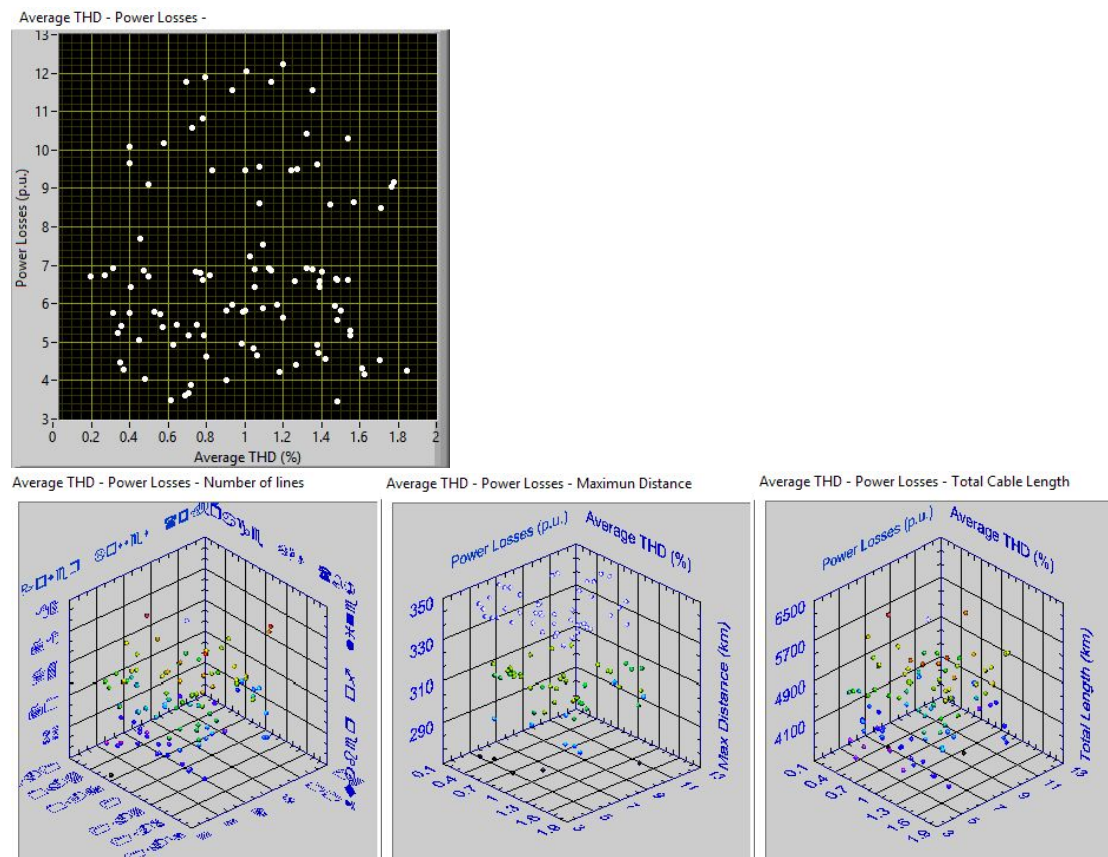
100 chromosomes generated after obtain minimum distance tree for each chromosome and eliminate not valid chromosomes. 01:24:53.34 = 5093.34 seconds
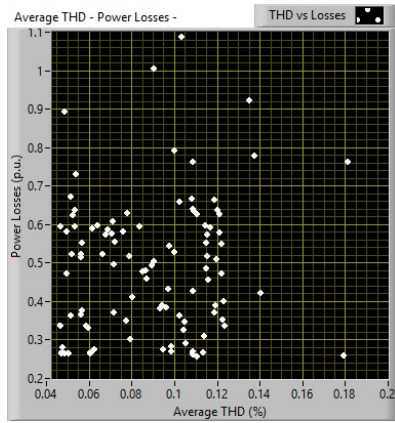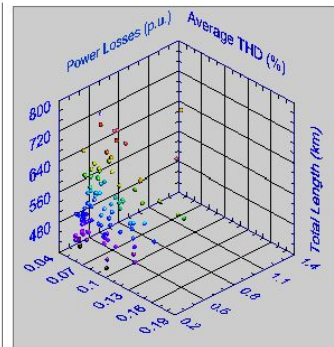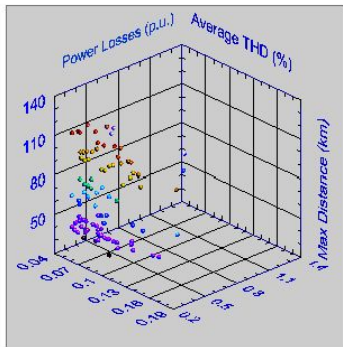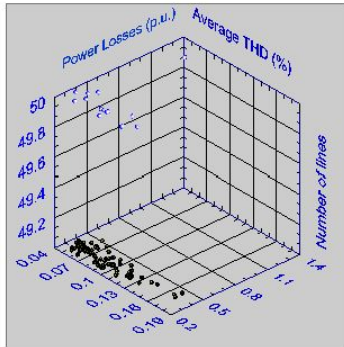
Generation of chromosomes number 1
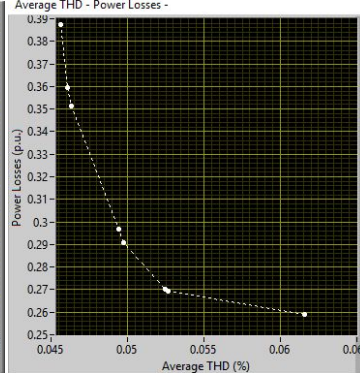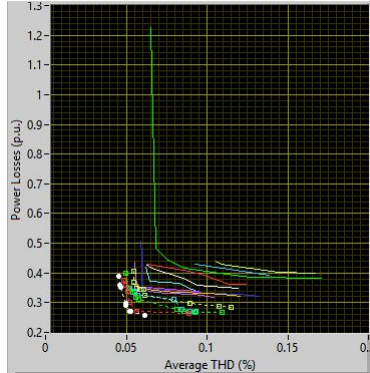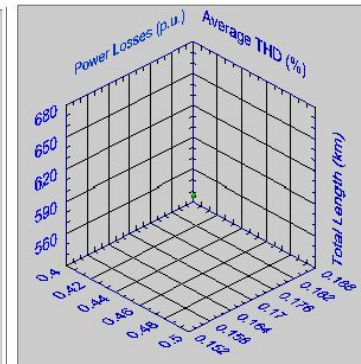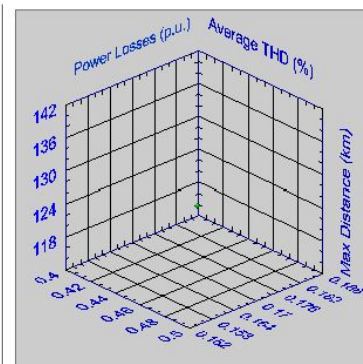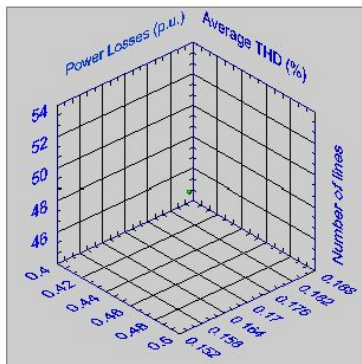
	THD (%)	Power losses (p.u.)	Number of lines	Maximun distance (km)	Total cable length (km)
1	0.0456	0.3875	49	56.1914	438.8648

2	0.0461	0.3597	49	40.4055	401.8721
3	0.0463	0.3515	50	40.4055	424.0210
4	0.0494	0.2967	49	40.4055	499.8752
5	0.0497	0.2907	49	40.4055	441.3737
6	0.0525	0.2700	49	65.7126	438.5422
7	0.0526	0.2693	49	113.0968	451.0615
8	0.0616	0.2589	49	40.4055	503.4154

Generation of chromosomes number 1,000

	THD (%)	Power losses (p.u.)	Number of lines	Maximun distance (km)	Total cable length (km)
1	0.0447	0.3722	49	111.7604	418.4618
2	0.0461	0.3597	49	111.7604	401.8721
3	0.0463	0.3515	50	111.7604	424.0210
4	0.0466	0.2893	49	111.7604	440.0372
5	0.0496	0.2811	50	111.7604	432.7067
6	0.0515	0.2772	50	111.7604	398.1801
7	0.0517	0.2731	49	133.9574	499.9185
8	0.0525	0.2700	49	113.0968	438.5422
9	0.0526	0.2693	49	113.0968	454.3281
10	0.0536	0.2674	49	113.0968	433.9902
11	0.0565	0.2653	50	111.7604	467.6053
12	0.0607	0.2609	49	133.9574	534.8170
13	0.0616	0.2589	49	113.0968	503.4154

Total processing data time
35:07:17.141 = 126437.141 seconds
13 chromosomes generated as the best options after 1,000 generations.
*** End of Graphs report ***

*** Results ***
Base: 10000000
Number of lines and Transformers: 49
Generation Nodes: 14
**Load Nodes: 24**
Total Nodes: 38
Number of elements in derivation: 2
Load nodes with harmonics injected: 8
Number of harmonics to be considered: 7
Processing time of Power Flow and Harmonic Propagation Study : 00:00:0.791 = 0.791 seconds
Map of the North Sea with connection option 1
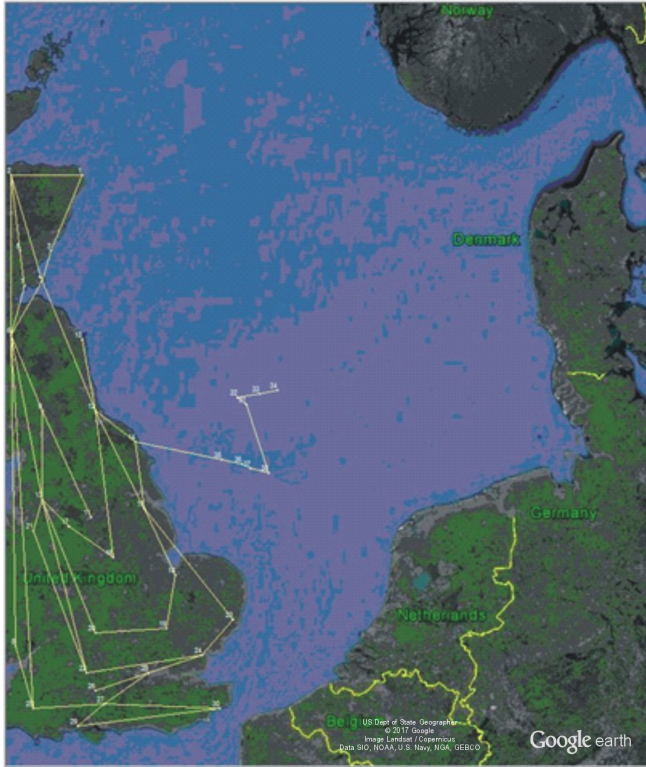

Number of iterations: 5
Error : 1.573259E-5
Generation : 2.886195 p.u.
Demand : 2.514000 p.u.
Power Losses: 0.372201 p.u.
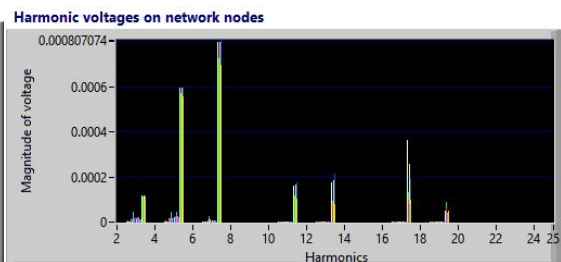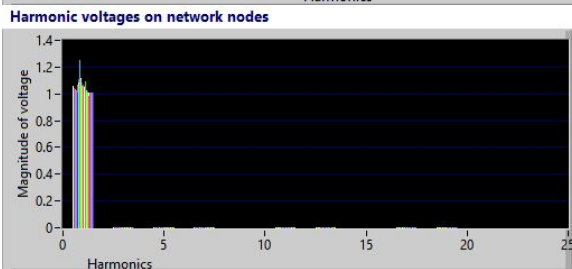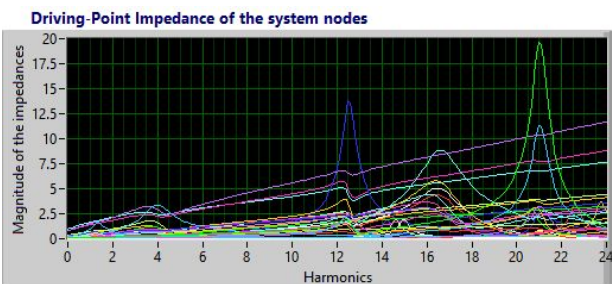
*** Results ***
Base: 10000000
Number of lines and Transformers: 49
Generation Nodes: 14
Load Nodes: 24
Total Nodes: 38
Number of elements in derivation: 2
Load nodes with harmonics injected: 8
Number of harmonics to be considered: 7
Processing time of Power Flow and Harmonic Propagation Study : 00:00:0.809 = 0.809 seconds
Map of the North Sea with connection option 2

Number of iterations: 5
Error : 1.563636E-5
Generation : 2.873681 p.u.
Demand : 2.514000 p.u.
Power Losses: 0.359686 p.u.
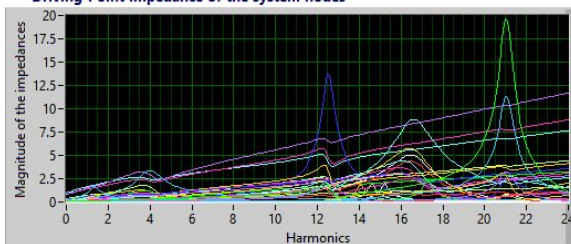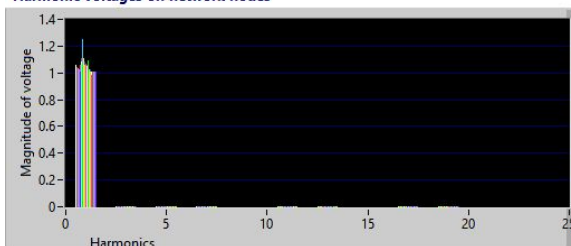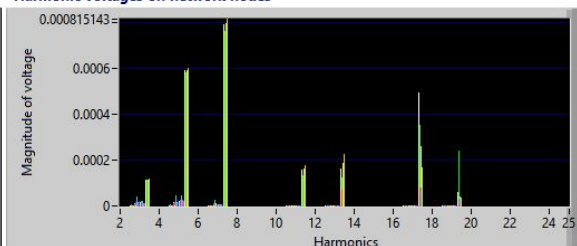
*** Results ***
Base: 10000000
Number of lines and Transformers: 50
Generation Nodes: 14
Load Nodes: 24
Total Nodes: 38
Number of elements in derivation: 2
Load nodes with harmonics injected: 8
Number of harmonics to be considered: 7
Processing time of Power Flow and Harmonic Propagation Study : 00:00:0.81 = 0.81 seconds
Map of the North Sea with connection option 3

Number of iterations: 5
Error : 1.565756E-5
Generation : 2.865504 p.u.
Demand : 2.514000 p.u.
Power Losses: 0.351510 p.u.
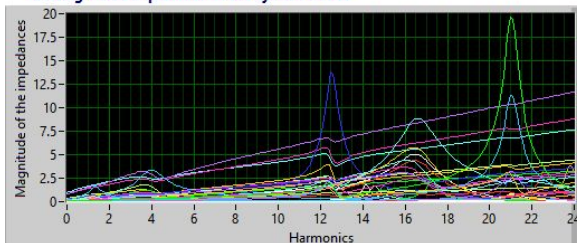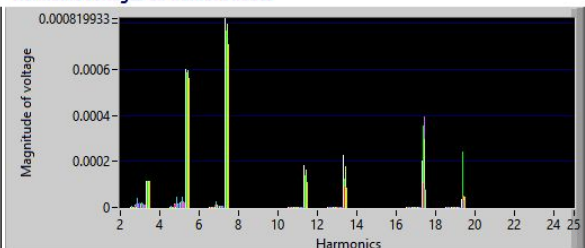
*** Results ***
Base: 10000000
Number of lines and Transformers: 49
Generation Nodes: 14
Load Nodes: 24
Total Nodes: 38
Number of elements in derivation: 2
Load nodes with harmonics injected: 8
Number of harmonics to be considered: 7
Processing time of Power Flow and Harmonic Propagation Study : 00:00:0.808 = 0.808 seconds
Map of the North Sea with connection option 4
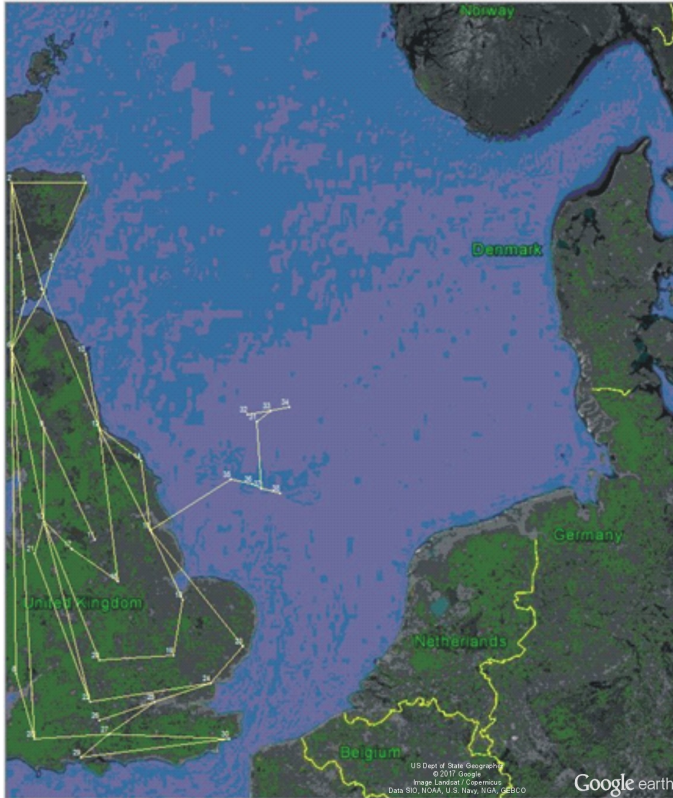
Number of iterations: 5
Error : 5.002647E-7
Generation : 2.803282 p.u.
Demand : 2.514000 p.u.
Power Losses: 0.289282 p.u.
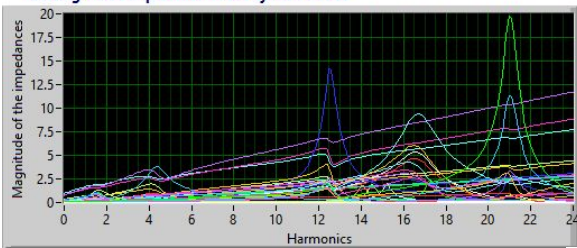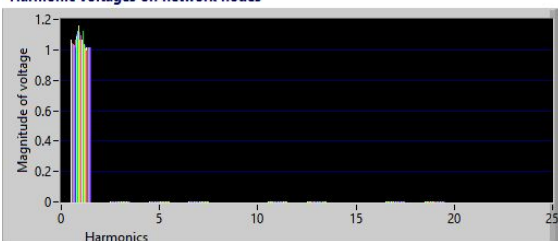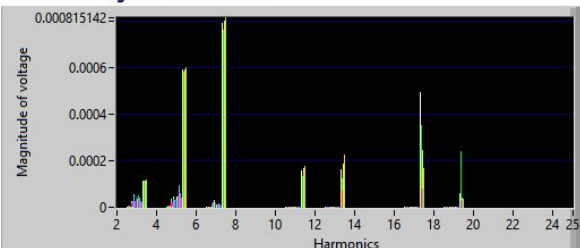
*** Results ***
Base: 10000000
Number of lines and Transformers: 50
Generation Nodes: 14
Load Nodes: 24
Total Nodes: 38
Number of elements in derivation: 2
Load nodes with harmonics injected: 8
Number of harmonics to be considered: 7
Processing time of Power Flow and Harmonic Propagation Study : 00:00:0.844 = 0.844 seconds
Map of the North Sea with connection option 5

Number of iterations: 5
Error : 5.078555E-7
Generation : 2.795146 p.u.
Demand : 2.514000 p.u.
Power Losses: 0.281147 p.u.
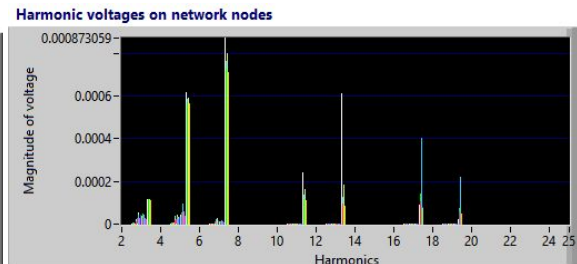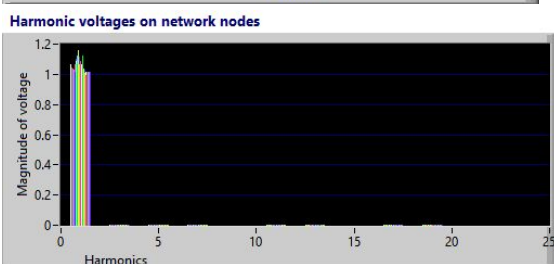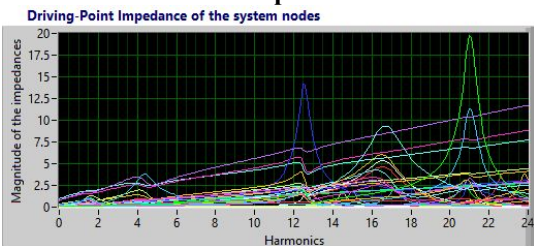
*** Results ***
Base: 10000000
Number of lines and Transformers: 50
Generation Nodes: 14
Load Nodes: 24
Total Nodes: 38
Number of elements in derivation: 2
Load nodes with harmonics injected: 8
Number of harmonics to be considered: 7
Processing time of Power Flow and Harmonic Propagation Study : 00:00:0.83 = 0.83 seconds
Map of the North Sea with connection option 6
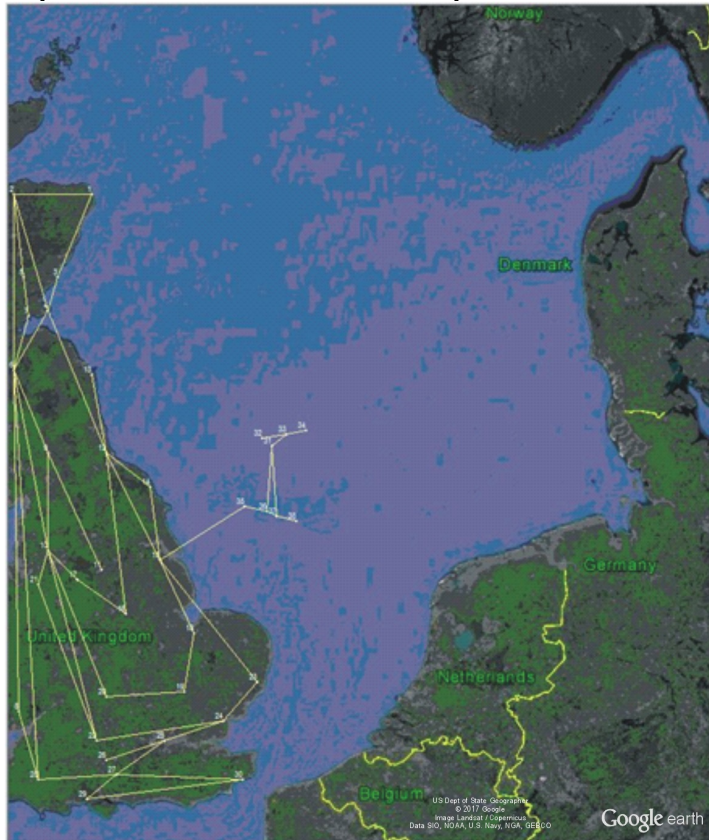
Number of iterations: 5
Error : 5.133731E-7
Generation : 2.791186 p.u.
Demand : 2.514000 p.u.
Power Losses: 0.277186 p.u.
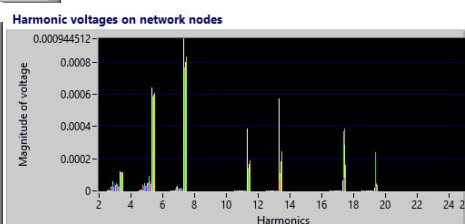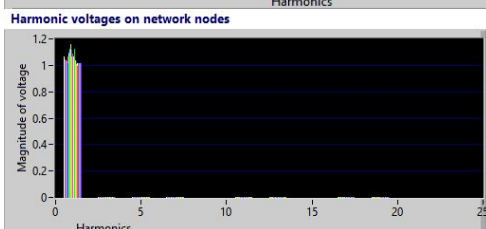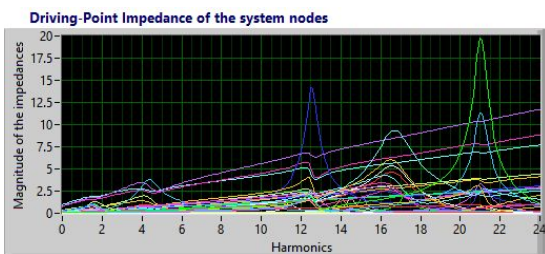
*** Results ***
Base: 10000000
Number of lines and Transformers: 49
Generation Nodes: 14
Load Nodes: 24
Total Nodes: 38
Number of elements in derivation: 2
Load nodes with harmonics injected: 8
Number of harmonics to be considered: 7
Processing time of Power Flow and Harmonic Propagation Study : 00:00:0.877 = 0.877 seconds
Map of the North Sea with connection option 7
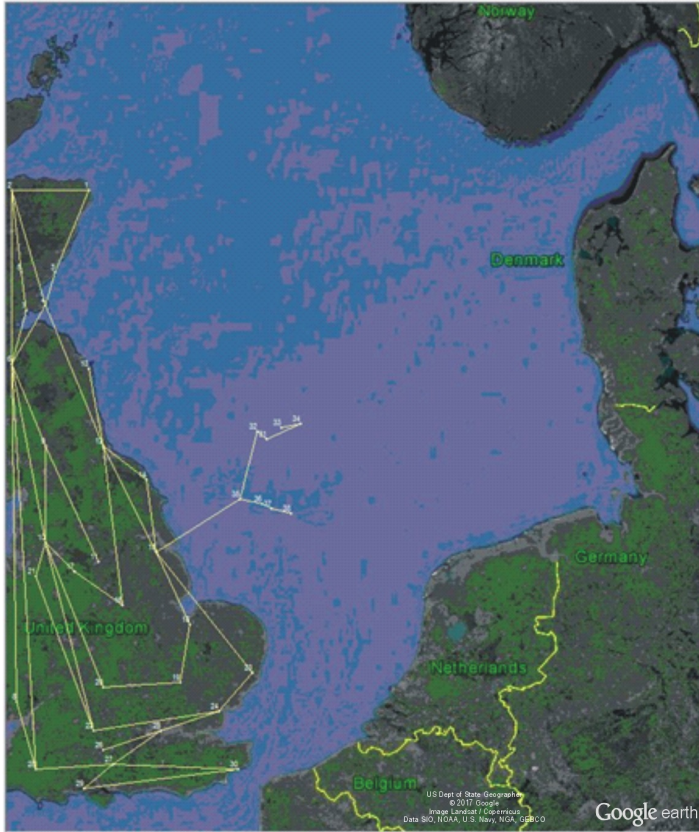
Number of iterations: 5
Error : 5.206746E-7
Generation : 2.787107 p.u.
Demand : 2.514000 p.u.
Power Losses: 0.273107 p.u.
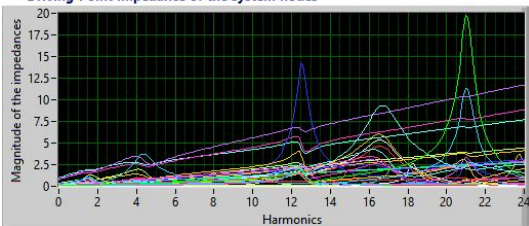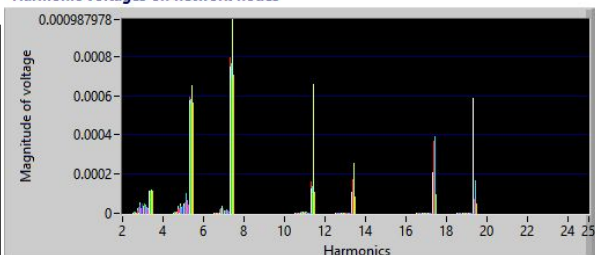
*** Results ***
Base: 10000000
Number of lines and Transformers: 49
Generation Nodes: 14
Load Nodes: 24
Total Nodes: 38
Number of elements in derivation: 2
Load nodes with harmonics injected: 8
Number of harmonics to be considered: 7
Processing time of Power Flow and Harmonic Propagation Study : 00:00:0.808 = 0.808 seconds
Map of the North Sea with connection option 8

Number of iterations: 5
Error : 5.271583E-7
Generation : 2.783984 p.u.
Demand : 2.514000 p.u.
Power Losses: 0.269984 p.u.
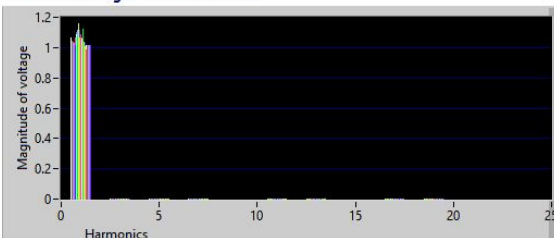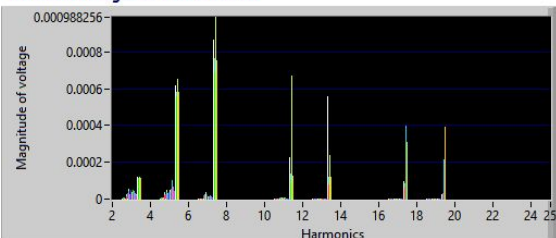
*** Results ***
Base: 10000000
Number of lines and Transformers: 49
Generation Nodes: 14
Load Nodes: 24
Total Nodes: 38
Number of elements in derivation: 2
Load nodes with harmonics injected: 8
Number of harmonics to be considered: 7
Processing time of Power Flow and Harmonic Propagation Study : 00:00:0.811 = 0.811 seconds
Map of the North Sea with connection option 9

Number of iterations: 5
Error : 5.286706E-7
Generation : 2.783313 p.u.
Demand : 2.514000 p.u.
Power Losses: 0.269313 p.u.

*** Results ***
Base: 10000000
Number of lines and Transformers: 49
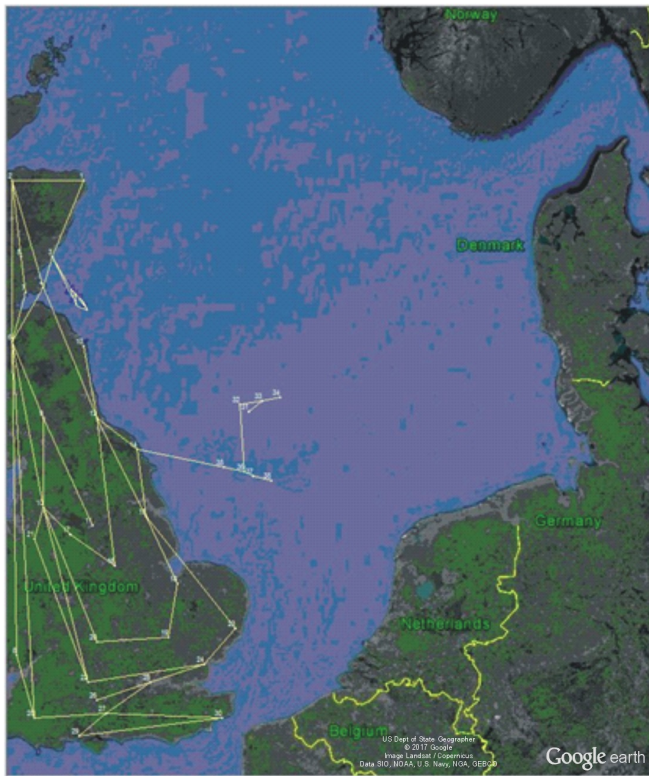**Generation Nodes: 14**
Load Nodes: 24
Total Nodes: 38
Number of elements in derivation: 2
Load nodes with harmonics injected: 8
Number of harmonics to be considered: 7
Processing time of Power Flow and Harmonic Propagation Study : 00:00:0.832 = 0.832 seconds
Map of the North Sea with connection option 10
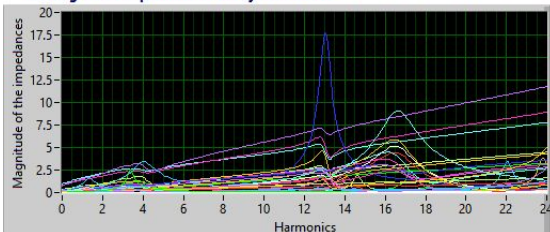

Number of iterations: 5
Error : 5.331946E-7
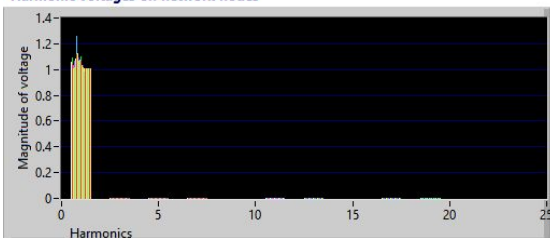**Generation : 2.781383 p.u.**
Demand : 2.514000 p.u.
Power Losses: 0.267383 p.u.
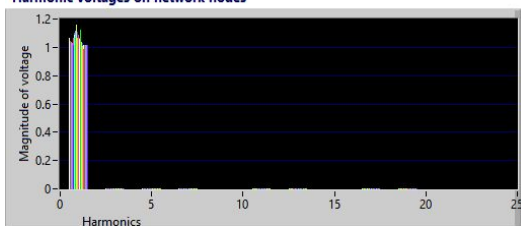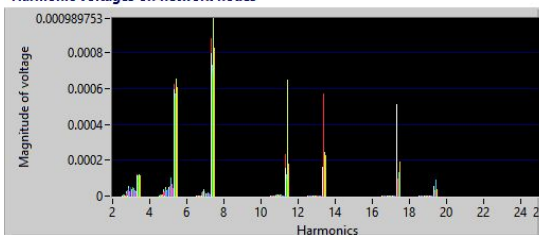
*** Results ***
Base: 10000000
Number of lines and Transformers: 50
Generation Nodes: 14
Load Nodes: 24
Total Nodes: 38
Number of elements in derivation: 2
Load nodes with harmonics injected: 8
Number of harmonics to be considered: 7
Processing time of Power Flow and Harmonic Propagation Study : 00:00:0.821 = 0.821 seconds
Map of the North Sea with connection option 11

Number of iterations: 5
Error : 5.386987E-7
Generation : 2.779285 p.u.
Demand : 2.514000 p.u.
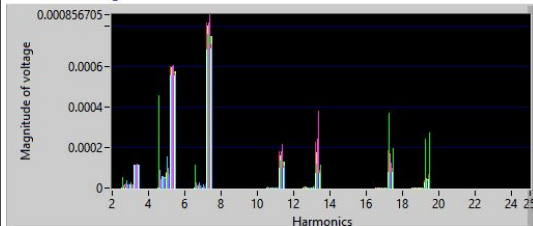**Power Losses: 0.265285 p.u.**
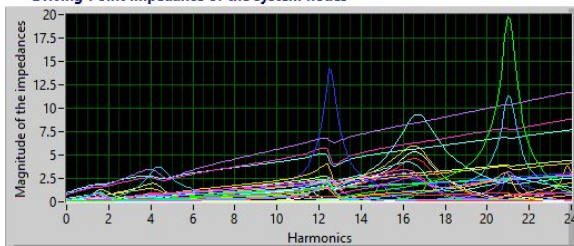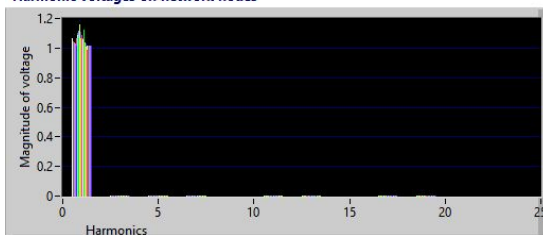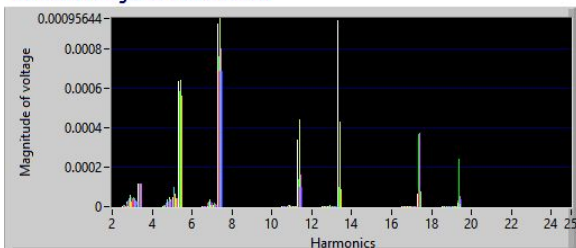
*** Results ***
Base: 10000000
Number of lines and Transformers: 49
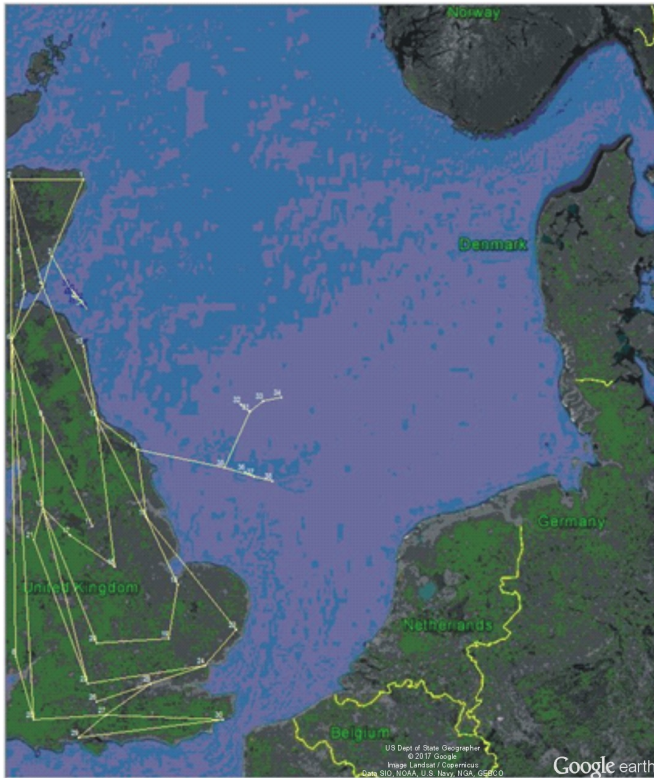**Generation Nodes: 14**
Load Nodes: 24
Total Nodes: 38
Number of elements in derivation: 2
Load nodes with harmonics injected: 8
Number of harmonics to be considered: 7
Processing time of Power Flow and Harmonic Propagation Study : 00:00:0.815 = 0.815 seconds
Map of the North Sea with connection option 12
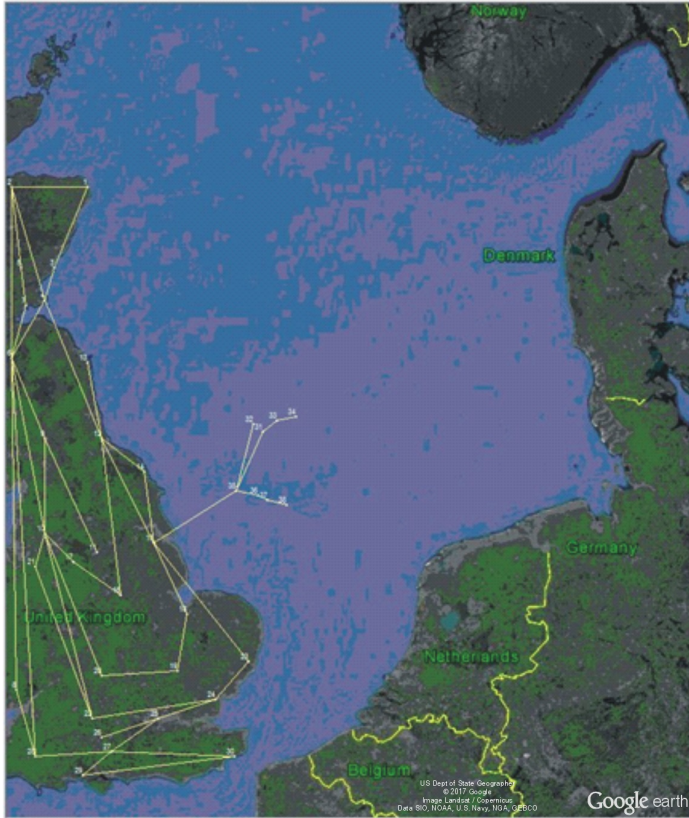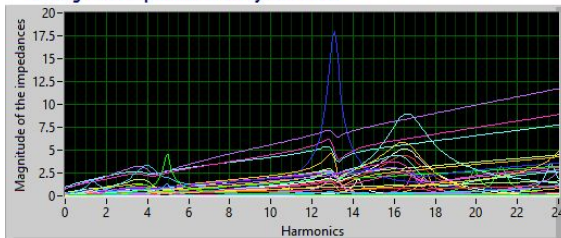

Number of iterations: 5
Error : 5.516490E-7
Generation : 2.774914 p.u.
Demand : 2.514000 p.u.
Power Losses: 0.260914 p.u.
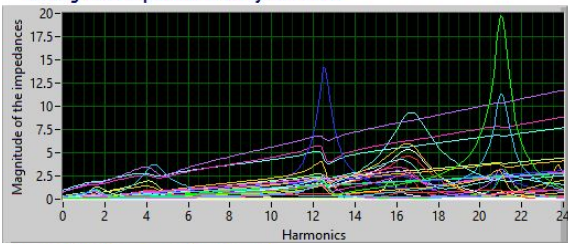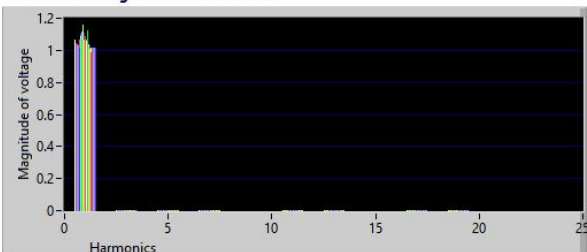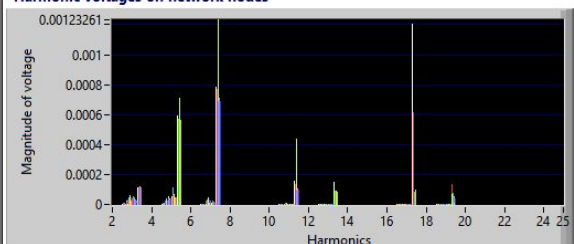
*** Results ***
Base: 10000000
Number of lines and Transformers: 49
Generation Nodes: 14
Load Nodes: 24
Total Nodes: 38
Number of elements in derivation: 2
Load nodes with harmonics injected: 8
Number of harmonics to be considered: 7
Processing time of Power Flow and Harmonic Propagation Study : 00:00:0.806 = 0.806 seconds
Map of the North Sea with connection option 13
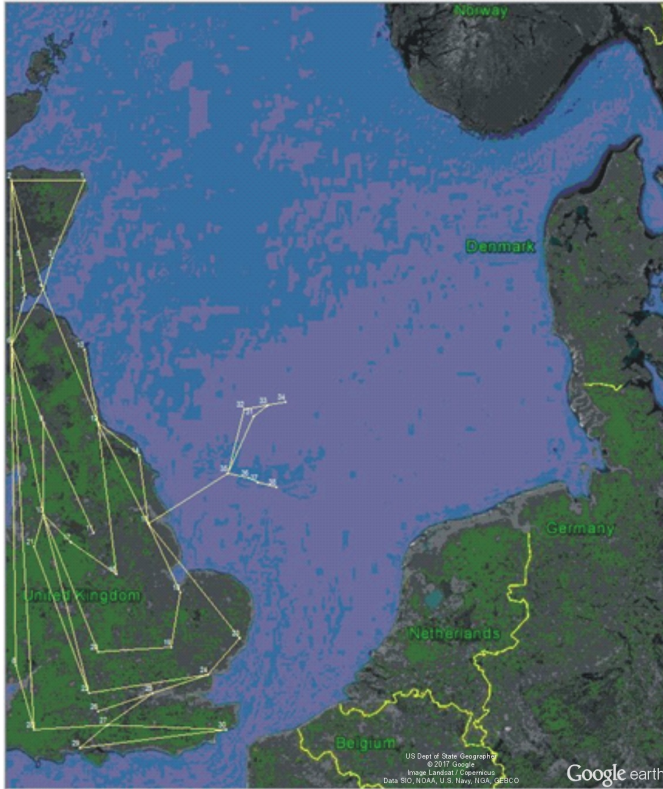
Number of iterations: 5
**Error : 5.582700E-7**
Generation : 2.772923 p.u.
Demand : 2.514000 p.u.
**Power Losses: 0.258923 p.u.**
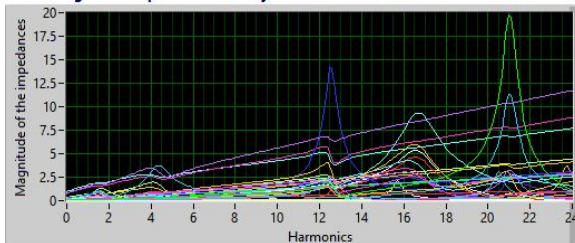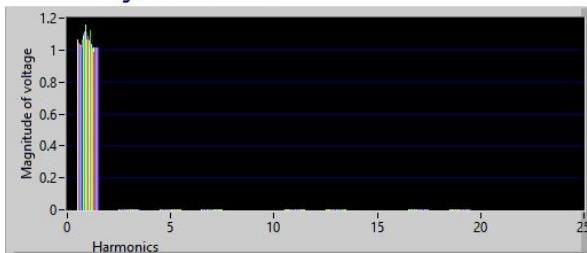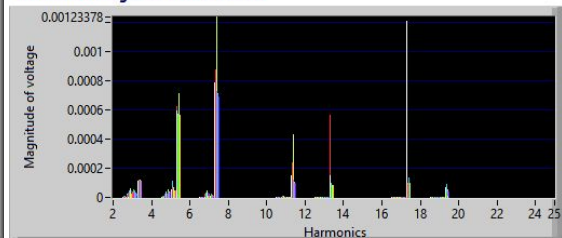
H.4   Results for Scenario 3

As in Scenarios 1 and 2, results were obtained from the report generated by the algorithm, only are presented the Pareto front of the first and last generation and the best configurations that the algorithm generates. Network data and reports are not attached because if it is included for each configuration, it is much information.

For Scenario 3 were proposed 150 chromosomes as the first generation because 15 nodes can be interconnected, with this number of nodes were generated 500 offsprings because time was increased and new generations did not create new better chromosomes.

H.4.1   150 chromosomes

*** Report ***
Total of Chromosomes Generated for the Initial Population: 150
Maximum Distance: 45 km
Pareto Fronts Considered: 15
Generation time: 00:05:42.215 = 342.215 seconds
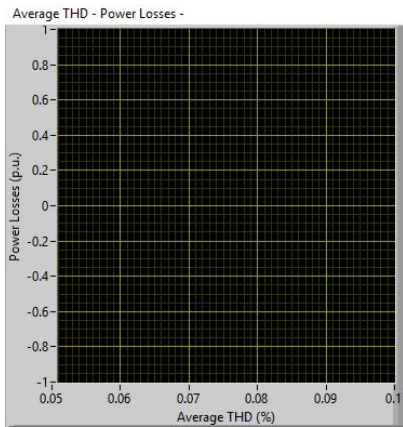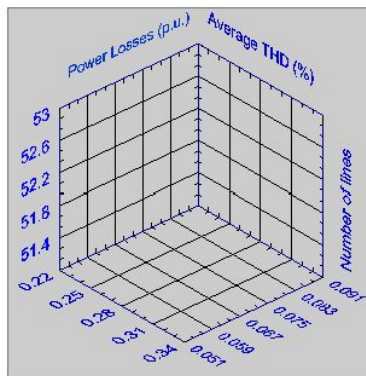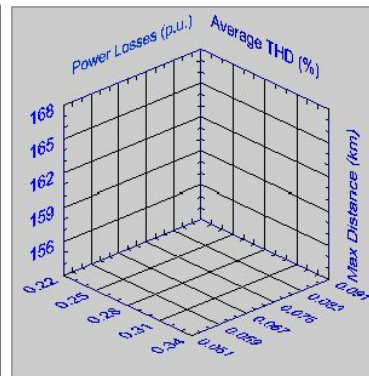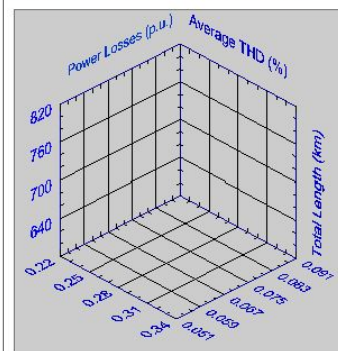
150 chromosomes generated after obtain minimum distance tree for each chromosome and eliminate not valid chromosomes. 09:23:46.931 = 33826.931 seconds
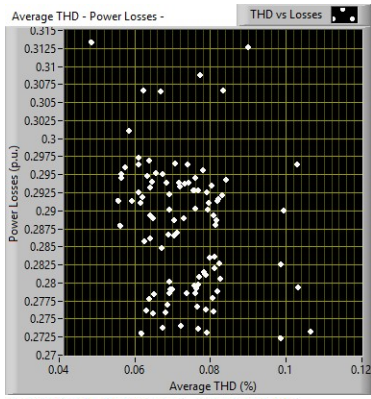
Average THD - Power Losses - Number of lines
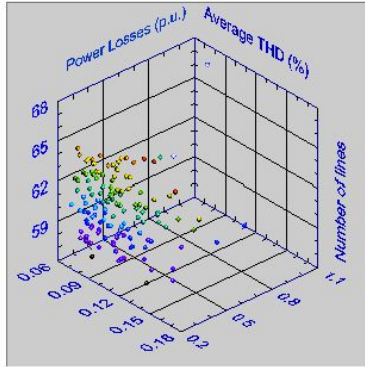
Average THD - Power Losses - Maximun Distance
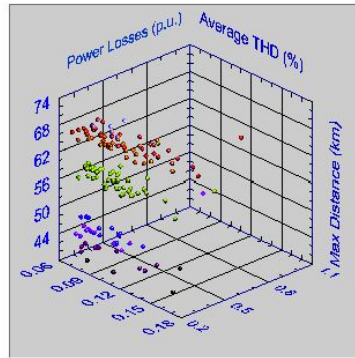
Average THD - Power Losses - Total Cable Length
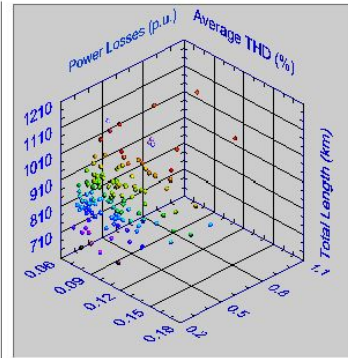
Generation of chromosomes number 1

Fronts of Pareto
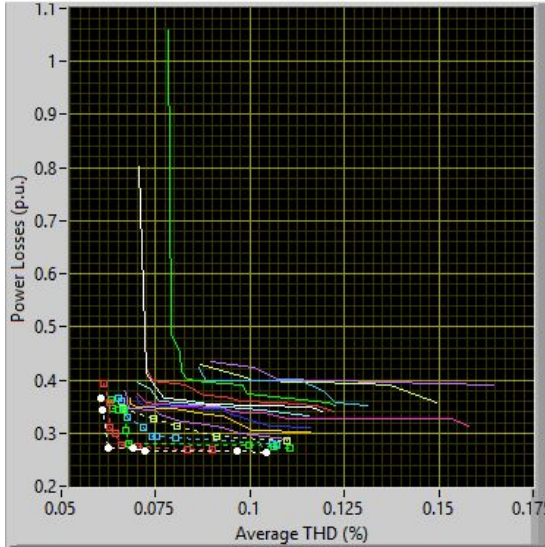
Average THD - Power Losses -
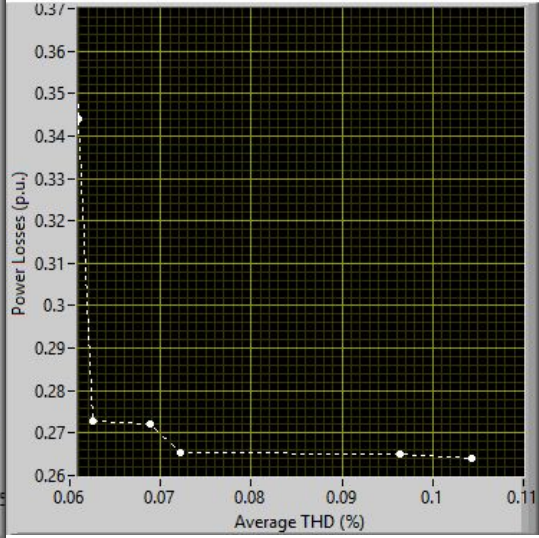
Average THD - Power Losses - Number of lines
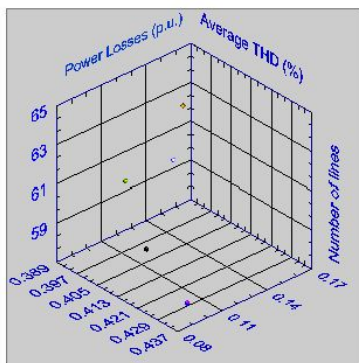
Average THD - Power Losses - Maximun Distance
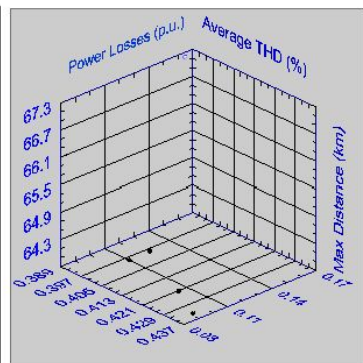
Average THD - Power Losses - Total Cable Length
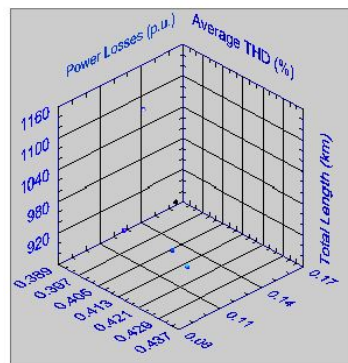
	THD (%)	Power losses (p.u.)	Number of lines	Maximun distance (km)	Total cable length (km)
1	0.0605	0.3655	60	43.5368	761.8323
2	0.0609	0.3440	57	45.8963	614.8928
3	0.0625	0.2728	60	65.7126	715.1140
4	0.0689	0.2721	62	56.1914	796.6288
5	0.0722	0.2655	60	40.4055	839.4981
6	0.0965	0.2650	59	57.0326	784.0425
7	0.1043	0.2639	61	39.2933	928.6563

Generation of chromosomes number 102

	THD (%)	Power losses (p.u.)	Number of lines	Maximun distance (km)	Total cable length (km)
1	0.0605	0.3655	60	115.3429	761.8323
2	0.0609	0.3440	57	111.7604	614.8928
3	0.0610	0.2753	57	111.7604	645.4751
4	0.0617	0.2694	57	111.7604	611.6694
5	0.0629	0.2669	60	113.0968	681.3083
6	0.0722	0.2655	77	411.0729	4456.0700
7	0.0965	0.2650	75	385.0543	3666.7357
8	0.1043	0.2639	79	411.0729	5082.5616

Total processing data time

61:00:31.083 = 219,631.083 seconds

8 chromosomes generated as the best options after 500 generations.

*** End of Graphs report ***

*** Results ***
Base: 10000000
Number of lines and Transformers: 60
Generation Nodes: 21
Load Nodes: 24
Total Nodes: 45
Number of elements in derivation: 2
Load nodes with harmonics injected: 15
Number of harmonics to be considered: 7
Processing time of Power Flow and Harmonic Propagation Study : 00:00:1.189 = 1.189 seconds
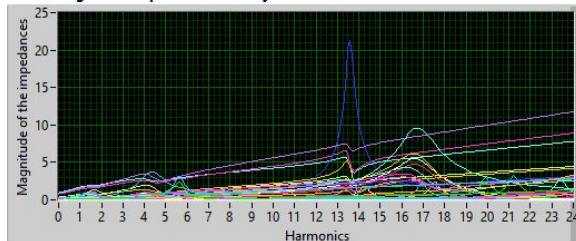**Map of the North Sea with connection option 1**
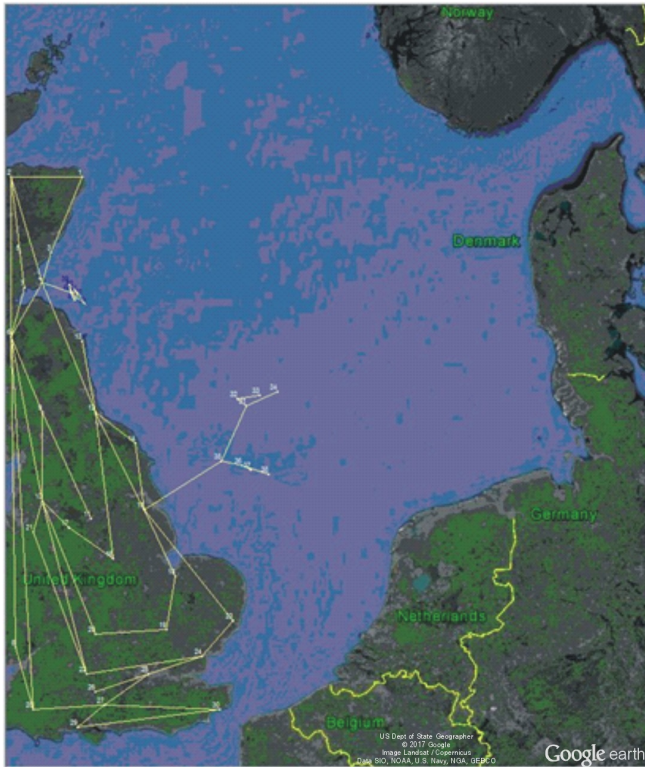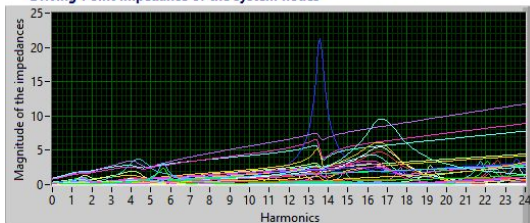

Number of iterations: 5
Error : 1.658474E-5
Generation : 2.599476 p.u.
Demand : 2.234000 p.u.
Power Losses: 0.365482 p.u.

*** Results ***

Base: 10000000

Number of lines and Transformers: 57

Generation Nodes: 21

Load Nodes: 24

Total Nodes: 45

Number of elements in derivation: 2

Load nodes with harmonics injected: 15

Number of harmonics to be considered: 7

Processing time of Power Flow and Harmonic Propagation Study : 00:00:1.243 = 1.243 seconds

Map of the North Sea with connection option 2

Number of iterations: 5

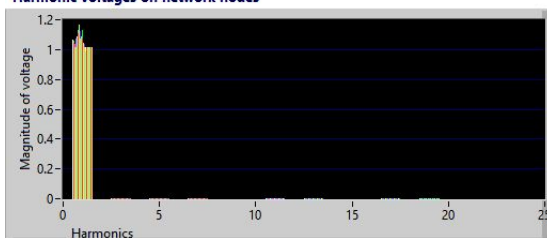**Error : 1.633949E-5**

Generation : 2.578006 p.u.

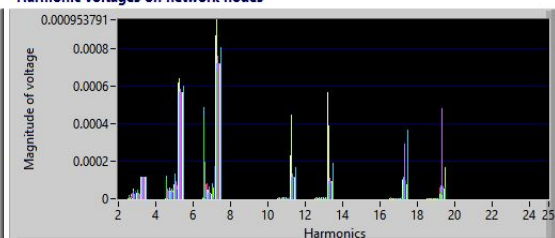**Demand : 2.234000 p.u.**

Power Losses: 0.344012 p.u.
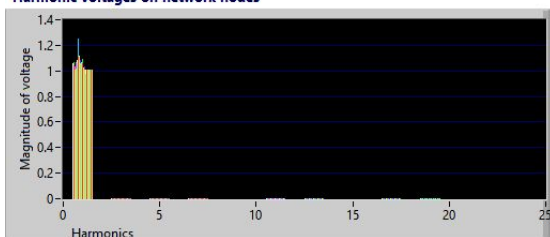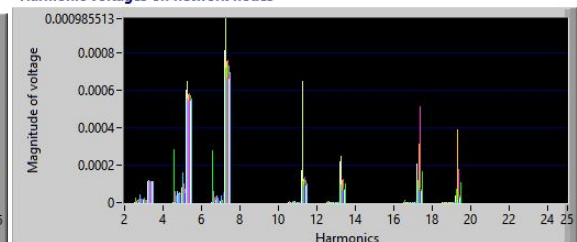
*** Results ***
Base: 10000000
Number of lines and Transformers: 57
Generation Nodes: 21
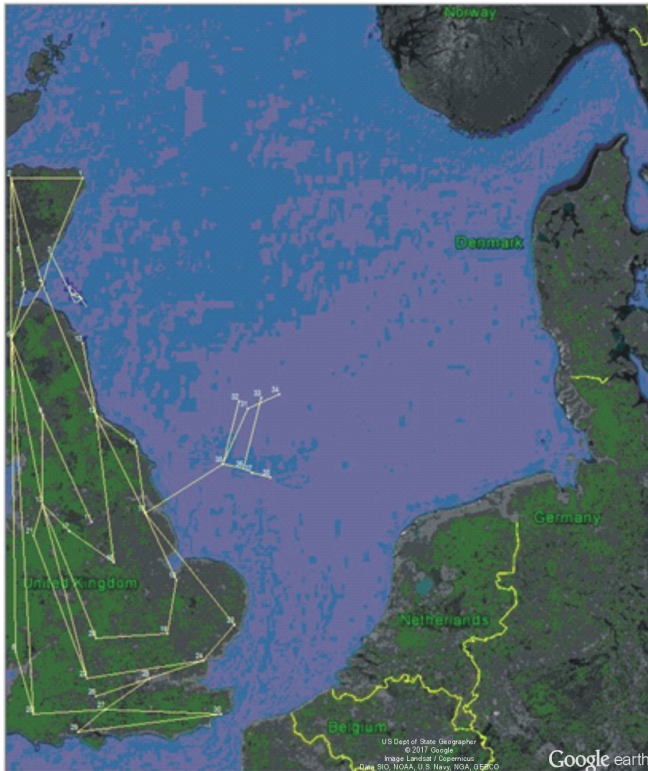**Load Nodes: 24**
Total Nodes: 45
Number of elements in derivation: 2
Load nodes with harmonics injected: 15
Number of harmonics to be considered: 7
Processing time of Power Flow and Harmonic Propagation Study : 00:00:1.242 = 1.242 seconds
Map of the North Sea with connection option 3
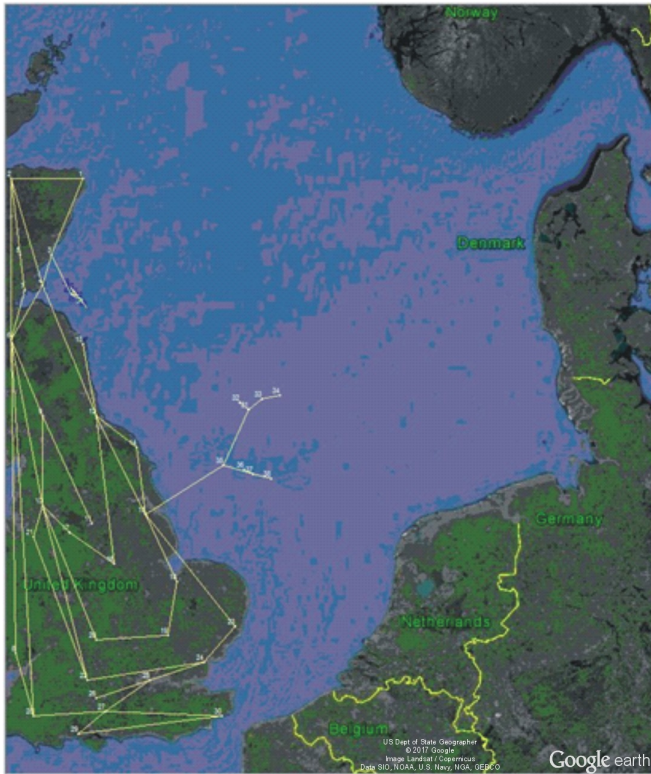
Number of iterations: 5
Error : 5.613597E-7
Generation : 2.509265 p.u.
Demand : 2.234000 p.u.
Power Losses: 0.275265 p.u.
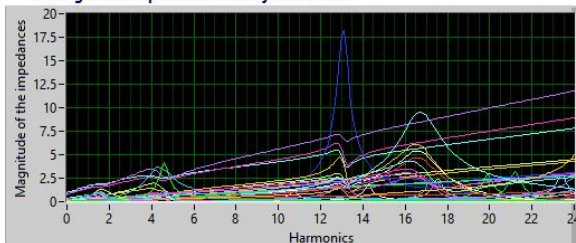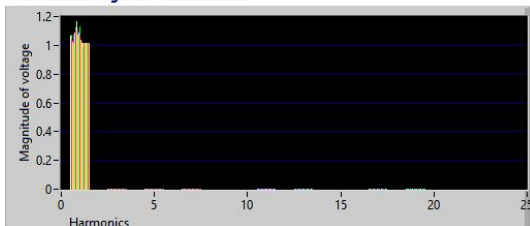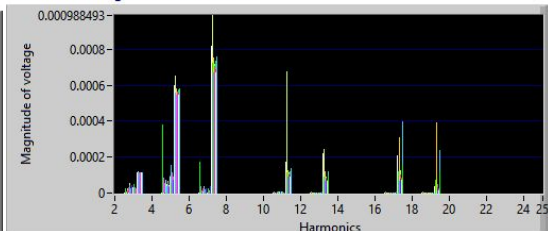
*** Results ***
Base: 10000000
Number of lines and Transformers: 57
Generation Nodes: 21
Load Nodes: 24
Total Nodes: 45
Number of elements in derivation: 2
Load nodes with harmonics injected: 15
Number of harmonics to be considered: 7
Processing time of Power Flow and Harmonic Propagation Study : 00:00:1.198 = 1.198 seconds
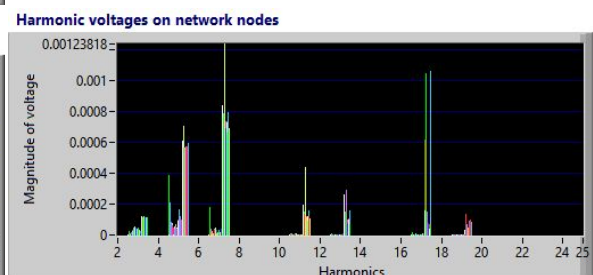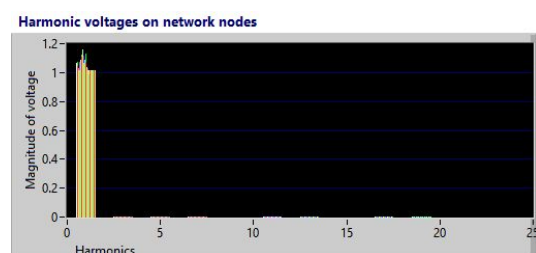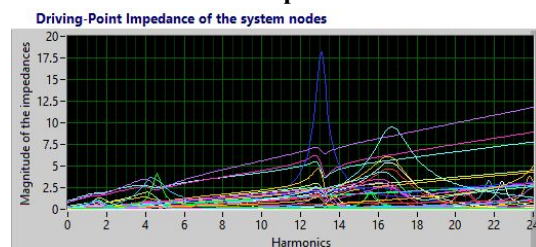**Map of the North Sea with connection option 4**
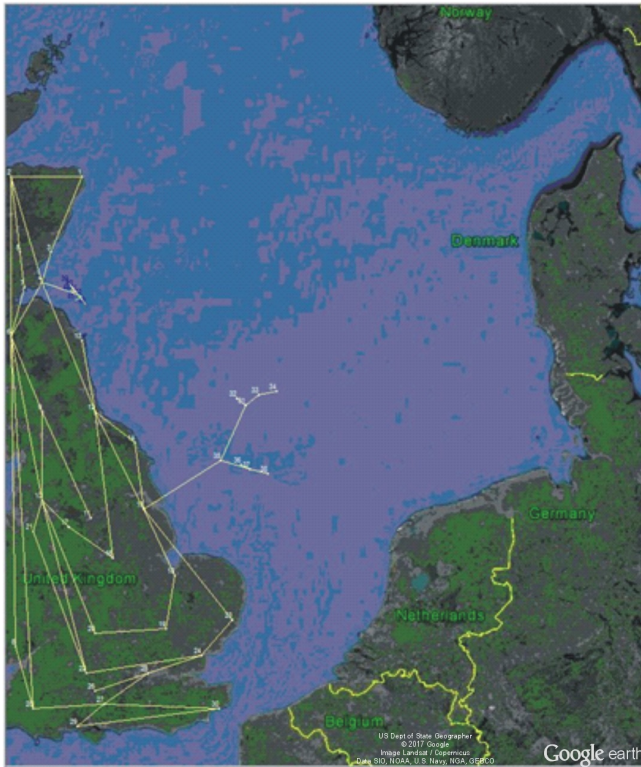
Number of iterations: 5
Error : 5.656639E-7
Generation : 2.503418 p.u.
Demand : 2.234000 p.u.
Power Losses: 0.269418 p.u.
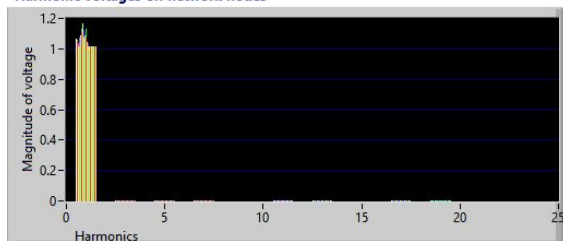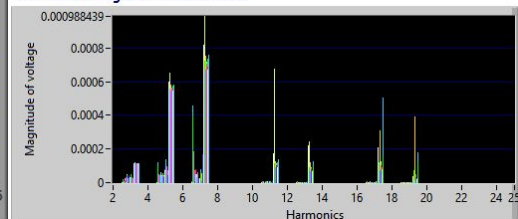
*** Results ***
Base: 10000000
Number of lines and Transformers: 60
Generation Nodes: 21
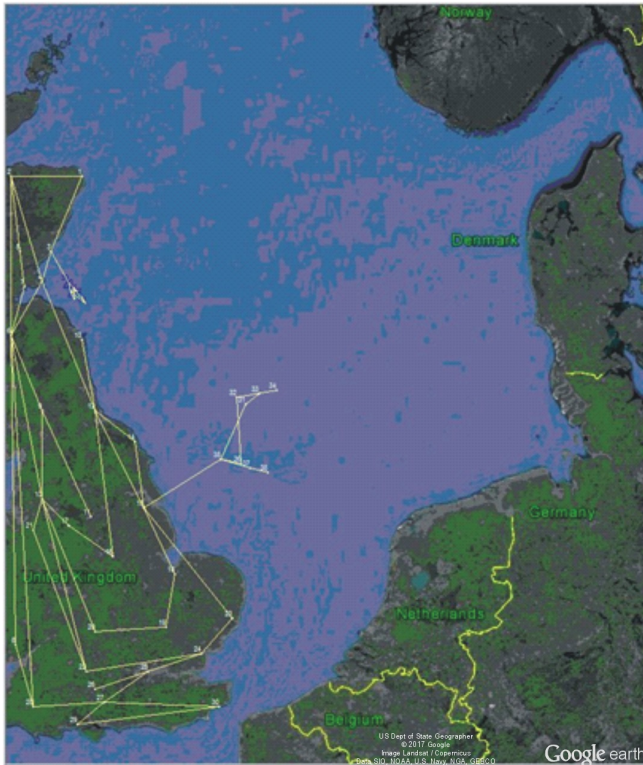**Load Nodes: 24**
Total Nodes: 45
Number of elements in derivation: 2
Load nodes with harmonics injected: 15
Number of harmonics to be considered: 7
Processing time of Power Flow and Harmonic Propagation Study : 00:00:1.267 = 1.267 seconds
Map of the North Sea with connection option 5

Number of iterations: 5
Error : 5.700629E-7
Generation : 2.500920 p.u.
Demand : 2.234000 p.u.
Power Losses: 0.266920 p.u.

*** Results ***
Base: 10000000
Number of lines and Transformers: 60
Generation Nodes: 21
Load Nodes: 24
Total Nodes: 45
Number of elements in derivation: 2
Load nodes with harmonics injected: 15
Number of harmonics to be considered: 7
Processing time of Power Flow and Harmonic Propagation Study : 00:00:1.244 = 1.244 seconds
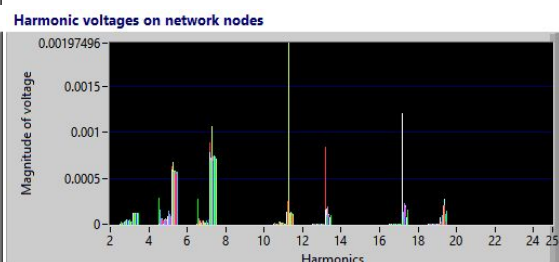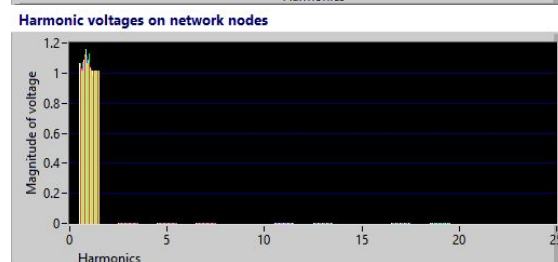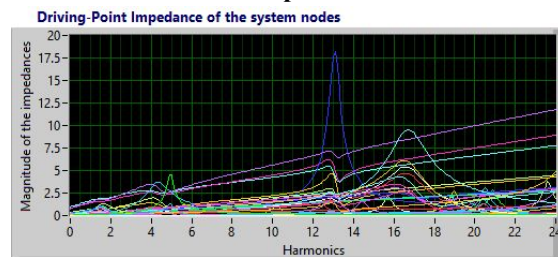**Map of the North Sea with connection option 6**

Number of iterations: 5
Error : 5.857226E-7
Generation : 2.499542 p.u.
Demand : 2.234000 p.u.
Power Losses: 0.265542 p.u.

*** Results ***

Base: 10000000

Number of lines and Transformers: 59

Generation Nodes: 21

Load Nodes: 24

Total Nodes: 45

Number of elements in derivation: 2

Load nodes with harmonics injected: 15

Number of harmonics to be considered: 7

Processing time of Power Flow and Harmonic Propagation Study : 00:00:1.212 = 1.212 seconds

Map of the North Sea with connection option 7

Number of iterations: 5

Error : 5.768252E-7

Generation : 2.498968 p.u.

Demand : 2.234000 p.u.

Power Losses: 0.264969 p.u.

*** Results ***
Base: 10000000
Number of lines and Transformers: 61
Generation Nodes: 21
Load Nodes: 24
Total Nodes: 45
Number of elements in derivation: 2
Load nodes with harmonics injected: 15
Number of harmonics to be considered: 7
Processing time of Power Flow and Harmonic Propagation Study : 00:00:1.229 = 1.229 seconds
Map of the North Sea with connection option 8
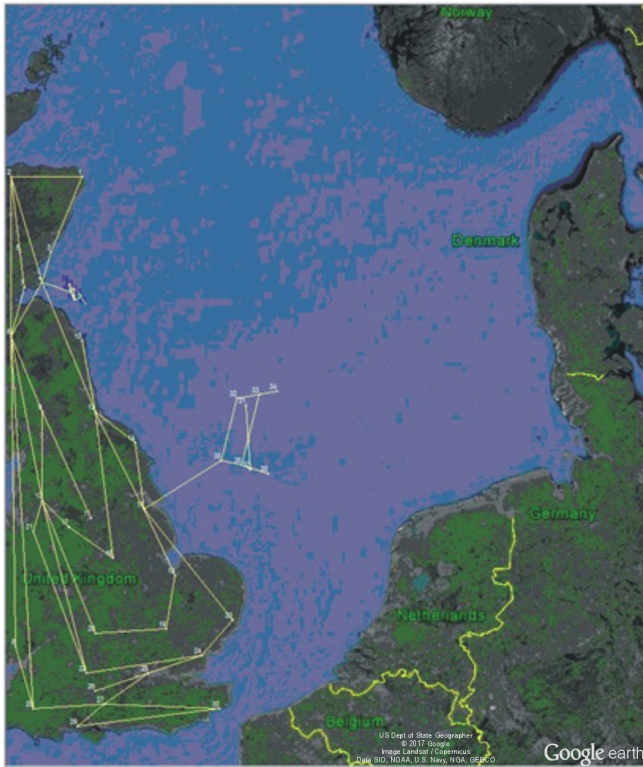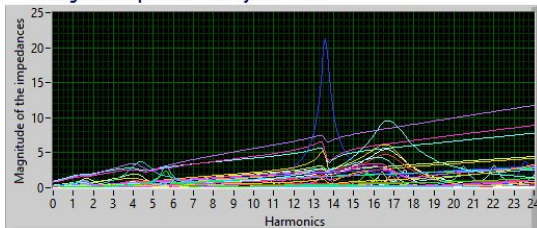

Number of iterations: 5
Error : 5.779442E-7
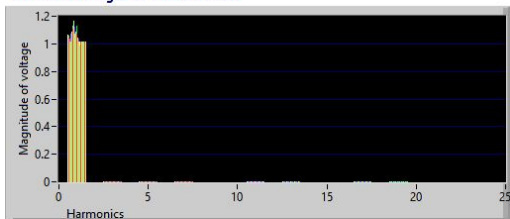**Generation : 2.497892 p.u.**
Demand : 2.234000 p.u.
Power Losses: 0.263892 p.u.